ELECTRICAL LOAD CONTROL

OF

A WIND TURBINE GENERATOR

A thesis
submitted for the degree
of
Doctor of Philosophy
in
Electrical Engineering

by

I.P.Milner

Department of Electrical
and
Electronic Engineering

University of Canterbury

Christchurch, New Zealand

1984

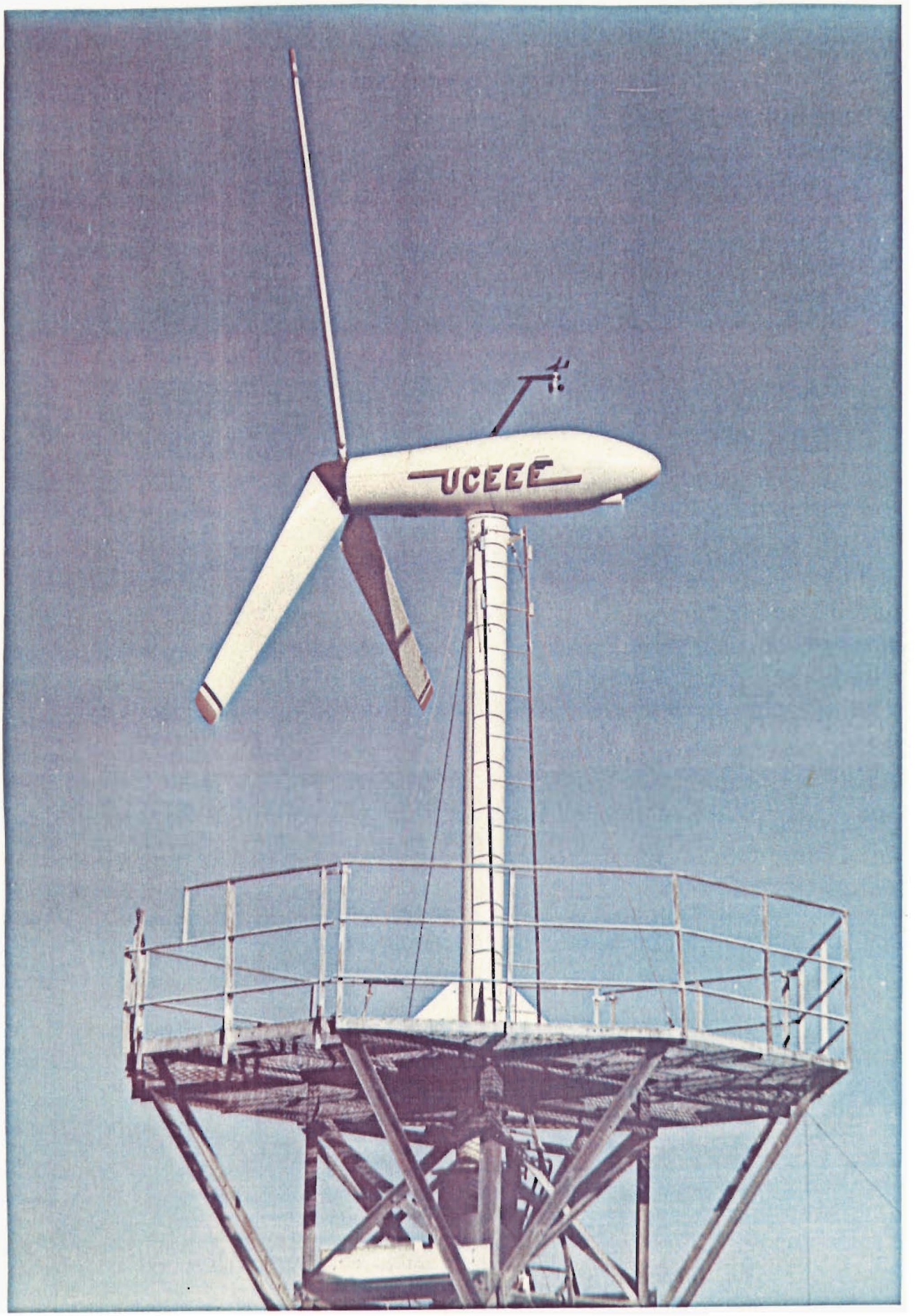

To my wife Lynne and
my children
Peta and Jessica

ABSTRACT

The thesis describes a method for control of wind turbine generator power coefficient by variation of load with wind speed changes.

Steady state characteristics of horizontal axis propeller type wind turbines are shown and development of the tip speed ratio - power coefficient curve is given. Taking account of the theory of the horizintal axis propeller turbine, a three bladed windmill of six metres diameter with fixed pitch was designed and constructed.

Self excited induction generators are described in detail in terms of the steady state characteristics. It is shown that the currently used induction machine equivalent circuit model, employed for determination of the steady state characteristics, inadequately describes the observed operation of the machine. This is shown using phasor diagrams. An alternative equivalent circuit model is suggested.

A controllable rectifier was designed and used in conjunction with the self excited induction generator. The rectifier is capable of operating over a wide frequency range with large amounts of harmonic present at the input.

Use of the self excited induction generator in conjunction with the controllable rectifier in the wind turbine generator is described and shown to provide a practical form of turbine load control. Control of the turbine power coefficient is obtained by controlled variation of rectifier delay angle. A microprocessor is used to determine power available in the wind and subsequently estimates the required load power to obtain the desired power coefficient.

Results of the turbine operating in windy conditions show that such a system can operate satisfactorily.

Suggestions are also made for further research to be carried out on the wind turbine generator.

TABLE OF CONTENTS.

ACKNOWLEDGEMENTS.

I wish to express sincere gratitude to my supervisor, Dr. D.B. Watson, for his support during the period which I have been involved with the Wind Generation Project. His comments and constructive criticisms have been of great assistance.

A vote of thanks is given to all academic staff and postgraduate students in the Department who have provided encouragement and interesting discussions. Thanks also the workshop staff for their valued assistance, particularly to Mr. R.H. Young who spent many long nights working with me in order that hardware would be completed.

Acknowledgement is made for the financial support given by New Zealand Electricity as well as for the many drawings prepared by the Christchurch Drawing Office. Their assistance is greatly appreciated. The University Grants Committee are especially recognised for their funding of the project.

A special thanks is due to Dr. C.J.Chesmond of the Queensland Institute of Technology who gave me the initial encouragement to undertake a Ph.D.

I wish also to thank my parents for managing to keep a wayward son on the straight and narrow and my wife's parents for their support and assistance over the last few years.

Last, and by far most importantly, I owe my wife Lynne and my children gratitude which can never be repaid for their patience, tolerance and moral support, which always seemed to be there when needed the most. The past few years have given a deep respect of the importance of my family to me.

LIST OF FIGURES.

CHAPTER 7

CHAPTER 8

LIST OF PLATES.

LIST OF TABLES.

LIST OF PRINCIPAL SYMBOLS.

CHAPTER 2.

a	Axial interferrence factor.
a'	Rotary interferrence factor.
A	Disc area.
C_D	Drag coefficient.
C_L	Lift coefficient.
C_p	Power coefficient.
C_{pm}	Maximum power coefficient.
C_t	Thrust coefficient.
C_r	Root chord of blade.
C_t	Tip chord of blade.
C_q	Torque coefficient.
D	Drag.
F	Force.
H_1	Upstream head.
H_2	Downstream head.
L	Lift.
$\dot{m}$	Air mass flow rate.
M	Moment.
p_a	Free air pressure.
p_{01}	Air pressure immediately upstream of disc.
p_{02}	Air pressure immediately downstream of disc.
P	Turbine power.
P_m	Turbine power at C_{pm}.
P_W	Wind power.
Q	Torque.
r	Radius.
r_r	Root radius of blade.
R	Tip radius.
R_T	Test radius.
S	Blade plan area.

T	Thrust.
U_1	Free air velocity.
U_2	Air velocity downstream of disc.
U	Air velocity through disc.
V	Vector sum of wind velocity components.
x	Local speed ratio.
X	Tip speed ratio.
X_m	Tip speed ratio at C_{pm}.
α	Angle between V and blade chord line.
θ	Pitch angle (θ = 90 - true pitch).
ν	Rotational velocity component of flow.
ρ	Air density.
ω	Local angular velocity of fluid.
Ω	Turbine angular velocity.

Subscripts:

PT	Along plane of blade chord at test point.
NT	Normal to the plane of blade chord at test point.

CHAPTER 3.

C	Capacitance.
E	Internal emf.
E_g	Generated emf.
E_0	Source emf.
E_R	Emf induced by residual flux.
E_s	Saturation emf.
f_1	Stator electrical frequency.
f_m	Frequency for measured magnetisation characteristic.
I	Total load current.
I_0	Total magnetising current (Including iron loss current).
I_1	Stator current.
I_2'	Rotor current referred to stator.
I_c	Capacitive current.
I_{fe}	Iron loss current.
I_m	Magnetising current.
I_p	Active component of load current.

I_q	Reactive component of load current.
I_R	Current resulting from residual flux.
I_x	Magnetising current at zero volts.
j	"j" operator.
L_0	Magnetising inductance.
L_1	Stator leakage inductance.
n	Rotor mechanical speed in rps.
p	Number of pole pairs.
P_c	Capacitor leakage loss.
P_{cu1}	Stator copper loss.
P_{cu2}	Rotor copper loss.
P_{fe}	Iron loss.
P_l	Machine power loss.
P_L	Load power.
P_T	Total power loss.
R_0	Iron loss resistance.
R_1	Stator resistance.
R_2'	Rotor resistance referred to stator.
R_L	Load resistance.
s	Slip.
V	Stator terminal voltage.
X_0	Magnetising reactance.
X_1	Stator leakage reactance.
X_2'	Rotor leakage reactance referred to stator.
X_c	Capacitive reactance.
X_L	Load reactance.
β_1	Angle between fundamental terminal volts and fundamental generated emf.
β_3	Angle between fundamental terminal volts and third harmonic generated emf.
ν	Harmionic number.
φ	Phase angle.
Φ_R	Residual flux.
ω_1	Stator electrical angular frequency.
ω_2	Rotor electrical angular frequency.

CHAPTER 4.

$e_{a,b,c}$	Instantaneous phase-neutral voltages.
e_{ab}	Instantaneous phase-phase voltage, a-b phases.
E	Peak phase-neutral voltage.
I	AC input current.
I_d	DC current.
I_p	Active component of input current.
I_q	Reactive component of input current.
R_L	Load resistance.
t	Time.
T	Period of one conduction cycle.
v_d	Instantaneous value of DC voltage.
V	Phase-neutral rms voltage.
V_d	DC voltage.
α	Delay angle.
γ	Overlap angle.
φ	Phase angle.
ω	Angular frequency.

CHAPTER 5.

A	Cross sectional area.
C_D	Drag coefficient.
d	Neutral axis - centre line distance.
E	Modulus of elasticity.
F	Force.
F	Centrifugal force.
I	Moment of inertia.
H	Angular momentum of turbine.
M	Moment.
l	Section length.
r_d	Effective radius.
r	Radius of gyration.
R_T	Test radius.
S	Blade plan area.

U	Wind velocity.
Z	Section modulus.
γ	Blade bending angle.
δ	Coning angle.
ε	Strain.
θ	Pitch angle (θ = 90 - true pitch).
$\dot{\phi}$	Yaw angular velocity.
ρ	Air dendity.
σ	Stress.
Ω	Turbine angular velocity.

Subscripts:

AN	Component normal to blade chord plane from centrifugal force.
AP	Component along blade chord plane from centrifugal force.
NT	Component normal to blade chord plane from aerodynamic forces.
PT	Component along blade chord plane from aerodynamic forces.
N	Component normal to blade chord plane from centrifugal and aerodynamic forces.
P	Component along blade chord plane from centrifugal and aerodynamic forces.
A	Normal to disc.
B	Radially along blades.
b	Blade.
g	GRP component.
s	Steel component.
s	Shear.
s	Spar.
t	Tensile.
tg	Tensile for GRP.
ts	Tensile for steel.
sg	Shear for GRP.
ss	Shear for steel.
sp	Spindle.

CHAPTER 7.

A	Turbine disc area.
C	Capacitance.
C_p	Turbine power coefficient.
f_1	Frequency.
I	AC current.
I_c	Capacitive current.
I_d	DC current.
I_m	Magnetising current.
I_q	Reactive component of current.
P_A	Actual load power.
P_D	Dead zone power.
P_R	Required load power
P_W	Wind power.
R_L	Load resistance.
U_1	Free wind velocity.
V	AC phase-neutral voltage.
V_d	DC voltage.
α	Delay angle.
ν	Harmonic number.
φ	Phase angle.
ρ	Air density.

CHAPTER 8.

A	Turbine disc area.
C_p	Turbine power coefficient.
R_L	DC load resistance.
R'_2	Generator rotor resistance referred to stator.
s	Slip.
U_1	Free wind velocity.
V	AC phase-neutral voltage.

CHAPTER 1.

INTRODUCTION.

1.1: A Short History of Windmills.

Wind has been the servant of mankind for many centuries providing the motive force for sea travel, water pumping and the grinding of grains. Some of the earliest references to windmills date back to the seventeenth century B.C. (Golding 1955) when the Babylonian Emperor, Hammurabi, studied the possibility of using them for irrigation. The Hindu classic Arthasastra (400 B.C.) (UN 1981) refers to wind powered machines used for raising water. It is uncertain as to the length of time that windmills have been used by the Persians but it is known that they were commonplace around the seventh century A.D.. With the expansion of the Moslem civilization, windmill use spread widely and eventually found its way to Europe and even as far as China. By the early nineteenth century windmills were accepted widely for varied uses in Europe, particularly for the grinding of grain crops.

Invention of the steam engine, internal combustion engine and widespread use of electricity initiated a major discontinuance in the use of windmills in many parts of the world. Despite this, windmills still found applications in rural areas such as for water pumping and battery charging. These were usually small multiple blade types and with the advent of aviation research developed into more sophisticated models.

Up until the end of the Second World War most windmills were small, ranging up to about 5kW capacity, but some larger machines were constructed. The Central Wind Power Institute of Moscow commissioned the construction of a 100kW pilot plant for electricity generation near Balaclava, Crimea (Golding 1955, Warne 1983) in 1931. During World War II, and largely through the work of Palmer Putnam, a 53m diameter machine of 1250kW rating was constructed at Grandpa's Knob in Vermont, USA. This mill operated with varying degrees of

success for about six years and ultimately destroyed itself by shedding one of its two eight ton blades.

Since World War II interest has steadily increased in the use of wind power for electricity generation with major work being done in the Scandanavian countries, the United States and other parts of Europe. Developments include the American ERDA/NASA series of mills:- the MOD-0 (Taylor 1982 ,Puthoff 1975) machine at Plumbrook, Ohio rated at 100kW and 38m in diameter, and the four MOD-0A wind turbines (Stiller 1983) of 200kW rating. In 1971 the MOD-1 machine of 2MW capacity was commissioned followed by the installation of three MOD-2 mills at Goodnoe Hills, Washington. These were 91m in diameter with a 2.5MW rating. The latest in the line of these machines, and yet to be commissioned, are the MOD-5A (General Electric) and the MOD-5B (Boeing). The MOD-5A is a 7.3MW machine of 130m diameter while the MOD-5B is of 7.2MW capacity at 128m diameter. The Hawaiian Electric Company is intending to install a MOD-5A on Oahu starting early in 1984 with operation in early 1985. Other developments from the USA include the 3MW Bendix- Schackle turbine and the 4MW WTS-4 and 3MW WTS-3 of Hamilton- Standard.

European efforts include the 2MW wind generator at Tvind (Jensen 1983) on the West Jutlannd coast which has 54m diameter blades and has met with substantial success, and the West German Growian turbine (Hau 1982) of 3MW capacity at Kaiser- Wilhelm- Koog. Several efforts in Europe at developing mills in the 50kW to 200kW range have also met with substantial acceptance (Stodhart 1975, et al).

1.2: The Wind Resource.

Wind power can simply be described as a manifestation of solar power: the movement of air in Earths atmosphere resulting from the effects of solar energy reaching Earth. Of the 5.2×10^{24} Joules per annum of solar energy (Warne 1977) reaching the Earth only about 9×10^{22} Joules is converted into air movement with an estimated 3.6×10^{18} Joules being extractable from the

0m to 100m air layer. This means that 10^6 to 10^7 MW (UN 1981, Jayadev 1976) is available in the Earths winds, largely based on the estimates of Von Arx. On a local basis approximately 350TWh (Wood 1981) of energy is available in New Zealand from the wind, which is substantially in excess of the energy requirements for the whole country. Although it is impracticle to ever attempt to recover all of this energy, the figure does demonstrate the potential of the power in the wind and it could be likely that even a small contribution from the wind could be of economic benefit.

Nearly all windmills to date have been sited on land although recent efforts to initiate sea based studies have been made (Lindley 1980, Milborough 1982), as well as proposals for jet stream designs (Arbouw 1982). For mills constructed within the first 100m of the boundary layer of the atmosphere the effects of the structure of the land surface are most important as it is here where turbulance and gusts are pronounced. It has also been known for some time (Putnam 1948, Golding 1955) that mean wind speeds are enhanced on the summits of suitably selected hills, a factor which because of the relationship between wind speed and potentially available wind power, is of great interest. Some recent studies (Bradley 1983, et al) have more clearly defined the phenomenom. Another feature of wind flow over the surface of the Earth which has a great effect on large wind turbines is the "mean velocity profile ". This is caused by the shearing of the wind near the land surface and results in an increase in mean wind speed as height increases.

Although the energy available from a given wind turbine site does not greatly vary from year to year it is found that variations in daily and seasonal patterns may appear. This situation is critical to windmill users as it affects factors such as energy storage and load matching. Gusts are also significant on two counts: firstly in terms of structural design of the turbine and secondly in terms of energy extraction, since a significant amount of wind energy is contained within them. Study of wind patterns at windmill sites has thus taken on significant importance and many studies have been made (Bhumralkar 1980, et al) to assess these effects.

1.3: Windmills - Types and Uses.

1.3.1: Turbine Types.

Classification of windmills can come under two broad areas:-

(a) According to the relationship between wind direction and relative turbine shaft orientation and can be either axial flow machines (wind flow parallel to the shaft) or cross flow machines (wind flow normal to the shaft).

(b) According to the construction of the turbine. This classification is more common and classes them as either being horizontal axis wind turbines (HAWT's) or vertical axis wind turbines (VAWT's).

Earliest windmills probably used sails as the blades. It is known that the Persians used a vertical axis mill (Golding 1955) which used this type of blade. In modern times sailwing mills are still in use in some parts of the world (UN 1981), the majority of which are of the horizontal axis type. One of the advantages of sailwing mills is that their structure often can survive high wind speeds, primarily due to the fact that the blades are fabric and shred before the support structure fails. The other advantages of this construction are the low cost, low technology factors which make this form of wind energy converter particularly favorable to third world nations for irrigation purposes.

Primitive horizontal axis mills were constructed with canvas sails spread over wooden framework, and since they had no yawing mechanism they were erected so as to face the prevailing wind. The first attempts to provide a yawing mechanism were thought to have come from Germany (Golding 1955) and it is also known that Leonardo da Vinci designed windmills where the support structure itself rotated. It was not until the construction of the Dutch windmills that 'modern' designs were born. These incorporated a

fixed support structure with a yawing nacelle, and were mainly used for milling purposes.

Commonly used for irrigation worldwide are the multi-bladed farm type windmills which are rugged and inexpensive and have reliably served farms for nearly a hundred years. They are characterized by a multitude of flat or slightly curved metal blades on a horizontal axis and a tail to point the blades into the wind. When excess windspeed occurs a latching mechanism on the tail steers the blades sideways into the wind to prevent damage.

The problem with all the above mills is that they are generally of low efficiency and do not lend themselves to large scale construction, ie., multi-megawatt scale. Modern approaches to this finally led to several designs of both the horizontal axis and vertical axis types. The Darrieus rotor designed by G.J.M. Darrieus in France in 1927 is one such vertical axis design and is used mainly in the phi configuration although a delta configuration is also possible. The main difference between the Darrieus rotor and earlier vertical axis machines is that the Darrieus relies on aerodynamic lift to obtain rotation rather than differential drag and is a highly efficient wind energy converter which holds great promise for the future. One drawback with this design is that it is not self starting and requires some additional mechanism to perform this function. More recent studies (Baker 1983) have overcome this difficulty.

The Gyromill is another form of vertical axis mill which relies on aerodynamic lift for torque production and has a particularly high efficiency. The disadvantage with the Giromill is that its construction is unsuited for large scale.

The Savonius mill has been proposed as an inexpensive design for use in rural areas such as for irrigation. Recent work (Baird 1983) shows that the simplicity and ruggedness of these mills can give more than adequate performance in such applications. They are inefficient and not suitable for large designs.

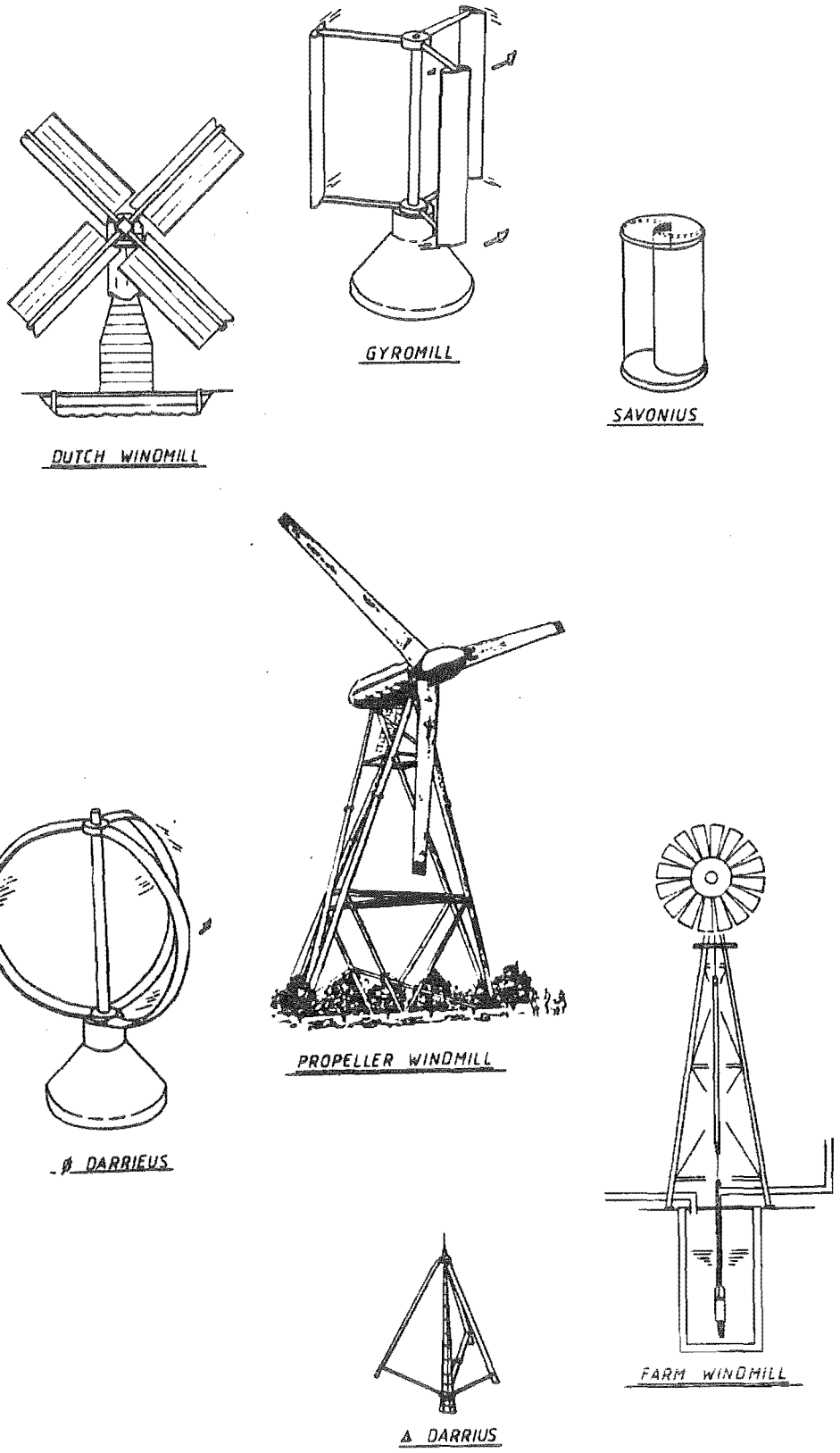

Figure 1.1: Common Windmill Types.

The most proven design is the propeller type turbine as it combines rugged construction with high efficiency. The largest of these mills are of two bladed design with low solidity and high speed. The major difficulties arising with the propeller type turbines are ones of blade costs and cyclic loads due to tower shadow and wind profile. Three bladed mills offer advantages in terms of resonance problems but add extra capital cost to the turbine. Some designs have even been studied using one blade with the appropriate counterweight.

Propeller type turbines are categorized as either upwind types or downwind types. Upwind type machines have the blades on the upwind side of the support structure and need to be steered into the wind. Downwind types have the blades on the downwind side of the support structure and do not necessarily need to be steered. The advantage that upwind type machines have is the lesser effect of the support structure on the wind flow over the blades. In downwind type mills this effect is called tower shadow.

Many efforts to improve the performance of propeller turbines have been made. Tipvanes (van Holten 1978) have been used as an effective method and this shows promise for the future. Shrouding (Igra 1978) is another method applicable to smaller mills.

It is because the propeller type turbine is so well proven that this design was chosen for the purposes of this project. Three blades were used in the downwind position so that steering would not be required.

1.3.2: Generator Types.

Variations in generator types used in wind turbine generators (WTG's) have been under considerable study for many years. For WTG's connected to the electricity grid, control of voltage and frequency are of prime imoportance. The solution to providing a constant frequency is to allow the windmill to operate at constant speed and drive a synchronous generator.

This led to WTG's of the constant speed, constant frequency class (CSCF). For reasons explained in Chapter 2 constant speed windmills are not efficient for any one given configuration over a range of wind speeds. This led to the variable speed, constant frequency class (VSCF) of WTG. In these some method of translating the variable speed shaft to constant frequency is required and an array of designs has appeared to accomplish this. These include mechanical means such as variable ratio gearboxes, hydraulic drives and others.

Electrical means of achieving this have also been proposed such as ADA (AC-DC-AC conversion) (Watson 1979, et al) where the variable frequency AC from the generator is firstly converted to DC and then inverted to constant frequency AC. More elaborate systems have also been proposed such as the frequency modulated generator (FMG) (Jayaveviah 1975, Ramakumar 1975), the rotor fed induction generator (Jayadev 1975) and the double output induction generator (DOIG) (Yadavalli 1976). With the decreasing costs of solid state power devices it appears now probable that the ADA proposals will come to the forefront of VSCF systems.

A third and lesser known group of windmills also exists. These are the systems where frequency does not play a significant role in the load, such as for heating. Such systems could operate with varying speed and varying frequency (VSVF) and indeed could operate with the electrical output in DC form. Such windmills are currently available and markets appear to be significant (Stodhart 1975, et al). Recent studies have been made using DC generators (Suzuki 1982) and others using AC commutator generators with rectifiers (Buehring 1981). Both these designs are suited to low power applications such as heating but suffer from brushgear maintenance problems.

This difficulty is solved by using the self excited induction generator, which uses a brushless squirrel cage induction machine and is both rugged and relatively inexpensive. Several control proposals have been made (Arrillaga 1978, et al) and it is one of these proposals which is of concern in this thesis, with a view to eventually using the WTG for glasshouse heating.

1.4: Project Aims and History.

The objective of the project is to develop a wind generation research facility suitable to the requirements outlined below and also to allow further studies of a varied nature to be carried out. This objective being satisified, the following studies were undertaken:

(1) To further study the operational characteristics of the self excited induction generator and its interaction with controlled rectifiers.

(2) To construct a controllable rectifier which could successfully operate over a wide range of frequncies and with large quantities of harmonics at the input, and to test its operation in conjunction with the self excited induction generator.

(3) To develop a microprocessor based control system to allow the generator/rectifier combination to be used to control windmill shaft loading and hence power transfer from the wind to the turbine shaft, using a fixed pitch wind turbine.

The project was started in early 1980 with the mechanical design and construction phase being complete some two years later. Design and construction of the control system was completed in mid 1983 with system debugging requiring a further six months. During the coures of work, the author performed the following tasks:-

. Initial conception and development of criteria for the construction of the wind turbine generator such that the above objectives could be carried out.

. Design all mechanical and aerodynamic components for the wind turbine.

. To design all electrical systems, digital and analogue electronics, power electronics and microprocessor components.

. Develop control algorithms and to implement and debug these in software.

. Undertake computer studies of wind turbine performance.

. To supervise construction and erection at all phases of the project.

. Test the operation of the system.

. Design and construct a wind recording system capable of operating in a remote location. This system is described in Appendix 6.

Chapter 1 has given an outline of windmill history and current technology. Chapter 2 gives the basis of the operation of HAWT's. Chapter 3 outlines the evaluation and theory of the self excited induction generator while Chapter 4 describes the operation of controlled rectifiers. Chapter 5 describes mechanical construction of the WTG and Chapter 6 outlines operation of the control system used for the wind turbine. Chapter 7 combines the theory of Chapters 2, 3 and 4 and forms the basis for the load control of the WTG and gives test results. Chapter 8 outlines proposals by the author for further work to be carried out and Chapter 9 gives conclusions.

CHAPTER 2.

WIND TURBINE CHARACTERISTICS.

2.1: Introduction.

The extent to which windmills will be used for the generation of electrical power will depend on the cost effectiveness of the wind generation plant. Factors which influence a cost effective design are similar to those for any other generating plant, such as site, lifespan, capital and maintenance costs and of particular importance here is efficient extraction of power from the source. It is therefore necessary, in a study of efficient power transfer from wind to turbine shaft, to have an understanding of the aerodynamic performance of the wind turbine. Chapter 2 outlines theory which has been developed for wind turbines, mainly based on well established theories for aircraft propellers and places particular emphasis on the momentum theory.

2.2: Actuator Disc Theory.

The study of windmill aerodynamics has its roots in marine engineering in the momentum theories developed for ships propellers by Rankine and Froude, and later adopted by Betz for use on windmills (Golding 1955). The theory uses an expression for the momentum of a stream of moving air on an actuator disc and considers the pressures and velocities of air on the free upstream side of the disc and also in the disc wake. The following initial assumptions are made (Wilson 1974, Warne 1977):

(1) The turbine is represented as an actuator disc creating a discontinuity in pressure in a stream tube. An infinite number of blades is therefore assumed.

(2) The fluid (air) is incompressible and non viscous.

(3) The flow is steady and non rotational, i.e., translational flow only is considered.

(4) For air downstream of the actuator disc the velocity is axial and constant over the stream tube section and there is no pressure discontinuity across the stream tube boundary.

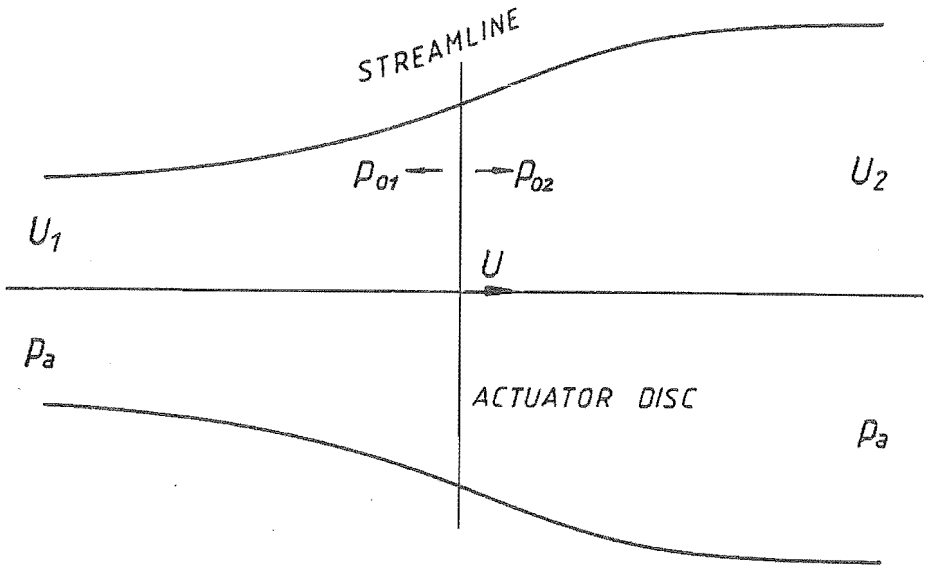

Figure 2.1: Actuator Disc - One Dimensional Representation.

Consider the flow past the wind turbine shown in Figure 2.1. Bernoulli's equation can be applied between the free air stream and the upwind side of the turbine and also between the downwind side of the turbine and the wake.

$$H_1 = p_a + U_1^2 . \rho/2 = p_{01} + U^2 . \rho/2 \qquad (2.1)$$

and

$$H_2 = p_a + U_2^2.\rho/2 = p_{02} + U^2.\rho/2 \qquad (2.2)$$

where H_1 is the upstream head and H_2 is the downstream head.

In addition, the thrust on the disc can be found from the momentum theorem.

$$T = \dot{m}.(U_1 - U_2) = A.(p_{01} - p_{02}) \qquad (2.3)$$

or

$$T = \rho.A.U.(U_1 - U_2) \qquad (2.4)$$

The power extracted by the turbine into its shaft is:

$$P = A.U.(p_{01} - p_{02}) \qquad (2.5)$$

Combining Equations (2.1) to (2.5) gives:

$$P = \rho.A.U.(U_1^2 - U_2^2)/2 \qquad (2.6)$$

ie.,

$$P = \rho.A.(U_1 + U_2).(U_1^2 - U_2^2)/4 \qquad (2.7)$$

where

$$U = (U_1 + U_2)/2 \qquad (2.8)$$

A rotor axial interference factor "a" is introduced such that:

$$U = U_1.(1 - a) \qquad (2.9)$$

thus

$$U_2 = U_1.(1 - 2a) \qquad (2.10)$$

Equating (2.4), (2.6), (2.9) and (2.10) gives the following:

$$P = [4a.(1 - a)^2].U_1^3.A.\rho/2 \qquad (2.11)$$

$$T = [4a.(1 - a)].U_1^2.A.\rho/2 \qquad (2.12)$$

Equations (2.11) and (2.12) are simplified to:

$$P = C_p.U_1^3.A.\rho/2 \qquad (2.13)$$

$$T = C_t.U_1^2.A.\rho/2 \qquad (2.14)$$

where

$$C_p = 4a.(1 - a)^2 \qquad (2.15)$$

$$C_t = 4a.(1 - a) \qquad (2.16)$$

C_p is defined as the power coefficient and has a maximum value of 16/27 or 0.593 when a = 1/3. The absolute maximum value of "a" is realized when the final wake velocity U_2 is zero. Returning to Equation (2.10), this occurs for a = 1/2 and represents the impractical case of a 100% efficient machine. In addition to the limits imposed on the power coefficient by the above the combination of friction, imperfect construction, etc. reduce it to more practical limits of about 0.45. In effect the power coefficient represents the ratio of shaft power absorbed from the wind to the actual power available in the wind.

C_t is defined as the thrust coefficient. Applying principles similar to those above places a limit on C_t of 8/9 or 0.889.

2.3: Effects of Wake Rotation.

An extension to the one-dimensional model can be made by considering the effects of wake rotation. As the non-rotational incoming air stream interacts with the turbine, rotational components will be introduced into the wake stream in addition to the translational components. The rotation of the wake will be in the opposite sense to that of the turbine rotation.

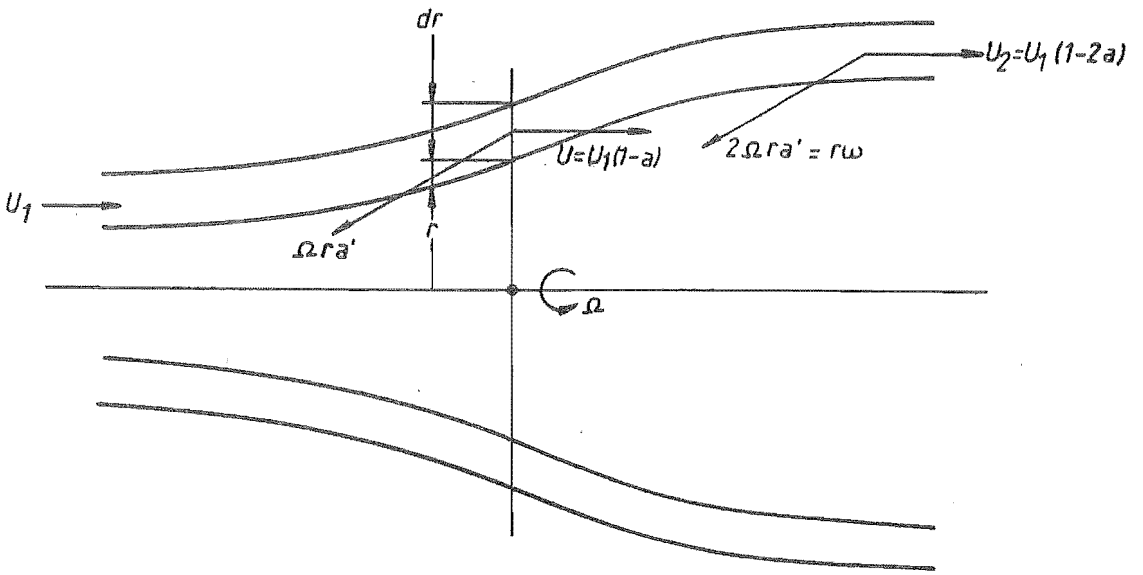

Figure 2.2: Actuator Disc Axial and Outflow Components at Annulus.

Consider the annulus shown in Figure 2.2 at radius "r" and thickness "dr". The axial outflow components and rotary outflow components come from velocities induced by helical vortices leaving the blades as they rotate. The elemental torque contribution from the annulus is:

$$dQ = \rho . r^2 . \omega . U . dA \qquad (2.17)$$

where ω is the local angular velocity of the fluid.

ie.,

$$dQ = 2\pi . r^3 . \rho . U . \omega . dr \qquad (2.18)$$

A rotary interference factor a' is used to simplify ensuing equations and is defined as:

$$a' = \omega/2\Omega \tag{2.19}$$

Equating (2.18), (2.19) and (2.9) gives:

$$dQ = 4\pi.r^3.\rho.\Omega.U_1.(1 - a).a'.dr \tag{2.20}$$

Considering the linear momentum for the annulus an expression can also be found for the elemental thrust:

$$dT = d\dot{m}.(U_1 - U_2) \tag{2.21}$$

or

$$dT = 2\pi.r.\rho.U_1.(1 - a).2U_1.a.dr \tag{2.22}$$

At the annulus the power extracted from the air flow is equal to the work done against the retarding torque per unit time. The elemental forces involved are given by Equations (2.20) and (2.22). To estimate the power, the velocity components must also be known and the axial component is given by Equation (2.9). The rotational component can be seen from Figure 2.2 and is:

$$v = \Omega.r + \Omega.r.a' = \Omega.r.(1 + a') \tag{2.23}$$

Equations (2.20), (2.22), (2.9) and (2.23) can now be equated.

$$(1 + a').\Omega.r.dQ/r = (1 - a).U_1.dT \tag{2.24}$$

or

$$(1 + a').a'.\Omega^2.r = U_1^2.(1 - a).a \tag{2.25}$$

or

$$(1 + a').a'.x^2 = (1 - a).a \tag{2.26}$$

Where the local speed ratio is defined as:

$$x = \Omega.r/U_1 \tag{2.27}$$

Returning to Equation (2.13) the power coefficient can now be redefined.

$$C_p = P/P_w = \int_0^R \Omega.dQ \ / \ (R^2.U_1^3.\pi.\rho/2) \qquad (2.28)$$

The tip speed ratio is defined as:

$$X = \Omega.R/U_1 \qquad (2.29)$$

Equating (2.27), (2.28) and (2.29) gives C_p as:

$$C_p = 8/X^2.\int_0^X (1 - a).a'.x^3.dx \qquad (2.30)$$

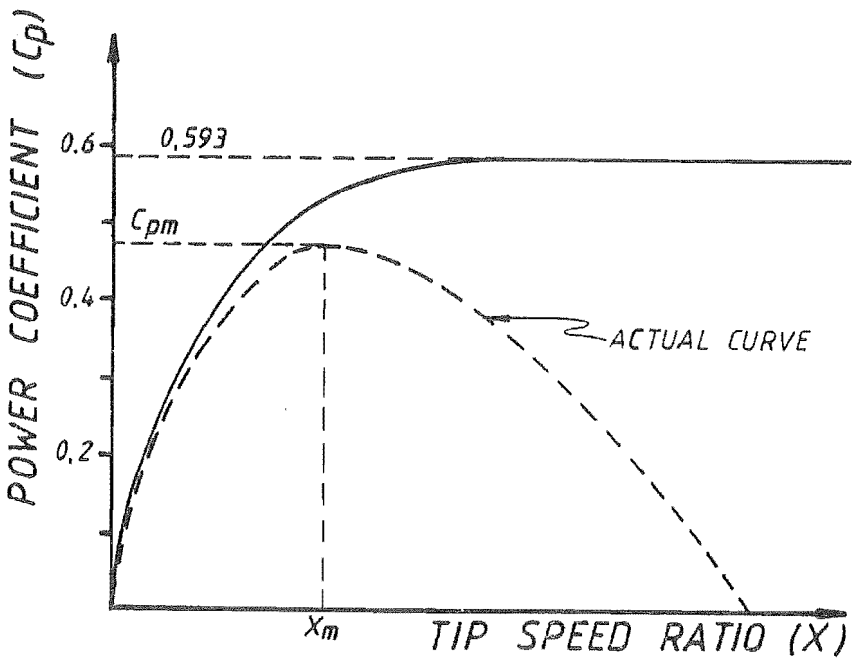

Figure 2.3: Wind Turbine Tip - Speed Characteristic.

For maximum values of C_p , (1 - a).a' must be a local maximum for every x. Numerical integration of Equation (2.30) in conjunction with Equation (2.26) yields the solid curve shown in Figure 2.3. The importance of this curve, which shows the effects of wake rotation, is that the previously determined maximum value of C_p (see Section 2.2) is only valid for high tip speed ratios and that for a tip speed ratio of zero the power coefficient is zero. This condition becomes obvious when it is seen that zero tip speed ratio corresponds to zero shaft rotation. The power loss at the lower tip speed ratios can be accounted for by considering the blade aerodynamics where the inner portions of the blades are operating in stall conditions. At higher tip speed ratios the effects of aerodynamic drag on the blades becomes predominant and the power coefficient again decreases, as shown by the broken curve in Figure 2.3, to the extreme where the power coefficient reaches zero. This shape can be compared with that more usually seen and the salient point to be observed is that there is a unique practical range of angular velocity for the turbine for each value of free air velocity which gives a maximum power transfer from the wind to the turbine shaft.

Figure 2.4 represents this characteristic in a different way. Each curve is drawn for a particular value of wind velocity and the tip speed ratio is varied. The peak of each curve is the optimum power transfer point and a locus of these points represents a curve of cubic form where tip speed ratio is optimum.

It is also possible to draw similar curves for the torque on the turbine shaft. The shaft torque can be found from the equation:

$$Q = P/\Omega \qquad (2.31)$$

Equating (2.31) with (2.29) and (2.13) gives:

$$Q = (C_p/X).\rho.A.U_i^2.R/2 \qquad (2.32)$$

or

$$Q = C_q.\rho.A.U_i^2.R/2 \qquad (2.33)$$

where

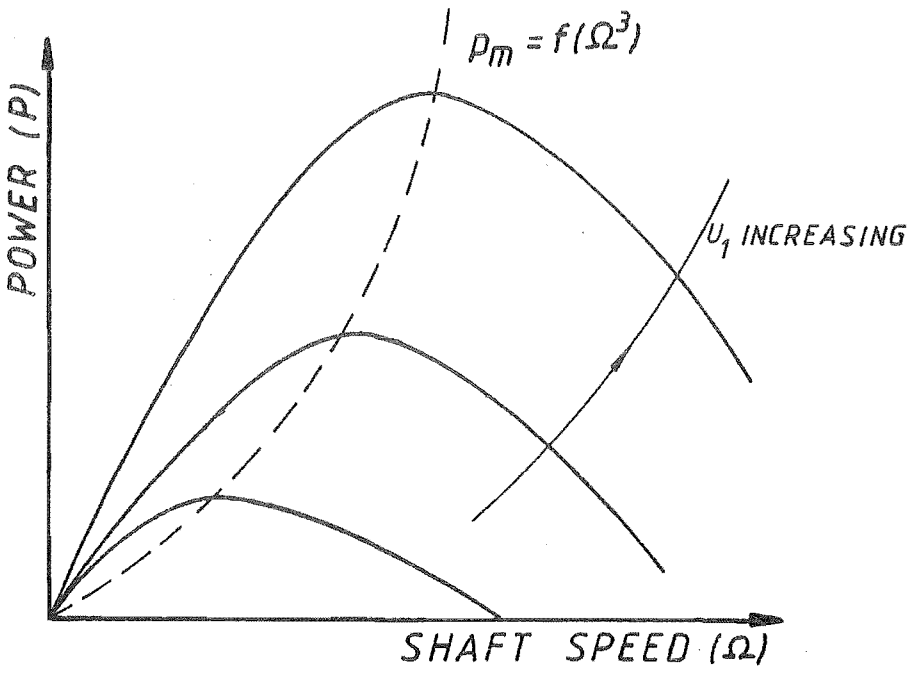

Figure 2.4: Wind Turbine Power - Speed Characteristic.

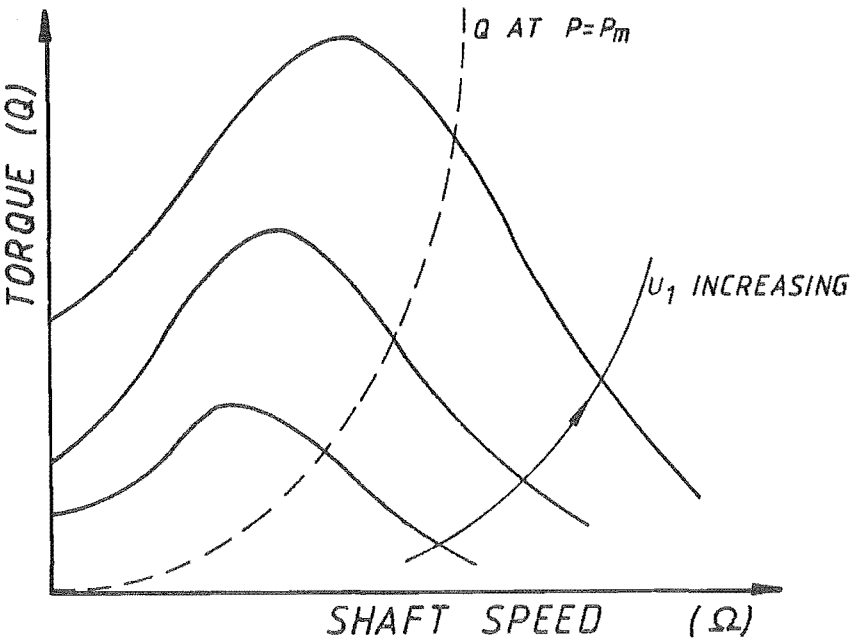

Figure 2.5: Wind Turbine Torque - Speed Characteristic.

$$C_q = C_p/X \qquad (2.34)$$

C_q is the torque coefficient. The torque curves are as in Figure 2.5.

Notice that the maximum power transfer occurs for higher angular velocities of the turbine shaft than do the maximum torque values.

2.4: Wind Turbine Blade Loadings.

The above analysis gives a description of the basic precepts of wind turbines, and the characteristics deduced are utilised in this thesis. However, the descriptions given in Section 2 and Section 3 of this chapter have been based on the momentum theory and as a result suffer from the initial assumptions, in particular that the turbine has been modelled as an actuator disc implying an infinite number of blades. It cannot be used to predict blade loading distributions, effects of non-uniform flows and the effects of the number of blades or the aerodynamic interaction between the blades. For the design of optimum rotors these factors must be taken into account.

Blade element theory was developed in part to answer some of these shortcomings. Although the origins of the theory are generally credited to Drzewiecki, W. Froude had published works on the subject some years earlier (Weick 1930). The Drzewiecki blade element theory considered the propeller as a twisted aerofoil with elemental sections where parameters such as torque, thrust, lift and drag can be individually determined. The air flow around each element is considered as being two dimensional and hence is totally independent on adjacent elements. Modifications to this simple blade element theory have also been made to account for blade interference and are outlined by Weick (Weick 1930).

The aerodynamic loadings on the blades of a turbine can be found using blade element theory by considering some arbitary element of blade of length dr at radius r as shown in Figure 2.6. The elements of lift and drag (von Misis 1959) are:-

$$dL = (\rho.C_L.V^2/2).dS \tag{2.35}$$

$$dD = (\rho.C_D.V^2/2).dS \tag{2.36}$$

where

$$dS = dr.\{C_r - (C_r - C_t).(r - r_r)/(R - r_r)\} \tag{2.37}$$

where dS is the area of the element.

dr is the length of the element.

r is the radius of the element.

V is the vector sum of the free wind velocity and the tangential velocity of the element resulting from blade rotation.

The forces and moments along the plane of the blade and normal to the plane of the blade at any test radius can thus be calculated:

$$F_{PT} = \int_{R_T}^{R} \{(dL.\sin(\alpha) - dD.\cos(\alpha)\} \tag{2.38}$$

for the force along the plane of the blade.

$$F_{NT} = \int_{R_T}^{R} \{(dL.\cos(\alpha) + dD.\sin(\alpha)\} \tag{2.39}$$

for the force normal to the plane of the blade.

$$M_{PT} = \int_{R_T}^{R} \{(dL.\sin(\alpha) - dD.\cos(\alpha)\}.r \tag{2.40}$$

for the moment along the plane of the blade.

$$M_{NT} = \int_{R_T}^{R} \{(dL.\cos(\alpha) + dD.\sin(\alpha)\}.r \qquad (2.41)$$

for the moment normal to the plane of the blade.

R_T is the test radius and R is the turbine radius.

Equations (2.38) to (2.41) are used in Chapter 5 to estimate blade loadings for estimates of blade strength.

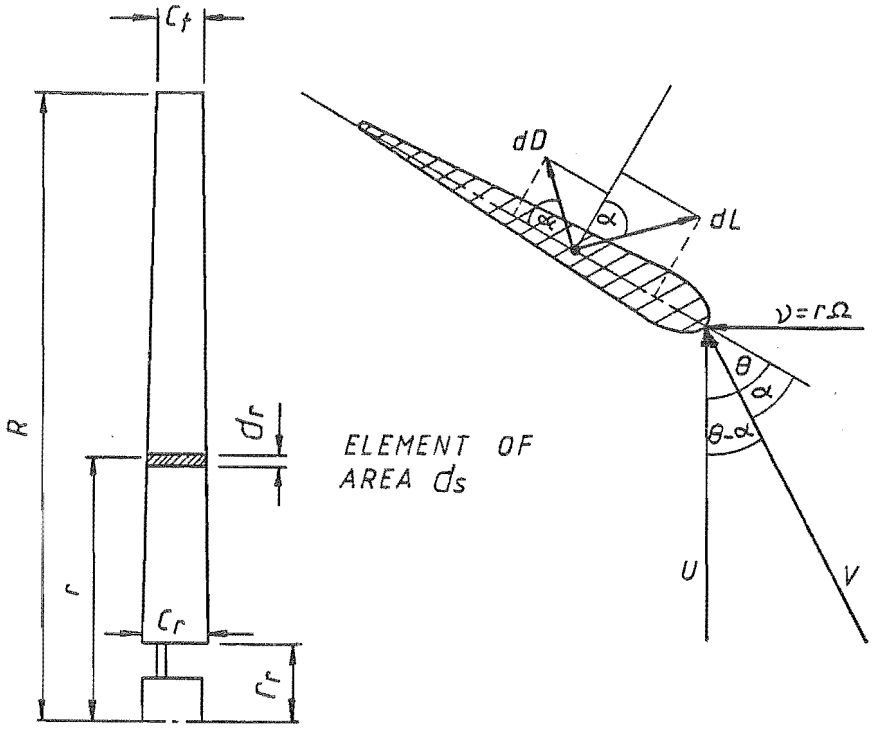

Figure 2.6: Blade Aerodynamic Loadings.

2.5: Summary.

The relationship between tip speed ratio and power coefficient for a propeller type wind turbine has been derived taking into account the effects of wake rotation. Useful curves relating torque and power to shaft speed have been derived. Blade element theory has been introduced to find equations which can be used to calculate the aerodynamic loadings on the blades.

CHAPTER 3.

THE INDUCTION GENERATOR.

3.1: Introduction.

In a paper in 1888 (Tesla 1888) Nicola Tesla outlined the principles of the polyphase induction motor and some years later Steinmetz (Steinmetz 1897) gave a description of its use as a generator. Steinmetz realized the importance of a source of reactive current for the induction generator and suggested that part of its load should consist of synchronous motors to supply this excitation current. Even so, Steinmetz did not fully appreciate the potential of induction generators. Early attempts to use asynchronous generators to supply the grid were described by Waters (Waters 1901) in 1901, and serious consideration of their usage for large scale generation of electricity was enunciated in 1910 in a paper by Spooner and Barnes (Spooner 1910). Some of the inherent advantages were described, particularly operation under fault conditions. More recently it was pointed out (de Mello 1981,1982) that a power system composed totally of induction generators could operate satisfactorily and may in fact have superior reliability to existing systems. Up until shortly before the Second World War the only source of excitation current considered pracitcal was the electricity grid. In 1935 Basset and Potter (Basset 1935) described a method of providing self excitation for the induction generator thus obviating the necessity of grid connection and the autonomous self excited induction generator (SEIG) was born.

The method described consisted of placing static capacitors over the terminals of the generator so that it draws the requisite lagging current for excitation as shown in Figure 3.1.

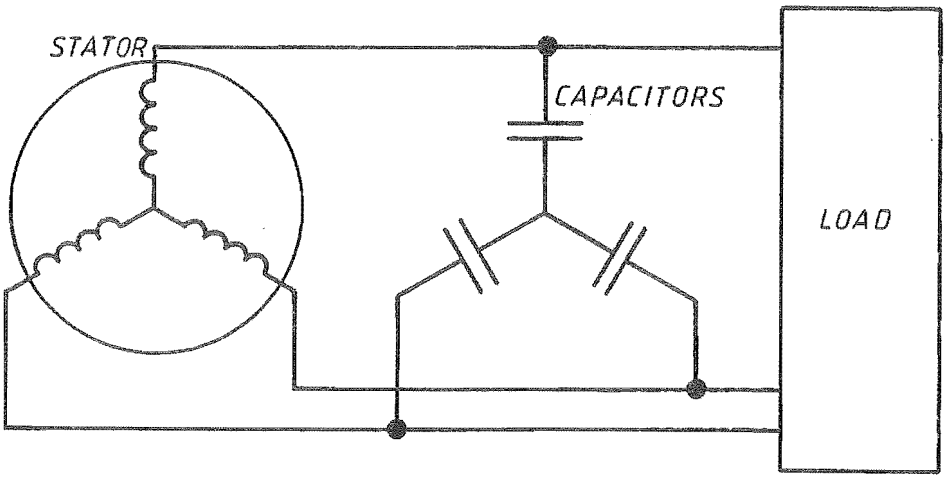

Figure 3.1: Capacitive Excitation of the Induction Generator.

Whilst grid connected wind generation plant using induction generators have been widely used and discussed in the literature (Golding 1955, et al) it has only been recently that consideration has been given to the self excited induction generator in autonomous wind turbine generators (Milner 1982, et al). The advantages of using the SEIG are ones of reliability, low cost and availibility, all of which are particularly applicable to autonomous applications.

3.2: Excitation of the Self Excited Induction Generator.

In its most rugged form the self excited induction generator consists of a squirrel cage induction motor with capacitive excitation as shown in Figure 3.1. The basic requirement for self excitation is the provision of currents of suitable phase to magnetise the iron of the machine. This is obtained from static capacitors so that the generator absorbs lagging VARS (ie., supplies leading VARS). Initial impetus comes from a small emf, E_R, generated by the machine resulting from driving the shaft through a residual field Φ_R in the iron, as shown in Figure 3.2. The emf will thus lag the residual field by 90 degrees, and since the capacitors are connected over the machine terminals a current I_R flows.

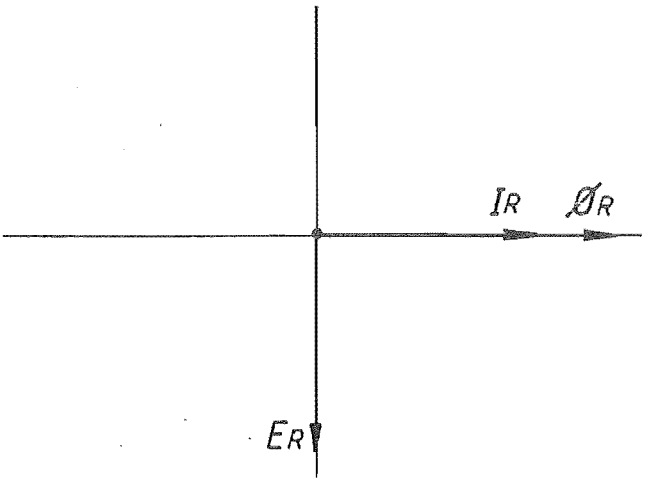

Figure 3.2: Phasor Diagram of SEIG Initial State.

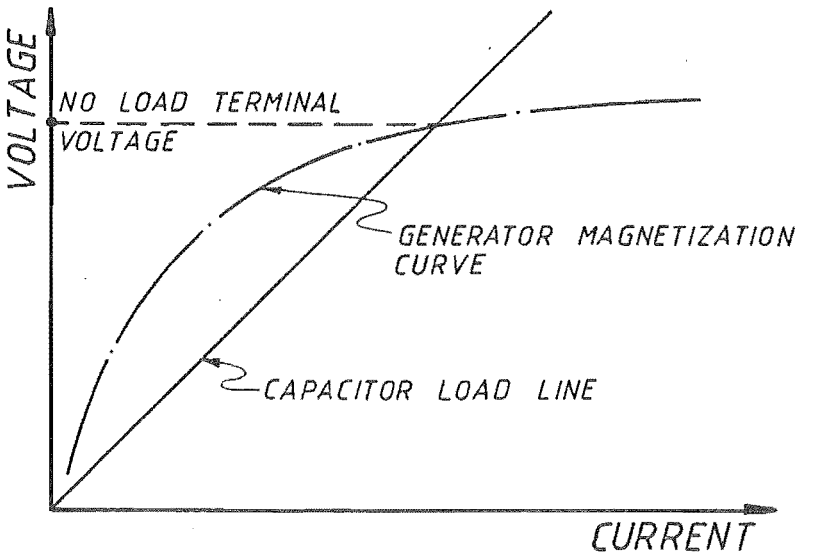

Figure 3.3: No Load Excited Generator Characteristic.

If series impedances are ignored, I_R leads E_R by 90 degrees due to the effect of the capacitors and thus generates a flux which is in phase with Φ_R. The total flux thus increases and the process is repeated, ie., the generated emf increases. This continues to a point where the load line for the capacitor intersects the magnetisation curve of the machine (see Figure 3.3) and it is then in an asynchronous excited state. The generated emf is of frequency proportional to the rotor speed less the slip.

The exact nature of this excitation process has been recently discussed (Elder 1983), and the analysis considers the machine operation as being in two possible states:

(1) A synchronous state occuring before excitation where the machine behaves like a permanent magnet AC generator with residual magnetism causing synchronous stator currents to flow. The equivalent circuit for this synchronous state (Figure 3.4) consists of the excitation capacitance, stator leakage reactance, stator resistance and magnetising reactance, and is in the form of a resonant circuit. The forcing function for the resonant circuit is the emf generated by the residual magnetism of the machine and is thus of frequency proportional to rotor speed. The normal response of such a circuit is as shown in Figure 3.6(a). This response must however be modified since the magnetising inductance varies as current changes as shown in Figure 3.5. The effect of this variation on the resonant circuit response is shown in Figure 3.6(b) and if rotor speed is increased from zero the current will be seen to jump at the point shown.

(2) An asynchronous state where the machine is excited. Analysis of this state taking the non-linear magnetising inductance into account yields the result shown in Figure (3.7). For self excitation to occur the resonant speed of the circuit must be exceeded and asynchronous currents will subsequently flow. For stable asynchronous operation of the machine it must operate at a particular point of resonance and for any one particular speed an upper stable point and a lower unstable operating point are possible. The stable point represents the machine in the excited state.

The lower point can either lead to excitation or the machine can drop back into the synchronous state as shown by Figure 3.8.

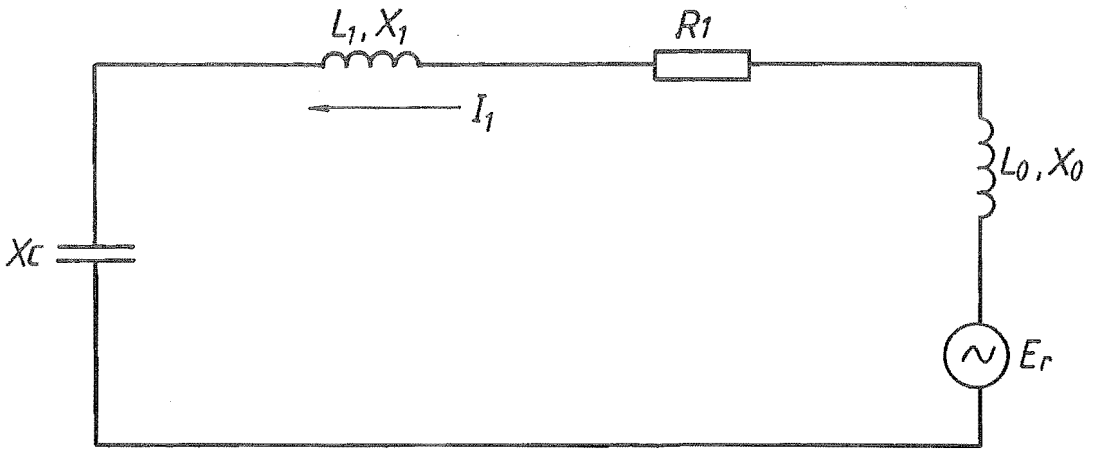

Figure 3.4: Equivalent Circuit of Machine Synchronous Mode.

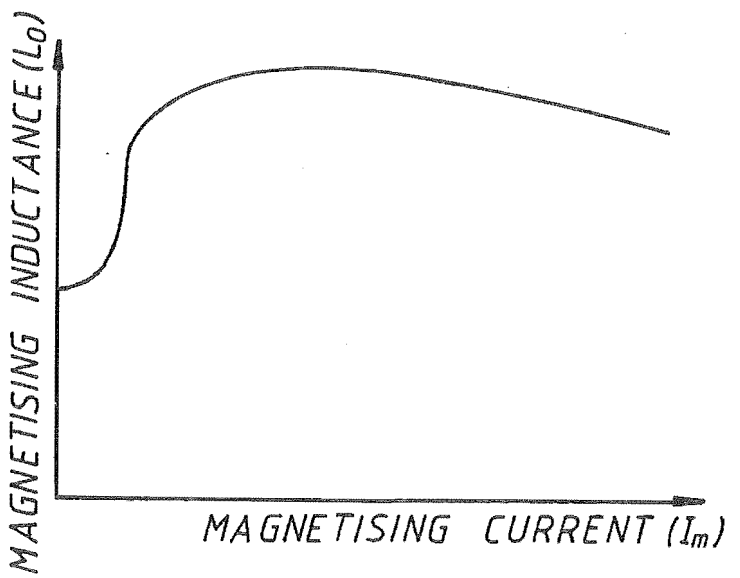

Figure 3.5: Magnetising Inductance Characteristic.

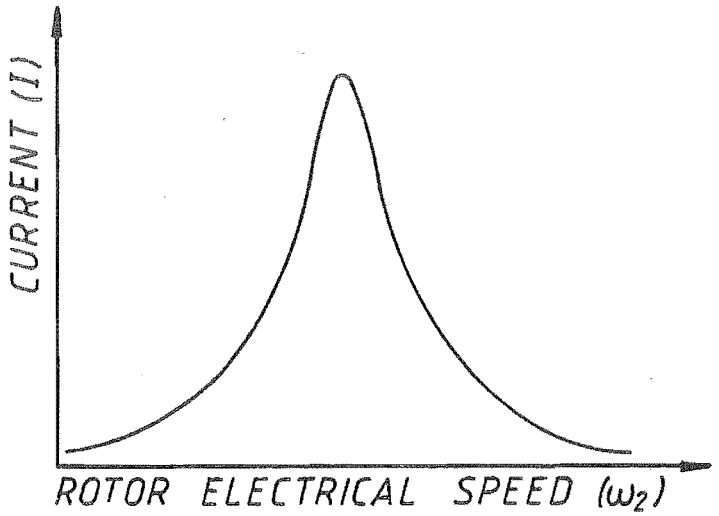

Figure 3.6(a): Normal Response of Synchronous State.

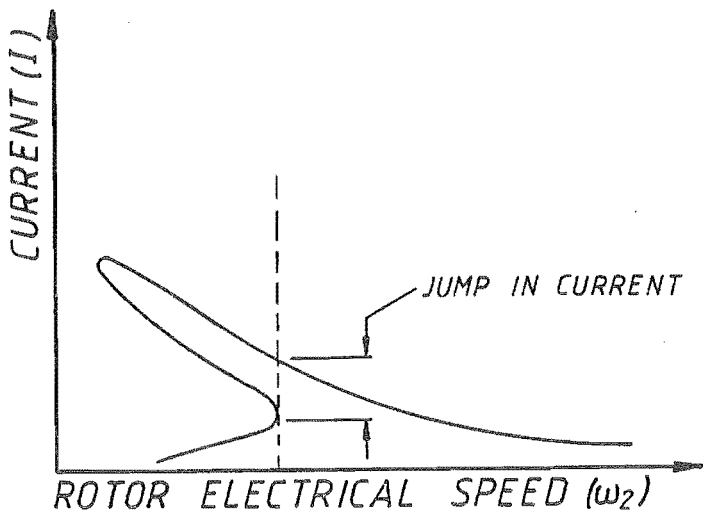

Figure 3.6(b): Modified Response of Synchronous State.

For a machine starting from rest in the synchronous state the current increases up to the knee. If speed is further increased the current jumps up to a value above the asynchronous curve and is in the region where asynchronous currents can flow. The currents will increase to the upper stable part of the curve as shown by Figure 3.7 and the machine will be in an excited state. The equivalent circuit is now as in Figure 3.9.

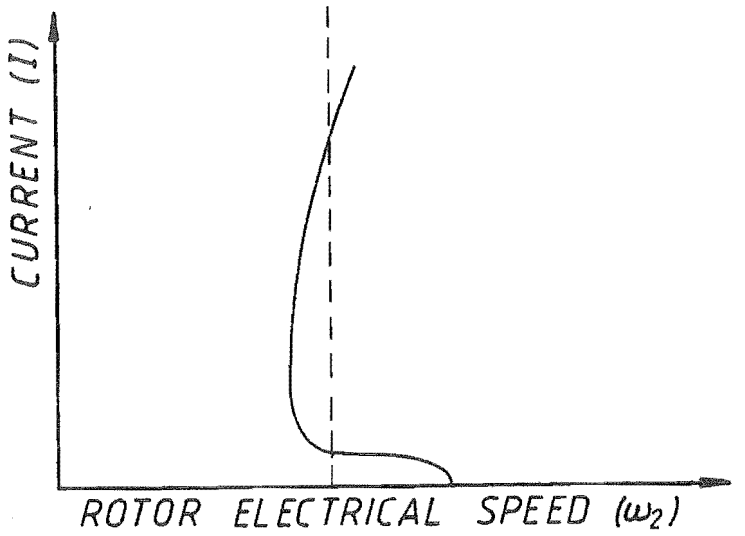

Figure 3.7: Characteristic of Asynchronous State.

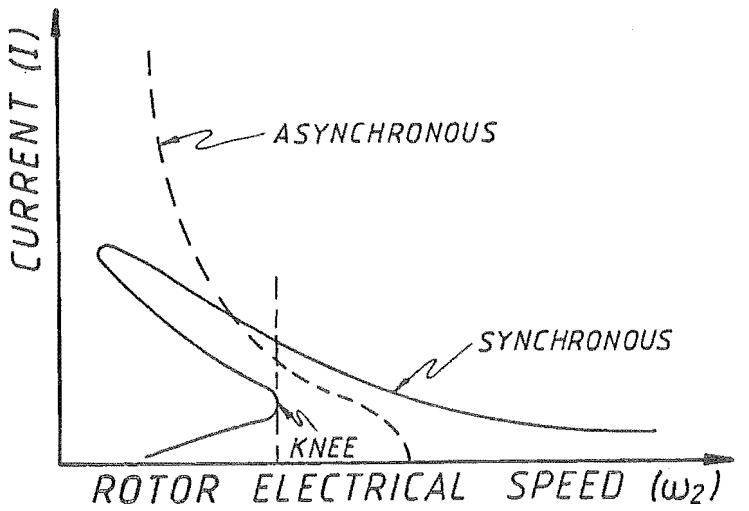

Figure 3.8: Synchronous and Asynchronous States.

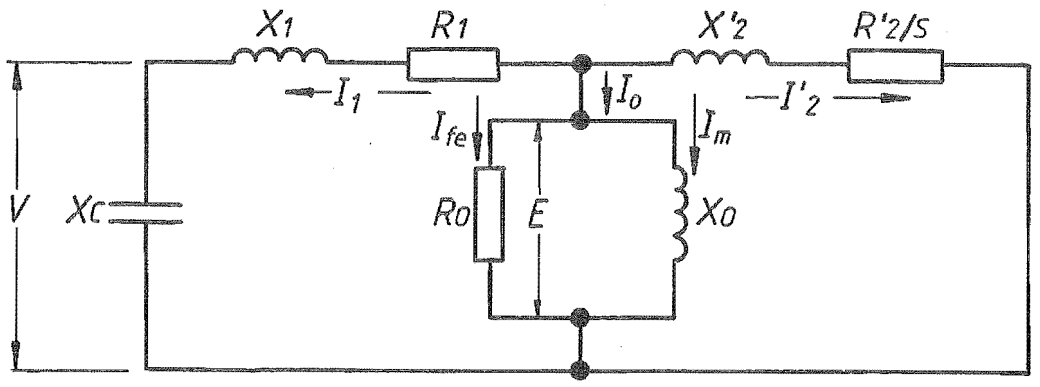

Figure 3.9: Equivalent Circuit of Asynchronous Mode of Machine - Unloaded.

3.3: Measurement of Machine Parameters.

3.3.1: Machine Parameters.

The generator used in the wind turbine is an 8 pole, 3 kW, three phase squirrel cage machine rated for 415 V, 50 Hz operation. Machine parameters can be determined from standard light load tests and locked rotor tests. Measured machine parameters at mains frequency are given in Table 3.1.

3.3.2: Magnetisation Characteristic.

The 50 Hz magnetising characteristic can be measured from the light load test used above by running the machine as a motor and varying the input voltage and is shown in Figure 3.10. This characteristic can be approximated to the form given in Figure 3.11, where the current I_x is the magnetising current when the voltage is zero and E_s is the saturation voltage.

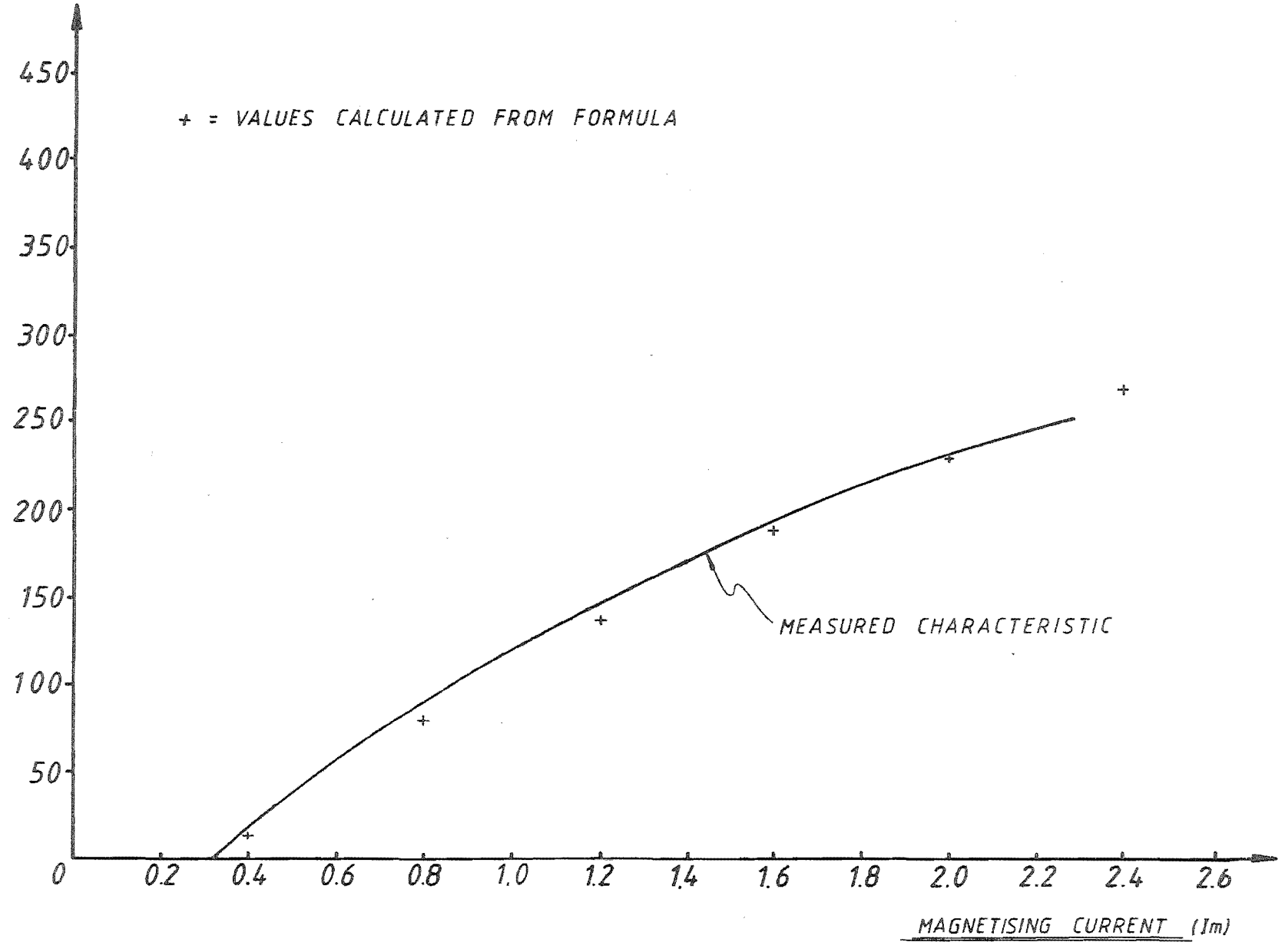

Figure 3.10: Measured 50Hz Magnetisation Characteristic.

Parameter	Symbol	Value
Stator Resistance	R_1	4.32 Ω
Rotor Resistance (refered to stator)	R_2'	5.34 Ω
Stator Leakage Reactance	X_1	* 8.97 Ω
Rotor Leakage Reactance (refered to stator)	X_2'	* 8.97 Ω
Iron Loss	R_0	1214 Ω

* $X_1 = X_2'$ for standard squirrel cage machines.

Table 3.1: Machine Parameters, at 50 Hz.

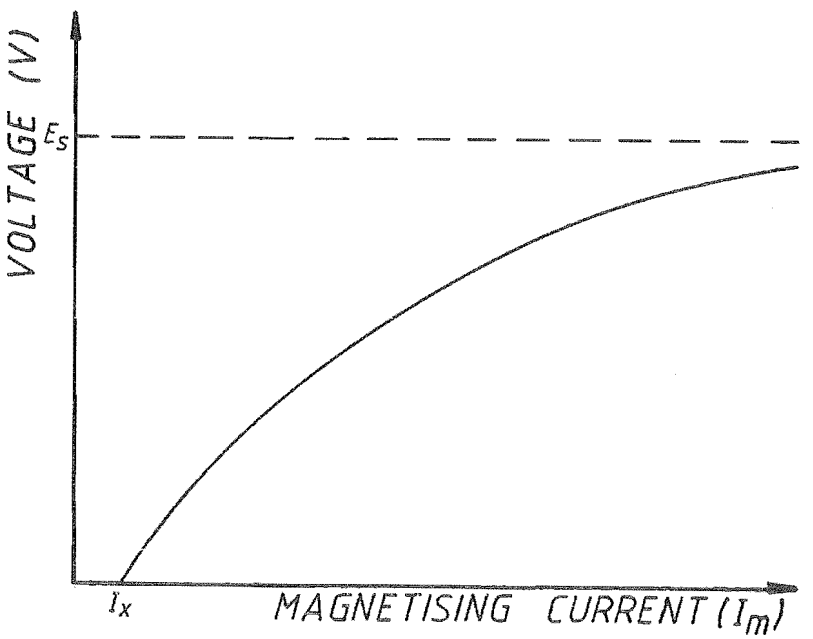

Figure 3.11: General Form of Machine Magnetisation Characteristic.

The curve of Figure 3.11 can be described approximately by Equation (3.1):

$$E = E_s.[1 - \exp\{-k(I_m - I_x)\}] \qquad (3.1)$$

Since generated voltage is directly proportional to the rate of flux change, Equation (3.1) can be modified for any frequency as shown by Equation (3.2) where f_m is the frequency at which the characteristic is measured (50 Hz) and f_1 is the stator frequency of the generated voltage.

$$E = E_s.[1 - \exp\{-k(I_m - I_x)\}].f_1/f_m \qquad (3.2)$$

For the measured characteristic of Figure 3.10 a fit to within 5% can be obtained using Equation (3.2) for the values shown below.

$E_s = 500$ V

$I_x = 0.32$ A

$k = 0.365$

$f_1 = 50$ Hz

This gives the simplified expression:-

$$E = 10.f_1.[1 - 1.12.\exp\{-0.365.I_m\}] \qquad (3.3)$$

Some values calculated from this expression for 50 Hz are compared with the experimental results on Figure 3.10.

3.4: Self Excited Induction Generator Operation.

To assess steady state operational characteristics of the self excited induction generator, bench tests were carried out using the test circuit of Figure 3.13. Capacitors of 94 μ F per phase were placed, star connected, over the terminals of the machine. The machine was arranged with star connected windings and a neutral connection made between the generator star point and the star point of the capacitors.

Instrumentation was used to provide readings of terminal voltage, stator current, capacitor current and load current and phase angle. Photographs of oscilloscope traces of terminal voltage were also taken and are shown in Plates 3.1 (a) to (c).

Two bench tests were carried out, viz:-

(i) An unloaded test

(ii) A loaded test where the load consisted of a complex R-L circuit

The equivalent circuit for the induction machine is shown in Figure 3.14 and in addition to the expected elements, the excitation capacitance is also shown. The complex load is dotted in for the case of the loaded machine.

3.4.1: Unloaded Condition.

Under no load conditions the power input to the machine shaft is used to overcome internal losses and capacitor leakage power losses (refer to Figure 3.12). The capacitors supply the magnetising current for the machine and the capactive current is related to the terminal voltage by:-

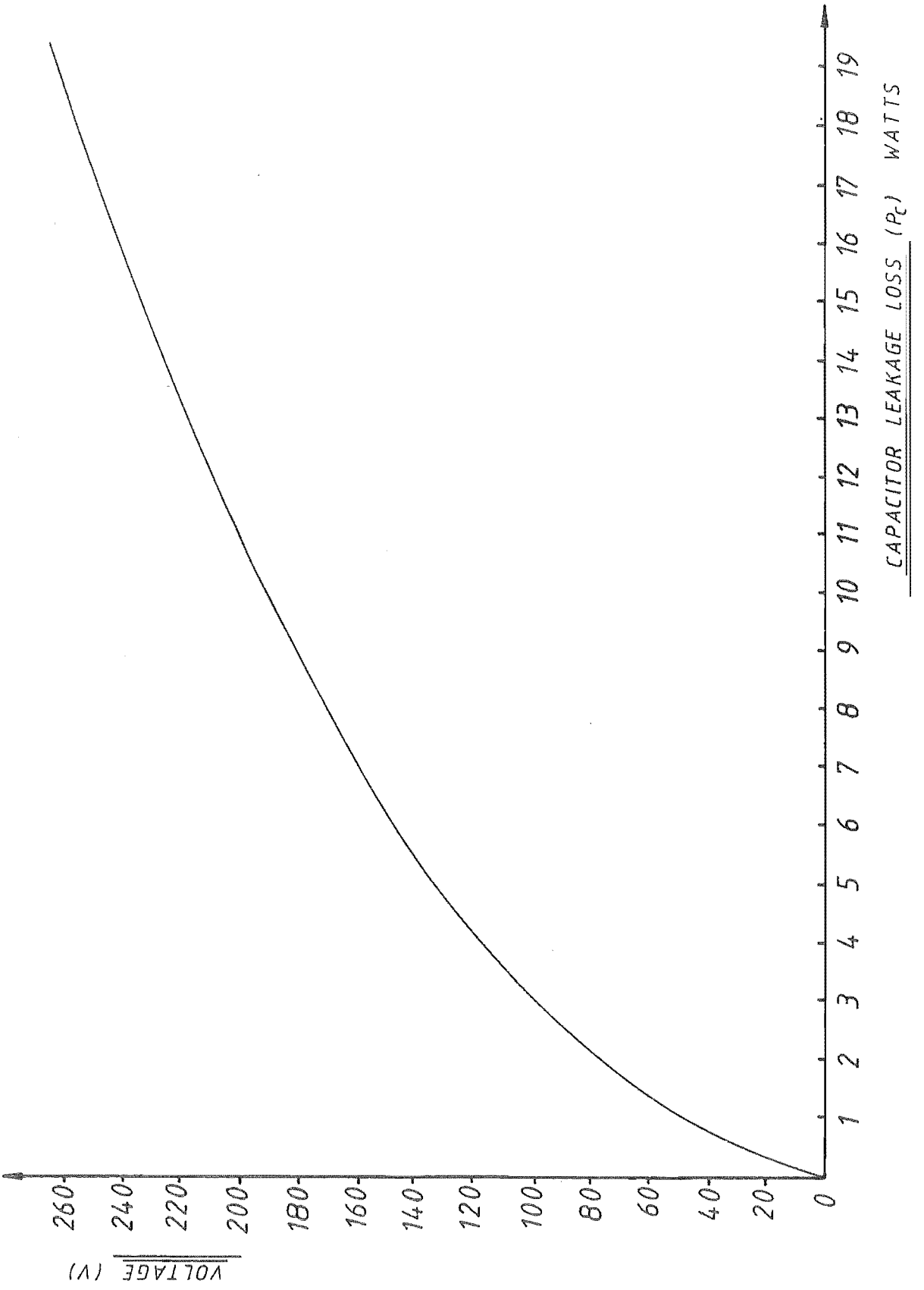

Figure 3.12: Capacitor Power Losses Due to Leakage

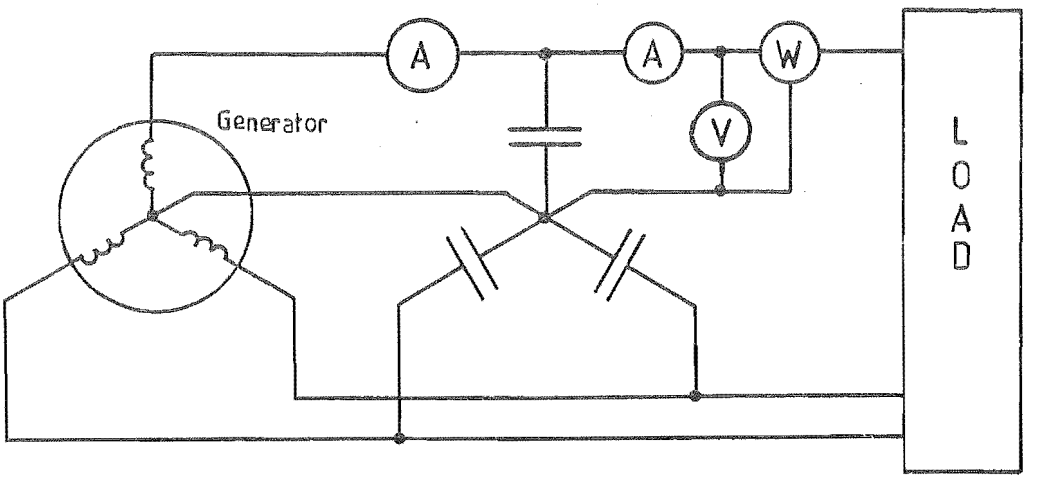

Figure 3.13: Generator Bench Test Circuit

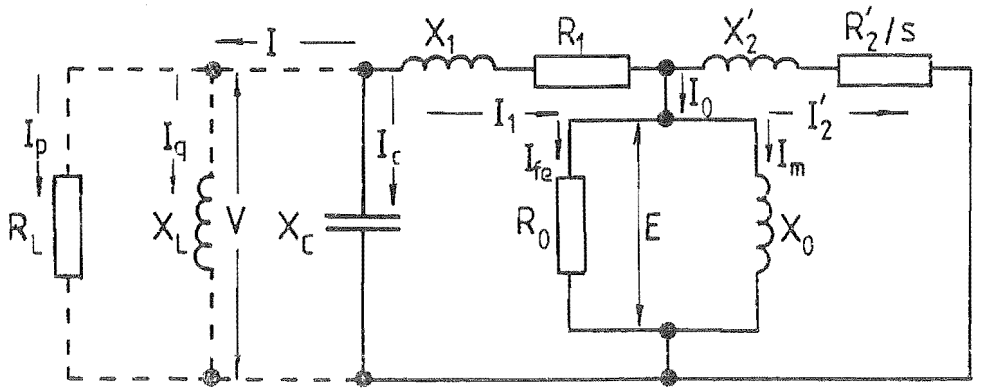

Figure 3.14: Induction Generator Equivalent Circuit

$$I_c = V/X_c = 2.\pi.f_1.V.C \qquad (3.4)$$

The reference phasor for the construction of the phasor diagram is the terminal voltage of 245 V, with the machine terminals used as the current node. The stator current is equal in magnitude to the capacitor current. The internal emf E can be determined from the terminal voltage and the voltage drops over the stator parameters R_1 and X_1. Notice that, due to the phase relationship between the terminal voltage V and the stator current I_1, the magnitude of the internal emf is less than the terminal voltage - characteristically similar to the Ferranti Effect. Application of the internally generated emf to Equation (3.3) gives the value of the magnetising current I_m. The current in the iron loss leg of the circuit can be calculated from:-

$$I_{fe} = E/R_o \qquad (3.5)$$

Vector summation of I_m and I_{fe} gives the total magnetisation current I_o of 4.19A. Calculation of the rotor current I'_2 (referred to the stator) is made by subtracting the magnetisation current phasor I_o from the stator current phasor. Since the slip of the machine will be negative, the value of the voltage $I'_2.R'_2/s$ will approximately be equal to the internal emf E (since $I'_2.X'_2$ will be small compared to $I'_2.R'_2/s$) and will be in phase opposition to I'_2.

3.4.2: Loaded Conditions.

When the generator is operating under loaded conditions, it follows the torque-slip curve of Figure 3.16(a). The generator is now connected to the complex load shown in the equivalent circuit of Figure 3.14 and therefore, is supplying active and reactive components of current into the load. The phasor diagram must now be modified to account for these in-phase and quadrature components I_p and I_q respectively. Since the generator cannot supply the lagging current I_q into the load, its source must be the excitation capacitors and if the load lagging reactive current increases, the amount of lagging reactive current available for generator excitation decreases with a corresponding drop in generated voltage.

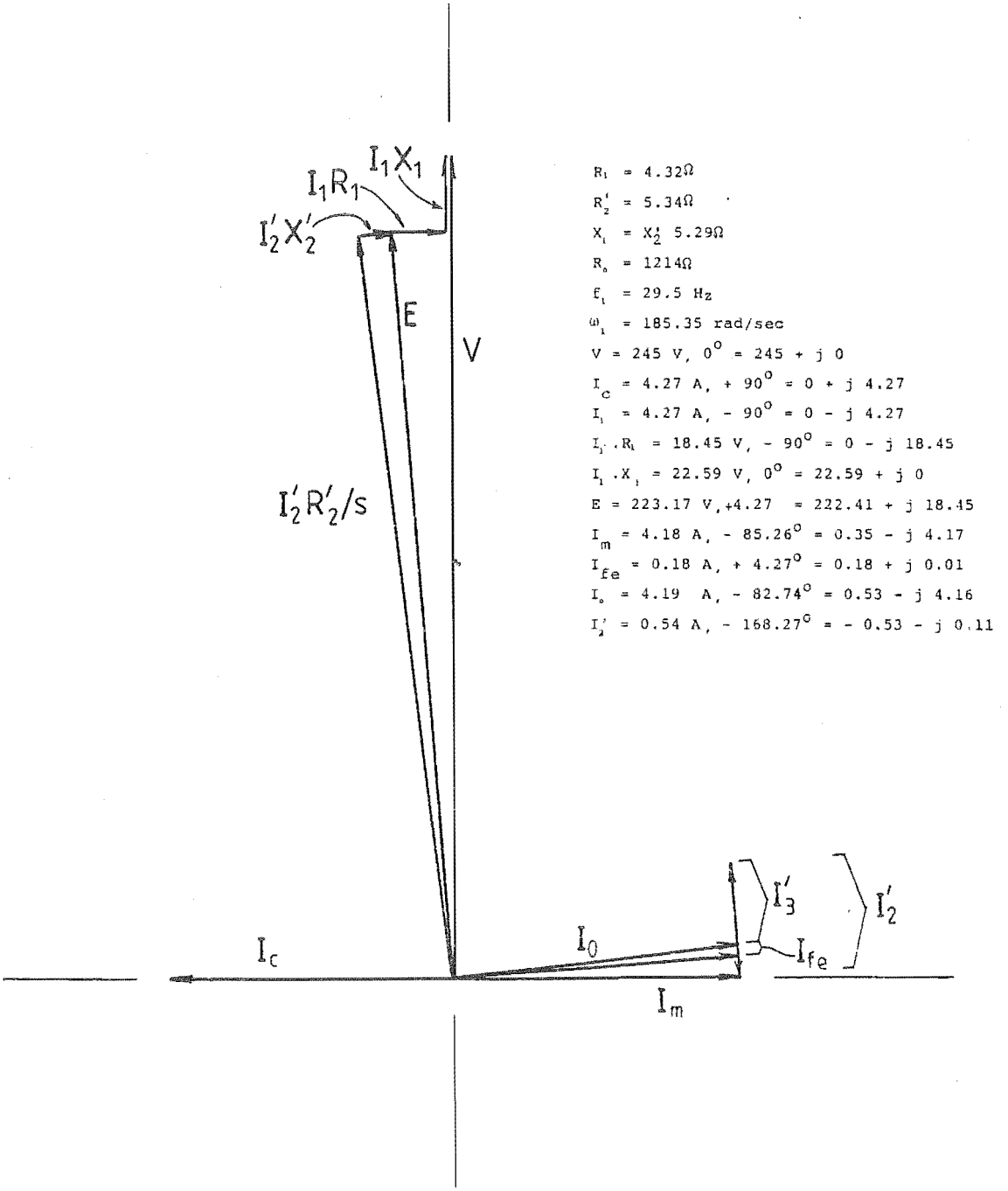

Figure 3.15: Phasor Diagram of Unloaded Generator for Measured 245V Terminal Voltage at 29.5Hz.

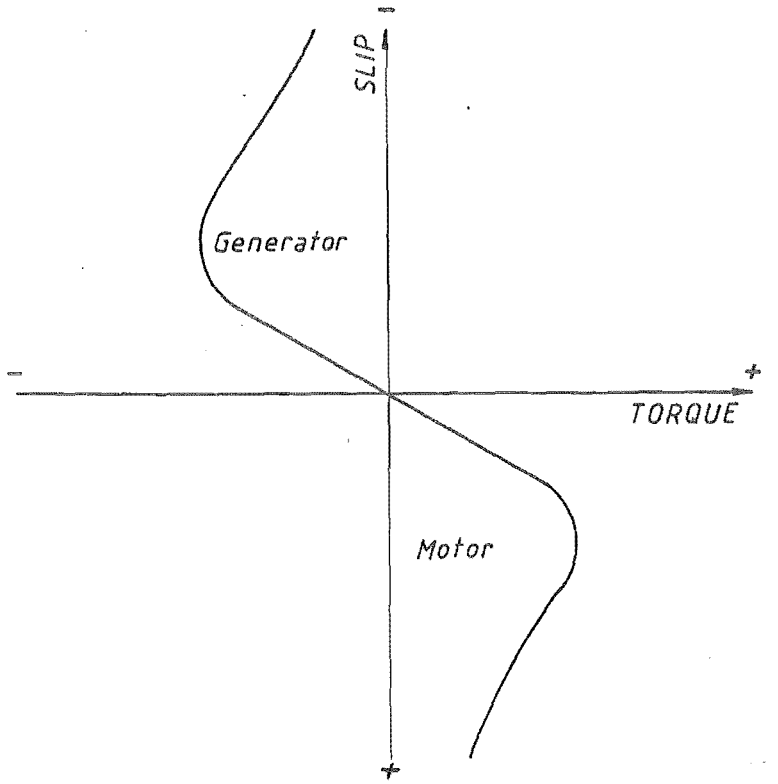

Figure 3.16(a): Torque - Slip Characteristic.

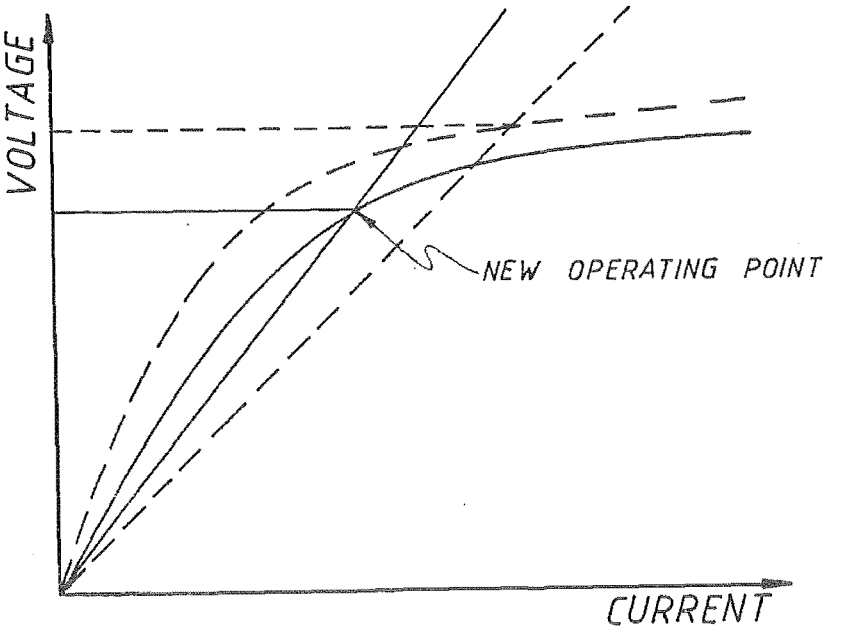

Figure 3.16(b): Loaded Excited Generator Characteristic.

The generated frequency of the machine is dependent on the rotor speed and the slip and is:-

$$f_1 = n.p/(1 - s) \qquad (3.6)$$

The rotor speed is higher than the synchronous speed of the generated emf hence the slip is negative. Also, since power is being generated, the value of R'_2/s is negative. If the internal losses of the machine are, for the time, ignored, the generated and load powers are equal.

$$V^2/R_L = -V^2/(R'_2/s) \qquad (3.7)$$

Thus the slip is:-

$$s = -R'_2/R_L \qquad (3.8)$$

Equating (3.7) and (3.8) gives:-

$$f_1 = n.p/(1 + R'_2/R_L) \qquad (3.9)$$

It can be seen that as the load increases the generated frequency drops and the magnetisation characteristic falls into a lower curve as shown in Figure 3.16(b). Additionally, the load line of the capacitor goes to one of higher slope due to the increased capacitive reactance. The new generated voltage, as a result of the load increase, falls to the new value as described by the new intersection point. It is possible to restore the voltage (providing the drop was not execessive) by increasing the capacitance or by increasing shaft speed. It is only an increase in shaft speed which will restore frequency however.

The phasor diagram in the loaded case has been drawn for a terminal voltage of V = 208.5 V at f_1 = 50 Hz and a load current of I = 3.77 A at a phase angle of ϕ = - 61 degrees. It is similar to the unloaded case except that the quadrature lagging current being supplied to the generator from the capacitors (i.e., the generator supplies quadrature leading current to the capacitors) is reduced by the load quadrature current. An additional in-phase component of load current also exists due to R_L. The terminal voltage phasor V is used as the reference and the capacitive current I_c therefore leads it by 90 degrees. The load quadrature current is:-

$$I_q = I.\sin\phi \qquad (3.10)$$

I_q is in phase opposition to I_c as shown in Figure 3.17. The stator current I_1 can then be calculated by adding the phasors I_c, I_p and I_q. By taking the stator voltage drops $I_1.R_1$ and $I_1.X_1$ into account the internal emf E can be determined, hence the magnetising current I_m estimated from Equation 3.3. Using Equation (3.5) the iron loss component I_{fe} can be estimated and subsequently vectorially added to I_m to give the total magnetisation phasor I_o. Phasor subtraction of I_o from the stator current phasor I_1 will give the rotor current I_2' referred to the stator.

Conventional theory for the induction motor predicts that the phasor sum of the voltages $I_2'.R_2'/s$ and $I_2'.X_2'$ will give the internal emf E. This is illustrated by the broken lines of Figure 3.17 where the line parallel to I_2' is the path along which $I_2'.R_2'/s$ should follow (remembering that the slip is negative for a generator). The line normal to $I_2'.R_2'/s$ to the head of the internal emf phasor E represents the geometrically calculated value of $I_2'.X_2'$ and is approximately 68V. However, it is seen that if the value of $I_2'.X_2'$ is calculated using the value of I_2' of 2.56A and the value of X_2' of 8.97 a figure of 23V is obtained. This discrepancy is not in accord with existing theory and further consideration is required to explain the abnormality.

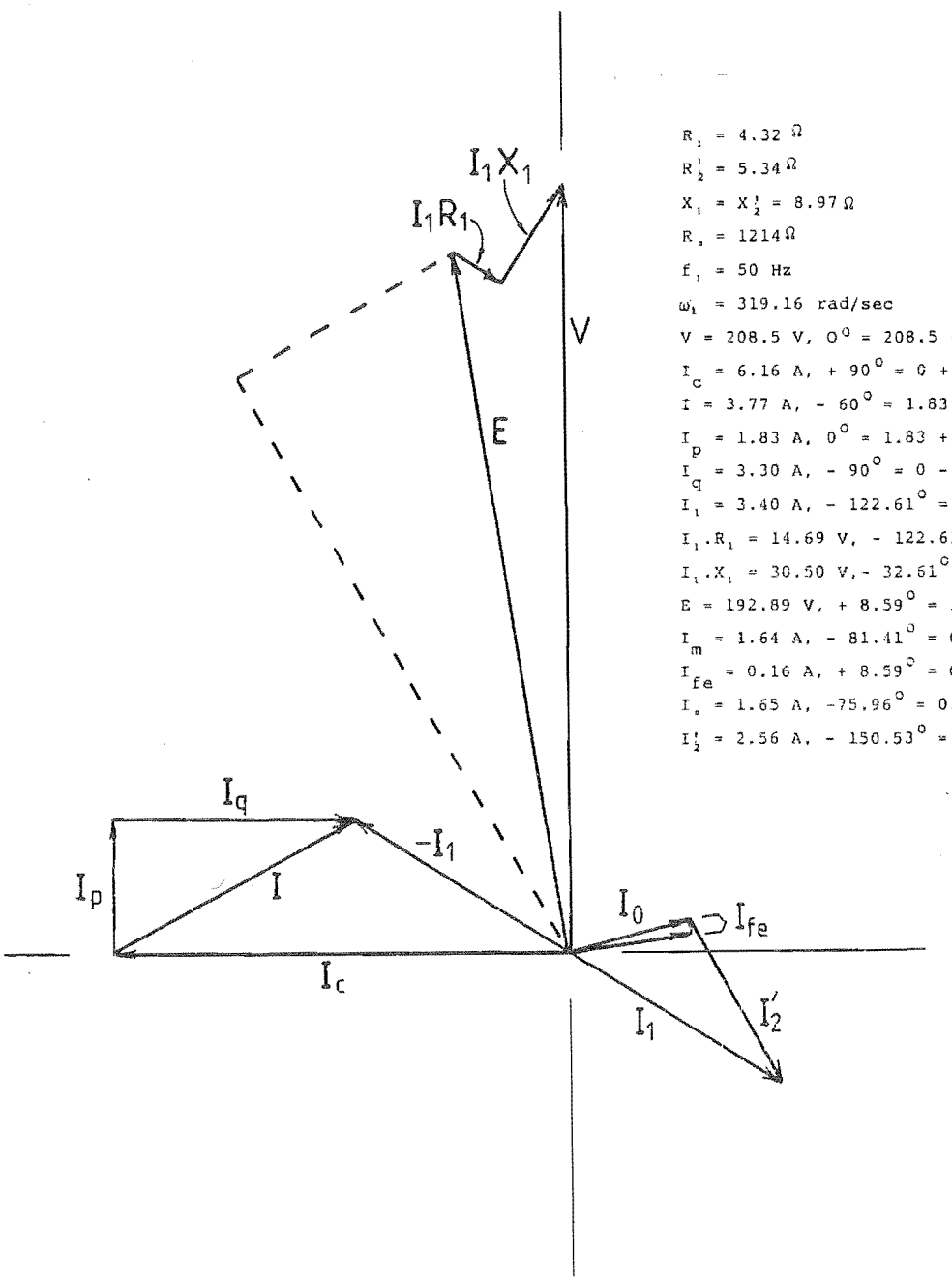

$R_1 = 4.32\ \Omega$

$R_2' = 5.34\ \Omega$

$X_1 = X_2' = 8.97\ \Omega$

$R_o = 1214\ \Omega$

$f_1 = 50$ Hz

$\omega_1 = 319.16$ rad/sec

$V = 208.5$ V, $0^\circ = 208.5 + j\ 0$

$I_c = 6.16$ A, $+ 90^\circ = 0 + j\ 6.16$

$I = 3.77$ A, $- 60^\circ = 1.83 - j\ 3.30$

$I_p = 1.83$ A, $0^\circ = 1.83 + j\ 0$

$I_q = 3.30$ A, $- 90^\circ = 0 - j\ 3.30$

$I_1 = 3.40$ A, $- 122.61^\circ = - 1.83 - j\ 2.86$

$I_1.R_1 = 14.69$ V, $- 122.61^\circ = - 7.92 - j\ 12.37$

$I_1.X_1 = 30.50$ V, $- 32.61^\circ = 25.69 - j\ 16.44$

$E = 192.89$ V, $+ 8.59^\circ = 190.73 + j\ 28.81$

$I_m = 1.64$ A, $- 81.41^\circ = 0.24 - j\ 1.62$

$I_{fe} = 0.16$ A, $+ 8.59^\circ = 0.16 + j\ 0.02$

$I_o = 1.65$ A, $-75.96^\circ = 0.40 - j\ 1.60$

$I_2' = 2.56$ A, $- 150.53^\circ = - 2.23 - j\ 1.26$

Figure 3.17: Phasor Diagram of Loaded Generator for Measured 208.5V Terminal Voltage at 50 Hz.

3.5: Modified Equivalent Circuit.

The observed irregularity in the phasor diagram can be accounted for by allowance for the power losses in the machine due to harmonic current. These arise from non-linearities in the B-H curve for the machine and since it is operating under a four wire system currents of the third harmonic will flow through both the stator and rotor circuits. Verification of the existence of these harmonics can be obtained from the waveforms of the terminal voltage in Plate 3.1 and the theoretical waveforms of Figure 3.23. The magnitude of the harmonic current is:-

$$I_\nu = V_\nu . \nu . \omega_1 . C \qquad (3.11)$$

where

V_ν is the harmonic voltage
I_ν is the harmonic current
ν is the harmonic number

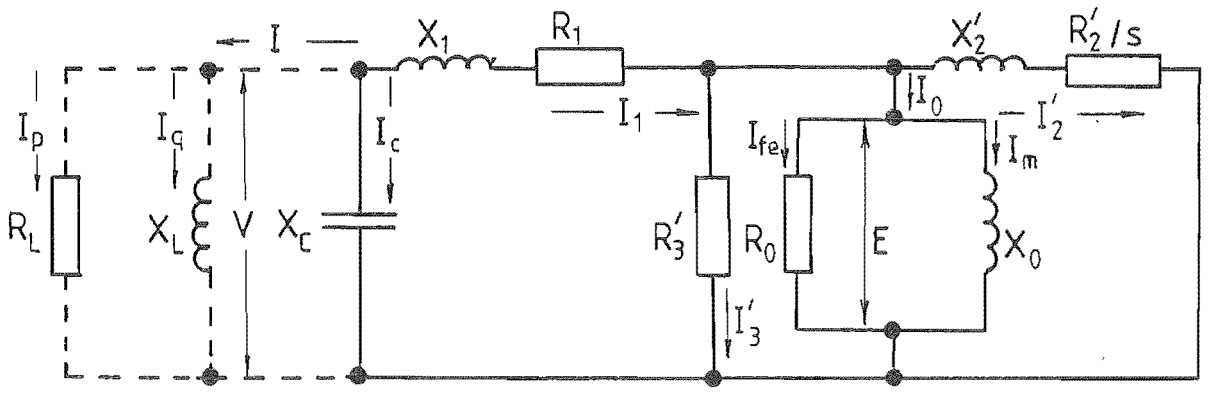

Figure 3.18: Modified Equivalent Circuit

The total third harmonic loss P_3 will be generated from the third harmonic current I_3 passing through the stator and rotor resistances, i.e.,

$$P_3 = I_3^2 (R_1 + R'_{23}) \qquad (3.12)$$

where

R'_{23} is a value of rotor resistance (referred to the stator) giving the appropriate rotor loss to third harmonic currents.

This third harmonic power loss can be accounted for by adding to the equivalent circuit a fictitious shunt loss component R'_3 referred to the fundamental frequency as shown in Figure 3.18, so that:-

$$P_3 = E^2/R'_3 = E.I'_3 \qquad (3.13)$$

where

I'_3 is the equivalent fundamental current through the additional loss element R'_3.

The phasor diagrams previously drawn for the unloaded and loaded cases can now be redrawn.

For the unloaded case, calculation of the internal emf proceeds as previously. See Figure 3.19.

The third harmonic current can be evaluated from Equation (3.11) where the third harmonic voltage over the machine terminals is estimated to be 35% of the fundamental or approximately 85 V phase to neutral. This gives a harmonic current of I_3 = 4.62 A. For a subsequent power loss of P_3 = 265 W per phase and internal emf of E = 223.2 V, a value for I'_3 can be found to be 1.19 A where I'_3 is the equivalent fundamental current through the additional loss element. The rotor current I'_2 can then be found by substracting the phasors I_o and I'_3 from the stator current I_1. The voltage

phasors $I_2' R_2'/s$ and $I_2'.X_2'$ summate to give E, the internal emf. Although the power loss to third harmonic makes little change in the unloaded case, a significant difference can be seen for the loaded situation.

In the loaded case shown in Figure 3.20, the internal emf is as calculated previously to be 192.9 V with an estimated third harmonic voltage of 30% of the fundamental at the generator terminals. The third harmonic current actually flowing is $I_3 = 5.54$ A (refer to Equation (3.11)).

A power loss of $P_3 = 395$ W per phase together with the internal emf of E = 193 V gives a value for the equivalent fundamental current I_3' through the additional loss element of 2.3A. Phasor subtraction of magnetisation current I_o and harmonic loss current I_3' from the stator current I_1 yield a value of $I_2' = 4.78$ A for the rotor circuit. Phasor addition of $I_2'.R_2'/s$ and $I_2'.X_2'$ now correctly gives the internal emf E which was not possible with the circuit of Figure (3.14).

3.6: Effects of Machine Saturation.

When operating in the normal excited state the terminal voltage of the machine is determined by the intersection point of the capacitor load line and the magnetisation curve as shown by Figure 3.3 and 3.11. As the terminal voltage is increased by an increase in excitation capacitance, i.e., by lowering the slope of the load line, the machine operates at a point where the magnetisation curve is of lower slope and is at a point where the iron is nearing saturation. The effect of this on the terminal voltage is to clip the top of the normally sinusoidal waveform and as the machine is driven further into saturation the waveshape will theoretically approach a square form.

Fourier analysis of a clipped sinusoidal waveform will, in addition to a fundamental component, contain odd harmonic voltages, noteably third and to a lesser extent fifth.

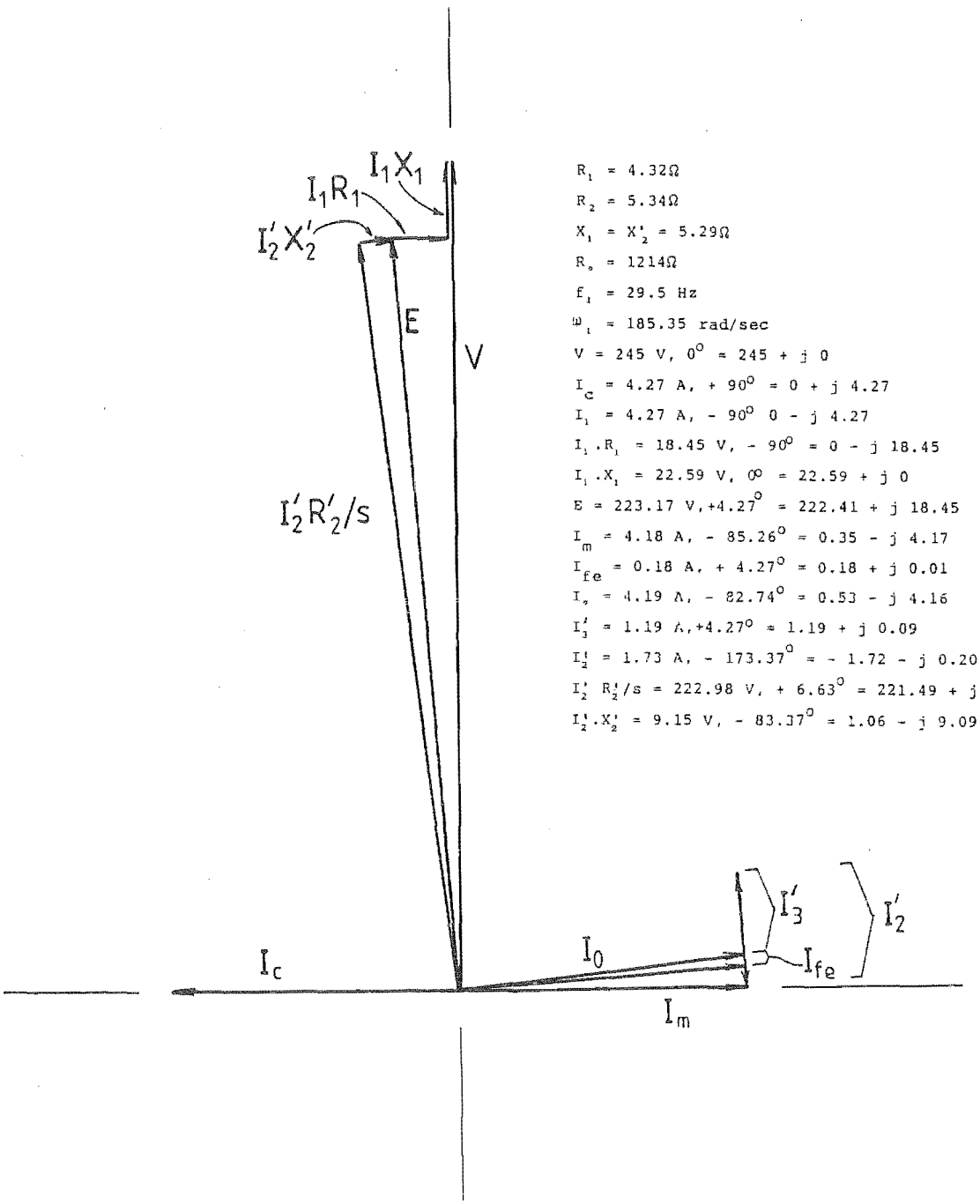

$R_1 = 4.32\Omega$

$R_2 = 5.34\Omega$

$X_1 = X'_2 = 5.29\Omega$

$R_o = 1214\Omega$

$f_1 = 29.5$ Hz

$\omega_1 = 185.35$ rad/sec

$V = 245$ V, $0^\circ = 245 + j\ 0$

$I_c = 4.27$ A, $+ 90^\circ = 0 + j\ 4.27$

$I_1 = 4.27$ A, $- 90^\circ\ 0 - j\ 4.27$

$I_1.R_1 = 18.45$ V, $- 90^\circ = 0 - j\ 18.45$

$I_1.X_1 = 22.59$ V, $0^\circ = 22.59 + j\ 0$

$E = 223.17$ V, $+4.27^\circ = 222.41 + j\ 18.45$

$I_m = 4.18$ A, $- 85.26^\circ = 0.35 - j\ 4.17$

$I_{fe} = 0.18$ A, $+ 4.27^\circ = 0.18 + j\ 0.01$

$I_o = 4.19$ A, $- 82.74^\circ = 0.53 - j\ 4.16$

$I'_3 = 1.19$ A, $+4.27^\circ = 1.19 + j\ 0.09$

$I'_2 = 1.73$ A, $- 173.37^\circ = - 1.72 - j\ 0.20$

$I'_2\ R'_2/s = 222.98$ V, $+ 6.63^\circ = 221.49 + j\ 25.74$

$I'_2.X'_2 = 9.15$ V, $- 83.37^\circ = 1.06 - j\ 9.09$

Figure 3.19: Phasor Diagram of Unloaded Generator for Measured 245V Terminal Voltage at 29.5Hz Using Modified Circuit

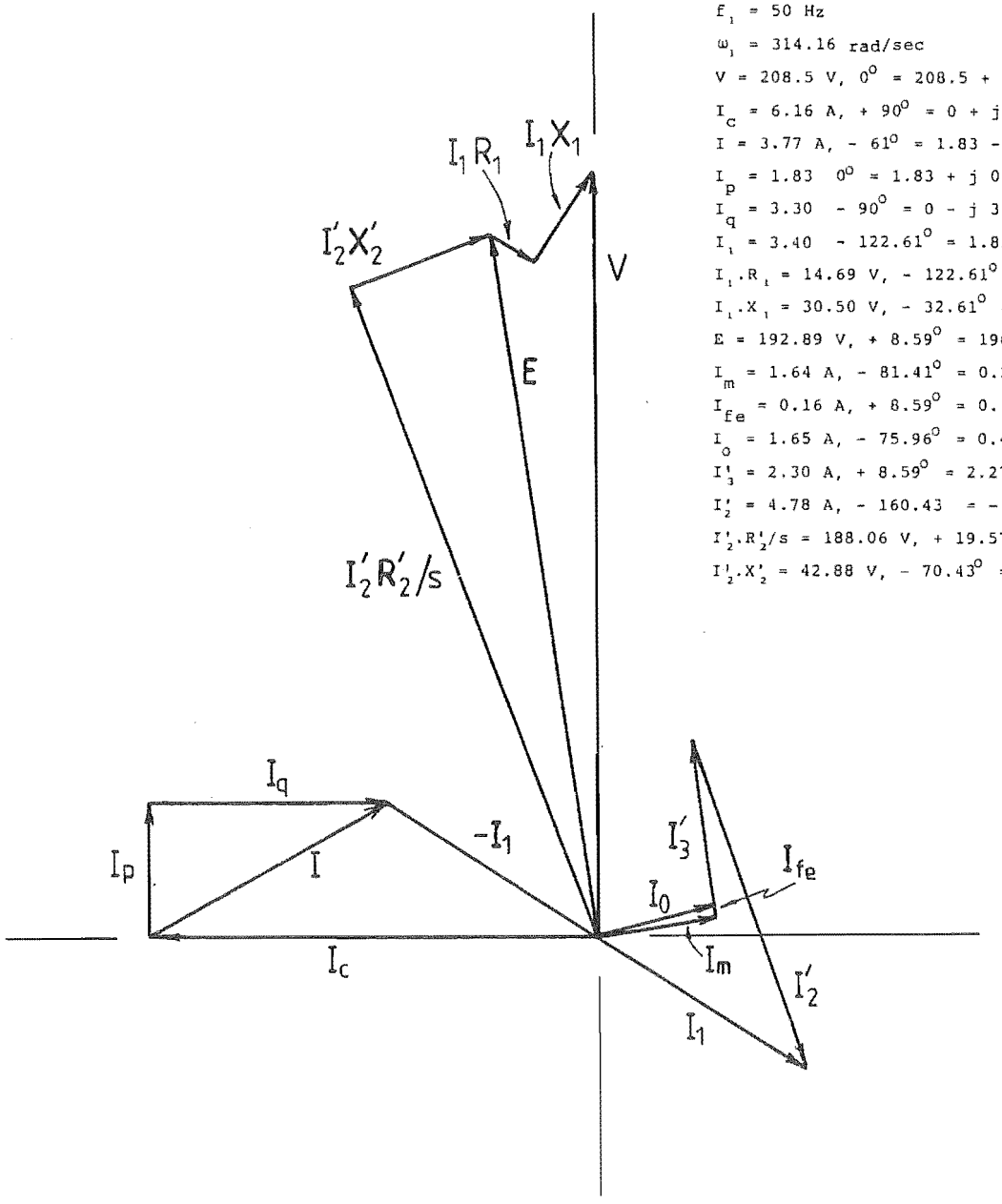

$R_1 = 4.32\Omega$

$R_2 = 5.34\Omega$

$X_1 = X'_2 = 8.97\Omega$

$R_c = 1214\Omega$

$f_1 = 50$ Hz

$\omega_1 = 314.16$ rad/sec

$V = 208.5$ V, $0^\circ = 208.5 + j\ 0$

$I_c = 6.16$ A, $+ 90^\circ = 0 + j\ 6.16$

$I = 3.77$ A, $- 61^\circ = 1.83 - j\ 3.30$

$I_p = 1.83\ \ 0^\circ = 1.83 + j\ 0$

$I_q = 3.30\ - 90^\circ = 0 - j\ 3.30$

$I_1 = 3.40\ - 122.61^\circ = 1.83 - j\ 2.86$

$I_1.R_1 = 14.69$ V, $- 122.61^\circ = - 7.92 - j\ 12.37$

$I_1.X_1 = 30.50$ V, $- 32.61^\circ = 25.69 - j\ 16.44$

$E = 192.89$ V, $+ 8.59^\circ = 190.73 + j\ 28.81$

$I_m = 1.64$ A, $- 81.41^\circ = 0.24 - j\ 1.62$

$I_{fe} = 0.16$ A, $+ 8.59^\circ = 0.16 + j\ 0.02$

$I_0 = 1.65$ A, $- 75.96^\circ = 0.40 - j\ 1.60$

$I'_3 = 2.30$ A, $+ 8.59^\circ = 2.27 + j\ 0.34$

$I'_2 = 4.78$ A, $- 160.43\ = - 4.50 - j\ 1.60$

$I'_2.R'_2/s = 188.06$ V, $+ 19.57^\circ = 177.20 + j\ 62.99$

$I'_2.X'_2 = 42.88$ V, $- 70.43^\circ = 14.36 - j\ 40.40$

Figure 3.20: Phasor Diagram of Loaded Generator for Measured 208.5V Terminal Voltage at 50Hz Using Modified Circuit.

If a large amount of hysteresis is present in the magnetisation the current waveform will become non-symmetrical about the peak, adding in additional harmonics. Generally, however, for most machines the hysteresis is relatively small and the only significant harmonic will be third.

This is evident from the series of traces shown in Plate 3.1. As the terminal voltage is increased, the third harmonic content also increases and existence of the harmonics above the third is not obvious. This situation becomes clearer by considering the equivalent circuit of the unloaded machine of Figure 3.9.

For the fundamental component, the rotor frequency ω_2 is higher than the frequency of the generated emf, ω_1, and slip is negative indicating power generation.

$$s = (\omega_1 - \omega_2)/\omega_1 \qquad (3.14)$$

For the harmonics, the frequency of the emf is now higher than the rotor frequency and the slip is positive indicating that the harmonic power is being absorbed by the machine. As the harmonic number ν increases the slip approaches unity and the value of R_2'/s approaches R_2'. Also, as the harmonic number increases the values of the rotor and stator leakage reactances increase while the capacitive reactance decreases. Since the terminal voltage is measured across the capacitors, the existence of harmonic voltages will become less evident as harmonic number increases. The values of the reactances in question are:-

$$X_C = 1/(\nu.\omega_1.C) \qquad (3.15)$$

$$X = \nu.\omega_1.L_1 \qquad (3.16)$$

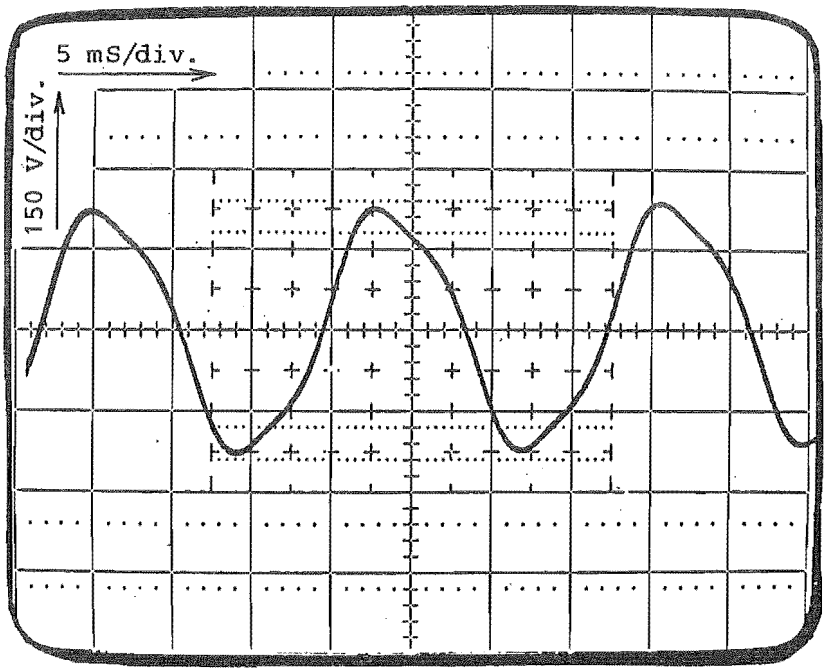

(a) Terminal Voltage 150 V.

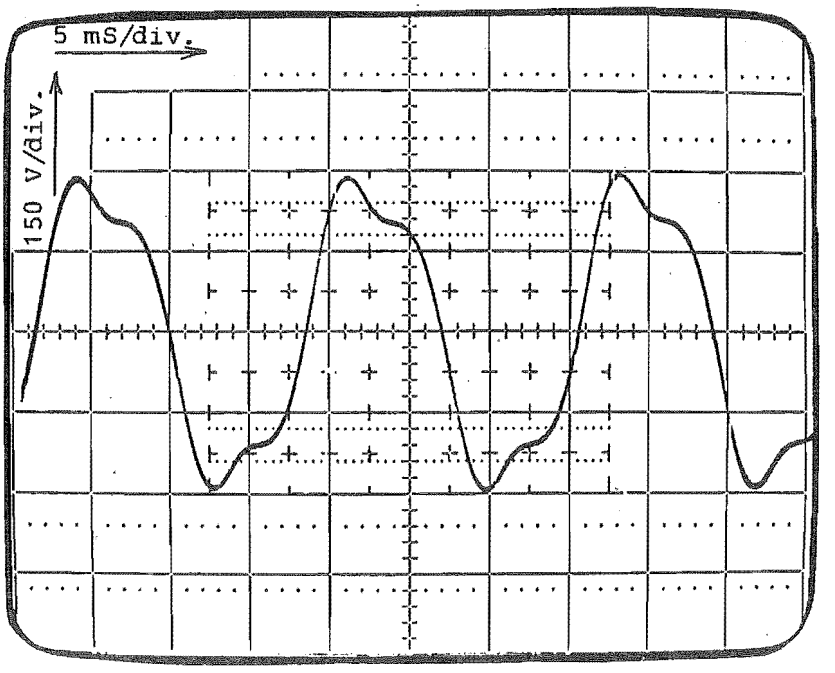

(b) Terminal Voltage 200 V.

Plate 3.1: No Load Generator Terminal Voltage Waveforms.

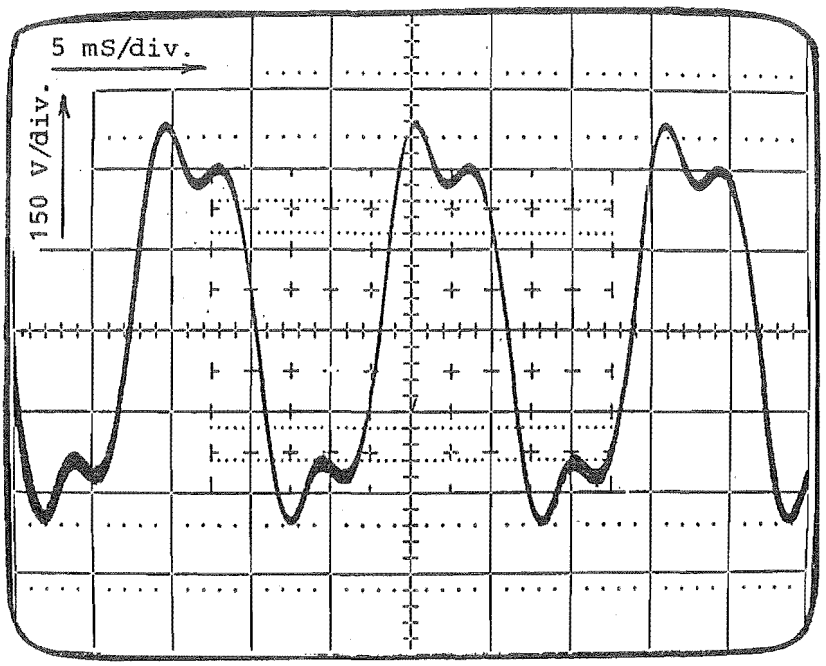

(c) Terminal Voltage 250 V.

Plate 3.1: No Load Terminal Voltage Waveforms.

$$X_2' = \nu . \omega_1 . L_2' \qquad (3.17)$$

where

ν is the harmonic number

ω_1 is the fundamental frequency

A further anomaly associated with Plate 3.1 (c) requires explanation in that the third harmonic wave lags the fundamental component. This is evident from the way in which the two third harmonic protrusions on top of the fundamental component are not of equal height. If the stator section of the equivalent circuit only is considered as in Figure 3.21 then the phasor diagram of Figure 3.22 can be drawn. The terminal voltage can be calculated from the stator current and the capacitive reactance for any particular harmonic.

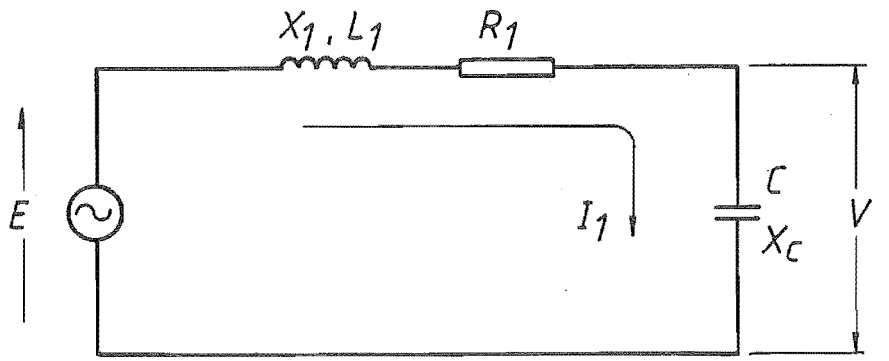

Figure 3.21: Stator Equivalent Circuit.

The internally generated voltages for the fundamental component and third harmonic will be in phase, i.e. a voltage zero is common to both waveforms, thus E_1 and E_3 are in phase. The terminal voltages can subsequently be drawn taking into account the changes in leakage reactance of the stator and capacitive reactance as the frequency is increased from fundamental to third harmonic.

The relative phase relationship between the terminal voltages can be found from the angles β_1 and β_3. Figure 3.23 shows the terminal fundamental and third harmonic voltage waveforms with the corresponding phase shift between the fundamental and third. Note that for Figure 3.23 the ωt axis is marked for fundamental angles only. The two terminal voltage waveforms are summed to give a waveshape as should be seen at the generator terminals. Comparison of Figure 3.23 to the actual waveforms of Plate 3.1 shows a close relationship.

3.7: Summary.

The mechanics of self excitation have been reviewed. Phasor diagrams have been drawn for the unloaded and loaded cases and found to not accurately relate to the equivalent circuit currently used. An alternative equivalent circuit model has been proposed which overcomes the difficulties. This proposed model will require further research and development. Harmonic voltages generated by the machine have been shown to be significant in the third only with higher orders being effectively 'short circuited' by the excitation capacitors. It has also been shown that the self excited induction generator will be operating under conditions of widely varying voltage and frequency when applied to the wind turbine.

$E_1 = 200 + j0$ V

$E_3 = 50 + j0$ V

$I_1 = 1.4 + j7.8$ A

$I_3 = 0.8 - j3.0$ A

$I_1.R_1 = 5.8 + j33.7$ V

$I_1.X_1 = -69.9 + j12.7$ V

$I_1.X_C = V = 264.7 - j42.4$ V

$I_3.R_1 = 3.6 - j12.9$ V

$I_3.\nu.X_1 = 80.2 + j22.2$ V

$I_3.X_C/\nu = V_3 = -33.6 - j9.3$ V

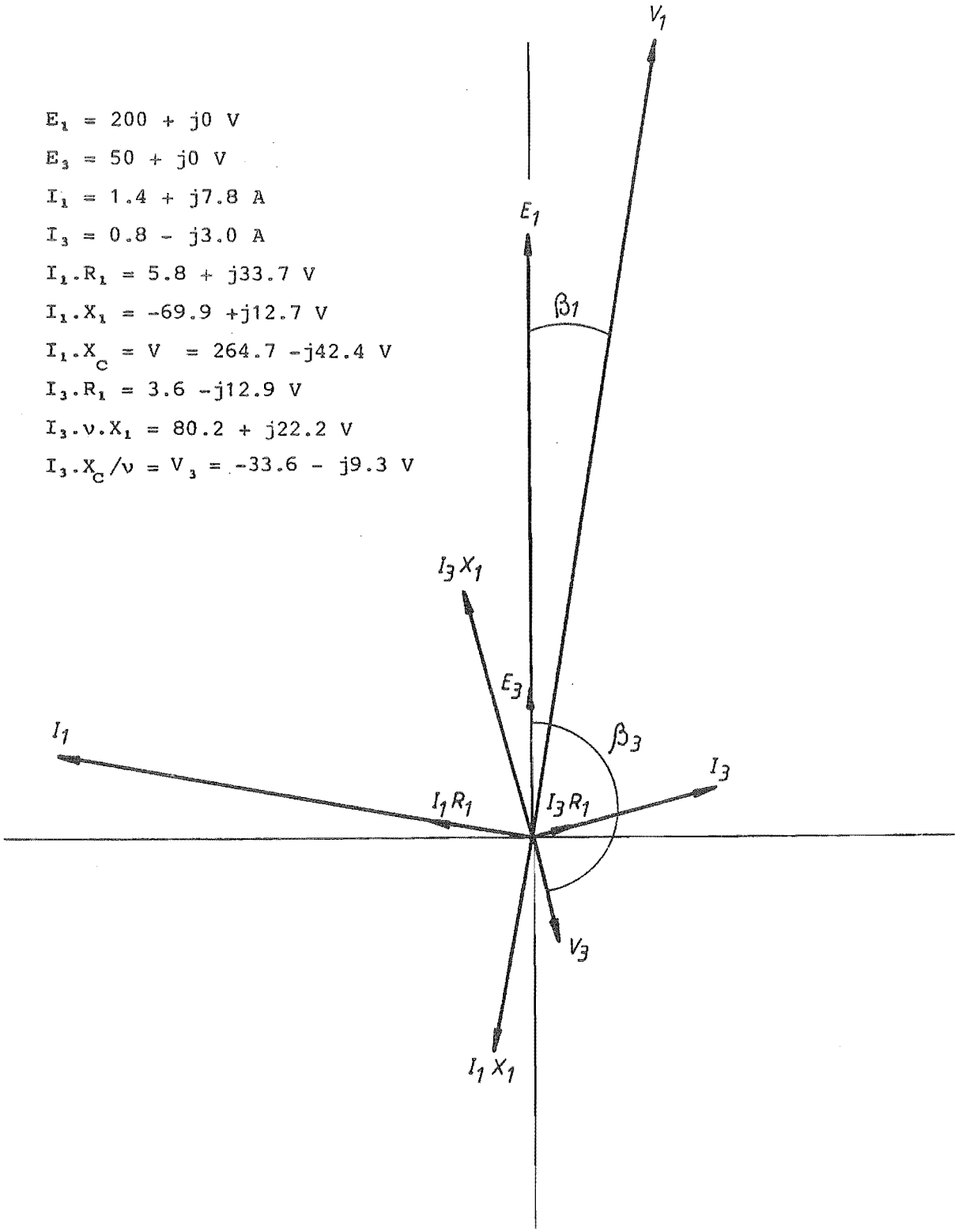

Figure 3.22: Phasor Diagram of Unloaded Machine Showing Fundamental and Third Harmonic Currents and Voltages.

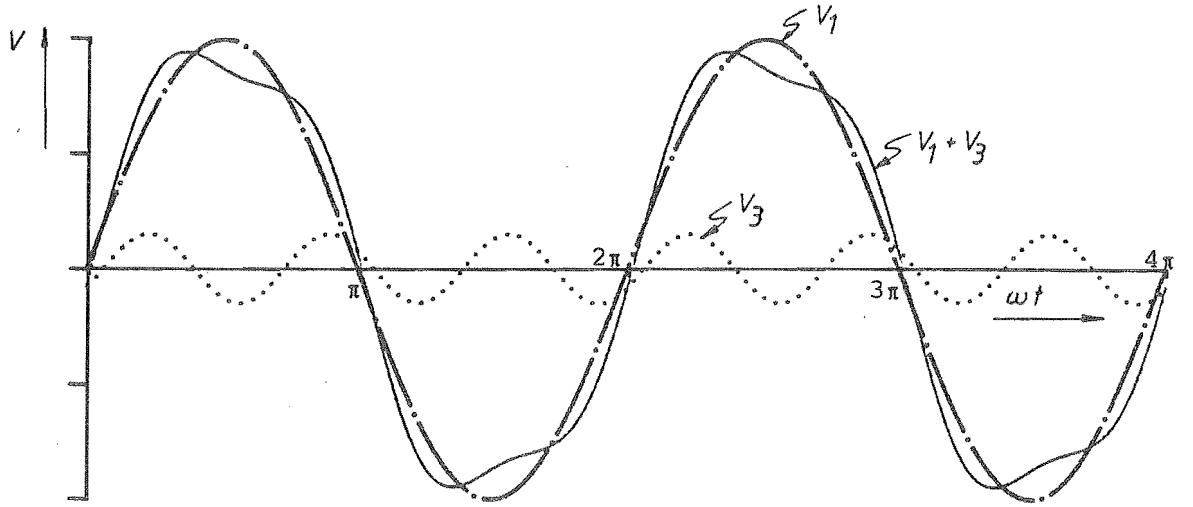

(a) V_1 = 1 Pu, V_3 = 0.15 Pu, 3rd Harmonic Phase Shifted 10°.

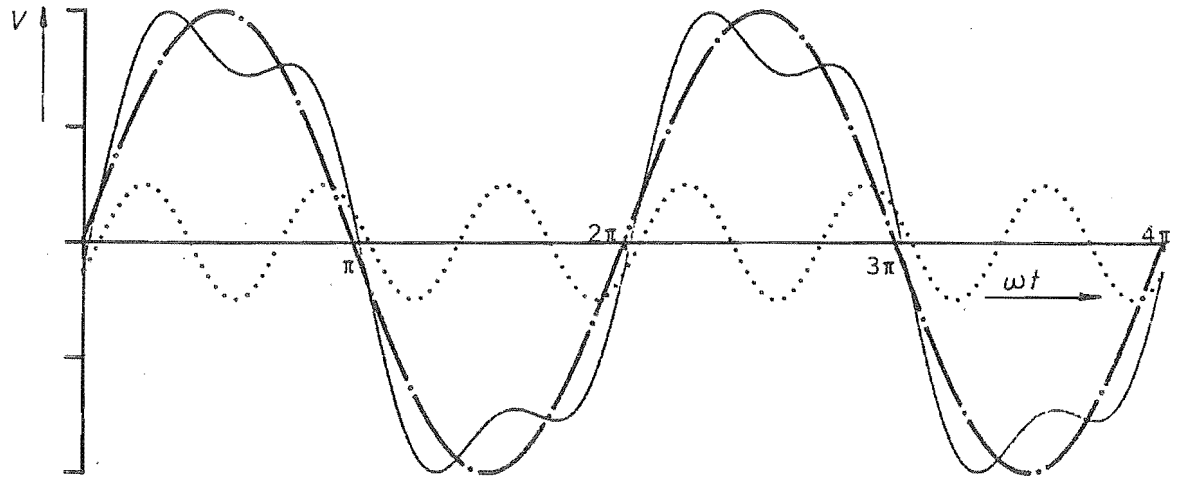

(b) V_1 = 1 Pu, V_3 = 0.25 Pu, 3rd Harmonic Phase Shifted 10°.

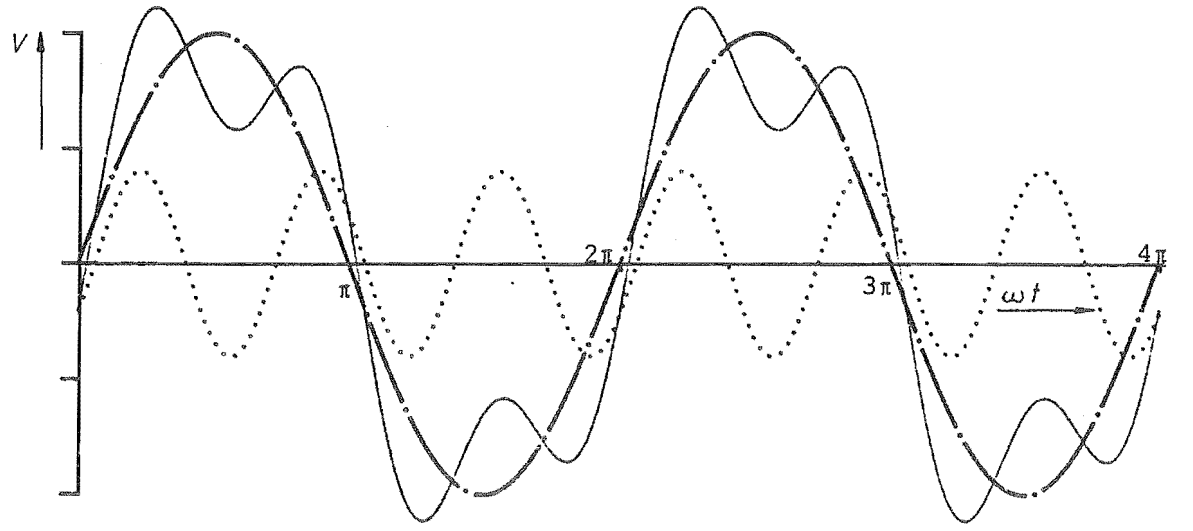

(c) V_1 = 1 Pu, V_3 = 0.4 Pu, 3rd Harmonic Phase Shifted 10°.

Figure 3.23: Predicted No Load Voltage Waveforms Showing Harmonic Phase Shift.

CHAPTER 4.

CONTROLLABLE RECTIFIER.

4.1: Introduction.

A characteristic of all rectifying devices is that they are nonlinear in that they conduct current readily in one direction and poorly, if at all, in the opposite direction. Although it had been known for a long time that the electric arc possessed a nonlinear characteristic it was not until 1905 that this property was applied to the construction of the mercury arc rectifier for the conversion of alternating current to direct current. The earliest devices were usually of a single cathode - multiple anode design using star or centre tapped transformers.

The development of semiconductor devices revolutionised the construction of rectifiers, firstly with the diode and later with the thyristor. The major advantages of these devices were that they were not as delicate as the mecury arc rectifier, they were relatively small and required no form of ignition as did the mecury arc rectifier. In the case of the thyristor only a low power control signal is required to turn them on. Developments in medium range power semiconductor devices include larger transistors capable of handling several hundred amperes and the gate turnoff thyristor. The gate turnoff thyristor has the ability to block at any point on the conduction cycle whereas normal thyristors do not turn off until they become reverse biassed and current goes to zero. The GTO cannot however turn off if the current rises above a certain level and also has the additional disadvantage of a high turn on voltage. Conventional thyristors have been used in the rectifier for the wind generator, as they provide a well proven and rugged means of rectification.

Uncontrolled rectification is obtained by use of either a half wave diode bridge or a full wave diode bridge. Figure 4.1 shows the basic form of uncontrolled diode rectifiers for half and full wave situations for both

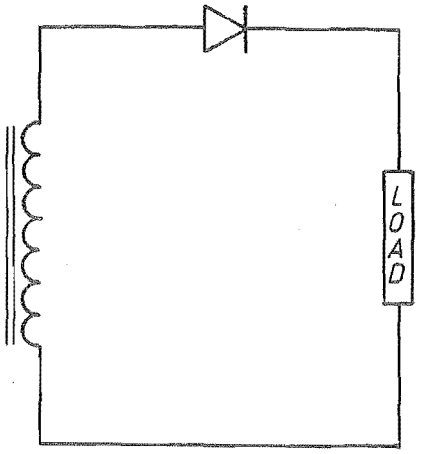

(a) 1 Phase, Half Wave.

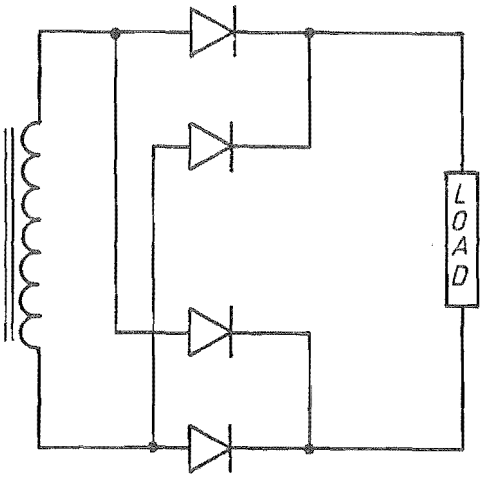

(b) 1 Phase, Full Wave.

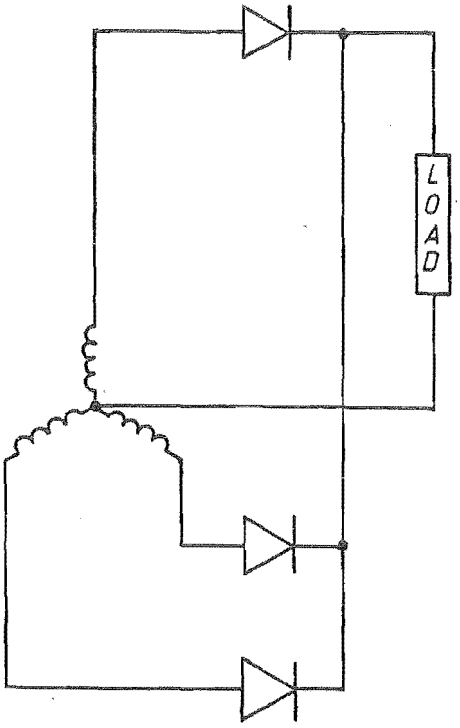

(c) 3 Phase, Half Wave.

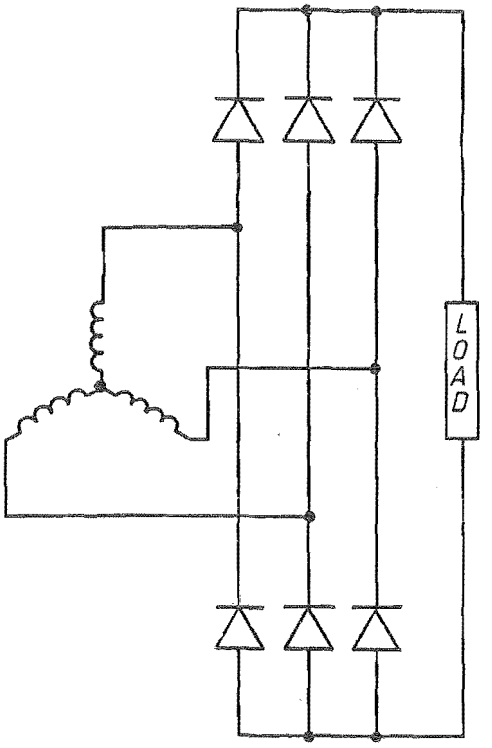

(d) 3 Phase, Full Wave.

Figure 4.1: Variations of Uncontrolled Rectifiers.

single phase and three phase supplies. The voltage of the DC output is dependent on the AC supply voltage and for practical purposes is fixed ie., uncontrolled. The output voltages for the circuits of Figure 4.1 are given in Table 4.1 where E is the peak AC phase-neutral voltage. The bridge rectifiers have two major advantages over half wave circuits. Since the bridge rectifier is a full wave rectifying device it is possible to obtain twice the output voltage as both the positive and negative half cycles are used. Additionally the phases for the bridge rectifier do not carry any net DC current since each conduction cycle causes the phases to carry two components in opposite directions. The absence of this DC current in the phases is a major advantage as it eliminates electrical heating effects in the AC source other than those due to the AC currents.

Input Type	Half Wave Voltage	Full Wave Voltage
1 Phase	E/π	$2.E/\pi$
3 Phase	$3\sqrt{3}\ .E/2.\pi$	$3\sqrt{3}\ .E/\pi$

Table 4.1: Uncontrolled Rectifier Output Voltages.

A great advantage of half wave rectifiers is that the output DC voltage can be easily referenced to some point in the AC circuit. For a single phase rectifier this would be one side of the source and for a three phase bridge reference is made to the neutral. For bridge rectifiers this is not possible since both the output terminals follow the AC voltages. Referencing either output to any of the AC terminals would place a short circuit on the supply. For bridge rectifiers either the AC must float or the DC output must float with reference to the other side of the bridge. Another advantage of half wave rectifiers is one of lower cost compared to bridge circuits.

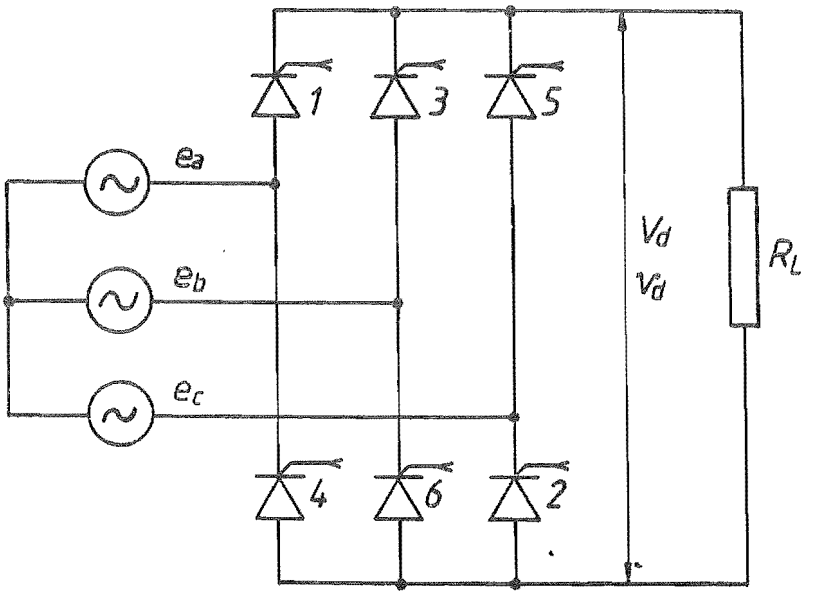

Figure 4.2: Three Phase Full Wave Controlled Bridge.

For the case where the rectifier is fed directly from a generator it is of particular importance to eliminate any possibility of DC currents flowing in the machine windings, since the machine rating would need to be reduced to account for the heating effects of the DC current. For this reason the bridge circuit has been selected for this project.

Controlled rectifiers are similar to uncontrolled rectifiers except that the diodes are replaced by thyristors, allowing control over which part of the half cycle conduction is allowed to begin. The circuit for a three phase fully controlled bridge is shown in Figure 4.2. Whilst diodes will always conduct when they become foward biassed, the conduction for thyristors can be delayed until an appropriate voltage is applied to the gate, ie., until the thyristors are fired. The thyristors cease to conduct when they become reverse biased and the current falls to zero. The electrical angle between the AC fundamental voltage zero and the instant when the thyristor is fired is the delay angle α ,as depicted in Figures 4.8 and 4.9, and as delay angle is increased the DC voltage output decreases. The advantage of the controlled rectifier is that by varying the delay angle it is possible to control the load, and thus provide a convenient method of controlling generator electrical load for the wind turbine.

4.2: The Controlled Bridge Rectifier.

For the bridge of Figure 4.2 operation would begin say with thyristors 1 and 2 conducting. As e_a becomes negative with respect to e_b thyristor 1 becomes reverse biassed since thyristor 3 has fired, resulting in thyristor 1 extinguishing. Similarly as e_a becomes negative with respect to e_c thyristor 2 will extinguish and 4 will conduct. The complete sequence of conduction is 1 and 2, 3 and 2, 3 and 4, 5 and 4, 5 and 6, 1 and 6, 1 and 2, etc. For rectifiers supplied from a source which is mainly inductive the transfer of current from one thyristor to the next will be slow and a period of overlap will occur where both devices are simultaneously conducting, causing what is referred to as commutation overlap, and can have substantial effects on the performance of rectifiers.

The equations which describe rectifier operation are well known and documented in the literature (Seymour 1968, Adamson 1960, Davis 1979). A set of simplifying assumptions is made and these assumptions are:-

(1) The foward voltage drop of the thyristors may be neglected.

(2) The reverse leakage current of the thyristors may be neglected.

(3) Circuit resistances (apart from the load) are small enough to have no appreciable effect.

(4) The rectifier is supplied from an infinite bus giving a pure sine wave of voltage.

(5) The rectifier output is smoothed hence average and rms values of the DC output are equivalent.

(6) The DC load has infinite inductance.

The DC voltage output can be found by equating input and load powers:-

$$3.V.I.\cos\varphi = V_d.I_d \qquad (4.1)$$

where V is the phase to neutral rms voltage.

For rectifiers where commutation overlap occurs the phase angle can be related to the delay angle and overlap angle by (Adamson 1960):-

$$\cos\varphi = [\cos\alpha + \cos(\alpha + \gamma)]/2 \qquad (4.2)$$

and

$$I = I_d.\sqrt{6}/\pi \qquad (4.3)$$

Equating (4.1), (4.2) and (4.3) gives:-

$$V_d = (3\sqrt{6}/2\pi).V.[\cos\alpha + \cos(\alpha + \gamma)] \qquad (4.4)$$

where γ is the overlap angle.

In terms of peak phase - neutral voltages, Equation (4.4) is:-

$$V_d = (3\sqrt{3}/2\pi).E.[\cos\alpha + \cos(\alpha + \gamma)] \qquad (4.5)$$

If commutation overlap is ignored then the DC voltage becomes:-

$$V_d = (3\sqrt{6}/\pi).V.\cos\alpha \qquad (4.6)$$

Equation (4.6) can also be related to the three phase bridge voltage when $\alpha = 0$. The active component of current can be found using Equation (4.2) and Equation (4.3):-

$$I_p = I.\cos\varphi \qquad (4.7)$$

or

$$I_p = (\sqrt{6}/2\pi).I_d.[\cos\ \alpha + \cos(\alpha + \gamma)] \qquad (4.8)$$

For the reactive component a similar approximation as used in Equation (4.2) can be used, ie.,

$$I_q = I.\sin\ \varphi \qquad (4.9)$$

or

$$I_q = (\sqrt{6}/2\pi).I_d.[\sin\ \alpha + \sin(\alpha + \gamma)] \qquad (4.10)$$

If commutation overlap is ignored these become:-

$$I_p = (\sqrt{6}/\pi).I_d.\cos\ \alpha \qquad (4.11)$$

$$I_q = (\sqrt{6}/\pi).I_d.\sin\ \alpha \qquad (4.12)$$

The above equations are valid for sinusoidal input voltages implying a pure sine wave source. For connection of the rectifier to a self excited induction generator the assumption of a sine wave source is not valid as was shown in Chapter 3. The difficulty arising for non - sinusoidal sources results from the possibility of the rectifier control circuits detecting spurious phase crossovers. Since these phase crossovers are used to determine thyristor firing timing, incorrect crossover detection will result in unwanted thyristor conduction.

The presence of harmonics in the AC voltage is therefore of considerable importance. Although the self excited induction generator has considerable inductance in its windings the presence of commutation overlap will be greatly reduced due to the presence of shunt capacitors over its terminals and has therefore subsequently been ignored in the following. It was also assumed in the above that the DC output was smoothed by some means, usually a reactor, however for the application used no smoothing was incorporated, necessitating the development of new voltage equations. This topic is persued in Section 4.3.3.

4.3: Rectifier Design and Operation.

4.3.1: Design Requirements.

The requirement of variable wind speed turbine operation was described in Chapter 2 and implied the generation of a variable frequency voltage. The rectification of this waveform therefore requires operation of the rectifier over a wide range of frequencies with a linear relationship between control voltage and true delay angle, regardless of what the frequency is. Additionally, since severely distorted waveforms are likely it is required that the rectifier operate reliably when large harmonic content is present at the input. The design implemented gives linear control from 5 Hz to 300 Hz on waveforms with abnormally large harmonic content.

4.3.2: Rectifier Design.

The rectifier consists of five main components (refer to Figure 4.3) viz:

(1) Phase Crossover Detector.

The phase crossover detector provides indication of when the phase to neutral input voltage waveforms cross, the indication being used as a reference for delay angle as shown in Figure 4.4. The detector outputs three crossover detection pulses and three reset pulses, one crossover detection pulse for each crossover between two phases and one reset pulse for each negative crossover between two phases. The reset pulses simply ensure correct sequencing of thyristor firings.

(2) Control Board.

The control board reads the phase crossover signals and generates the appropriate firing commands. Delay angle control is obtained from the 0 - 10 V control line on to the board where 0 V corresponds to no angular

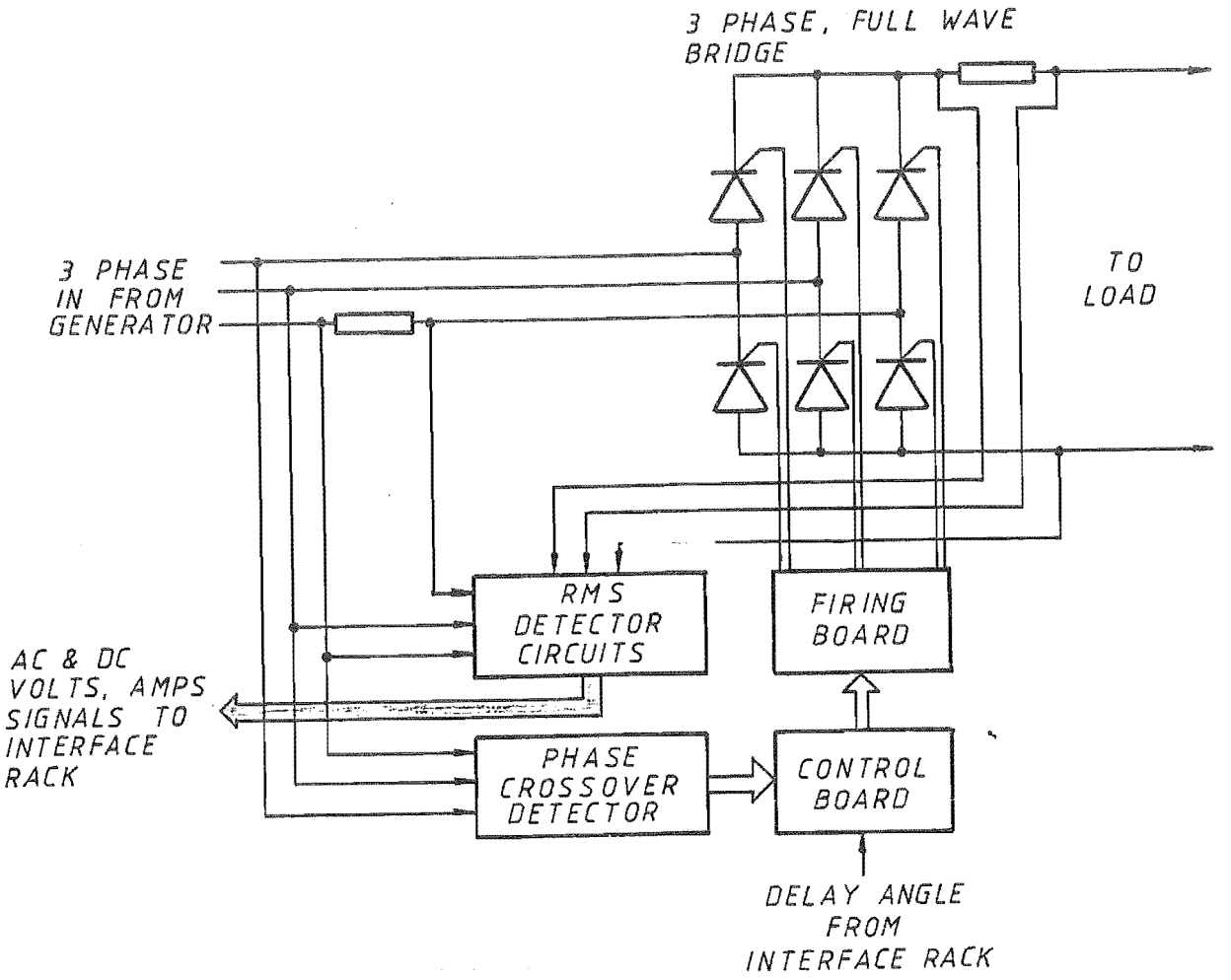

Figure 4.3: Controlled Rectifier Schematic.

delay (ie., full output voltage) and 10 V corresponds to full angular delay (blocking). When a phase crossover pulse is detected the control circuit generates a ramp of 120 degrees width, regardless of frequency. Refer to Figure 4.5. This is accomplished by the use of the circuit of Figure 4.6. The phase crossover pulses are passed through a monostable to produce sharp start pulses of about 100 μS width which coincide with the phase crossovers. These are filtered so that a DC voltage level is developed, its amplitude being proportional to the frequency of the incoming start pulses, ie., proportional to the frequency of input to the rectifier. This level provides the current I_f to the positive input of the integrator which generates the positive ramp, its slope depending on the value of I_f and therefore also dependent on input frequency. Reset is

provided by using the start pulses on the negative input to the integrator thus forcing the output to zero at each phase crossover. The diodes prevent any loading down effect each input may have on the other. A comparitor sends the command to begin firing when the control signal and ramp intersect. The firing command persists for a full 120 degrees but is only effective up until the thyristors become naturally reverse biassed at which stage they turn off, even though the firing command is still present. The rectifier is thus capable of operating over a wide range of input frequencies. A logical AND is performed between the firing command and a 65 kHz square wave from an oscillator to provide a train of firing pulses which can be transmitted through the pulse transformers of the firing board to the gates of the thyristors.

(3) Firing Board.

The firing board amplifies the six firing signals (to the six thyristors) to an appropiate level and isolates them through pulse transformers before being sent to the gates of the thyristors. The isolation is necessary for protection of the control circuits since the thyristor gates operate at input AC voltages.

(4) Rectifier Bridge.

The bridge is of a three phase, six pulse design as shown by Figure 4.3. The thyristors used are rated at 1 kV and 24 amperes. Snubbers are provided over each thyristor to protect against excess dV/dt. To enhance the fast commutation capabilities of the bridge it is necessary to obtain a large value of di/dt, requiring fast gate pulses, hence the use of the 65 kHz square wave for the generation of the firing pulses.

(5) Transducers.

Measurement of AC and DC voltage and current is made using voltage dividers and current shunts with true rms detector circuits. Since the waveforms on the AC side could be severely distorted and also since the DC

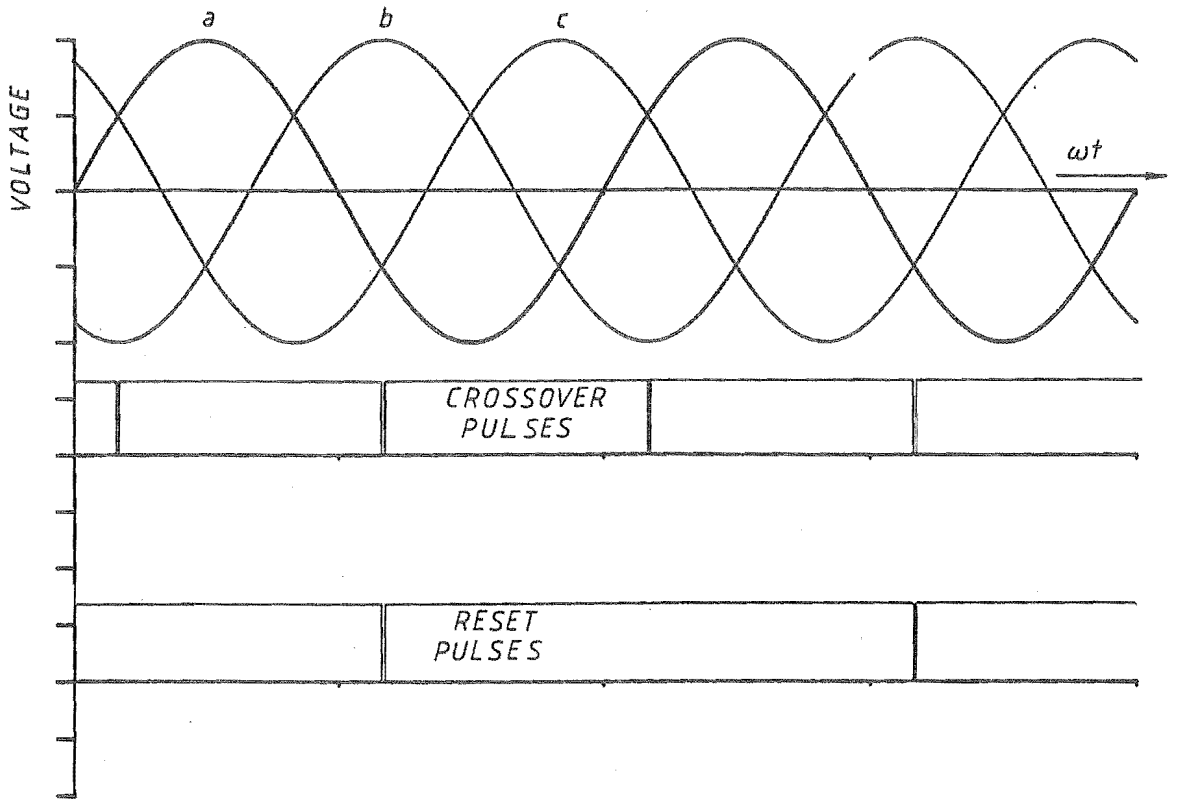

Figure 4.4: Phase Crossover Detector Operation.

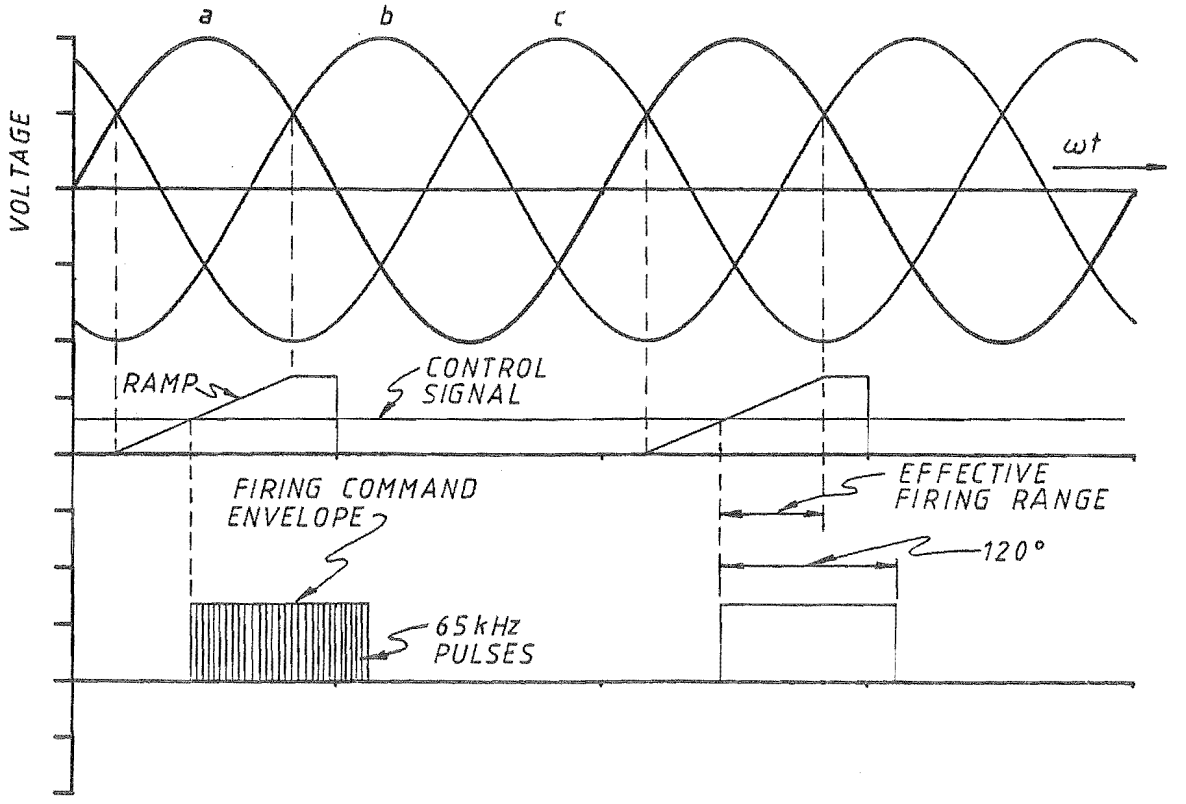

Figure 4.5: Control Board Operation.

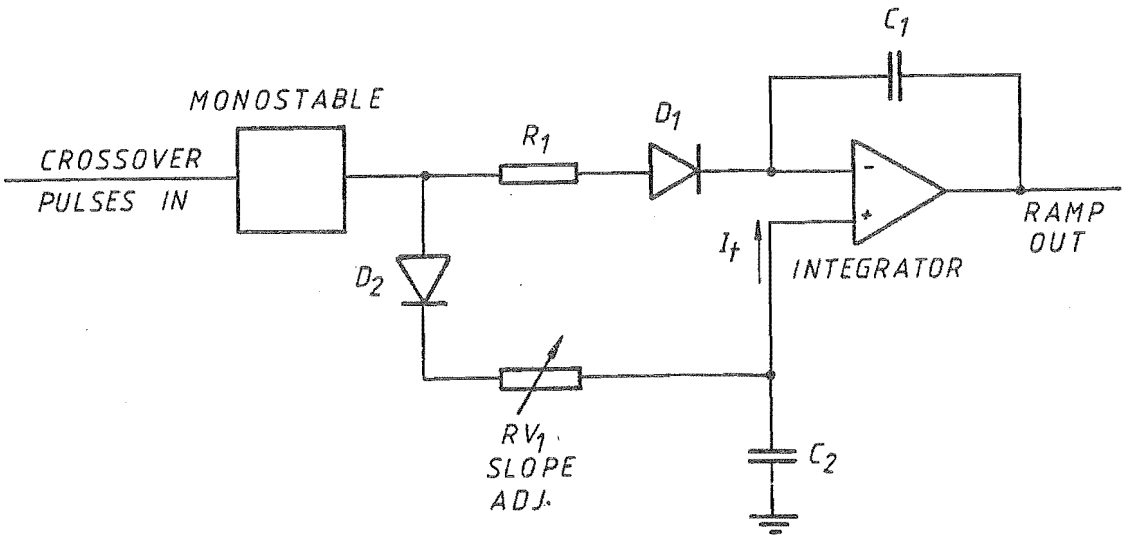

Figure 4.6: Variable Frequency Ramp Generation.

output is not smoothed by a reactor, all signals could not simply be averaged and hence required true true rms detection. The rms detectors shown in Figure 4.7 use four quadrant multipliers to square the incoming signal which is then averaged and the square roots then found by another set of four quadrant multipliers. The optical isolators provide isolation between the detector boards and the remainder of the control panel since the detectors float at line potentials.

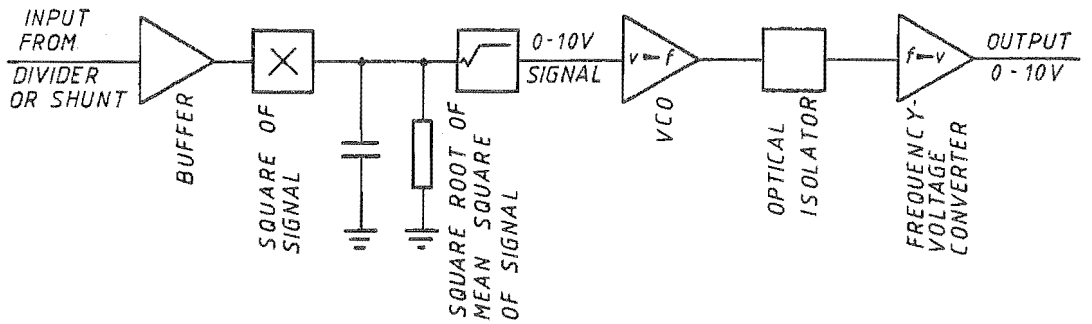

Figure 4.7: True RMS Detector Schematic.

4.3.3: Rectifier Operation.

The development of the following equations differs from that normally made in that commutation overlap is ignored and the assumption of a smooth DC output is not valid since a purly resistive load is used, ie., a reactor is not used in the DC circuit. It is therefore necessary to develop equations which determine the rms value of the voltage. Two separate equations have been developed for the cases of α less than 60 degrees, ie., the situation where the conduction cycles are a full 60 degrees wide and also for greater than 60 degrees. These two cases are illustrated in Figures 4.8 and 4.9.

(1) α <= 60 degrees. Refer to Figure 4.2.

Energy in rms signal = Energy in actual signal

ie.,

$$V_d^2.T/R_L = \int_{(\alpha/\omega)}^{(\alpha+\pi/3)/\omega} e^2/R_L \, dt \qquad (4.13)$$

where R_L is the resistive load.
T is the period for one conduction cycle.
E is the peak value of phase voltage.
e is the instantaneous value of phase voltage.
V is the rms phase voltage.

$$e = e_{ab} = \sqrt{3}.E.\sin(\omega t + \pi/3) \qquad (4.14)$$

Equating (4.7) and (4.8) gives:-

$$V_d^2 = 3.E^2/T.\int_{(\alpha/\omega)}^{(\alpha+\pi/3)/\omega} \sin^2(\omega t + \pi/3) \, dt \qquad (4.15)$$

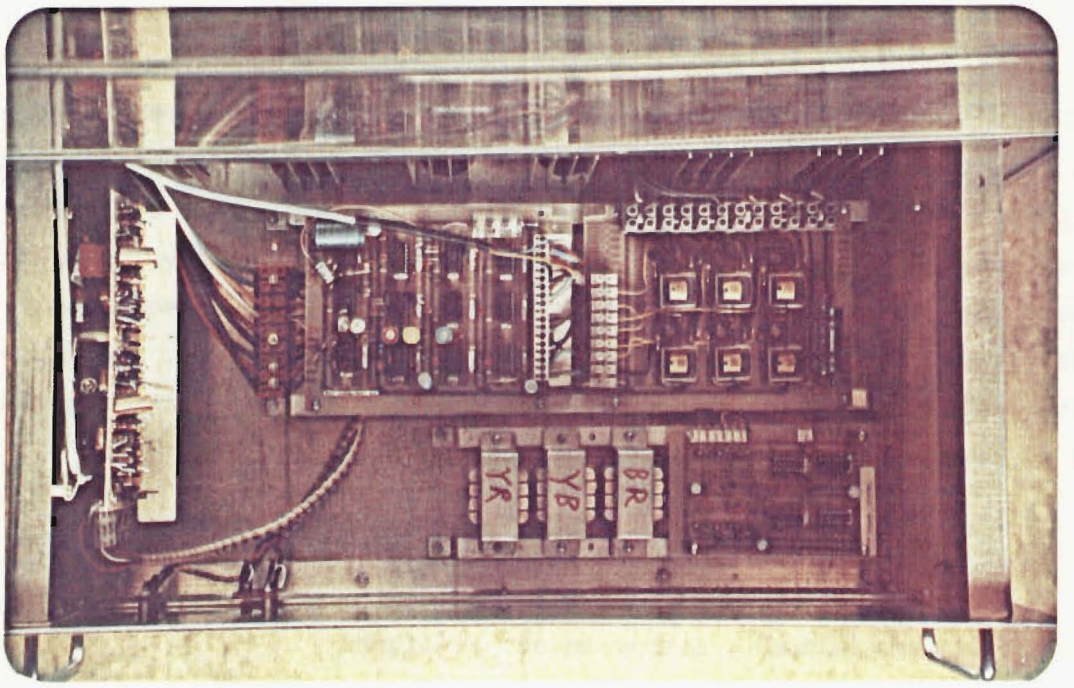

Plate 4.1: The Controllable Rectifier.

$$V_d^2 = 3.V^2/T.\omega \left[\pi/3 + \sqrt{3}/2 \cos(2.\alpha) \right] \qquad (4.16)$$

(2) $\alpha > 60$ degrees.

Analysis is similar to that above except that the period where conduction does not take place must be accounted for.

$$V_d^2 = 3.V^2/T.\omega \left[2\pi/3 - \alpha - 1/4.\sin(2.\alpha) + \sqrt{3}/4.\cos(2.\alpha) \right] \qquad (4.17)$$

Figure 4.10 shows the calculated values of normalised DC voltage for the rectifier with mains (sinusoidal) input and also the corresponding values of measured normalised DC voltage, exhibiting differences of less than 10%. Plates 4.2 (a), (b), (c), (d) show the phase voltage and DC output voltage

for delay angles of 90, 60, 30 and 0 degrees respectively. Notice that for delay angles of greater than 60 degrees the conduction cycles are less than 60 degrees wide. For the 60 degree delay angle, the conduction cycles are just 60 degrees wide and for delay angles of less than 60 degrees the conduction cycles are 60 degrees wide.

4.4: Summary.

A general overview of rectifiers has been given. Design and operation of the rectifier are described with emphasis placed on the unusual frequency and harmonic content requirements. Equations have been developed for the rms voltage of the unsmoothed output waveform and compared with test results for mains input.

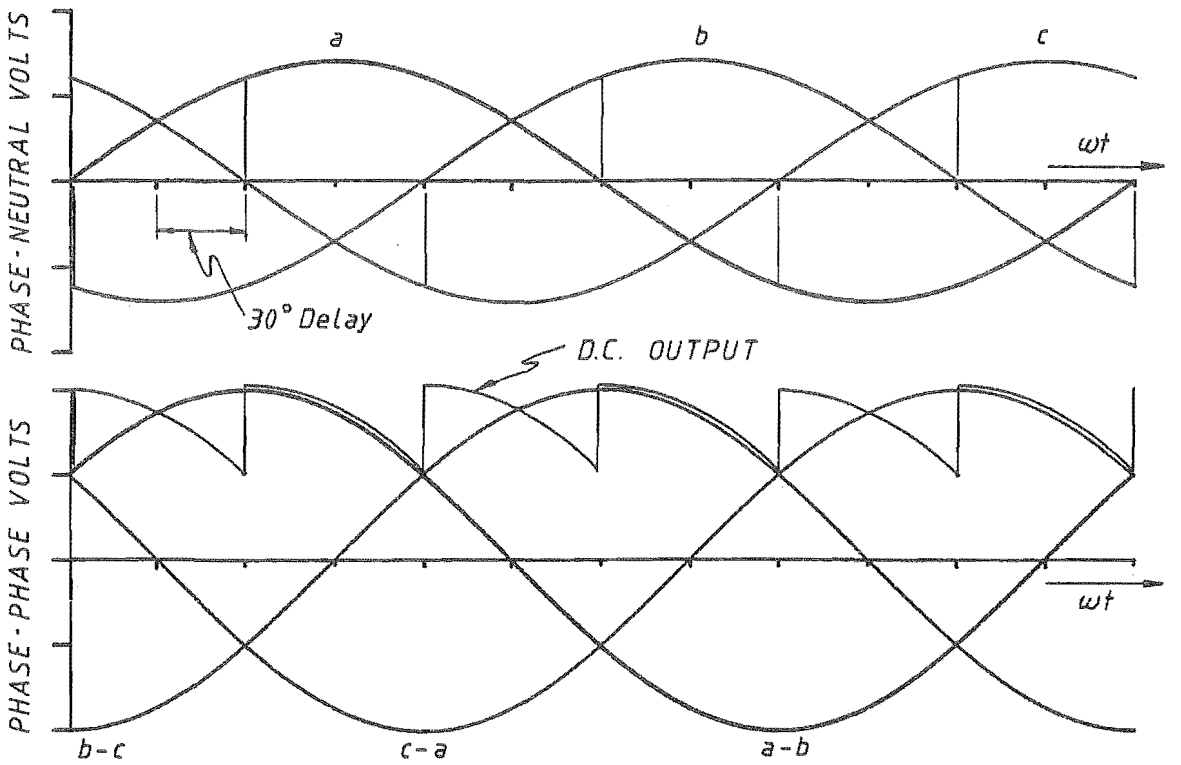

Figure 4.8: DC Output Voltage for $\alpha < 60$ Degrees.

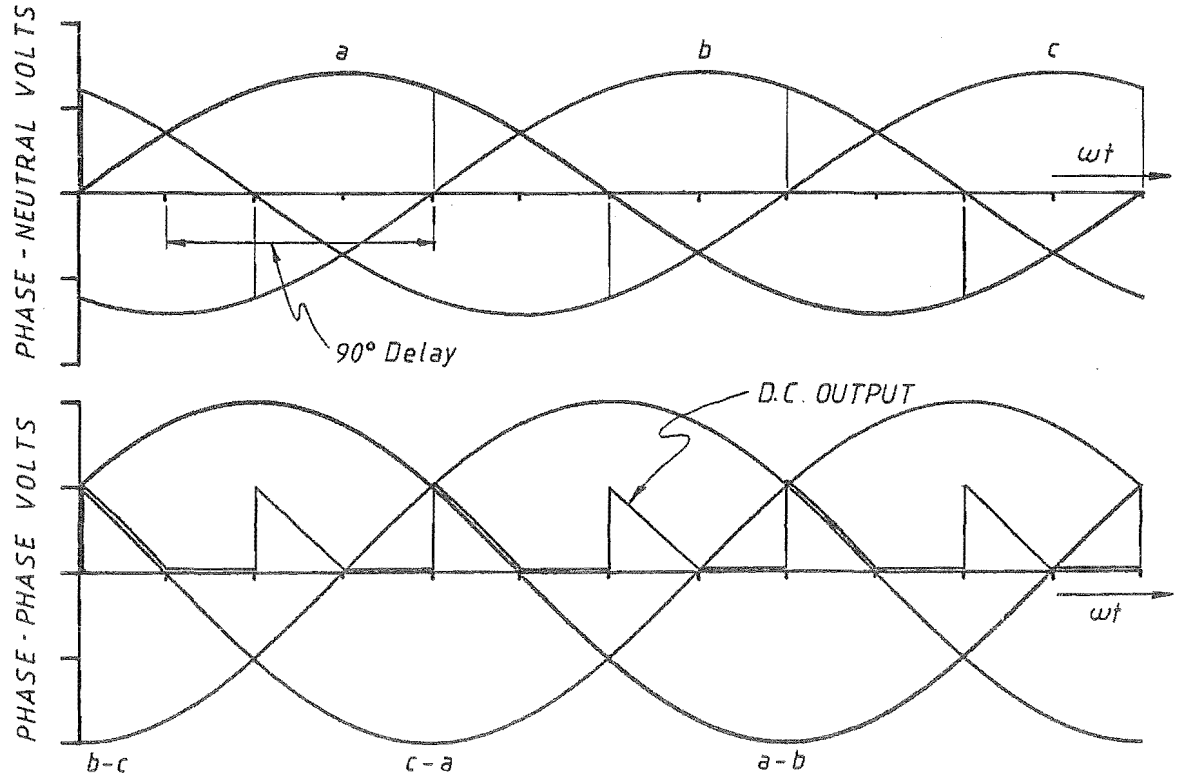

Figure 4.9: DC Output Voltage for $\alpha > 60$ Degrees.

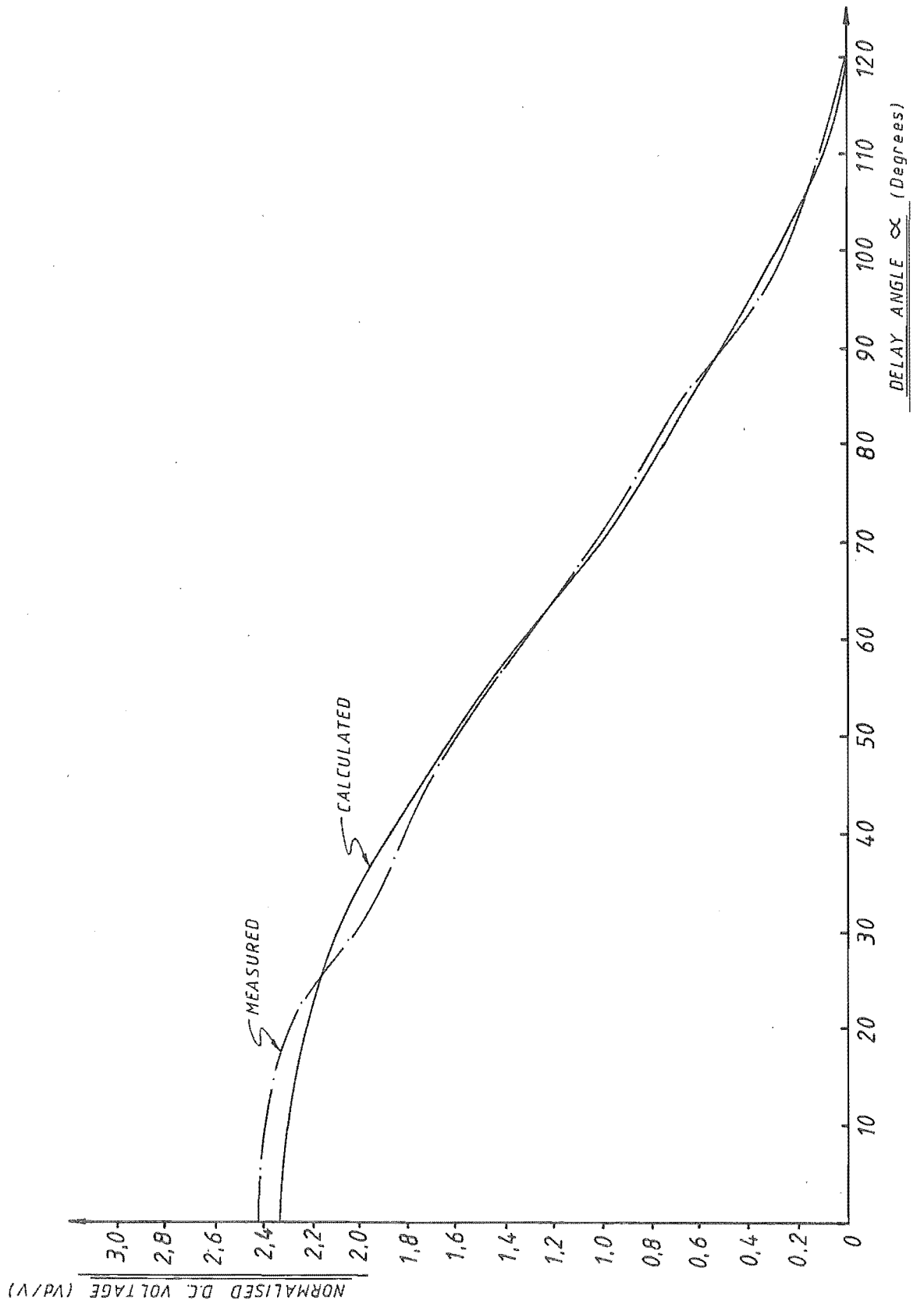

Figure 4.10: Comparison of Measured and Calculated Voltages of Rectifier Output as Delay Angle Varies for Mains Input.

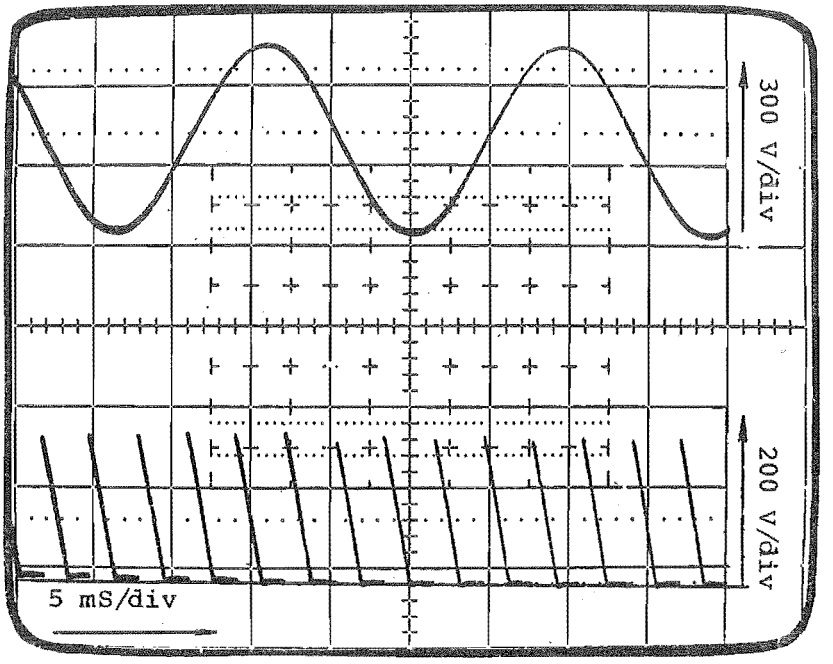

(a) α = 90 Degrees.

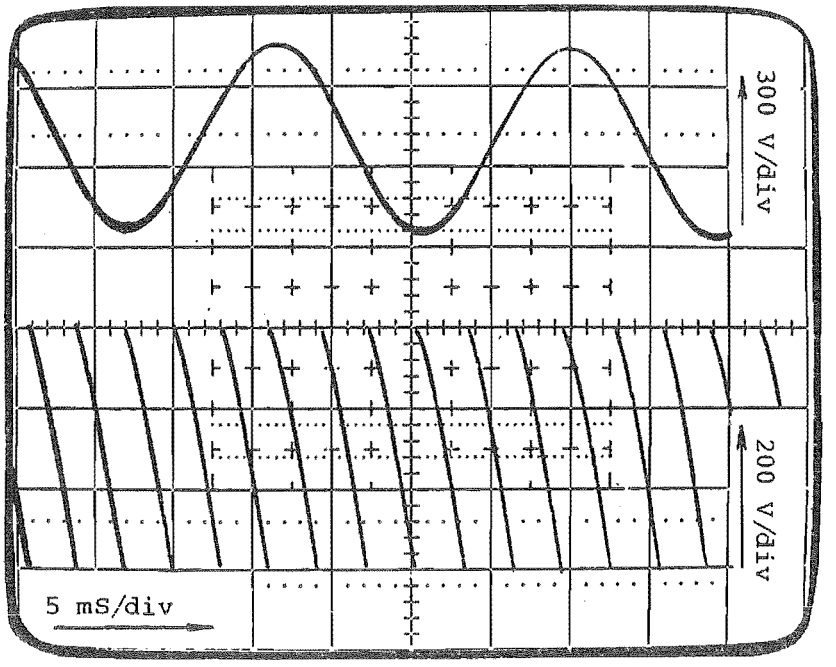

(b) α = 60 Degrees.

Plate 4.2: DC Output Voltage Waveforms.

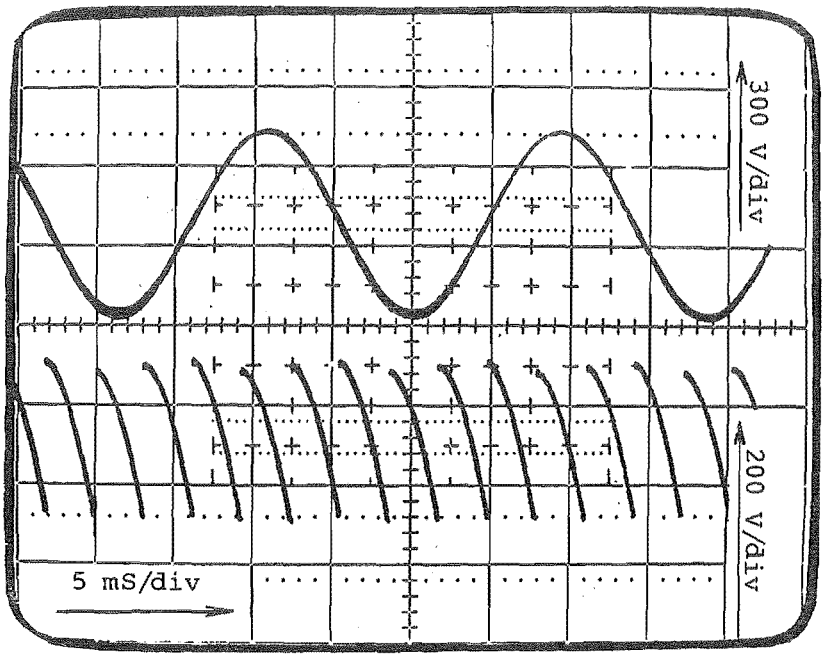

(c) α = 30 Degrees.

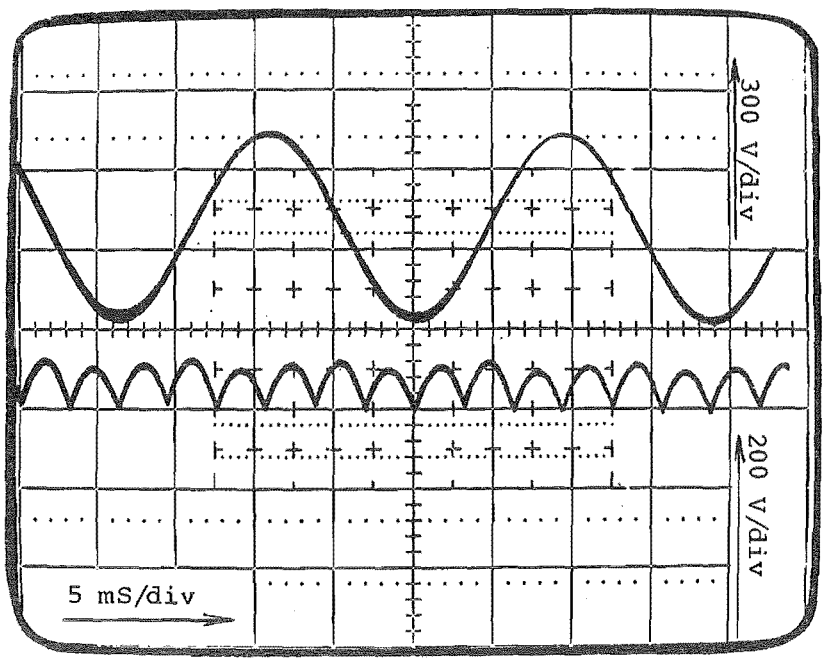

(d) α = 0 Degrees.

Plate 4.2: DC Output Voltage Waveforms.

CHAPTER 5

THE WIND TURBINE.

5.1: Introduction.

Chapter 5 gives a description of the mechanical components of the wind turbine generator. The Introduction outlines the design of the turbine by giving a short description of the major components. The sections following this deal with the steady state loads of the machine and since turbine blades constitute an area where failure is common, particular emphasis has been placed on loads associated with them. The effects of transient and cyclic loads have not been included in the following, however safety factors have in general been kept high (refer to Oberg, 1966, p351) to take account of these. Final results of the calculations have been included in the following sections and show estimates of stress and safety factors. Appendix 2 gives details of parameters used in the calculations.

The windmill is a horizontal axis downwind type with three fixed pitch blades as shown in Figure 5.1. Since a recent study (Miller 1983) has shown that optimal twisting of blades only results in about a 5% improvement in turbine performance it was not considered essential, or of value for the purpose of this project, to involve the added constructional complication of blade twisting. The blades are of RAF 39 profile and the pitch can be altered with the wind turbine at rest. The downwind or self steering feature was used as it obviated any necessity for continual control of turbine orientation, thus simplifying the design of the control system. To provide the torque required for self steering by the action of drag on the blades, the hub is mounted 1000mm back from the yaw shaft. Yaw rate is damped to prevent excess precession loading.

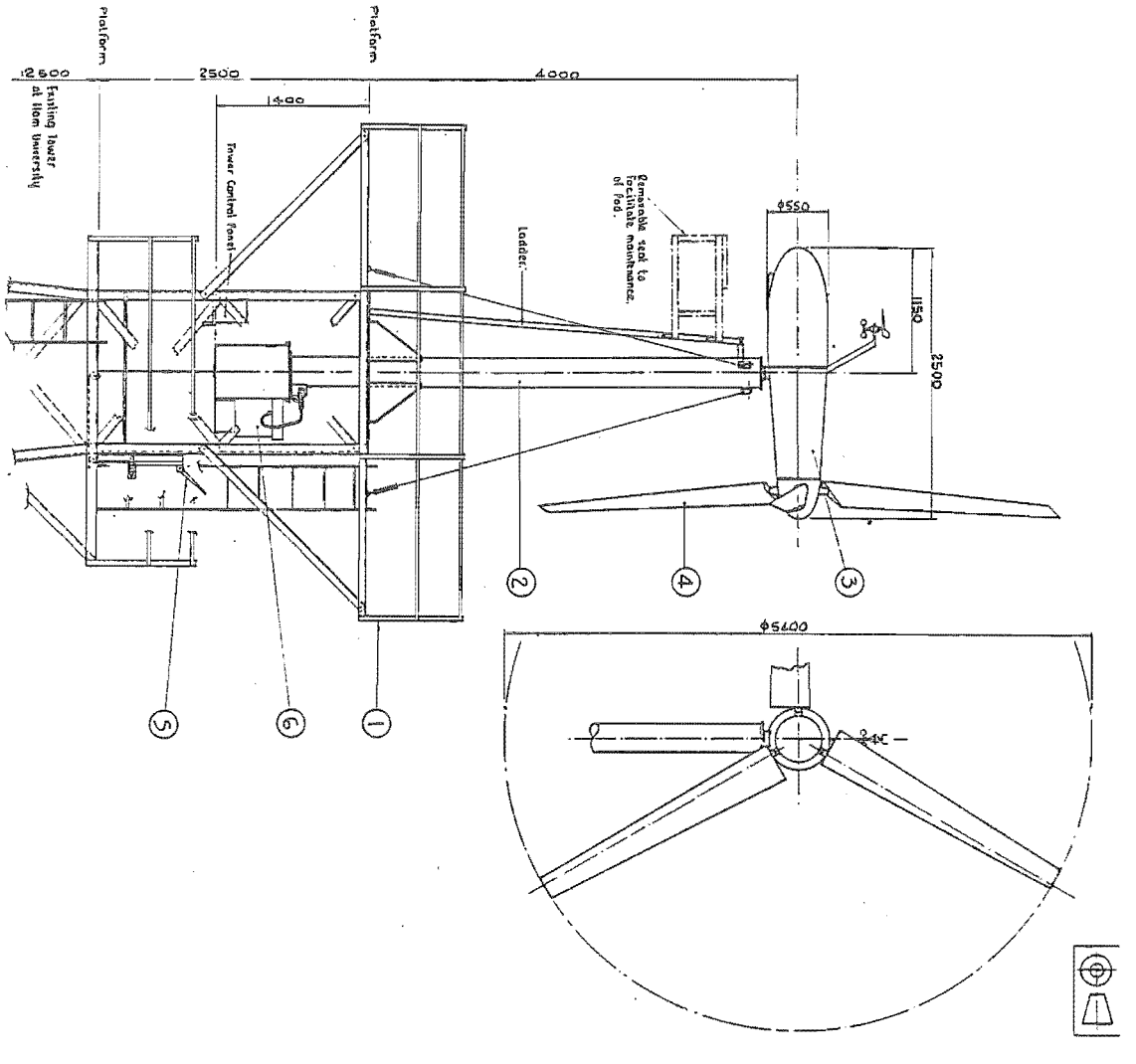

No. off	Item	Drawing No	Detail of Material Description	Remarks
1	1	–	Support tower or structure to suit	
1	2	1618 3658 (a)	Column Assembly	
1	3	FEM 154 (a)	Pod Assembly	
3	4	1618 3618 (a)	Fan blades etc	
1	5	1618 (a)	Handbrake Assembly	
1	6	1618	Hydraulics etc	
1	7			
	8			
	9			
	10			
	11			
	12			

Figure 5.1: Wind Turbine Generator Pictorial.

The hub drives a shaft supported by two bearings (Refer to Figure 5.2) through a flexible coupling to a gearbox of 1:10 step up ratio. The generator mounts directly onto the end of the gearbox with gear coupling. The purpose of the flexible coupling is to reduce the effects of shock and misalignment in the drive train. The main shaft bearings are self aligning with the rear bearing taking all of the axial loading.

The pod mounts a 4m long vertical yaw shaft inside a steel column and is supported by two self aligning bearings as shown in Figure 5.3. Support gussets are used for added strength in the welded joint between the column and bedplate. The bedplate has been simply bolted to a steel lattice tower of some 15m height so that the whole turbine structure can be resited to other towers. The yaw shaft is hollow to allow cables to pass through with sliprings located at the lower end to facilitate connection of power and signal cables.

A yaw drive mechanism is located at the base of the support column under the bedplate and comprises a herringbone gear mounted on the yaw shaft and the pinion mounted on a hydraulic motor. The pump and pump drive for these hydraulics are located on a separate stand along with hydraulic valves and oil tank.

The braking mechanism used to bring the turbine to rest consists of a brake disc located immediately forward of the rear main shaft bearing. It is a 305mm diameter disc with two hydraulic calipers. Each caliper has separate actuation from 24V DC servos operated from isolated DC supplies for improved security. Shaft angular deceleration rate is monitored and held below 2 rad/sec^2 or about 100 rpm to 0 rpm in 5 sec. A hand controlled cable (operating through the vertical shaft) can also be used to operate both calipers, the handle being located below the bedplate.

In all of the following calculations safety factors have been estimated on the ultimate strength of the materials.

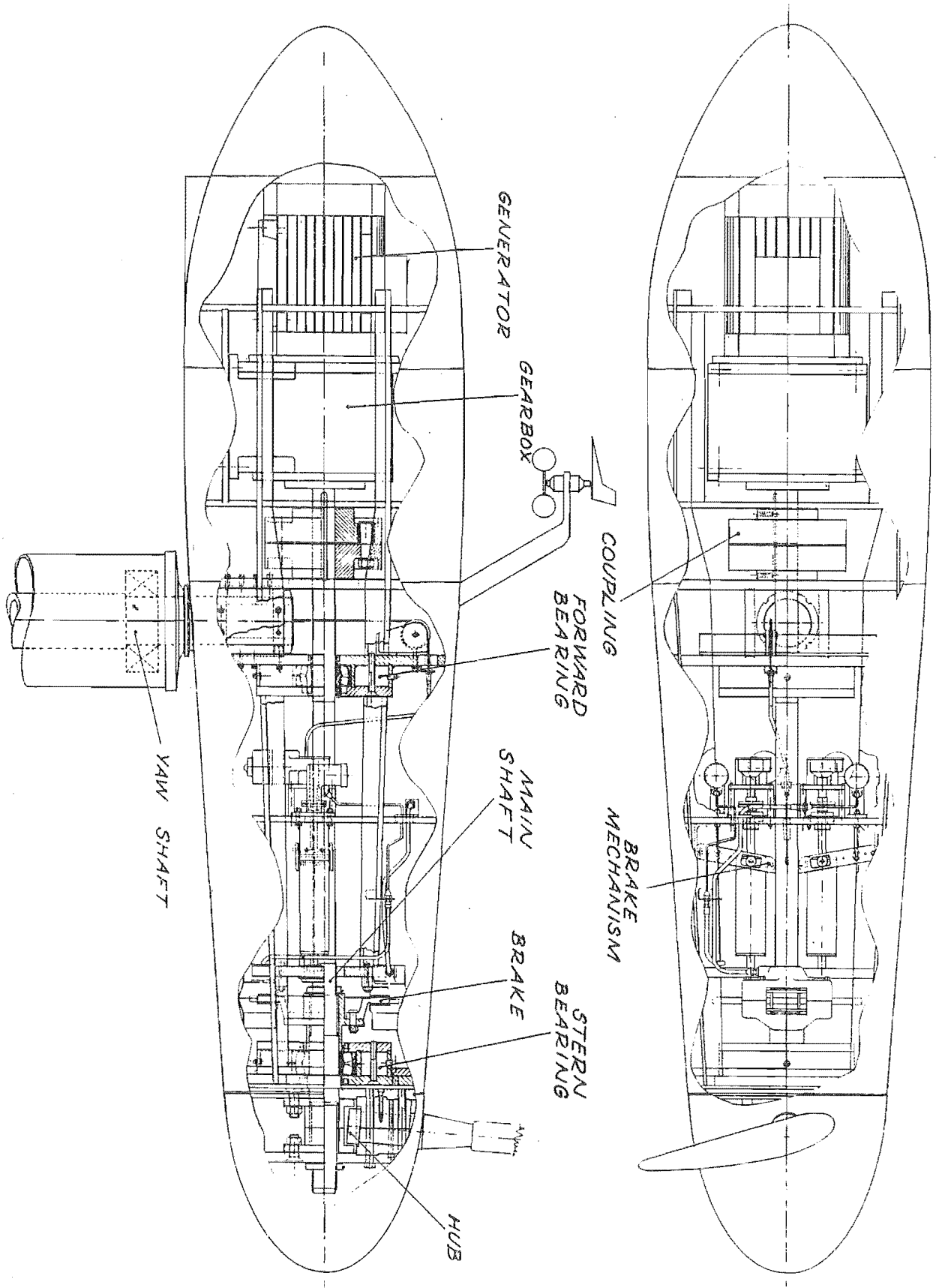

Figure 5.2: Pod Cutaway.

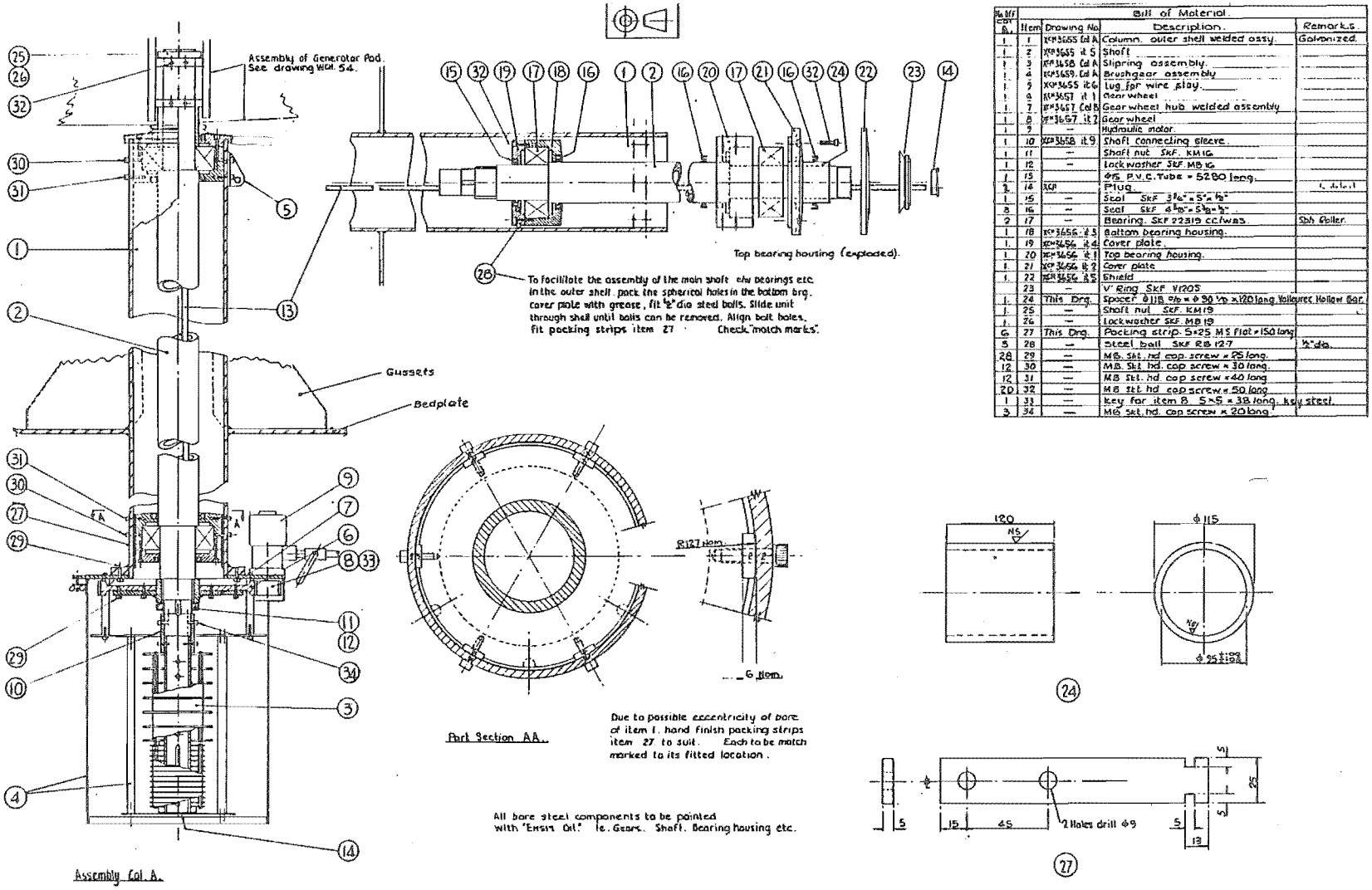

No. off Col. A.	Item	Drawing No.	Description.	Remarks
1	1	KP3655 Col A	Column. outer shell welded assy.	Galvanized.
1	2	KP3655 it 5	Shaft	
1	3	KP3658 Col A	Slipring assembly.	
1	4	KP3659. Col A	Brushgear assembly	
1	5	KP3655 it 6	Lug for wire stay.	
1	6	KP3657 it 1	Gear wheel	
1	7	KP3667 Col B	Gear wheel hub welded assembly	
1	8	KP3667 it 2	Gear wheel	
1	9	—	Hydraulic motor.	
1	10	KP3658 it 9	Shaft connecting sleeve.	
1	11	—	Shaft nut SKF. KM16	
1	12	—	Lockwasher SKF. MB16	
1	13		φ15 P.V.C. Tube = 5280 long.	
3	14	RCA	Plug	1 dia.
1	15	—	Seal SKF 3⅛" × 5" × ½"	
8	16	—	Seal SKF 4⅜" × 5⅛" × ½"	
2	17	—	Bearing. SKF 22319 cc/w33.	Sph Roller.
1	18	KP3656 it 3	Bottom bearing housing.	
1	19	KP3656 it 4	Cover plate.	
1	20	KP3656 it 1	Top bearing housing.	
1	21	KP3656 it 2	Cover plate	
1	22	KP3656 it 5	Shield	
	23	—	V Ring SKF V120S	
1	24	This Drg.	Spacer ϕ118.5 in × ϕ30 in × 120 long Tellurex Hollow Bar.	
1	25	—	Shaft nut SKF KM19	
1	26	—	Lockwasher SKF MB19	
6	27	This Drg.	Packing strip. 5×25 MS flat × 150 long	
5	28	—	Steel ball SKF RB 12.7	½" dia.
28	29	—	M6. Skt. hd cap screw × 25 long.	
12	30	—	M8. Skt. hd. cap screw × 30 long.	
12	31	—	M8 Skt. hd. cap screw × 40 long	
20	32	—	M8 Skt hd cap screw × 50 long	
1	33	—	key for item 8. 5×5 × 38 long. key steel.	
3	34	—	M6 skt. hd. cap screw × 20 long	

Figure 5.3: Support Structture Assembly.

5.2: Blades and Hub Assembly.

5.2.1: Design of Blades.

The blades have been designed for ease of construction and are composed of the three main parts shown in Figure 5.4. The spindles are of alloy steel, chrome plated over the entire surface to reduce rusting and subsequently heat treated to prevent hydrogen embrittlement. The spars are composed of four folded sections of 1.2 mm sheet galvanised steel which are riveted together with monel rivets, providing a very light and strong design. Each spindle and spar are connected using 5 mm countersunk screws along each of the four sides of the spars. To improve the strength of this joint the sheet steel is formed into the countersink of the screw holes in the spindle. Epoxy resin glue has also been used in order that water will not collect between the two surfaces.

The blade is formed with polyurethane foam sandwiched over 3mm marine ply to give added stiffness during construction. Refer to Figure 5.4. The polyurethane foam simply provides the form for the required profile and was shaped before bonding to the ply. The polyurethane is glued into the spar with epoxy resin and then sealed with a further coat of epoxy resin and covered with two layers of diagonally opposed 50mm wide, 165 gm. weight E-glass tape to give a total thickness of 5mm in epoxy resin. The ultimate tensile strength of the glass reinforced plastic (GRP) is 250MPa (Holloway 1978). The GRP skin is also directly bonded to the spar.

Load estimates have been made at four points, marked A,B,C,D on Figure 5.4, for two cases:-

(i) With the mill shutdown (locked rotor) and a 30 m/s wind impinging on to the blades at right angles. The blade is assumed to be a flat plate under this condition with a drag coefficient of 1.3 (calculated for a slender flat plate of ratio b/a=0.3/2.7 - Von Misis, p97, Fig. 53).

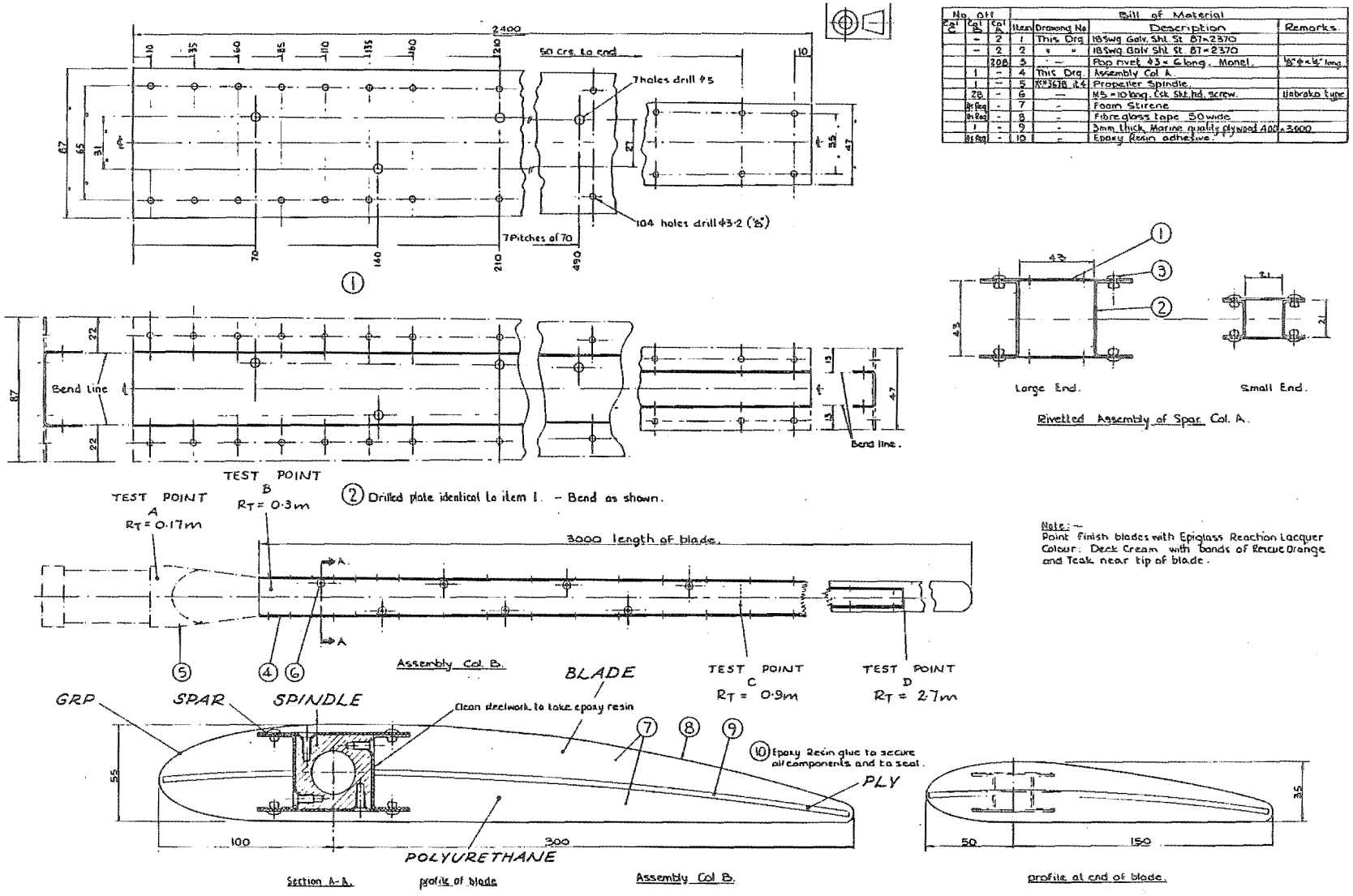

No. Off			Item	Drawing No	Description	Remarks
	–	2	1	This Drg	18 Swg Galv. Sht. St. 87×2370	
	–	2	2	" "	18 Swg Galv. Sht. St. 87×2370	
		208	3	– –	Pop rivet 4·3 × 6 long. Monel	⅛" ⌀ × ¼" long
	1	–	4	This Drg	Assembly Col A	
	1	–	5	X^P 3618 it 4	Propeller Spindle.	
	28	–	6	– –	M5 × 10 long. Csk. Skt. hd. screw.	Unbrako type
	As Req	–	7	–	Foam Stirene	
	As Req	–	8	–	Fibreglass tape 50 wide	
	1	–	9	–	3mm thick. Marine quality plywood 400 × 3600	
	As Req	–	10	–	Epoxy Resin adhesive.	

Note:–
Paint finish blades with Epiglass Reaction Lacquer Colour: Deck Cream with bands of Rescue Orange and Teak near tip of blade.

Figure 5.4: Blade Construction.

(ii) With the mill rotating (free rotor) at maximum speed and at a specified pitch angle in a 30 m/s wind speed. The pitch angle used is 75 degrees (true pitch of 15 degrees).

5.2.2: Locked Rotor Calculations.

The shear force at any test point on the blade will be given by the aerodynamic drag for the blade section beyond the test point and is:-

$$D = 1/2.\rho.C_D.S.U_1^2 \qquad (N) \qquad (5.1)$$

The moment acting as a result of this force is the drag times the effective radius at which the drag is considered to be operating at one point and is:-

$$M = D.r_d \qquad (Nm) \qquad (5.2)$$

The stresses at the test point are thus:-

$$\sigma_t = M/Z \qquad (MPa) \qquad (5.3)$$

$$\sigma_s = D/A \qquad (MPa) \qquad (5.4)$$

where Z is the section modulus and A the cross-sectional area of the test point. For test points A and B where the cross-sections are not composite the calculations are relatively simple. Point A has a simple hollow circular section as shown by Figure 5.5 and point B a hollow square section as shown by Figure 5.6.

The cross-section at point C is complicated by the other blade components forming a composite structure as shown by Figure 5.7. If the polyeurathane former and ply components are ignored, the section is composed of the spar and GRP components shown by Figures 5.8 and 5.9. In Figure 5.9, the GRP is approximated to an elliptical shape. In order to calculate the stresses in each component the two parts were assumed to share angle γ about the neutral axis n-n, as shown by Figure 5.10. The strain for each component can be estimated as:-

$$\Delta l_g/l = d_g.\tan(\gamma)/l = \varepsilon_g \qquad (5.5)$$

$$\Delta l_s/l = d_s.\tan(\gamma)/l = \varepsilon_s \qquad (5.6)$$

or

$$\varepsilon_g = (d_g/d_s).\varepsilon_s \qquad (5.7)$$

The modulus of elasticity for each part is:-

$$E_g = \sigma_{tg}/\varepsilon_g \qquad (5.8)$$

$$E_s = \sigma_{ts}/\varepsilon_s \qquad (5.9)$$

Equating (5.7), (5.8) and (5.9) gives

$$\sigma_{tg} = (d_g/d_s).(E_g/E_s).\sigma_{ts} \qquad (5.10)$$

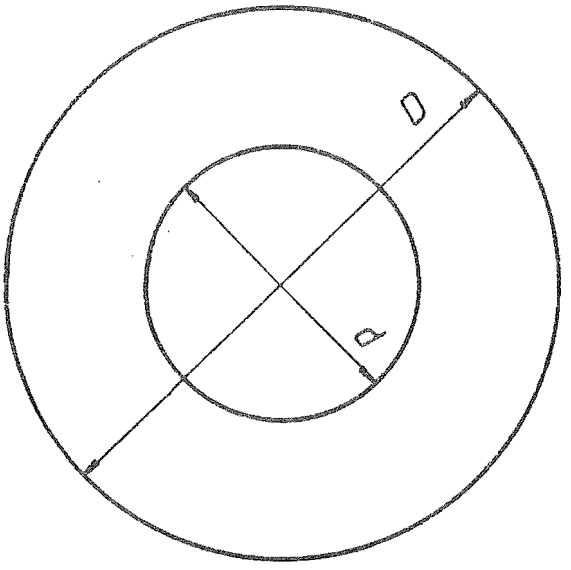

Figure 5.5: Point A Cross Section.

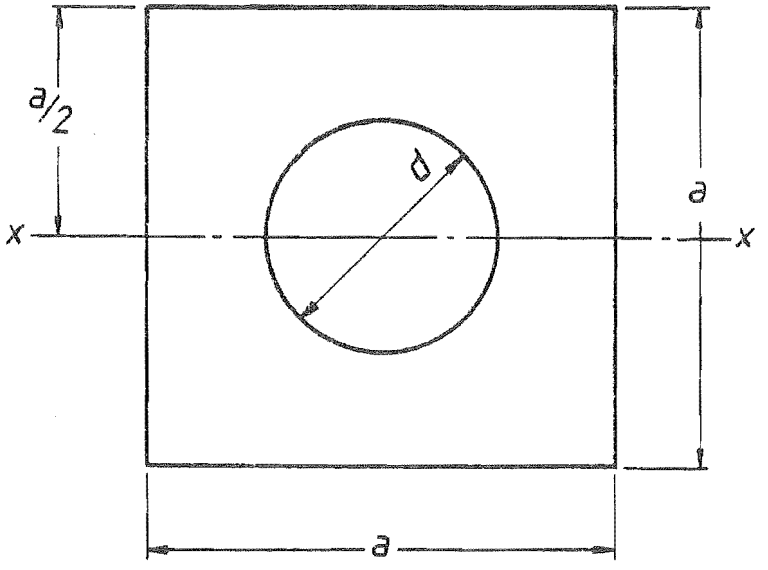

Figure 5.6: Point B Cross Section.

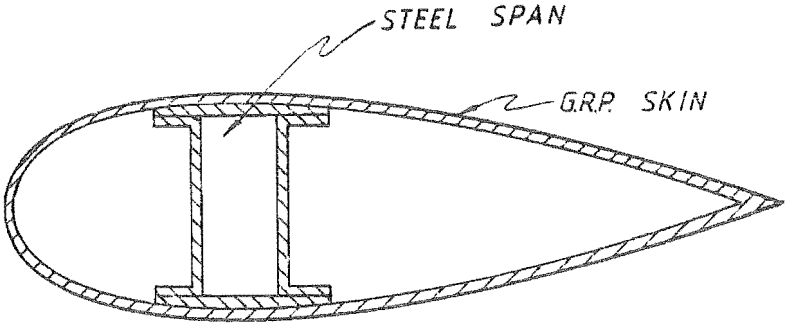

Figure 5.7: Point C Cross Section.

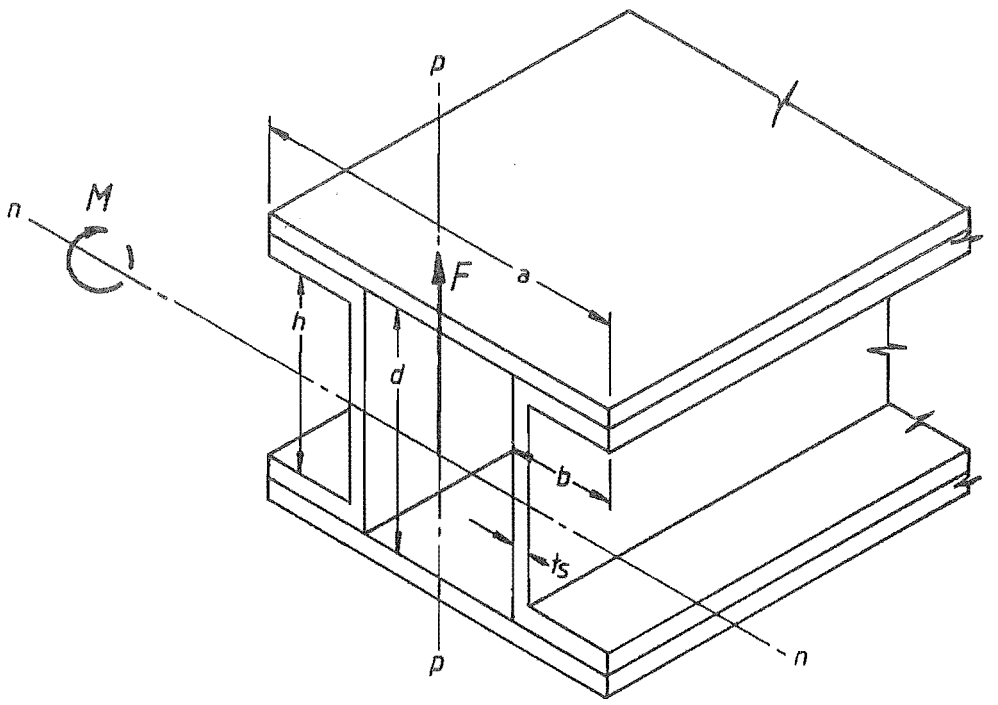

Figure 5.8: Point C Spar Cross Section.

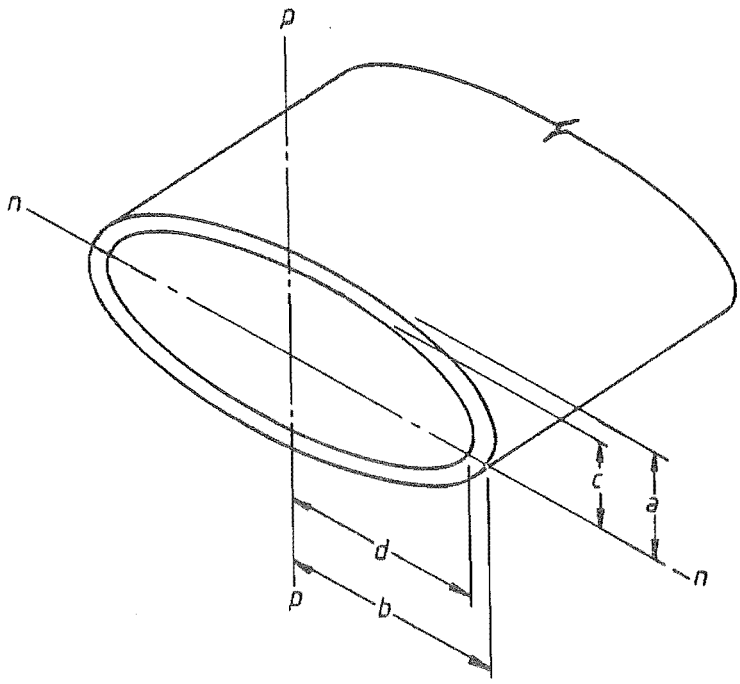

Figure 5.9: Point C GRP Cross Section.

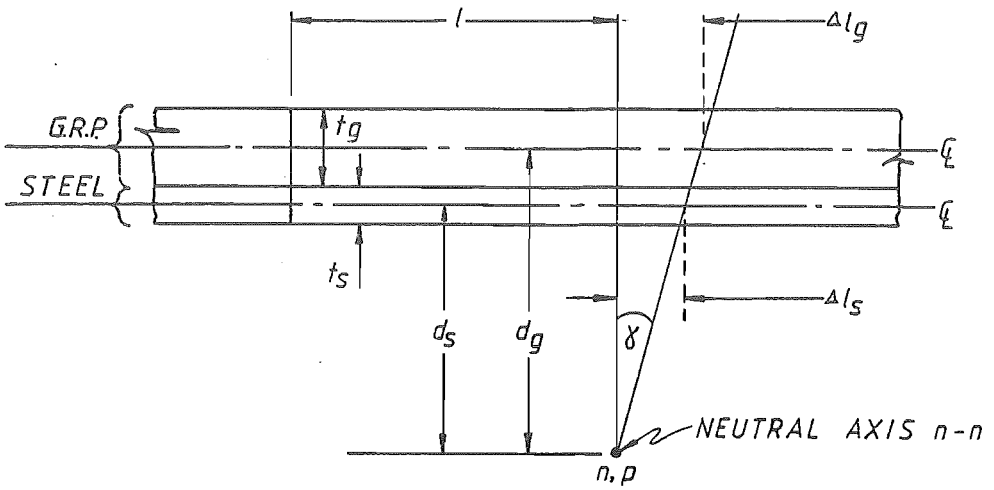

Figure 5.10: GRP/Steel Strains, nn Axis.

Since d_g, d_s, E_g and E_s are all known values, the GRP stress can be calculated as a fixed fraction of the steel stress. So far as the stresses induced by bending alone are concerned,

$$\sigma_{ts} = M_s/Z_s \qquad (5.11)$$

$$\sigma_{tg} = M_g/Z_g \qquad (5.12)$$

where M_s and M_g are the relative portions of the bending moment taken by the spar and GRP respectively and if M is the total moment, then:-

$$M = M_s + M_g \qquad (5.13)$$

Equating (5.10), (5.11), (5.12) and (5.13) gives:-

$$M_g = M.K/(1 + K) \qquad (5.14)$$

where

$$K = (d_g/d_s).(E_g/E_s).(Z_g/Z_s) \qquad (5.15)$$

The total moment can be calculated from Equation (5.2), and hence the steel and GRP tensile stresses can be estimated. Also, if the spar is assumed to carry all of the shear stress, then:-

$$\sigma_{ss} = D/A_s \qquad (5.16)$$

At point D the situation is again simple since the GRP is carrying all of the load, and the section is as shown in Figure 5.9. The stesses are thus:-

$$\sigma_t = M/Z_g \qquad (5.17)$$

$$\sigma_s = D/A_g \qquad (5.18)$$

For the four test points on the blade the results of the calculations for the locked rotor case are as shown in Table 5.1.

Point A tensile stress	42 MPa (26)
Point A shear stress	1 MPa (*)
Point B tensile stress	55 MPa (20)
Point B shear stress	< 1 MPa (*)
Point C tensile stress, spar	33 MPa (12)
Point C shear stress, spar	1 MPa (*)
Point C tensile stress, GRP	4 MPa (63)
Point C shear stress, GRP	-
Point D tensile stress	< 1 MPa (*)
Point D shear stress	< 1 MPa (*)

Figures in parentheses indicate safety factors

* indicates a safety factor > 100

Table 5.1: Locked Rotor Blade Loads.

5.2.3: Free Rotor Calculations.

In the free rotor calculations the effects of the centrifugal forces must be added to the aerodynamic effects, and it is therefore required to calculate the mass and radius of gyration for the structure. For point A, the calculation includes the spindle, spar and blade and the radius of gyration is:-

$$r = \sqrt{(I_{sp} + I_{s} + I_{b})/m} \qquad (5.19)$$

where I_{sp}, I_{s}, I_{b} are the moments of inertia for spindle, spar and blade respectively. The interation of centrifugal force and coning angle are shown by Figure 5.11. The direct centrifugal force F_{t} is composed of two components, F_{B} along the blade and F_{A} normal to the blade. The effect of F_{B} is to directly add tensile stress at the test point. The effect of F_{A} is to subtract from the axial drag moment.

$$F_t = m.\Omega^2.r \qquad (5.20)$$

$$F_A = F_t.\sin(\delta) \qquad (5.21)$$

$$F_B = F_t.\cos(\delta) \qquad (5.22)$$

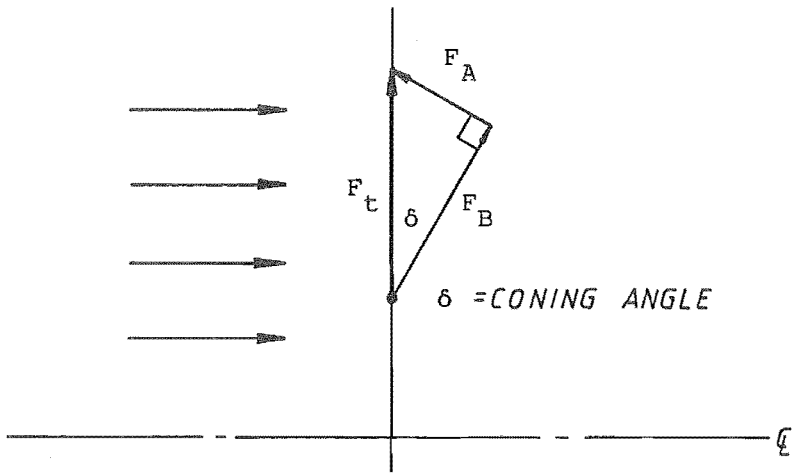

Figure 5.11: Centrifugal Force Effects.

Since the blade is inclined at a pitch angle θ , it has components normal to the plane of the blade and also along the plane (chord) of the blade, and are:-

$$F_{AN} = F_A.\sin(\theta) \qquad (5.23)$$

$$F_{AP} = F_A.\cos(\theta) \qquad (5.24)$$

For a test radius of R_T the moments can also be calculated as:-

$$M_{AN} = (r - R_T).F_{AN} \qquad (5.25)$$

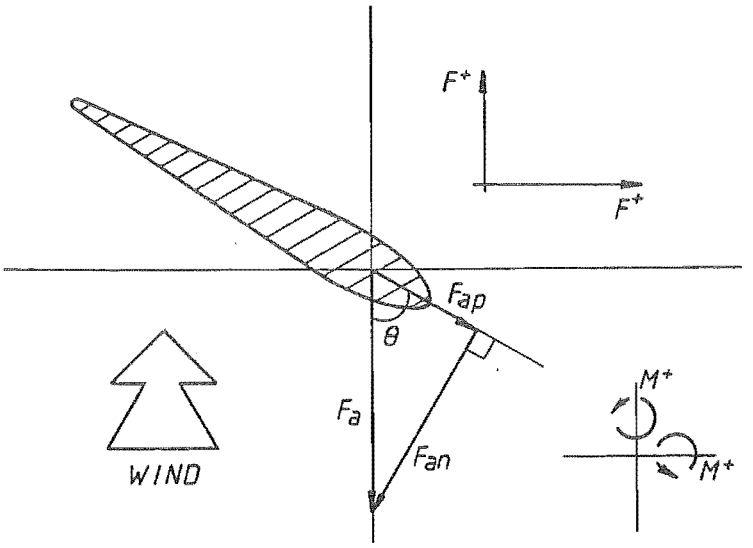

Figure 5.12: Centrifugal/Coning Forces.

$$M_{AP} = (r - R_T).F_{AP} \qquad (5.26)$$

The aerodynamic loadings on the blades are found using Equations (2.38) to (2.41). These equations have been implemented in a computer program BLADEB, the results of which can then be used in conjunction with the centrifugal effects. The results of BLADEB are shown in Appendix 1. The forces at the test point along the plane (chord) of the blade and normal to this are F_{PT} and F_{NT} . The associated moments are M_{PT} and M_{NT} .

Combining the centrifugal effects with the aerodynamic effects:-

$$F_P = F_{PT} + F_{AP} \qquad (5.27)$$

$$F_N = F_{NT} + F_{AN} \qquad (5.28)$$

$$M_P = M_{PT} + M_{AP} \qquad (5.29)$$

$$M_N = M_{NT} + M_{AN} \qquad (5.30)$$

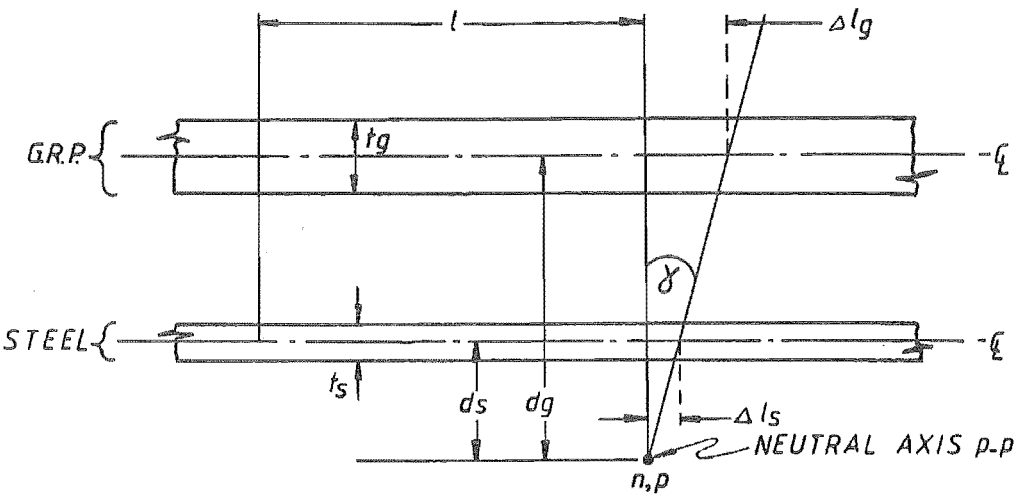

Figure 5.13: GRP/Steel Strains, pp Axis.

For test points A, B, D the stress calculations are relatively simple since the cross-sections are non-composite and:-

$$\sigma_t = (M_P/Z_P) + (M_N/Z_N) + (F_B/A) \qquad (5.31)$$

$$\sigma_s = \sqrt{F_P^2 + F_N^2}\ /A \qquad (5.32)$$

where Z_N is the section modulus about the n-n neutral axis and Z_P is the section modulus about the p-p neutral axis. For test point C the structure is composite. For the normal moments the calculation is similar to that used in the fixed rotor case for the composite structure. For the plane moments, a similar principle has been used as shown by Figure 5.13. The resulting equations are similar to those previously used. For conditions outlined in 5.2.1, the results of the calculations are given in Table 5.2.

Point A tensile stress	54 MPa (20)
Point A shear stress	< 1 MPa (*)
Point B tensile stress	90 MPa (12)
Point B shear stress	< 1 MPa (*)
Point C tensile stress, spar	80 MPa (5)
Point C shear stress, spar	< 1 MPa (*)
Point C tensile stress, GRP	9.3 MPa (27)
Point C shear stress, GRP	-
Point D tensile stress	2.5 MPa (100)
Point D shear stress	< 1 MPa (*)

Figures in parentheses indicate safety factors

* indicates a safety factor > 100

Table 5.2: Free Rotor Blade Loads.

5.2.4: Hub Assembly.

The hub assembly is shown in Figure 5.14. Torque is transmitted from the hub to the main shaft through a 16 tooth spline. Hub stress calculations have been made assuming all load is taken on one clamp plate only, with loading coming from the generator input torque and also from the aerodynamic and centrifugal effects on the blades. The generator was assumed to be running at full load and the additional loading estimated by using the free rotor equations of 5.2.3 giving a clamp plate stress (tensile) of 4.2 MPa with a safety factor of 95. The clamp bolt stress is 15.7 MPa with a safety factor of 70.

5.3: Drive Train.

The main shaft, shown in Figure 5.15 is of alloy steel, machined and stress relieved. The stern bearing is a spherical roller bearing of 60 mm bore and carries all axial load and all radial load on the hub end. The forward bearing is a spherical roller, taper sleeve bearing of 45 mm bore.

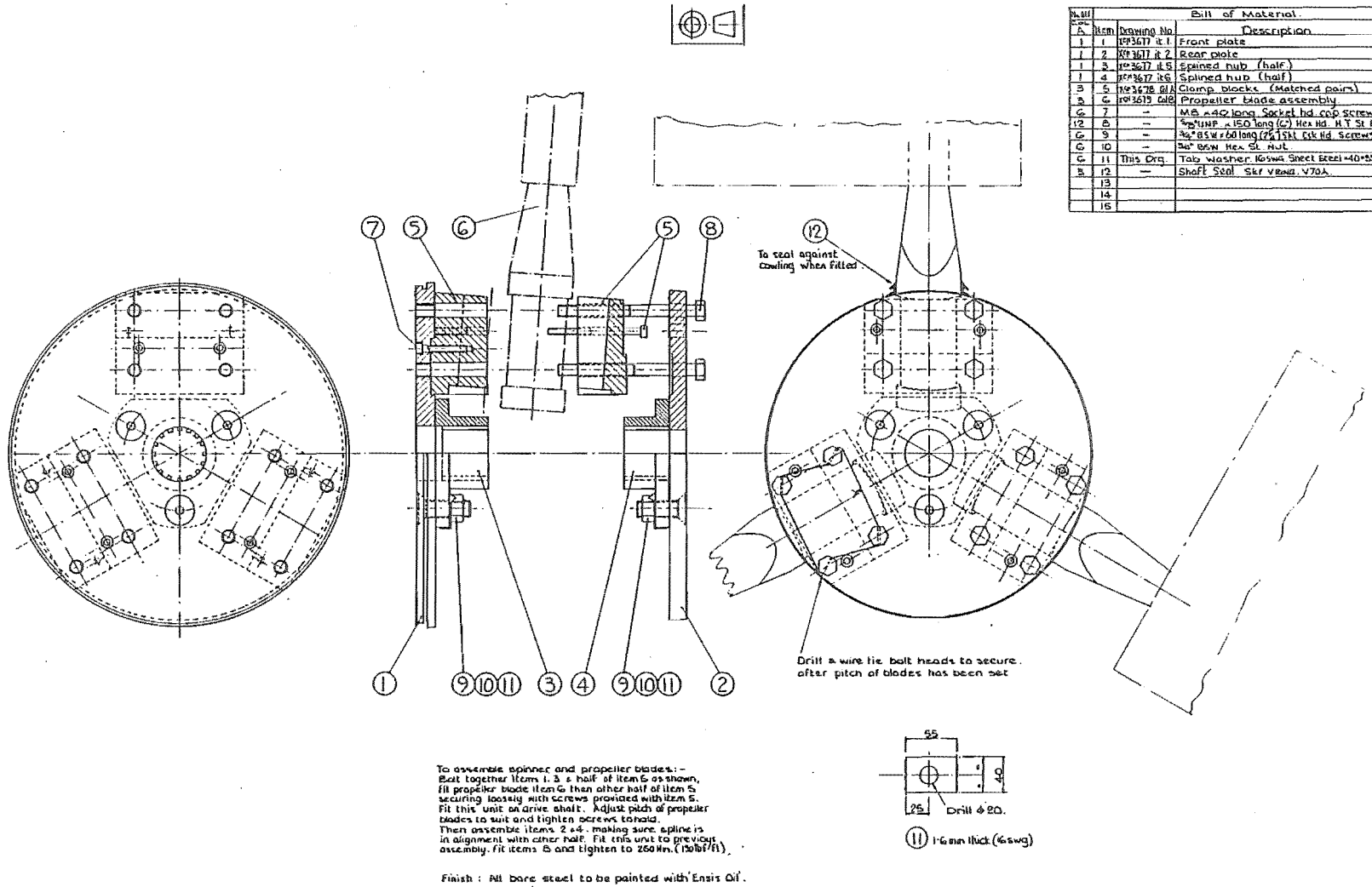

Figure 5.14: Hub Assembly.

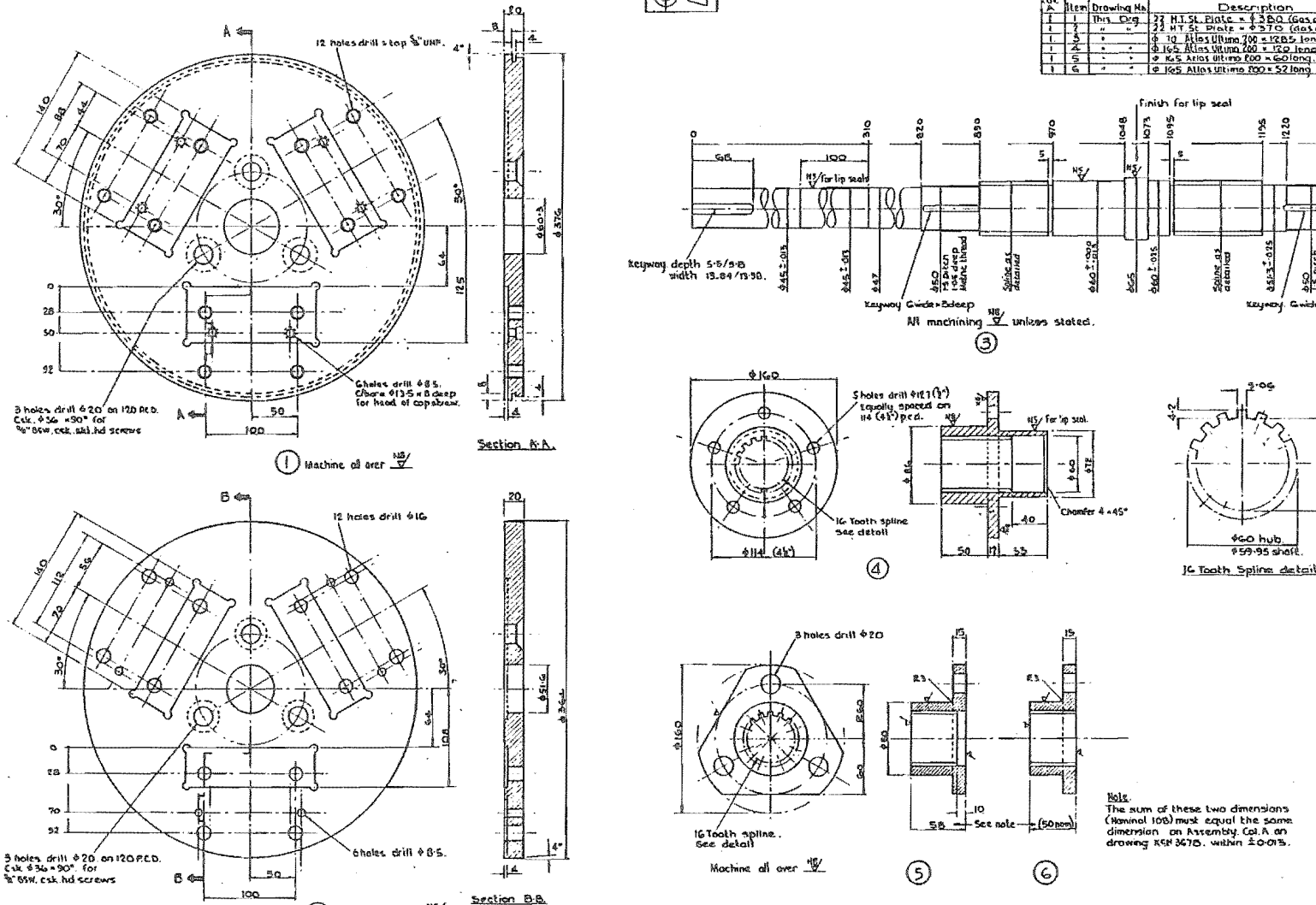

Figure 5.15: Main Shaft Details.

Both bearings run in oil baths. The hub drives the shaft through a 16 tooth spline. The brake hub also uses a 16 tooth spline. The flexible coupling is of the multiple pin type keyed to the shafts and is rated at 20 kw at 100 rpm. The gearbox is of 15 kw rating, 1:10 step up with helically cut gears running in an oil bath.

The main shaft loadings are outlined in Figure 5.16. The loadings assume a precession couple to be present:-

$$M = H.\dot{\varphi} \qquad (5.33)$$

where H is the angular momentum of the mill and

$\dot{\varphi}$ is the angular velocity of yaw.

and

$$H = I.\Omega \qquad (5.34)$$

where I is the moment of inertia of the hub and blades (gearbox, generator, coupling are ignored).

The axial force was estimated from program BLADEB, and the torsional load calculated for full generator loading. A misbalance of 1 Kg midway along a blade was assumed. The precession couple was estimated for 200 rpm on the main shaft with 6 rpm on the yaw axis. The main shaft combined stresses are summarized in Table 5.3.

Splines on the main shaft were designed according to standard practice (Oberg 1966) and bearing selection was made according to manufacturers standard instruction. The results are also shown in Table 5.3.

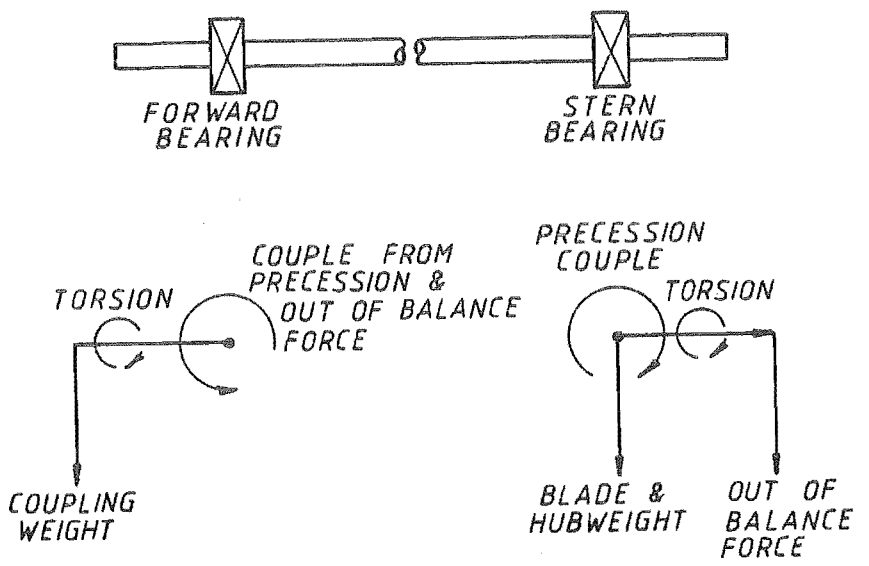

Figure 5.16: Main Shaft Loads.

Member	Stern End	Foward End
Main shaft tensile stress (max)	58 MPa (19)	138 MPa (8)
Main shaft shear stress (max)	40 MPa (21)	95 MPa (9)
Main shaft spline stress	0.2 MPa (*)	
Bearing load dynamic	2.2 kN (90)	
Bearing load static	3.9 kN (40)	

Figures in parentheses are safety factors.

* indicates safety factor > 100

Table 5.3: Main Shaft Assembly Loads.

5.4: Support Column.

The support column is a seamless pipe of 254 mm inside diameter and 19 mm wall thickness, seamless pipe being employed due to its ease of use, ie., bearings are easily mounted inside the pipe. It supports two 95 mm bore

spherical roller bearings through which the yaw shaft passes. Spherical roller bearings have been selected because of their ability to carry both radial and axial loads as well as being self aligning. The shaft is a 112 mm outside diameter and 63 mm inside diameter hollow bar which is bolted into the nacelle to facilitate separation of the nacelle and support structure. The bearings are grease packed and sealed. The lower bearing takes none of the axial loading. The column is welded into a 12 mm thick bed plate of 1500 mm sides and strengthened by four triangular gussets of 500 mm sides. The bedplate can simply be bolted to the steel lattice tower. Refer to Figure 5.3.

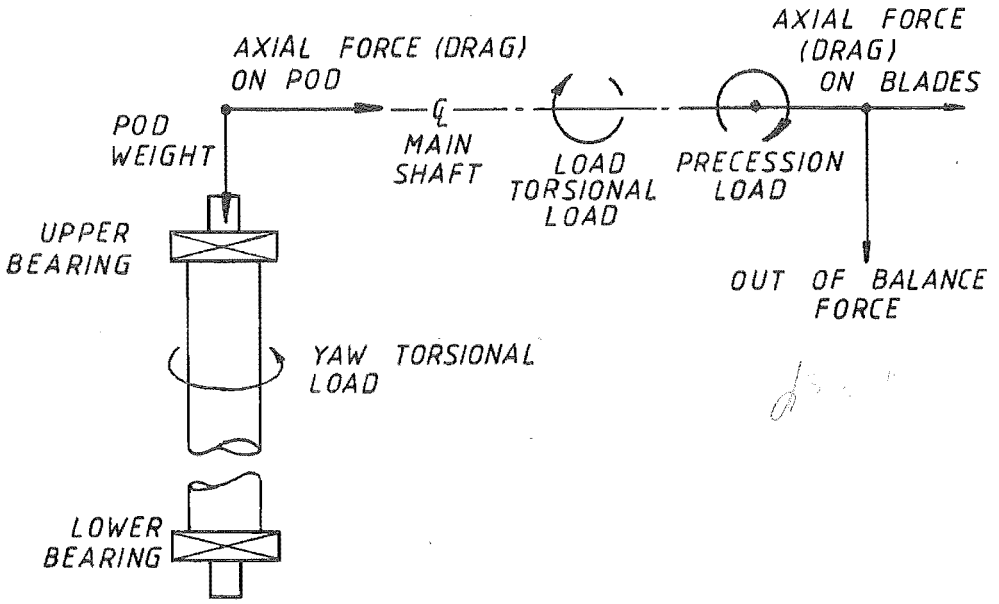

Figure 5.17: Yaw Shaft Loads.

The critical point in the upper region of the support structure occurs where the shaft extends past the upper bearing, and the shaft carries all of the load. The compressive and shear stresses are calculated by considering the shaft as a simple circular hollow section.

At the bed plate level the effects of the column must also be considered. This is done by considering the shaft and column as sharing bending, but the column only as taking all compressive loading since the lower bearing does not carry axial load. Table 5.4 gives a summary of the results.

Although the shaft is rotating only very slowly both dynamic and static calculations were made for the bearings, the results of which are given in Table 5.4 for the upper bearing only.

The spline which transmits the load between the shaft and the hydraulic motor is a 16 tooth spline of 90 mm major diameter. The load was assumed to be that required to drive the mill through a 30 m/s wind with the blades flat on to the wind.

The herringbone gear and pinion are of malleable cast iron with a pinion PCD of 58 mm and 18 teeth. The gear has a PCD of 420 mm and 134 teeth giving a ratio of 7.44:1. The ultimate tensile strength of the iron is 330 MPa with an ultimate shear strength of 200 MPa. Applying the same load conditions as for the spline gives the figures shown in Table 5.4.

Yaw shaft stress compressive, upper	35 MPa (11)
Yaw shaft stress shear, upper	19 MPa (11)
Yaw shaft stress compressive, lower	9 MPa (44)
Yaw shaft stress shear, lower	6 MPa (33)
Column stress compressive	7.5 MPa (53)
Column stress shear	3.7 MPa (54)
Upper bearing load, dynamic	20.96 kN (19)
Upper bearing load, static	13.26 kN (33)
Yaw shaft spline load	1150 Nm (58)
Yaw drive gear load	1150 Nm (11)
Yaw drive pinion load	155 Nm (11)

Figures in parentheses are safety factors.

Table 5.4: Yaw Shaft Assembly Loads.

5.5: Hydraulics.

5.5.1: Yaw Drive Hydraulics.

The yaw drive has three functions:-

(i) Under normal running conditions the hydraulic motor acts as a pump and forces the hydraulic oil through restrictors. This has the function of damping the yaw of self steering of the mill. In this state all hydraulic valves are in the rest position.

(ii) Under shutdown conditions the mechanism is used to steer the mill sideways into the wind before brake application. The direction of rotation is dependent on the relative positions of the wind direction and mill orientation (as detected by the wind vane) such that the least degrees of rotation are required for alignment. The pump drives fluid through the now energised Valves 1 and 2. The yaw direction will depend on which one of the two solenoids of Valve 2 are energised.

(iii) To lock the yaw, either solenoid of Valve 2 can be operated, but not both. Valve 1 must be in the rest position. The yaw is normally locked after the turbine has come to rest after braking.

The hydraulic motor is of a 5.7 kw continuous rating and is connected to a separate pump unit via two flexible hoses and a stop cock. The pump is driven by a three phase mains operated motor of 1.1 kw rating. Two spool valves are used to control flow as shown in Figure 5.18. Valve 1 is a 4/2 valve and Valve 2 is a 4/3 valve, both 12 volt solenoid operated and controlled from the Tower Control Unit. Figure 5.19 gives the truth table for the system.

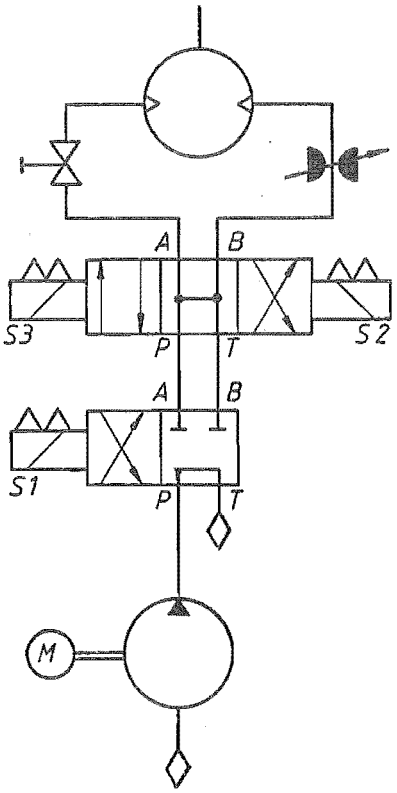

DIRECTION CONTROL VALVE (4/3)

Valve 2

MODE CONTROL VALVE (4/2)

Valve 1

Figure 5.18: Yaw Drive Hydraulics Circuit.

S2 \ S3	0	1
0	RUN	N/U
1	LOCK	N/A

OPERATION

S1 = 0

S2 \ S3	0	1
0	N/U	ROTATE CCW
1	ROTATE CW	N/A

OPERATION

S1 = 1

N/U = NOT USED
N/A = NOT ALLOWED

Figure 5.19: Yaw Drive Hydraulics Truth Table.

5.5.2: Brake Hydraulics.

The brake system is shown in Figure 5.20. Each of the two separate systems are supplied from isolated sources within the pod. Spring action is added into the operation in the compression cylinders so that the force applied to the hydraulic cylinder is dependent on servo displacement. Operation of the servos causes the springs to compress or release and by a lever system increase or release the hydraulic pressure. The brake control system has been designed in a closed loop form and is further discussed in Chapter 6.

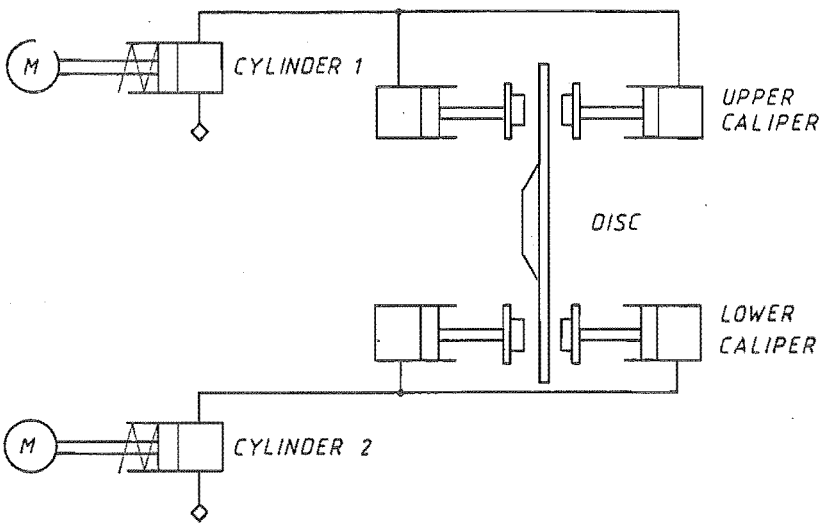

Figure 5.20: Brakes Hydraulics.

5.6: Summary.

Construction of the mechanical components of the wind turbine generator has been described with particular importance placed on the aerodynamic and centrifugal loadings of the blades. Loadings on other components have also been discussed, along with a description of the hydraulic systems. Calculated factors of safety indicate that the turbine should operate satisfactorily in wind speeds up to 30 m/sec.

CHAPTER 6.

CONTROL SYSTEM.

6.1: Introduction.

6.1.1: Control System Requirements Defined.

Flexibility is of prime importance in the design of the control system in order that variations in control and operation of the wind turbine generator are possible for future experiments. The philosophy of control system flexibility necessitates the design and construction of a general purpose main controller. Flexibility would be enhanced by the use of software for control and can provide a simple means of modifying control algorithms.

Functions required of the control system are:-

.Control of generator load so that wind turbine load can be controlled. This is the main control loop and is described in Chapter 7. The loop consists of reading wind speed to determine wind power available and then modifying rectifier delay angle to set the actual load power to a suitable value. Actual load power is to be determined form reading DC output voltage of the rectifier applied to a fixed load resistance.

.Sensing of control parameters including analogue and digital points. These parameters are used for indication as well as for control functions. Major parameters input include wind speed and rectifier output voltage for the main control loop and shaft speed, AC voltage and digital status signals for safety checking routines.

.Output of control parameters. These consist of both analogue signals and digital status signals. Rectifier delay angle is the main output

analogue signal. Status signals required for system startup and shutdown are also required to be output.

.Control of startup and shutdown sequencing for the wind turbine. Shutdown sequencing is to be independent of the main controller to cover the events of main controller software or hardware failure.

.Detection of failure of the main controller software or hardware. A circuit independent of the processor is required to detect processor failure and initiate shutdown procedure if it occurs.

.Detection of extreme operating conditions which would necessitate system shutdown. This includes the situations of excess wind speed and shaft speed and excess generator load.

.Sensing of failure of control circuits such as battery charger failure, DC supply undervoltage and failure and phase failure of the generator output.

.Security of controls where safety constraints are of importance. For instance, in the case of brake application where partial failure of the brake system should not prevent shutdown.

.To allow for the connection of data logging equipment for long term recording and also for the connection of telemetering equipment. Telemetery may be required in the case of installation of the wind turbine at a remote site.

.The system is to allow for fully automatic, semi-automatic and fully manual methods of control. For the fully automatic method, the processor is to have total control over all system functions. In cases where the operator requires control over some functions the processor is to censor operator requests to ensure that the system remains secure. A manual method of control is also required which will bypass the processor in all control functions.

6.1.2: Control System Layout.

The control system for the wind turbine generator is outlined in terms of physical locations in Section 6.1.2 followed by a functional description in Section 6.2. The design and operation of each unit in the system is then described in ensuing sections.

The wind turbine generator bases its control in three major areas as shown by Figures 6.1 and 6.2.

(A) The ground controls consist of five main components:-

(i) The main controller or processor which reads various analogue and digital points in the system, decides on what control action is necessary and then outputs the appropriate analogue or digital control parameters.

(ii) The control panel. This gives the operator an opportunity to observe system status and if deemed necessary to intervene in the plant operation.

(iii) The controllable rectifier which takes the 3 phase variable frequency, variable voltage from the generator and converts it to direct voltage. The rectifier is controlled from the processor or panel.

(iv) The interface rack. All signals to and from the processor and to and from the tower-ground cable pass through this rack. It provides the appropriate signal levels and conditioning.

(v) Power supplies for all ground controls. These include isolated supplies for the AC and DC voltage transducers.

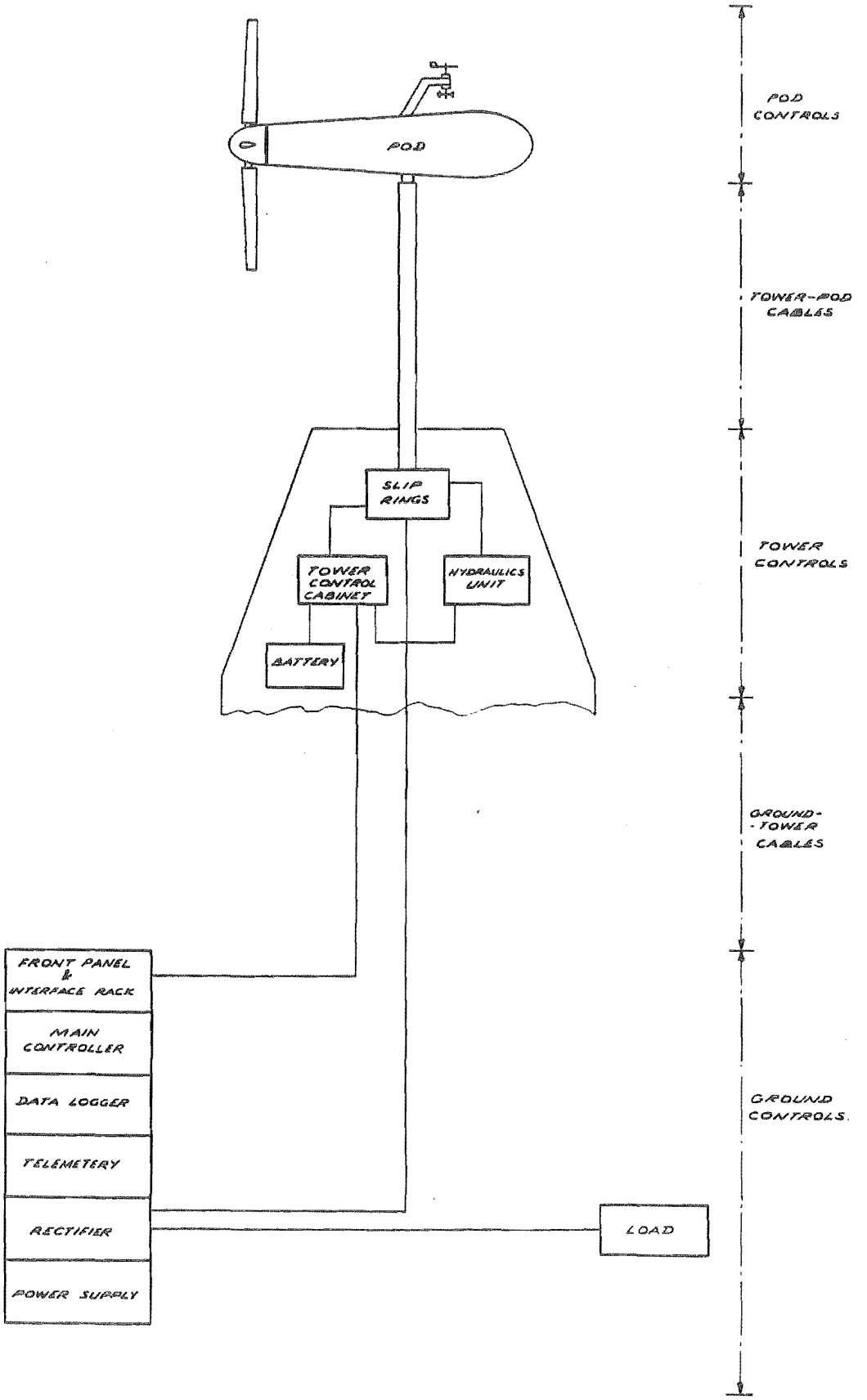

Figure 6.1: Control Centre Locations.

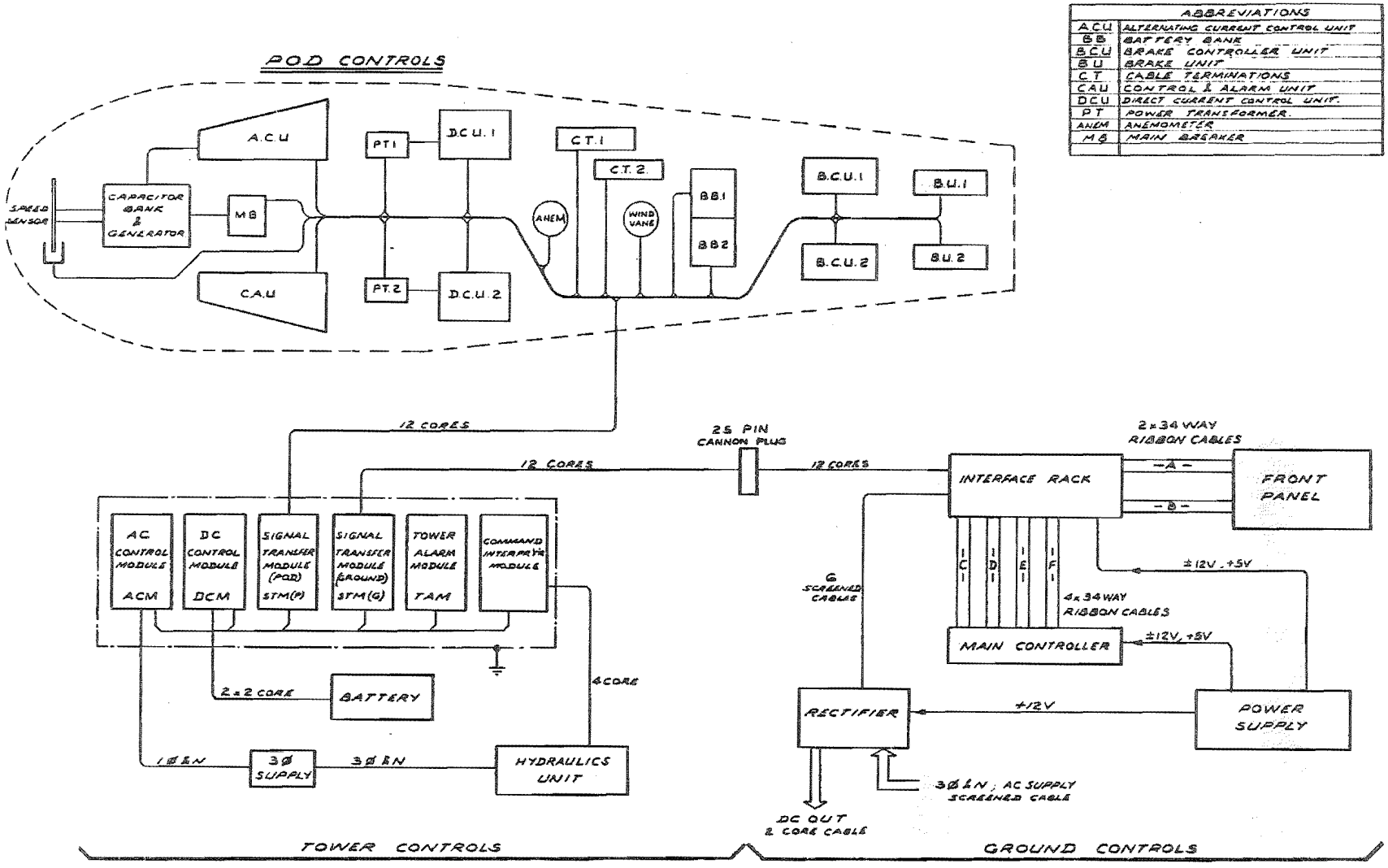

Figure 6.2: Control System Layout.

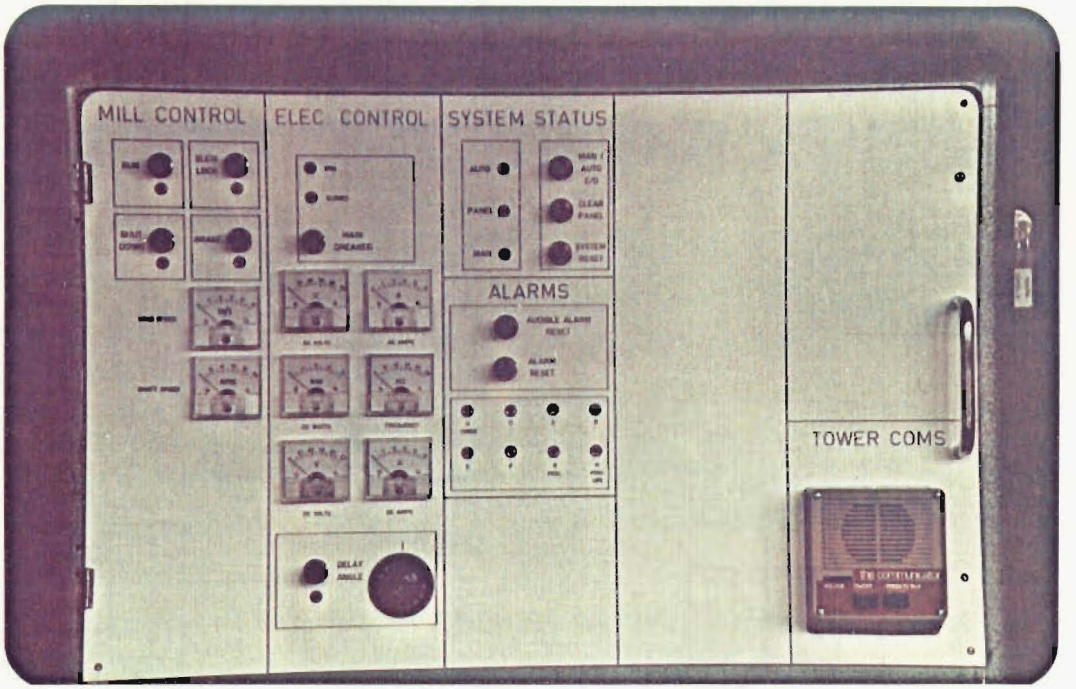

Plate 6.1: Ground Controls.

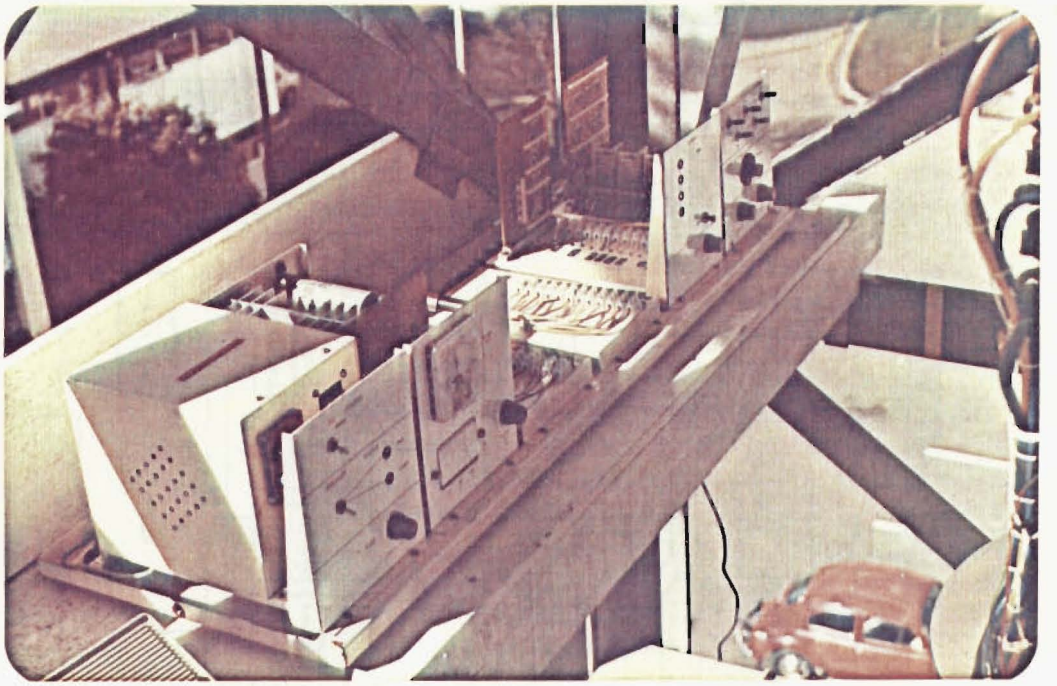

Plate 6.2: Tower Controls.

Connection from the ground controls to the tower controls is via a twelve core cable. Generator power reaches the recifier by a seperate three phase earth screened cable.

(B) The tower controls perform two functions:-

(i) To provide interconnection and buffering between the pod controls and ground controls.

(ii) To provide control of the yaw drive hydraulics and subsequent braking.

In addition, support equipment is necessary in the form of battery storage for electronics and the appropriate battery charging networks.

Generator power and signals run from slip rings at the support column base to the pod through the yaw shaft.

(C) Pod controls are divided into several units:-

(i) The AC Control Unit which controls the main breaker and generator excitation, as well as checking for generator phase failure.

(ii) The Control and Alarm Unit which collects information from alarm points and passes the alarm to the tower controls. It also drives the wind speed, shaft speed and wind vane tranducers.

(iii) The DC Control Units. Each of these two units provides battery charging for the pod battery banks as well as controlling the battery preservation circuits. Battery charger supply comes from the load side of the breaker.

(iv) Battery Banks. Each of the two banks provides 12V for pod electronics. Protection and switching relays are also incorporated.

(v) Brake Control Units. Each of these two units controls the deceleration rate of the main shaft of the mill under braking conditions and brake release control logic.

(vi) Brake Units. Each of these two units provides the hydraulic actuation of the brakes and are controlled from the brake control units.

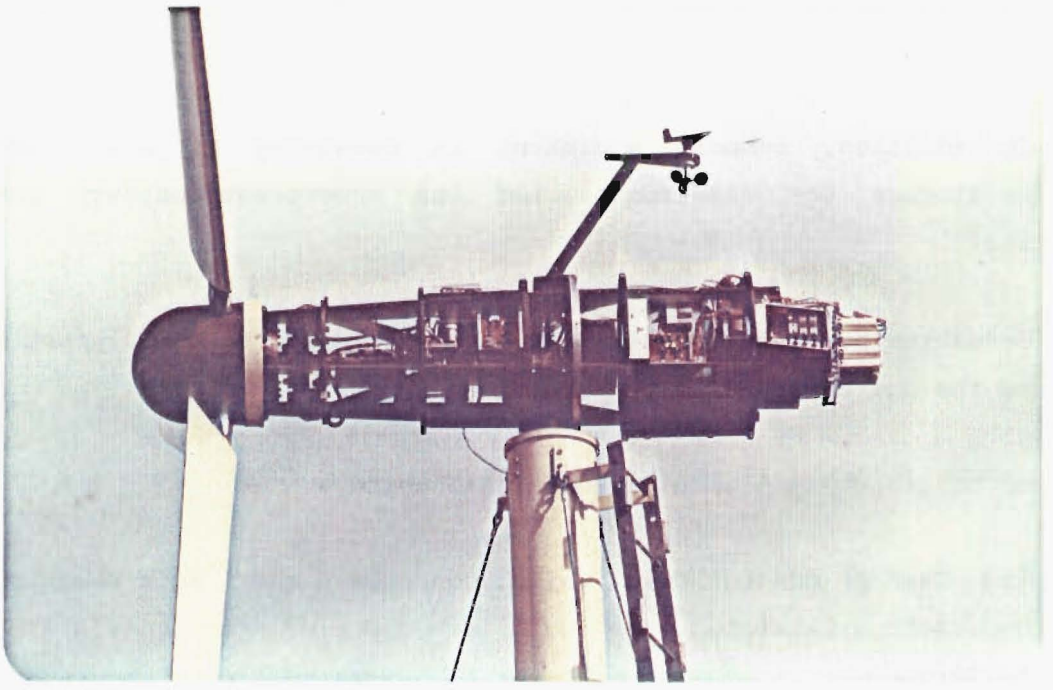

Plate 6.3: Pod Controls.

6.2: Control System - Functional Operation.

Functional operation of the control system is in four areas as follows.

6.2.1: Mill Control

The mill controls encompass all aspects of the mechanical operation of the mill, as shown by Figure 6.3.

At ground level the mill is controlled either from the panel (manual or panel) or from the processor (auto). The machine is allowed to operate in one of the four modes shown, and indication of the mode is given on the panel.

(1) RUN

Normal mode is RUN and is characterized by normal windmill operation where the yaw drive is free to rotate as determined by the current wind direction.

(2) SHUTDOWN

The SHUTDOWN mode is initiated when it is requred to terminate operation of the mill. The wind turbine may be required to be shutdown, ie., stopped for a variety of reasons. The possible causes of a shutdown command being issued are:-

(i) Processor Failure.

If the processor has been detected as failed the turbine is automatically shutdown by sub-control circuits.

(ii) At Operator Request.

The operator may wish to shut the turbine down to carry out maintenance.

(iii) At Processor Request.

The processor continually checks a number of parameters such as wind speed, shaft speed, etc. If these exceed predetermined values the processor will order a shutdown.

In each case the procedure for shutdown is similar. The command to shutdowm is received by the tower controls which then detect whether or not the turbine is aligned sideways with the wind in order to minimise input power to the shaft. This is done by the use of a wind vane mounted

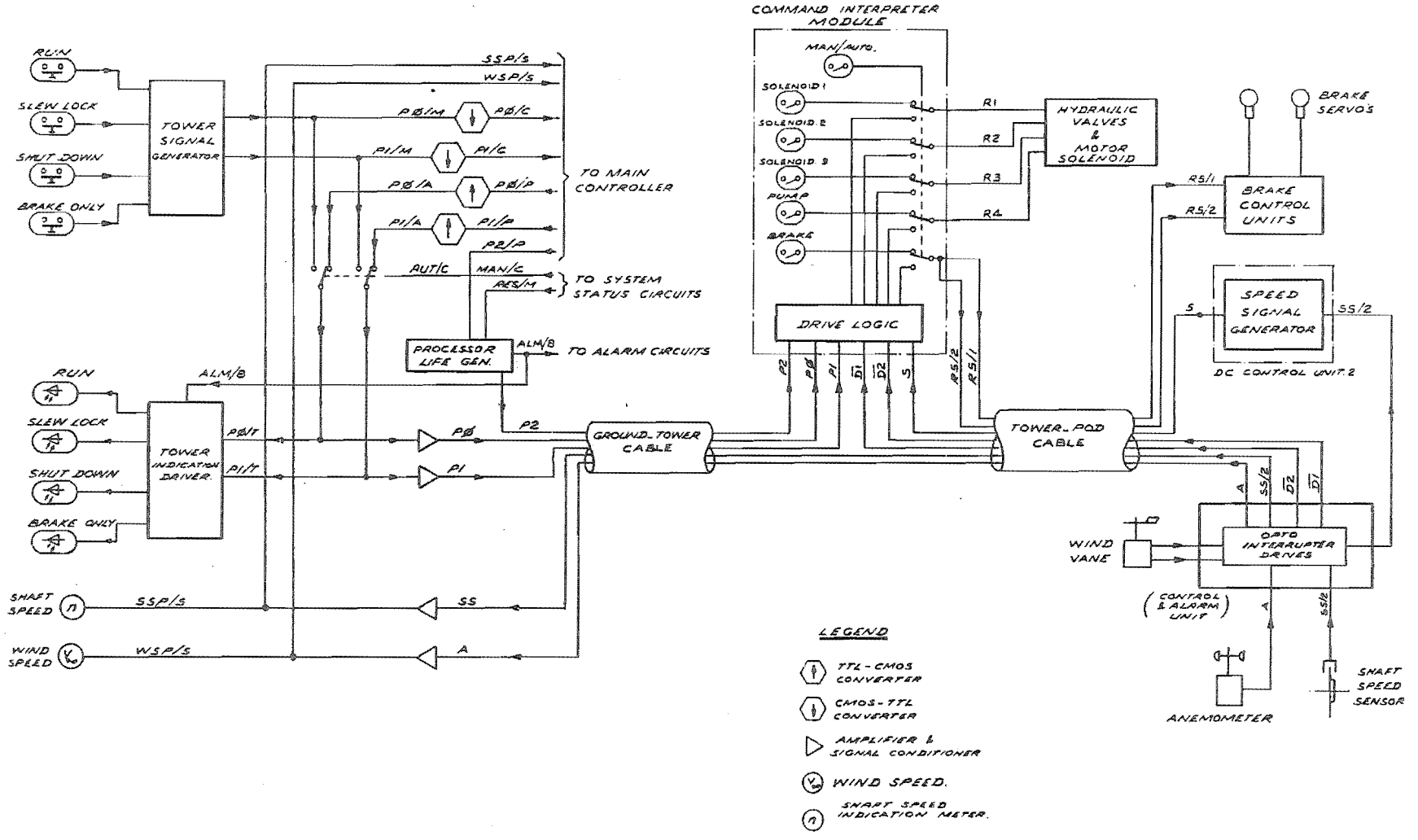

Figure 6.3: Mill Control Schematic.

on the pod. If the alignment is incorrect, the yaw hydraulics will start and rotate the pod to achieve correct alignment. When alignment is achieved, the brakes are applied and, on cessation of main shaft rotation, the yaw drive is locked.

(3) SLEW LOCK

SLEW LOCK is not normally requested from the ground unless in the manual state. This mode locks the yaw drive of the mill. The SLEW LOCK mode is used on the termination of shutdown procedure.

(4) BRAKE ONLY

BRAKE ONLY mode is not normally requested from ground, unlesss in emergency circumstances and only in the manual state. Processor software prevents a BRAKE ONLY command being issued in the auto or panel state.

These four modes generate the signals on three lines P0, P1, P2, as shown in Figure 6.3 and Table 6.1. If the line P2 at any stage falls low (P2 is generated from periodic pulses from the processor and if they fail, the life generator switches P2 low), it is automatically assumed that the processor has failed and shutdown procedure will be carried out. Additionally, the appropriate alarm will be actuated, both visually and audibly.

Mode	P0	P1	P2
Run	0	0	1
Shutdown	0	1	1
Slew Lock	1	0	1
Brake Only	1	1	1
Processor Fail	X	X	0

X = Don't Care.

Table 6.1: Mill Control Modes.

The three signal lines are received by the Command Interpreter Module (CIM) of the tower controls where it is decoded and the appropriate procedure initiated. A "low" on the P2 line is assumed to indicate a request for shutdown. For the shutdown procedure to operate correctly, it is also necessary to input additional signals to the Command Interpreter Module. For wind turbine shutdown alignment to be achieved two signals have been generated by the wind vane. D1/ indicates the relative position of the wind direction to the mill main shaft. When D1/ is "high", the mill is aligned with the main shaft normal to the wind direction within ± 6 degrees. D2/ simply indicates to the CIM which direction the yaw drive should rotate in order to achieve the shortest angular path. Once lineup is achieved, the CIM issues a brake command to the pod by forcing the two brake signal lines, R5/1, R5/2 "high". A slew lock command is issued, when the main shaft ceases rotation.

The yaw drive is controlled by four lines. R1, R2, R3 control the solenoids on the hydraulic valves - refer to Figure 5.19. R4 controls the pump motor contractor. Local operation of the yaw drive hydraulics is also possible.

Shaft speed and wind speed sensors are mounted at pod level and transmit signals to the ground controls for both panel indication and input to the main controller.

6.2.2: Electrical Control.

Electrical control is outlined by Figure 6.4 and has the two areas of operation shown below. These control the electrical components of the WTG such as generator excitation and electrical indication.

Measurement of AC and DC power quantities is made by the rms detector circuits in the rectifier and is indicated on the panel as well as sent to the main controller. The signal generated from the DC voltage transducer is used by the processor to determine generator shaft loading,

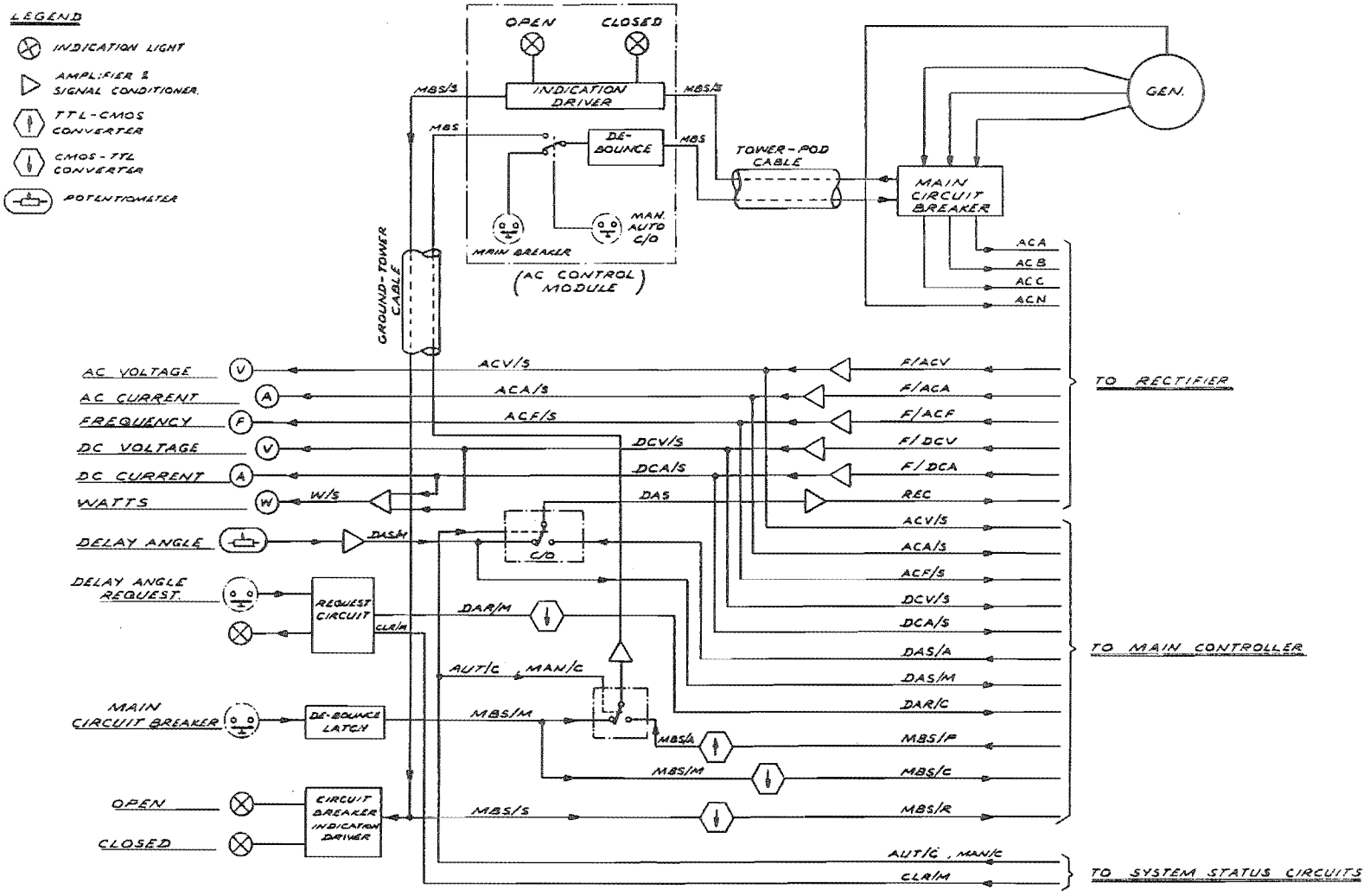

Figure 6.4: Electrical Control Schematic.

since a fixed resistive load is used (10 Ω). The rectifier can be controlled either from the front panel or from the processor, depending on the system status.

The generator main breaker can be controlled from the panel or from the processor, again depending on the system status. The breaker is controlled by one line from the ground controls, MBS, and its status is indicated on the panel via the MBS/S line which originates from the auxillary contacts on the breaker.

6.2.3: System Status Control.

System status describes the method (status) by which the windmill is controlled, and is generated as shown by the schematic of Figure 6.5. It refers to the method of system control and three states are possible:-

(i) Automatic State(AUTO). This is the normal status of control. All aspects of control are via the main controller under microprocessor supervision. Automatic state is obtained by operation of the 'panel clear' switch when in panel state. This sends the signal CLR/P to the processor to indicate that the operator wishes to return to processor control. A return line CLR/C from the processor provides indication of actual state.

(ii) Panel State(PAN). This is a semi-automatic control which allows the operator to intervene in system status. It is accessed from the automatic state by operation of any of the panel push buttons except the alarm and system status buttons. The advantage of this state over fully manual control is that the processor can censor operator requests to prevent inappropriate actions being taken. For example, if the operator requests a brake only command, the processor assumes that a shutdown command was required. Panel state is the normal startup state. Note that when in panel state the processor still controlls turbine load unless the 'delay angle request' switch is specifically operated.

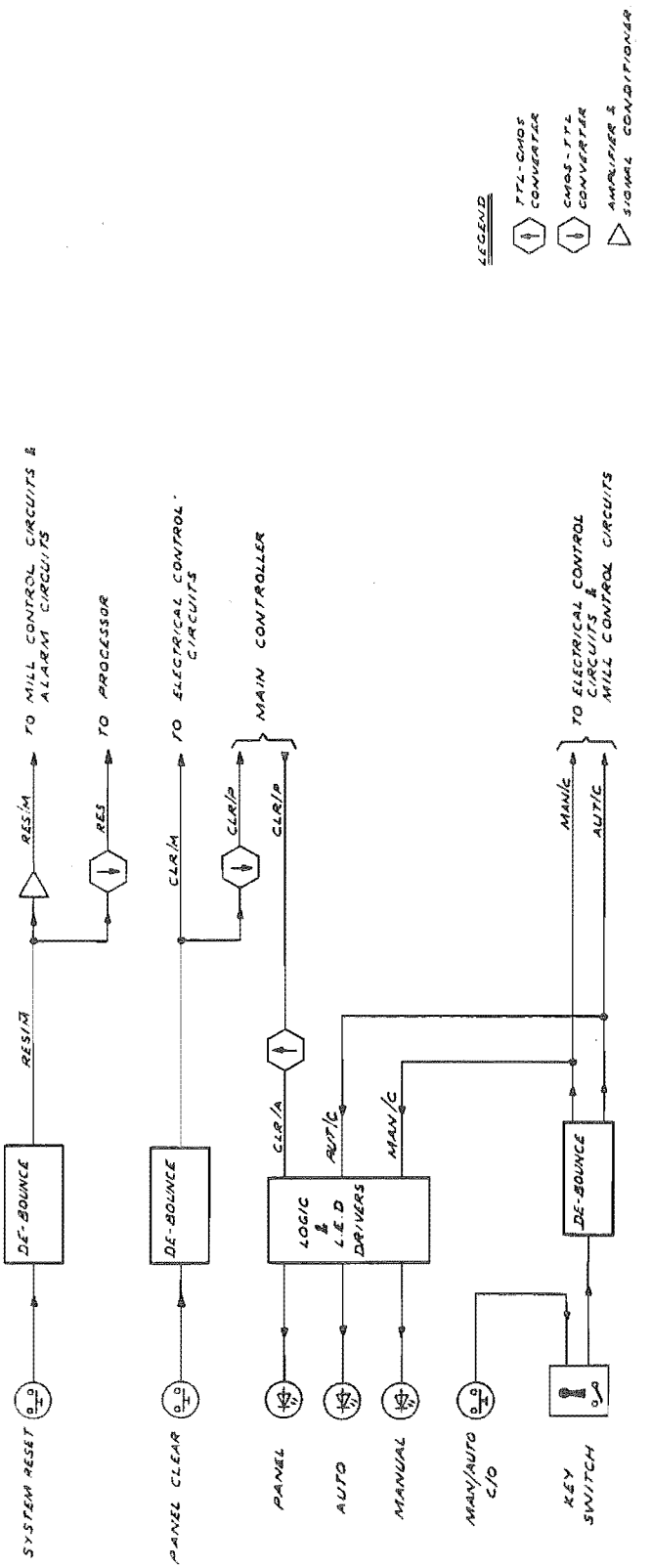

Figure 6.5: System Status Control Schematic.

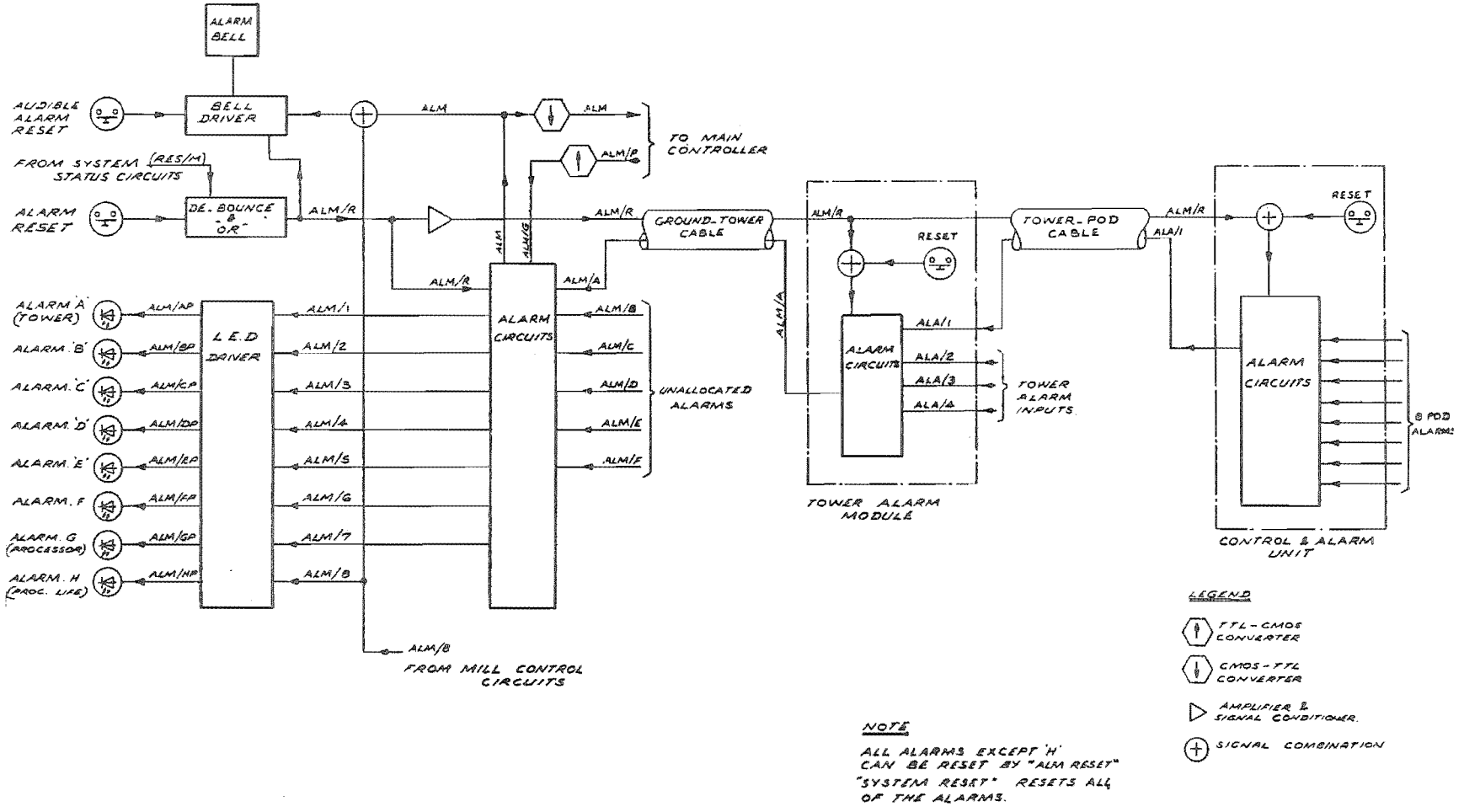

Figure 6.6: Alarms Control Schematic.

(iii) Manual State(MAN). This is a totally manual state and bypasses the main controller. This is obtained by operation of the 'manual/auto c/o' switch. A series key switch is incorporated to reduce the risk of unwanted operation. Changeover from auto to manual operates a series of analogue and digital switches with the MAN/C and AUT/C lines which bypass the processor when in manual state.

A key switch has been incorporated in the manual/auto changeover control to reduce the risk of unwanted operation.

6.2.4: Alarm Indication.

Alarm Level	Alarm Number	Alarm
Pod	1	Aux. DC Supply 1 Fail
	2	Aux. DC Supply 2 Fail
	3	Under Voltage Main DC Supply 1
	4	Under Voltage Main DC Supply 2
	5	Generator Phase Failure
	6	Spare
	7	Spare
	8	Spare
Tower	1	Alarm Input from Pod
	2	Battery Charger Supply Fail
	3	Spare
	4	Spare
Ground	1 (A)	Alarm Input from Tower
	2 (B)	Spare
	3 (C)	Spare
	4 (D)	Spare
	5 (E)	Spare
	6 (F)	Spare
	7 (G)	Alarm Input from Processor
	8 (H)	Processor Fail

Table 6.2: System Alarms.

The alarm system of Figure 6.6 allows up to eight ground alarms, four tower alarms and eight pod alarms to be input. Current software calls for system shutdown under any active alarms. Current alarms in use are given in Table 6.2.

All alarms can be reset from the ground controls either by the alarm reset" button or "system reset" button. The latter also resets the processor. A separate reset for the audible alarm has been provided. Tower and pod alarms can be reset from the Tower Alarm Module and the pod alarms can be reset from the Control and Alarm Unit in the pod.

6.3: Ground Controls Design.

6.3.1: Main Controller.

The main controller is microprocessor based and allows up to 16 analogue signals and up to 16 digital lines to be input with up to 8 analogue signals and 16 digital lines to be output, as shown by Figure 6.7. All analogue I/O is in the 0 - 10 V range with all digital I/O at T.T.L. level.

The four controller boards and processor board are interconnected by plugging on to a bus system consisting of a 10 bit interrupt bus, an 8 bit data bus, 8 bit address bus and 6 bit control bus. Up to a total of ten boards can be plugged on to the bus.

The processor board (See Figure 6.8) is based on an INTEL 8085 processor and has a total memory space of 4k EPROM and 2.25k static RAM. Inputs from the interrupt bus are latched onto a port and input to the RST 6.5 input of the processor. If an interrupt occurs on the first eight lines it is detected by the processor and the port read to find which interrupt has been activated. The last two interrupt lines are not normally used but can be patched directly to the RST 5.5 and 6.5 lines into the processor. The data bus address bus and control bus are input to the 8155 ports. Data direction on the address bus and data bus are software controlled from Port PA1 and data direction on the control bus is hardware plugged.

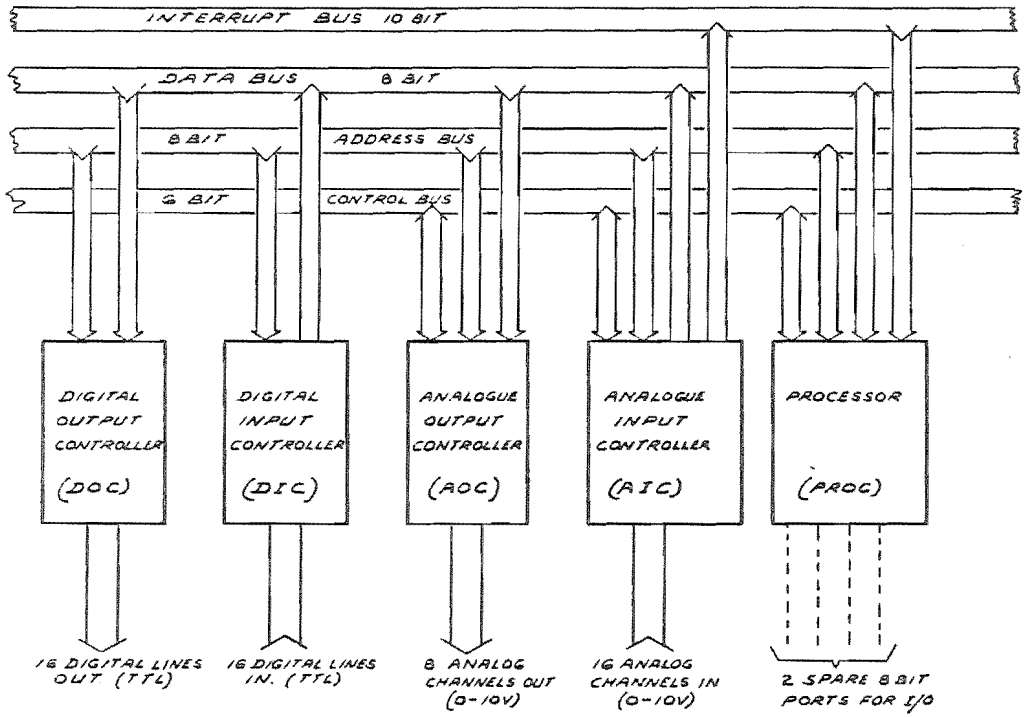

Figure 6.7: Main Controller Schematic.

RIBBON CABLES C D E & F CORE DESIGNATIONS				
CORE Nº	CABLE 'E' (DI) SIGNAL NAME	CABLE 'F' (DO) SIGNAL NAME	CABLE 'D' (AO) SIGNAL NAME	CABLE 'C' (AI) SIGNAL NAME
1	P0/C	P0/P	DAS/A	WSP/S
2	NC	NC	NC	NC
3	P1/C	P1/P		SSP/S
4	NC	NC		NC
5	DAR/C	P2/P		ACV/S
6	NC	NC		NC
7	MBS/C	MBS/P		ACA/S
8	NC	NC		NC
9	MBS/R	ALM/P		ACF/S
10	NC	NC		NC
11	CLR/C	CLR/P		DCV/S
12	NC	NC		NC
13	ALM			DCA/S
14	NC			NC
15				DAS/M
16				NC
17				TSR/SET
18				
19				
20				
21				
22				
23				
24				
25				
26				
27				
28				
29				
30				
31				
32				
33				
34				

NC = NO CONNECTION

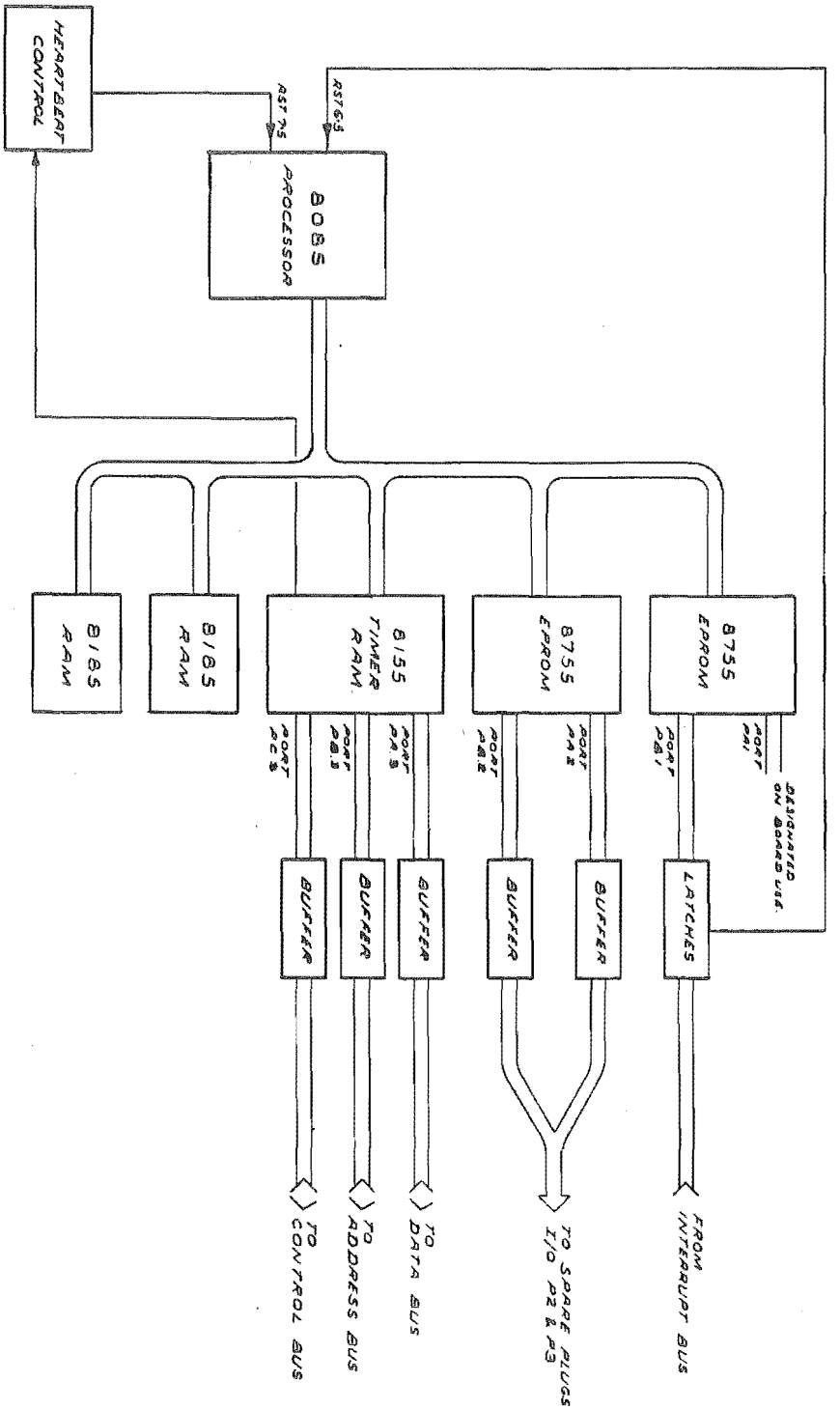

Figure 6.8: Processor Board Schematic.

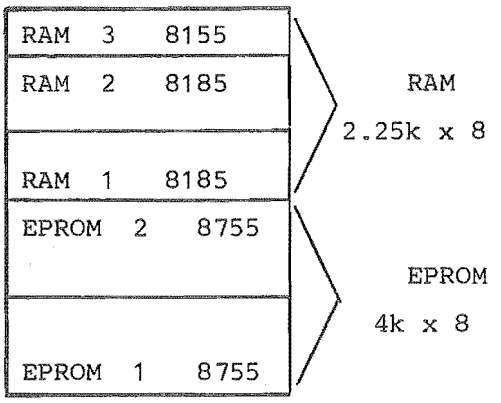

Figure 6.9: Processor Memory Allocations.

Two spare ports have been allowed for future connection to a data logger and telemetery. System timing is generated from a 10 m/s heartbeat into the RST 7.5 input of the processor. This is obtained from the system clock (6.144 MHz/2), a clock divider and the timer section of the 8155.

Additional features allowed for on the processor board are a tape recorder read/write facility in Kansas City format with the tape drive controlled by the processor. Sufficient address space is available for RAM expansion up to 4k.

The analogue input controller of Figure 6.10 consists of 16 sample/hold circuits with a single analogue to digital converter (8 bit) and analogue multiplexer. The analogue output controller is shown in Figure 6.11 and uses 8 separate 8 bit digital to analogue converters.

The digital input controller and digital output controller of Figures 6.12, 6.13 respectively use two groups of time multiplexed 8 bit data to obtain the 16 lines in each case.

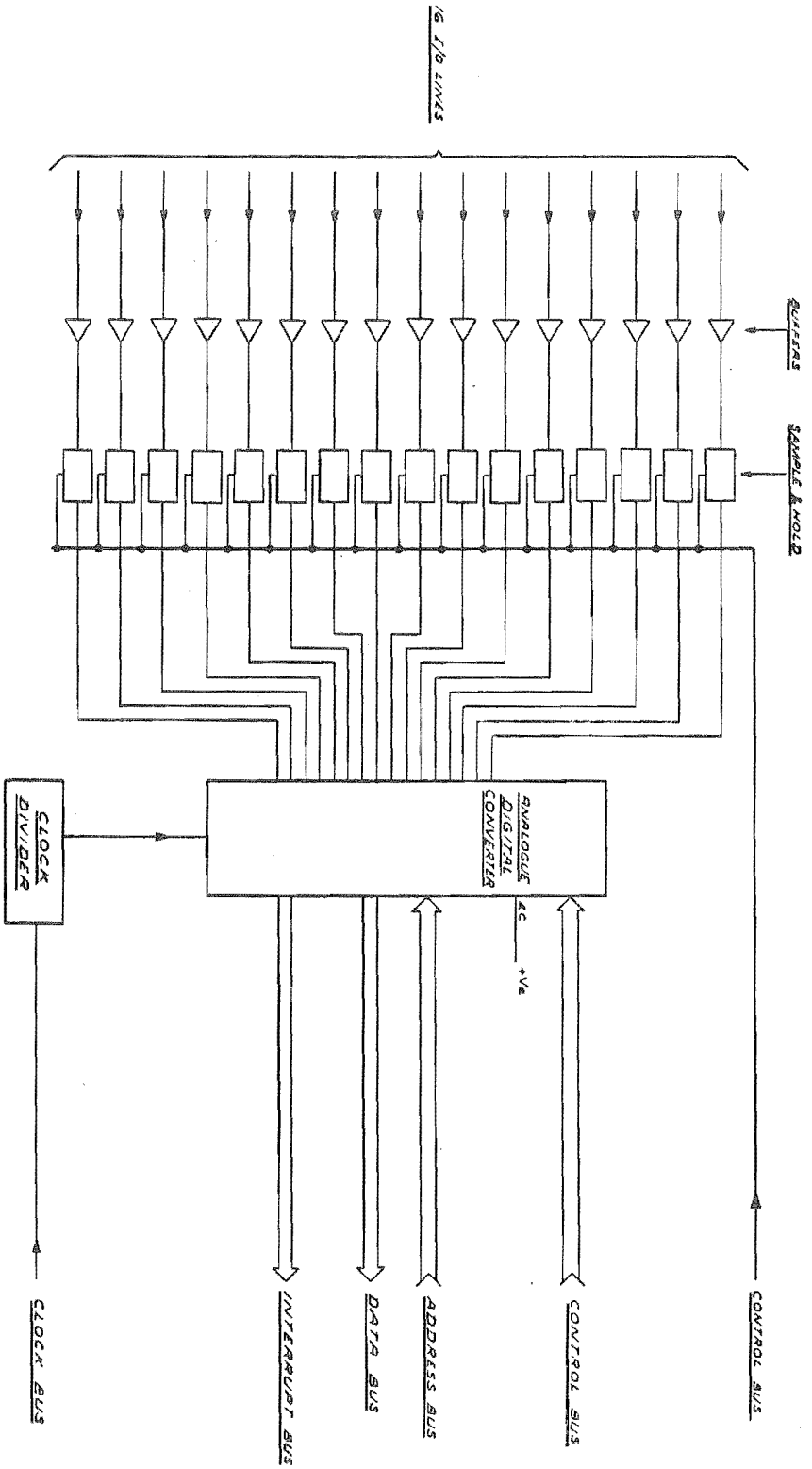

Figure 6.10: Analogue Input Controller.

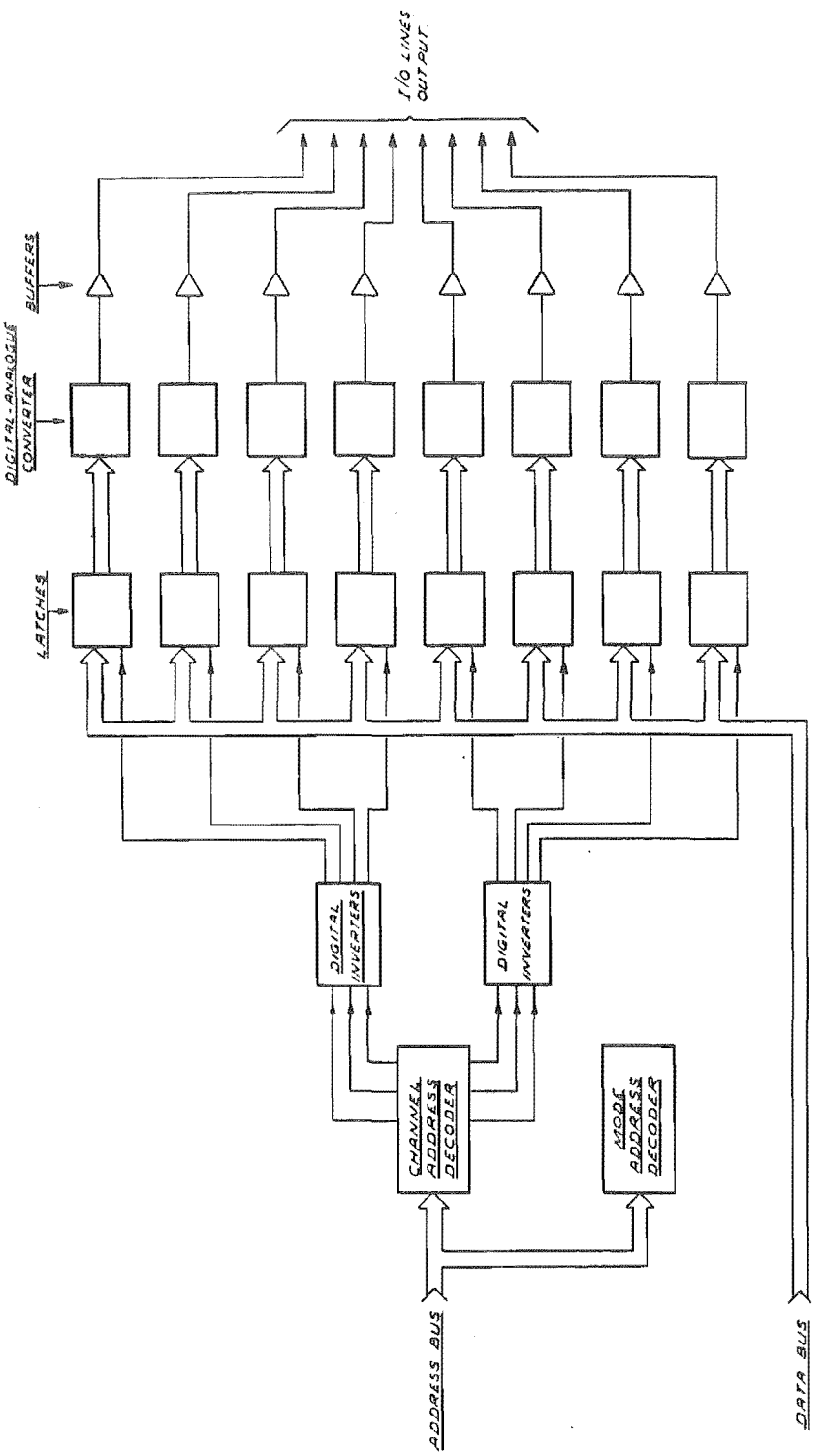

Figure 6.11: Analogue Output Controller.

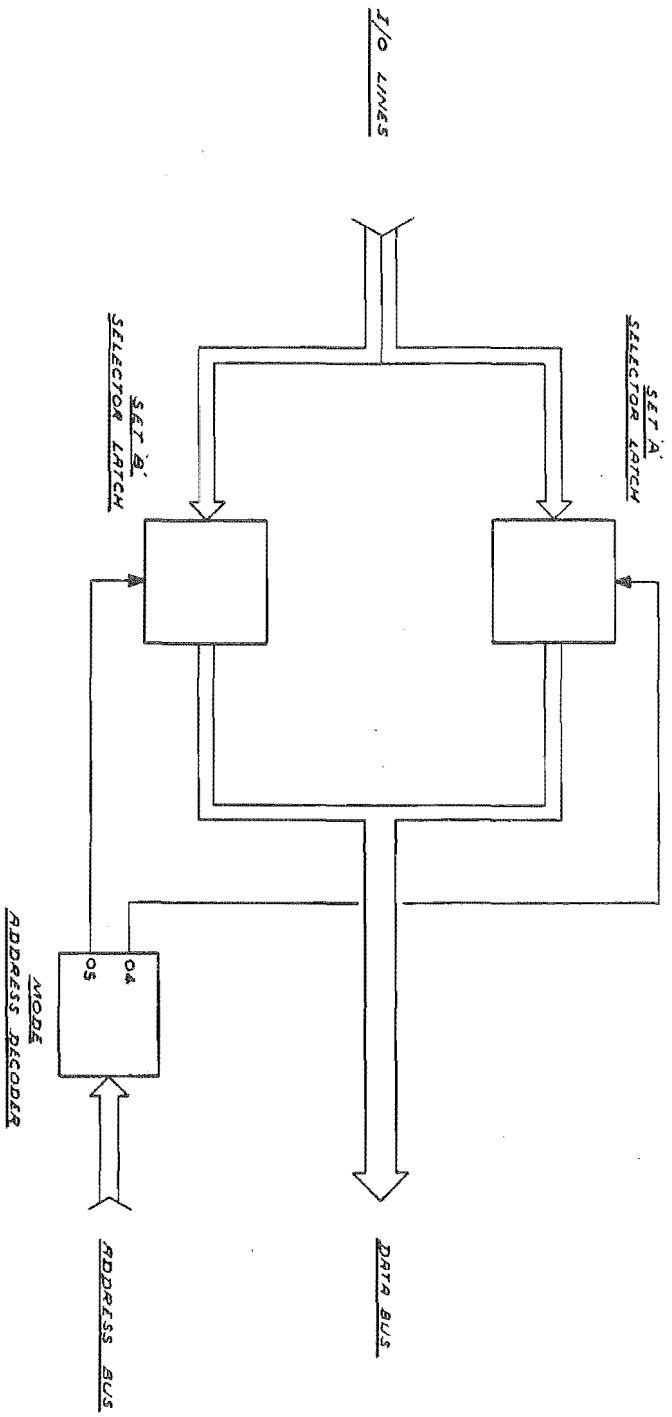

Figure 6.12: Digital Input Controller.

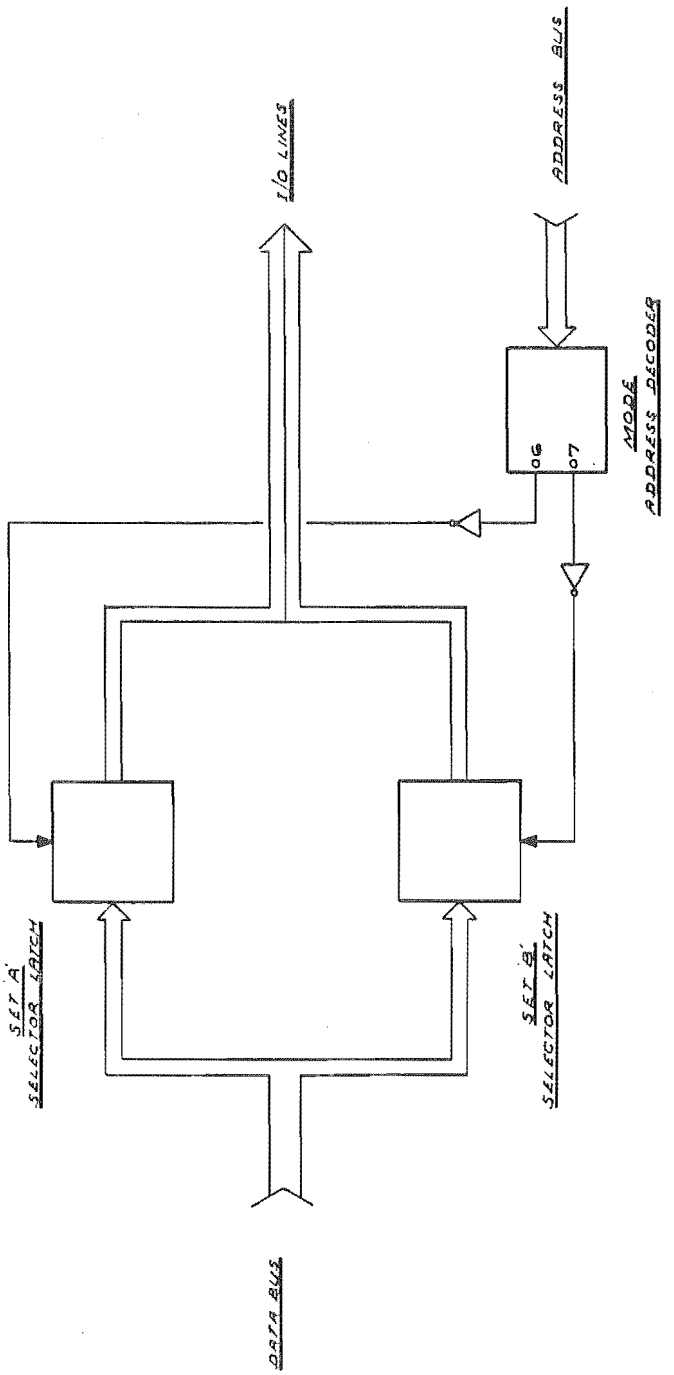

Figure 6.13: Digital Output Controller.

6.3.2: Main Controller Software.

Main controller software consists of a real-time, multi-tasking operating system and specialised tasks which perform system control functions. Refer to Figure 6.14 which shows the operating system modules. The tasks for the main load control routine are discussed in Chapter 7.

The operating system is designed to run many different tasks. It is a basic limitation of this version of the operating system that tasks are allowed to run to completion instead of being prempted if a high priority task is waiting to run. This means that the execution times of individual tasks are kept short. The maximum task length is about 10 mins (=(2**16-1)*10ms) after which system time keeping will fail. In practice to keep task response times acceptable much shorter task lengths should be used (say 10 to 100 ms). Current tasks in use are much shorter than the above and are not constrained by this limitation. Tasks such as console drivers which spend much of their time in delay loops should use the operating system delay function. A call to delay is equivalent to task termination for the purposes of these timing calculations.

Tasks can be run as a result of a demand from an interrupt service routine or according to one of the time based functions defined below. A task running as the result of an interrupt is equivalent to the system being interrupt driven and a task running according to time is equivalent to the system polling external events.

Interrupt service routines are not considered to be tasks. In general the interrupt service routine will capture data from an external device and place this data in a queue for later processing by a task that is demanded by the interrupt service routine, but not run until some time later.

The types of tasks at present defined in the system are:

1) A task which is run every 'N' periods of 10ms.

2) A task which is run once only, after 'N' periods of 10ms.

3) A task which is run only when demanded by another task or an interrupt service routine.

4) A task which is run every 10ms. (This is a special case of Type 1, but it is faster to process and requires less task table storage than a Type 1 task.)

Two special task types are also defined. The first is Type 0 which is the operating system task that implements the timing functions implied in some of the task definitions above. The second special task type is Type 15, which is a dummy task used in the task table to indicate the end of the task table.

The next section gives a description of each module in the operating system.

1) MILINT.

This module processes system interrupts. Timer interrupts increment the timer counter. Every timer interrupt (= 10ms) the schedular update task is run.

2) MILUP.

This is the highest priority task in the system. It is run every 10ms and updates the status of all other tasks where the task status is time dependant.

3) MILTSK.

This module contains 3 tables used to control and define task status within the system. Two of these tables are generated simultaneously by a macro deck. The three tables are:

1) TABIDX - The task table index table.

2) TABTSK - The prom image of the run time task status table.

3) TSKTAB - The ram resident run-time task status table.

TABIDX contains 2 bytes for each task in the system. These bytes define an index down either TABTSK or TSKTAB to the defined task. To find a task in either table these rules are followed.

1) Get System Task No. (= Place in task table, first task = Task 0.)

2) Multiply Task No. by 2.

3) Use result of 2 as an index down TARIDX.

4) Get index from TABIDX.

5) Use this as index down either TABTSK or TSKTAB give a pointer to the task control bits.

TABTSK is a prom resident image of the start up task table. TABTSK and TABIDX are generated simultaneously by macros. TSKTAB is the run time (Ram resident) task table - it is set up by MILGO.

The following section gives detailed descriptions of the task table entry for each type of task.

Task Type 0. Special task type for table update task.

Task Type 1. This type of task is run every N periods.

Task Type 2. This type of task is run once after N periods.

Task Type 3. This type of task is run on demand from a task or an interrupt service routine.

Task Type 4. This type of task is run every period.

Task Types 5 to 14 are not yet defined and cannot be specified.

Task Type 15. This is a dummy task used to mark the end of the task tables.

4) MILUTL.

This module contains utility functions that allow the caller tasks to perform the following functions.

i) Delay for N periods.

ii) Enable and disable a task.

iii) Set or reset the run flag of each task.

5) MILSHD.

This module does all the task starting. It scans down the task table looking for an enabled (and not delayed) task with its run bit set, or an enabled task with its restart (after a delay) bit set. When such a task is found the running flag is set and the task is started by an effective call. For a task being restarted after a delay the restart address is used. For a task being started because the run flag is set the task start address is used. If both the run flag and the restart flag are set the restart flag takes precedence. This means that a request to run a delayed task is held pending until after the delayed task has been restarted and allowed to run to completion. When the task finishes the running flag is reset and the schedular starts looking for work at the top of the task table. This means that tasks at the top of the table have a higher priority than those at the bottom of the table, and those at the bottom could conceivably never be run if higher priority tasks were run too often. The alternative of rotating priority can be implemented by changing a JMP instruction in the TSKRET routine.

6) MILT1.

This module provides a subroutine that is called from MILUP. The routine update task table entries for task type 1 every 10ms.

7) MILGO.

This module contains the system start up code. It performs the following functions:

i) Sets up the Task Table.

ii) Resets any pending interrupts.

iii) Initialises interrupt data queues.

iv) Initialises the timer to generate interrupts every 10/255 ms.

v) Clears miscellaneous flags.

The only tasks currently in use are MILPAN and MILRUN (see Chapter 7).

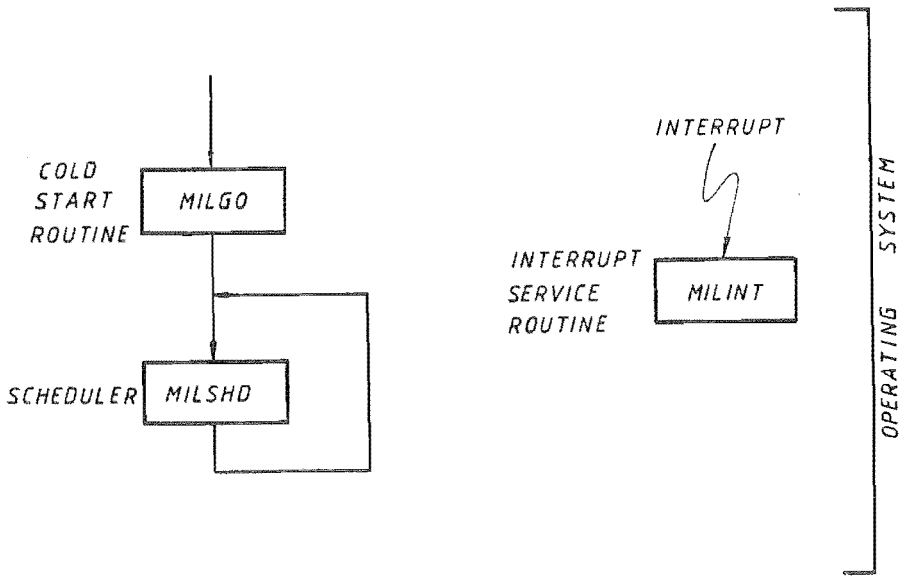

Figure 6.14: Main Controller Operating System.

6.3.3: Rectifier.

Rectifier design and operation is described in Chapter 4.

6.3.4: Panel.

The panel is shown by Plate 6.1. It provides the operator with indication of system operation and also with basic control functions. All control signals from the panel pass to the interface rack for conditioning before transmission to the required destination.

6.3.5: Interface Rack.

The interface rack has the main role of setting up signals to be used by other ground control units. Its major functions are:-

(i) To buffer incoming and outgoing signals.

(ii) To provide the necessary signal level conversions. These are between the main controller which is at TTL level and other components at 12V CMOS level.

(iii) To provide a single point for all incoming and outgoing signal lines.

(iv) To provide indication driving including LED displays and analog meter displays.

(v) To provide any signal conditioning which may be required such as filtering etc.

(vi) To carry out some hardwire logic control functions.

6.4: Tower Controls Design.

Layout of the tower controls is shown in Figure 6.15 and Plate 6.2.

6.4.1: AC Control Module.

This module serves two purposes:-

(i) To provide low voltage AC power to the DC Control Module for battery charging. An AC supply failure relay is incorporated to operate Alarm 2 of the Tower Alarm Unit.

(ii) To provide tower control and indication of the generator main breaker.

6.4.2: DC Control Module.

Battery charging is provided by this module. The battery charger is fully automatic with heavy and float charge rates.

The DC supplies for electronics to all other tower modules is also controlled from this module.

6.4.3: Signal Transfer Modules.

These simply provide a convenient termination point for cables to the pod and also to the ground. Suppression of slip ring noise is also made on signals from the pod.

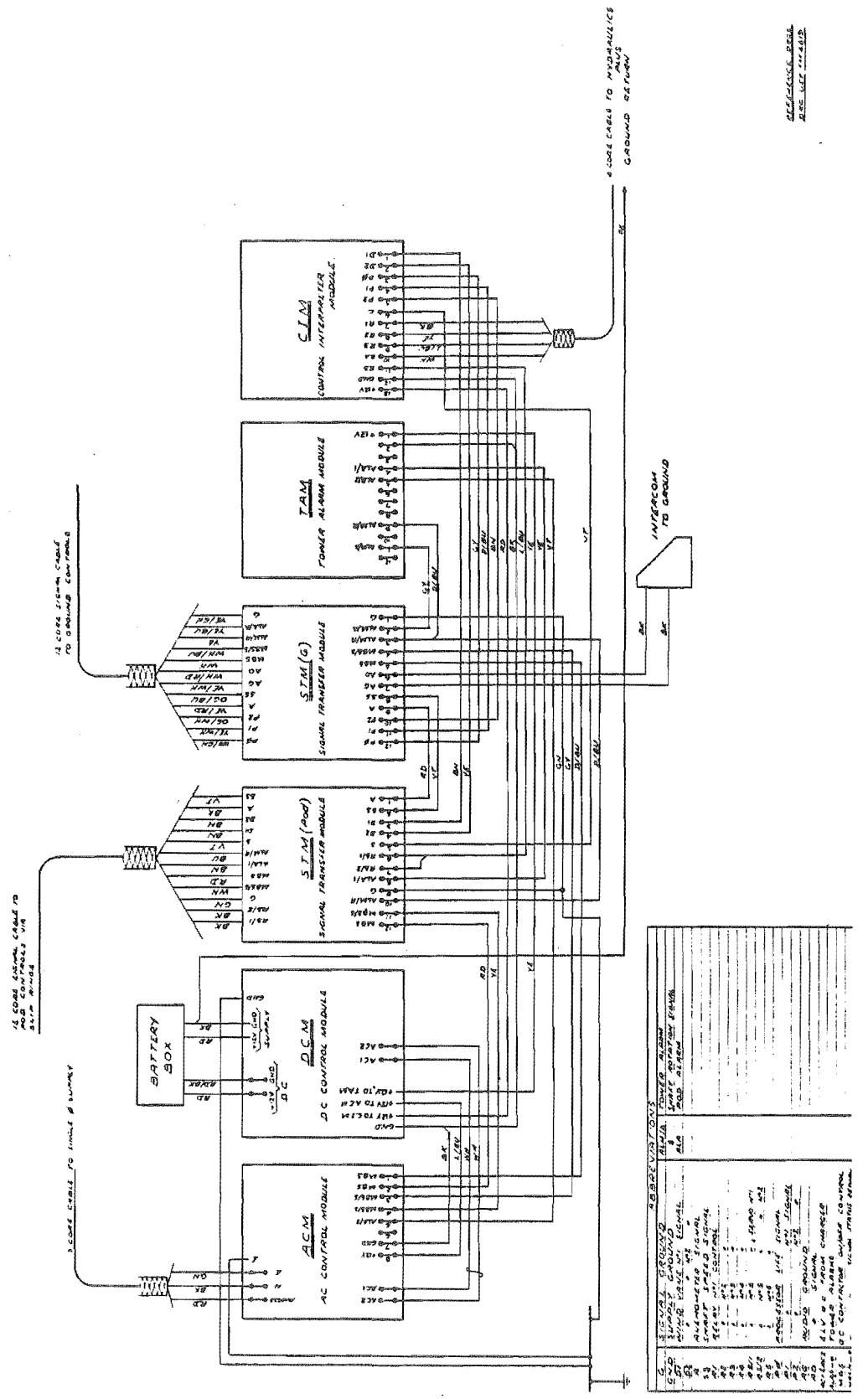

Figure 6.15: Tower Control Panel.

6.4.4: Tower Alarm Module.

This unit processes the alarm line from the pod and up to three others at tower level and transmits the result to ground. All alarms from tower level up can be reset at the Tower Alarm Module.

6.4.5: Command Interpreter Module.

This is the most important module of the tower controls, as it is responsible for shutdown sequencing of the system. The three control lines into the module were shown by Table 6.1. The role of each input and output signal is given in Table 6.3.

The Boolean equations governing these parameters are as follows. (Refer also to Figure 5.19):-

$$R5 = ((\overline{M0}.M1.\overline{D1}) + (M0.M1)) \ . \ (M1+M0) \qquad (6.1)$$

$$R4 = \overline{M0}.M1.\overline{Z}.D1 \qquad (6.2)$$

$$R3 = R4.D2 \qquad (6.3)$$

$$R2 = (R4.\overline{D2}) + (M0.\overline{M1}) + Z \qquad (6.4)$$

$$R1 = R4 \qquad (6.5)$$

where

$$M0 = P2.P0 \qquad (6.6)$$

$$M1 = (P2.P1) + \overline{P2} \qquad (6.7)$$

$$Z = R5.S \qquad (6.8)$$

P0	Control Line 0 from Ground
P1	Control Line 1 from Ground
P2	Control Line 2 from Ground
	P2 =0 Indicates Processor Failure
S	Main Shaft Rotation Sensor Line
	S = 1 Indicates Zero Shaft Rotation
$\overline{D1}$	Pod/Wind Alignment Sensor Line
	$\overline{D1}$ = 1 Indicates Alignment
$\overline{D2}$	Pod Yaw Direction Sensor Line

(a) Input Signals to CIM.

R1	Hydraulic Valve 1 Control Line
R2	Hydraulic Valve 2 Control Line 1
R3	Hydraulic Valve 2 Control Line 2
R4	Hydraulic Pump Motor Control Line
R5	Brake Control Line
	R5 = 1 Orders Braking

(b) Output Signals From CIM.

Table 6.3: I/O Lines for CIM.

The brake command 'R5' is issued only under the following conditions:-

(1) In the automatic or panel states after the pod has been successfully lined up with the shaft normal to the wind direction.

(2) In the manual state if a brake command is issued.

The brakes are to be released only if a RUN command is issued. The hydraulic pump signal 'R4' and control signals 'R2' and 'R3' for the valves are issued if pod/wind alignment is required. The valves are also operated

to lock the yaw after the main shaft has ceased to rotate following braking (Z). 'M0' and 'M1' are generated to test if line 'P2' is "low", ie., to test for processor security. Logic state analyser results of tests on the Command Interpreter Module are shown in Plate 6.4.

For Plate 6.4(a) a normal shutdown procedure is followed:-

(i) Normal operation with P0 = P1 = 0 and P2 = 1. No Hydraulics are energised.

(ii) Shutdown is ordered (P0 = 0, P1 = 1). The pump is started (R4 = 1), Valve 1 is energised (R1 = 1) and one side of Valve 2 is energised (R3 = 1, R2 = 0).

(iii) The effect of $\overline{D2}$ changing is shown, ie., the direction of yaw is reversed (R3 = 0, R2 = 1) and Valve 2 has the opposite side energised.

(iv) The condition of (ii) is again seen.

(v) Wind alignment is achieved, ie., $\overline{D1}$ = 1. Yaw drive stops (R1 = R2 = R3 = R4 = 0) and a brake command is issued (R5 = 1).

(vi) When the main shaft has ceased to rotate (S = 1) the yaw is locked by energising R2 only. Refer to Figure 5.19.

(vii) Normal run condition of (i) is set again.

For Plate 6.4(b) a slew lock command is issued:-

(i) Normal operation with P0 = P1 = 0 and P2 = 1.

(ii) P0 = 1 indicates a slew lock command has been issued. Valve 2 is energised on one side only (R2 = 1).

(iii) Normal operation again.

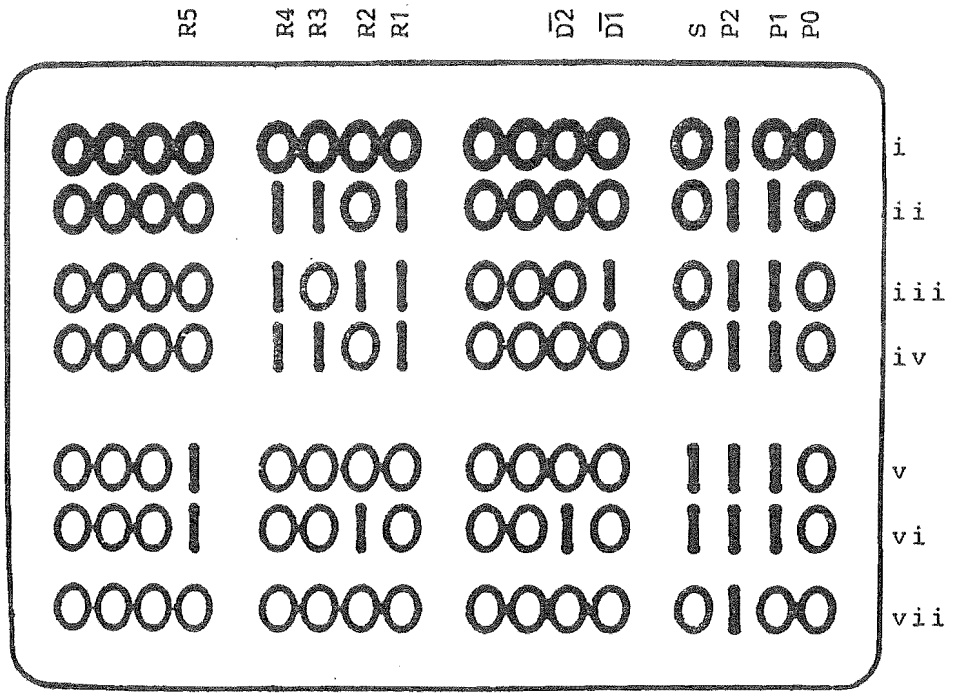

(a) Shutdown Command.

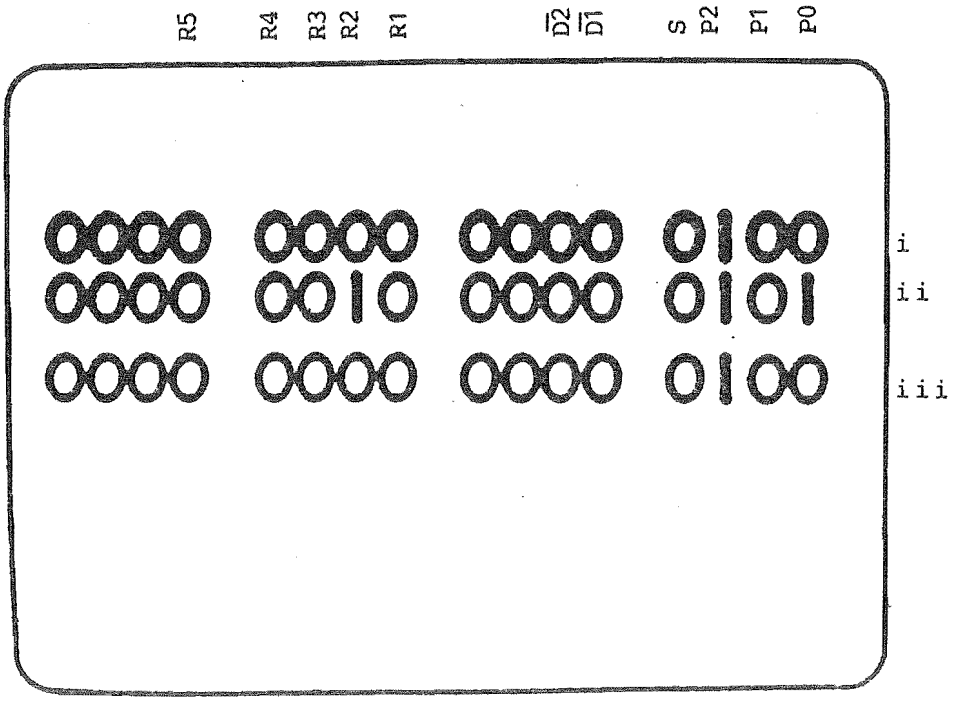

(b) Slew Lock Command.

Plate 6.4: Command Interpreter Logic Tests.

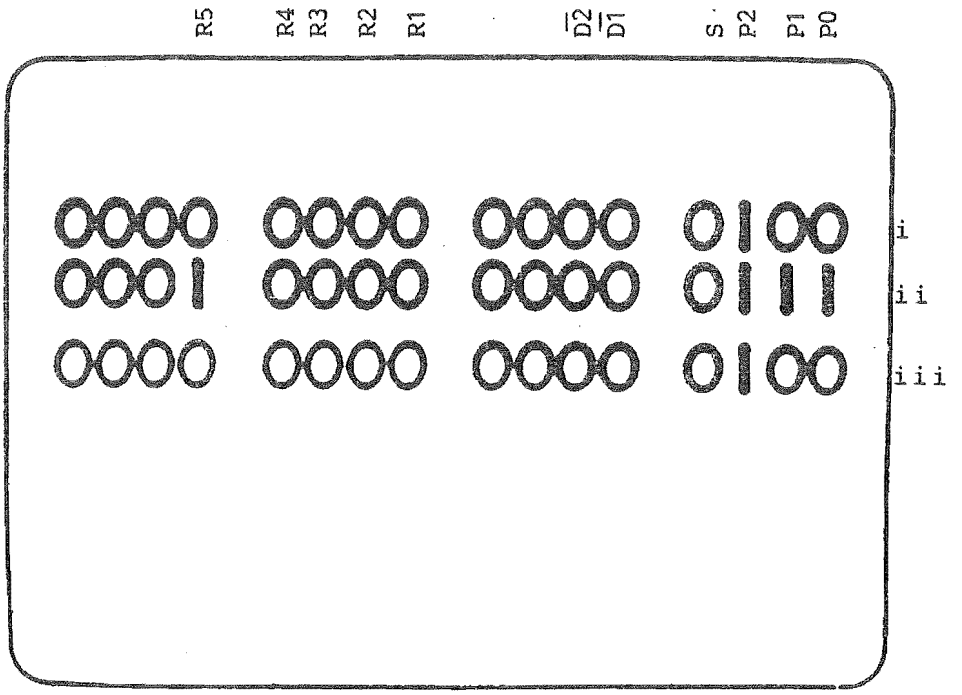

(c) Brake Only Commmand.

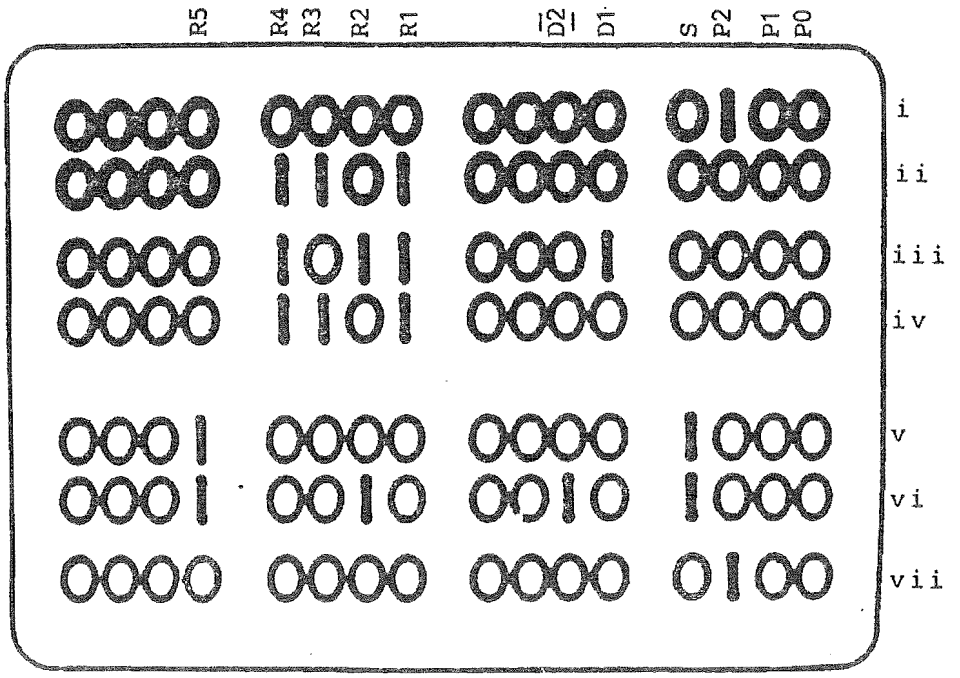

(d) Processor Failure.

Plate 6.4: Command Interpreter Logic Tests.

For Plate 6.4(c) a brake only command is issued:-

(i) Normal operation.

(ii) P0 = P1 = 1 indicates that a brake only command has been issued. R5 = 1 is issued to the brake control unit.

(iii) Normal operation.

For Plate 6.4(d) a processor failure is simulated:-

(i) Normal operation.

(ii) to (vi) P2 = 0 simulating a processor failure. This causes a standard shutdown procedure to be followed as outlined for Plate 6.4(a).

(vii) Normal operation.

6.5: Pod Controls Design.

The layout of the pod controls is given in Figure 6.16 and was also shown in Plate 6.3.

6.5.1: AC Control Unit.

This unit has the following functions:-

(i) Local control of the generator main breaker.

(ii) Detection of phase failure from the generator, the anticipated cause being circuit interruption by a blown main fuse on the generator terminals. Operation of the phase failure relays is locked out in the case when the generator is not excited. The resulting phase failure signals are sent to the Alarm and Control Unit for transmission to ground.

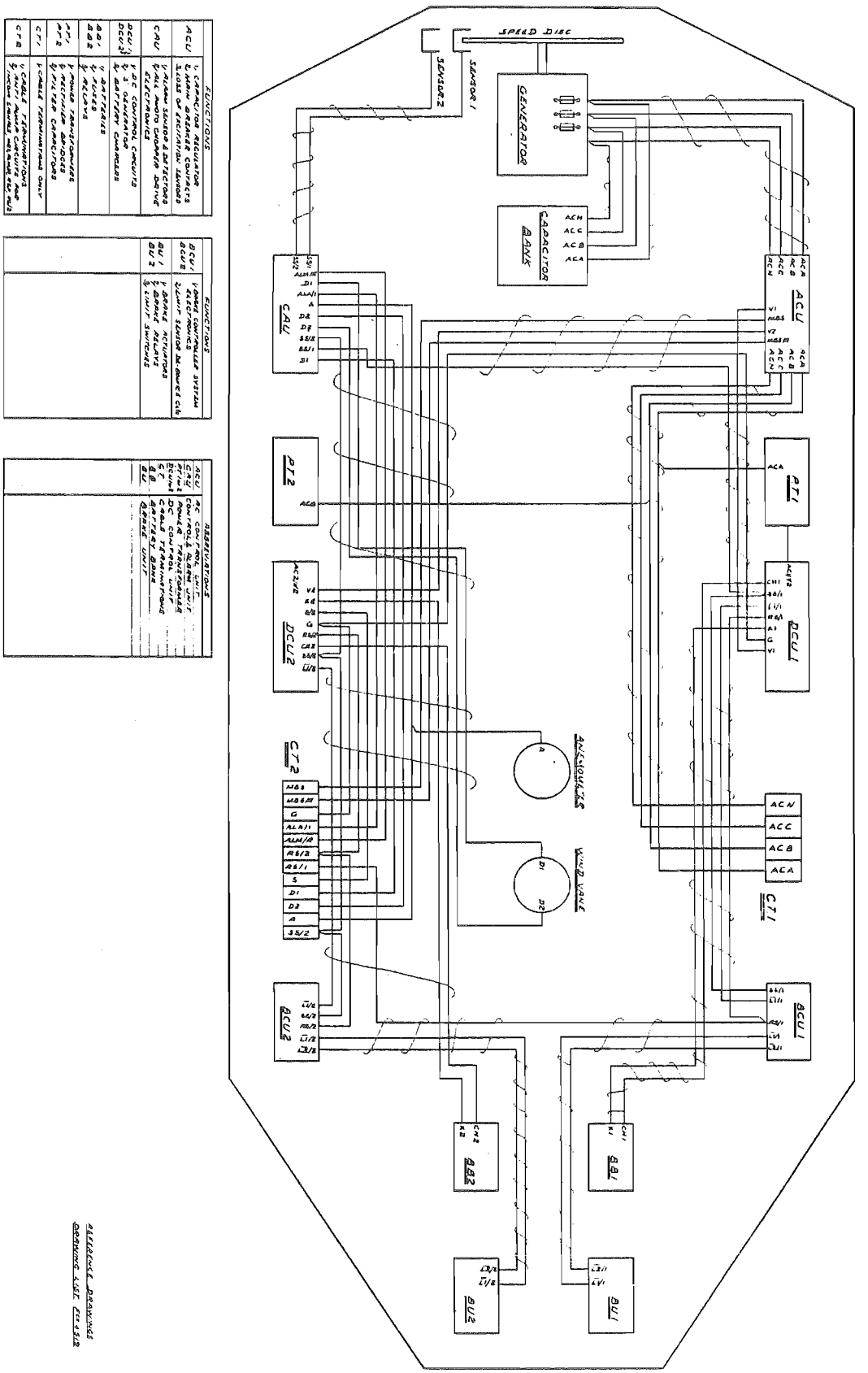

Figure 6.16: Pod Controls Layout.

6.5.2: Alarm and Control Unit.

All of the opto-interruptor detectors (anemometer, vane, shaft sensors) are driven by this unit and the outputs buffered before being sent to the appropriate destination.

Additionally, up to eight alarms can be input and were outlined in Table 6.2. Alarms 1 and 2 indicate the security of the two auxilliary supplies (see section 6.5.3). Alarms 3 and 4 indicate the status of the main supplies. If the levels of the main supplies fall below 10 volts an alarm is activated. Alarm 5 is the generator phase failure alarm. The power supplies for all circuits in the Control and Alarm Unit alarm section are designed such that it would be necessary for all DC supplies to fail for non-operation of the unit. If this situation occurs, an alarm is still indicated since the line to the Tower Alarm Module is active low.

6.5.3: DC Control Units.

These provide two basic functions:-

(i) Battery charging for the Battery Banks. The chargers are fully automatic with high and float charge rates.

(ii) To provide switching of the main DC supplies. The purpose of such switching is to preserve battery life when the chargers are not operating such as when the generator is not excited. In such cases, only the auxilliary supplies are activated and have a low current drain of about 300 mA. Main supplies are required for shutdown and only until shutdown is complete. This is indicated by the Boolean expression of Equation 6.9.

$$X = (R5.\overline{S}) + V + (\overline{R5}.SL) \qquad (6.9)$$

where

X = control line to main supply relays
= 1 for closed

R5 = brake control line
= 1 for application of the brakes

V = generator excitation status
= 1 if the generator is excited

S = shaft rotation status
= 1 for no shaft rotation

SL = S latched but cleared by $\overline{L1}$

$\overline{L1}$ = brake release sensor
= 1 when brakes are fully released

6.5.4: Battery Banks.

These consist of two indentical sets of 12V supplies. Each supply is from a sealed lead acid battery of 6 A hr rating.

6.5.5: Brake Control Units - Brake Units.

These control the deceleration rate of the mill when under braking. Final drive of the brakes is provided by the Brake Units. The signals input to the Brake Control Units are the brake command line R5, the brake limit sensors L1 (indicates release of brakes) and L2 (indicates max. brake pressure). Output signals are Rx and Ry which control the relays on the 24V servo drives of the Brake Units.

$$Rx = R5.E1.L2 \qquad (6.10)$$

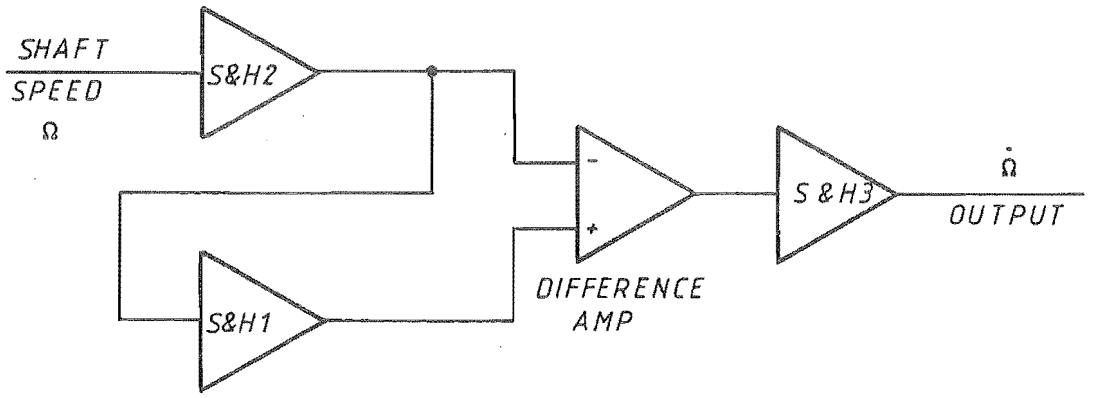

Figure 6.17: Brake Controller Deceleration Transducer.

$$Ry = (\bar{R5}.L1) + (R5.E2.L1) + Rx \qquad (6.11)$$

where

Rx = 0 indicates brake release

Rx = 1 indicates brake application

Ry = 1 turns the supplies on to the brake servos

R5 = 1 indicates braking is required

R5 = 0 indicates brake release is required

L1 = 0 indicates brakes are fully released

L2 = 0 indicates brakes are fully applied

E1, E2 are the deceleration rate error signals and indicate whether or not the angular deceleration rate is within the dead band of operation. For low deceleration rates, E1 = 1 and for high deceleration rates E2 = 1. If

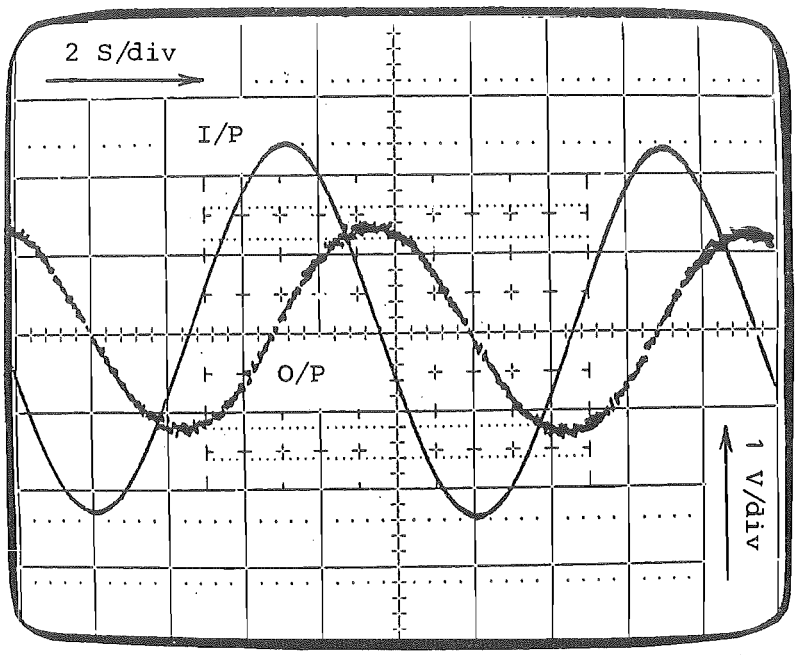

Plate 6.5: Deceleration Transducer Response.

the deceleration rate is within the required band, E1 = E2 = 0. In this case, the brake servos will be at rest.

Deceleration rate is detected from the shaft speed sensors using a series of cascaded sample and hold circuits as shown in Figure 6.17. Timing for the sample and hold circuits is generated so that samples are sequentially taken by units 1, 2 and 3. This, in effect, gives a very stable differentiator circuit operating in discrete steps. Plate 6.5 shows the output of the deceleration detectors for test sine wave inputs. The output is of the same form as the input with a 90 degree phase shift resulting from the differentiation.

Spring is introduced into the loop by the spring tube/lever system used to actuate the hydraulics.

6.6: Summary.

A brief description of the control system is given outlining the operation of the major components. Software for the mill load control is detailed in Chapter 7.

The requirements of the control system as shown in Section 6.1.1 have been satisfied:-

.A flexible operating system has been installed into the main controller. For modification of control algorithms a set of tasks defining control needs can be written and entered into the task table.

.Schematic diagrams detailing as constructed control and indication circuits are shown.

.Shutdown sequencing has been described in detail and shown by testing to be operating satisfactorily.

.Failure of the processor of the main controller results in system shutdown.

.Detection of extreme operating conditions or failure of sub-control circuits results in system shutdown.

.Construction of the brakes is such that failure of one hydraulic circuit does not affect operation of the duplicate circuit.

.Data logger and telemetering circuits can be connected to the main controller.

.The controls can operate as a fully automated system or allow for operator intervention which is censored by the processor. Fully manual operation is also possible.

CHAPTER 7.

SYSTEM CONTROL AND OPERATION.

7.1: Introduction.

It is the purpose of this chapter to combine the theory and design outlined in previous chapters and describe the operation of the wind turbine generator as a complete unit. The following are required:-

. Determination of the method of load control of the wind turbine generator. Interaction between the turbine, self excited induction generator and rectifier is required to be assessed when controlled by a microprocessor based controller.

. Design of software for control of the system.

. Assessment of operational performance. This is to be carried out on a step by step basis.

. Assessment of the complete system operating under windy conditions.

Section 7.2 shows the method used to control the steady state performance of the WTG giving details of the micrpocessor software used. Sections 7.3 and 7.4 give the results of laboratory tests carried out on the electrical components of the system while Section 7.5 gives results of tests carried out to measure harmonics in the system. Section 7.6 gives the test results for the complete system under windy conditions.

In all of the following tests a capacitance of 94 μF per phase has been used for generator excitation.

7.2: Wind Turbine Load Control.

7.2.1: General Considerations.

Wind turbine generators of fixed geometry demonstrate a tip speed characteristic similar to that shown in Figure 2.3. For a tip speed ratio of less than the optimum value, i.e., $X < X_m$ the turbine will be unstable. For $X > X_m$ the turbine is stable as it is in this region where an increased load will cause the turbine to reduce speed and hence reduce tip speed ratio. Under ideal conditions it is desirable to operate the WTG so that maximum power transfer from the wind to the turbine shaft is achieved, i.e., so that $C_p = C_{pm}$.

The described method, used to attain a controlled power transfer from the wind to the turbine shaft, consists of employing a combination of the self excited induction generator and the controlled rectifier (refer to Appendix 3, Milner 1982). By adjusting the rectifier delay angle, generator load and hence turbine load are controlled. For the investigations carried out here a fixed resistance load on the rectifier output is used as this provides a simple starting point for study. More complex loads may be considered for future investigations, eg., power inversion and grid connection.

Use of a frequency independent load on the generator, such as a fixed resistance heating bank fed from the rectifier, also simplifies the situation in that a shaft speed restriction is not required and the turbine is therefore free to rotate at whatever speed is suited to the tip speed characteristic. To increase flexibility of the system as a research facility the load controller has been designed so that a power coefficient can be selected by the operator in the range from zero up to C_{pm}. This allows for the installation of generators of somewhat lower rating than the turbine without risk of generator failure through overload and although such an arrangement would not allow C_{pm} to be reached it would be suitable for testing of different methods of control and generator types.

7.2.2: Method of Control.

The 6 metre diameter HAWT of three blade, fixed pitch design drives an 8 pole, three phase generator (described in Chapter 3) through a 1:10 step up gearbox. Refer to Figure 7.1. Turbine blade pitch has been set to 15 degrees. Although the generator is rated for 3 kW at 50 Hz and 415 V, it is possible to operate at a power output of up to 6 kW at higher frequency and voltage. Generator shaft speed is limited to less than 5000 rpm for a balanced rotor while voltage is restricted to 1000V phase to phase by insulation limitations.

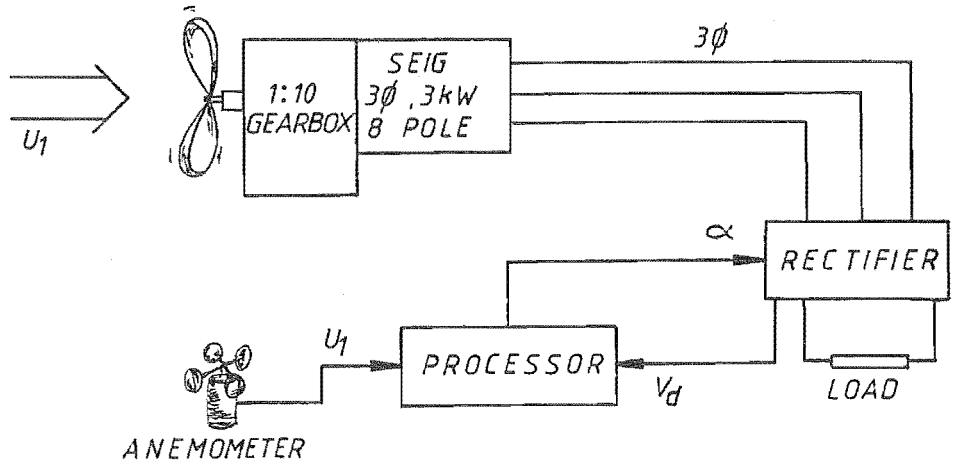

Figure 7.1: Wind Turbine Load Control System.

To obtain control of load the microprocessor reads the value of wind speed from the anemometer and estimates the power available in the wind. This value of power is subsequently multiplied by the power coefficient in order to give the required load power. Power coefficient is selected by potentiometer setting and is input as an analogue signal to the processor. The required load power is:-

$$P_R = P_W \cdot C_p \qquad (7.1)$$

where

$$P_W = (\rho.A.U_i^3)/2 \qquad (7.2)$$

For closed loop control the actual value of load power is determined from the value of DC voltage input to the processor from the electrical transducers (refer to Chapter 4, p64), ie.,

$$P_A = V_d^2/R_L \qquad (7.3)$$

Equation (7.3) is only valid while the rectifier load remains a fixed resistance.

Current control software used confines control to being three position in nature, ie., the actual load power relates to the required load power in any one of three ways:-

(1) Actual load less than required load.

(2) Actual load equal to required load.

(3) Actual load greater than required load.

The difficulty with control systems of this type is that preventative measures must generally be taken to ensure that the controlled parameter does not oscillate about the set point. This can usually be overcome successfully by introducing dead zone into the loop. For this system a sliding value of dead zone power has been used such that for large values of required power the dead zone is large and for small values of required power the dead zone is correspondingly small. For a power dead zone of P_D the three positions of control are shown by expressions (7.4) to (7.6).

$$P_A < (P_R - P_D) \qquad (7.4)$$

requires load to be increased.

$$(P_R - P_D) <= P_A <= (P_R + P_D) \qquad (7.5)$$

requires no change in load.

$$P_A > (P_R + P_D) \qquad (7.6)$$

requires load to be decreased.

This type of control is particularly suited to microprocessor applications such as the system used here. All calculations made by the processor are by use of unsigned integer values since the employment of floating mathematics routines excessively restricts processing time and memory storage capability. Actual load power can be matched to the required load by a series of estimative iterations. For the example of Figure 7.2, the actual power P_A is initially assumed to be zero with the rectifier fully blocking. The required power is P_R. The delay angle starts with blocking (α = 120 degrees) and decreases in steps of approximately 1 degree (120 x 2/255) until the actual power falls to within the dead zone region. If the processor detects that the power error is increasing the delay angle steps in the opposite direction.

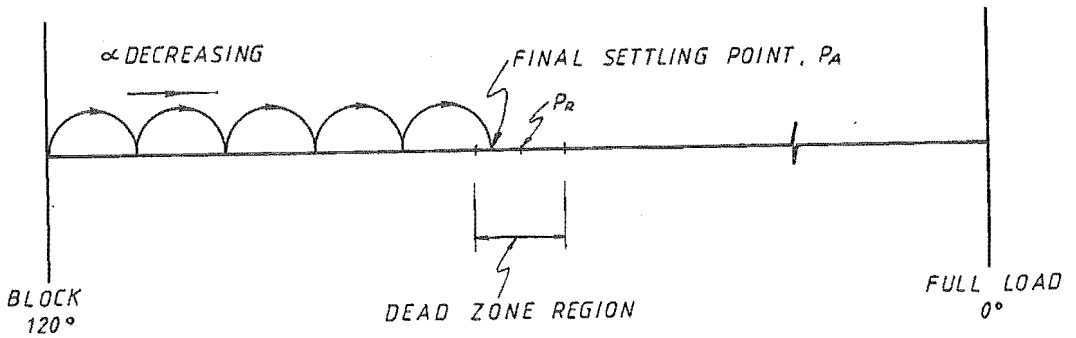

Figure 7.2: Iterative Load Control Steps.

The load control software is run as a result of being requested by the system control routine. To facilitate control of time variations of parameters the system control routine is called once every half second, which is approximately a quarter of the calculated mechanical time constant of the turbine. Scheduling of the running of the system control routine is determined by the operating system of the processor. It carries out the functions which control general operation of the control system (refer to Figure 7.3 and Appendix 4)., ie.,

(i) Control of system status for automatic and panel states. This requires routine scans of the control panel to be made to detect if the operator has requested control. It also censors the operator requests as a safegard against inappropriate actions being taken.

(ii) Generation of the processor life pulse. This is output to external circuits which sense if the system control routine is operating correctly. This is accomplished by detection of low frequency (less than 10 Hz) of the life pulses.

(iii) Calling of the load control routine. The load control routine is called every second scan of the system control routine. It is thus run once every second.

(iv) Detection of system alarms. If an alarm incoming to the processor via the Digital Input Controller is detected or if the processor detects a parameter which exceeds a predetermined maximum allowable value, a shutdown will be ordered.

The load control routine (refer to Figure 7.4 and Appendix 4) uses a look-up table in order to determine power values from wind speed readings, and has 256 entries corresponding to a 2^8 resolution of the anemometer. It caters for values of wind speed from 0 to 30 m/s, and the table entries are scalled to allow single entries in two bytes. Power coefficient is read from an analogue input and has a range of 0 to 0.5, but is restricted by the characteristics of the wind turbine to lower values. Multiplication of the

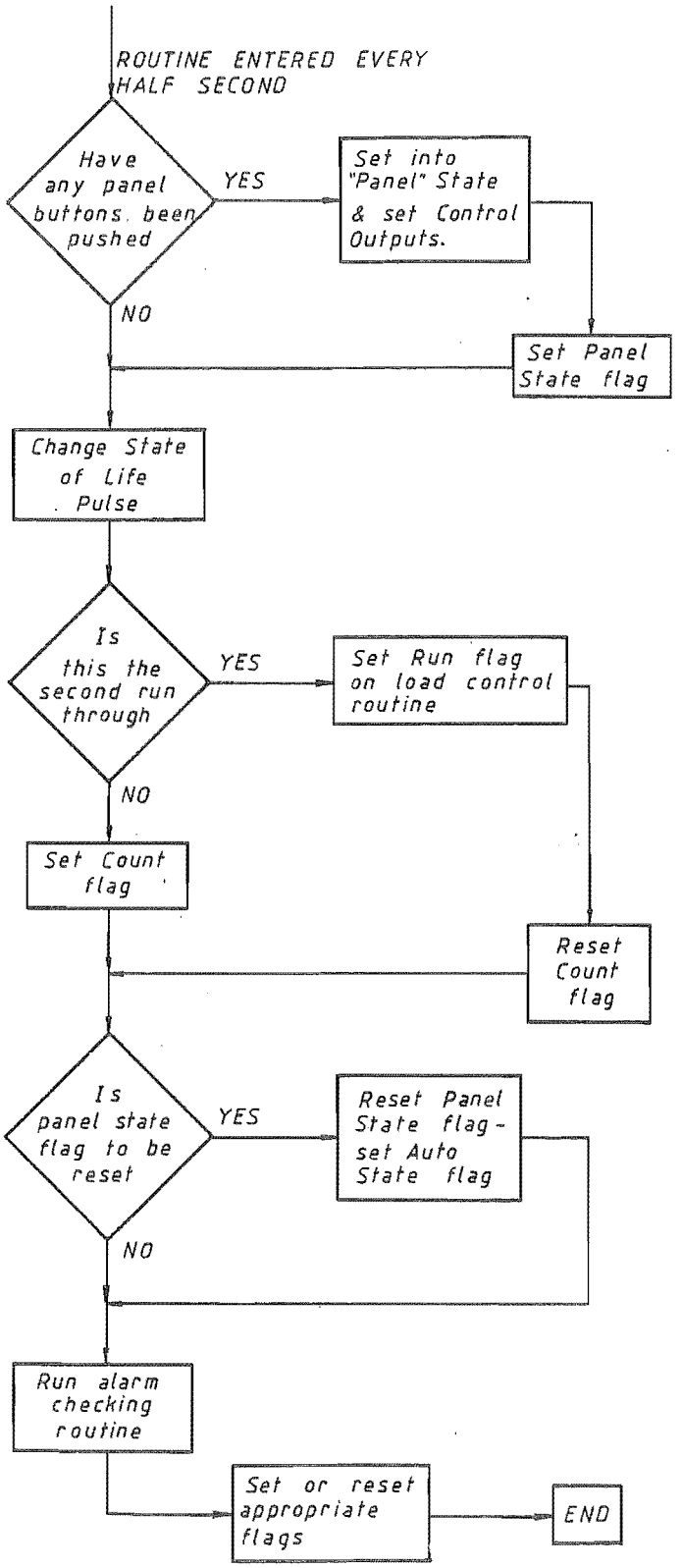

Figure 7.3: System Control Routine.

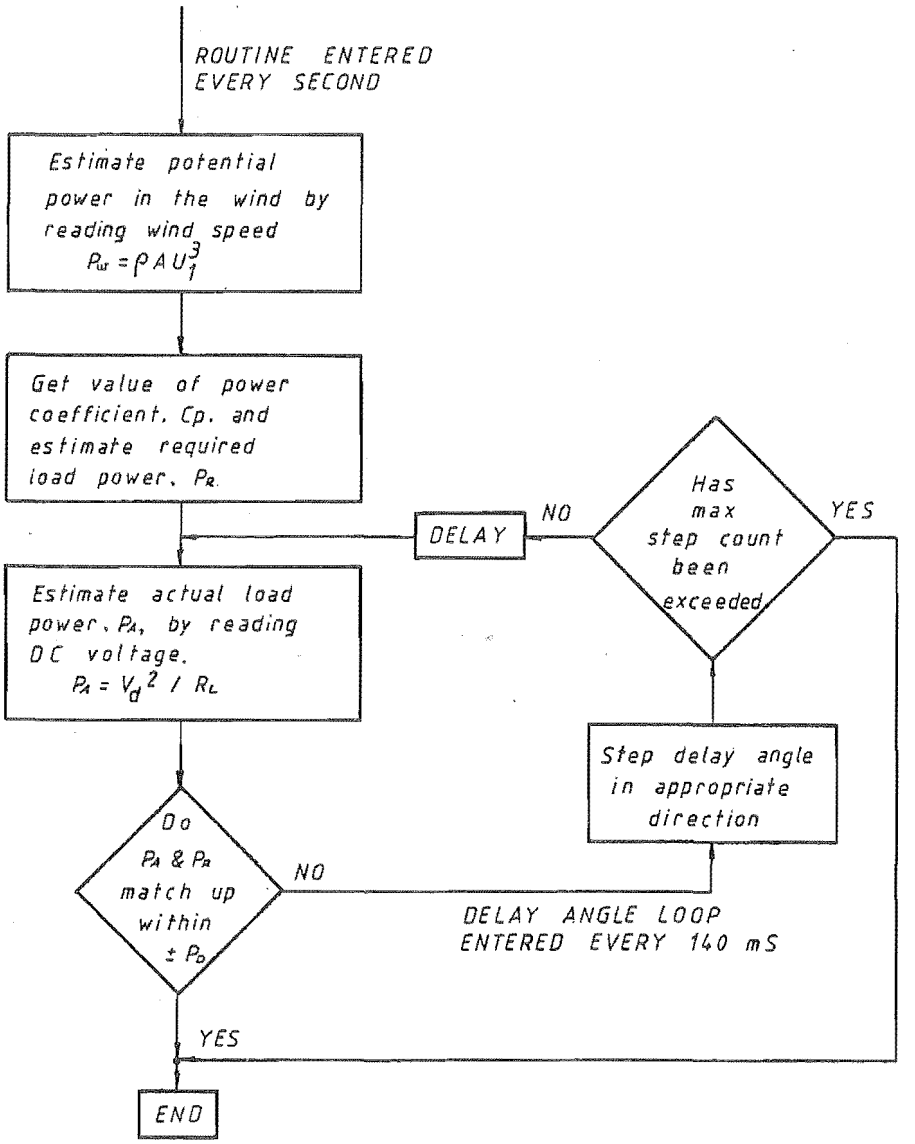

Figure 7.4: Load Control Routine.

wind power and the power coefficient gives the required power. Dead zone power is obtained from the wind speed reading as an index for a set of previously calculated values. Application of the DC voltage reading to Equation (7.3) gives the actual load power, where load resistance has been chosen to be 10 Ω. To change the resistance value on Line 101 of the load control routine listing needs only to be altered.

Required, dead zone and actual powers are compared and the delay angle modified in the appropriate direction. Loop count is checked and if above the maximum the routine is ended. Loop count is used to limit the number of iterative steps made on each run to prevent any possibility of software loop "lock-up". This maximum loop count has been set to 7. If the loop count maximum is not exceeded a delay of 140 ms is applied before a new power comparison is made. This allows time for the rectifier and electrical transducers to respond to the changes in delay angle. Although this time is dependent on the instant on the AC wave at which the change is made, frequency of the AC input, and transducer response time it has been fixed at a value which is greater than that expected under extreme conditions. The extreme condition would consist of operation at the lowest operating frequency of the rectifier (5 Hz) and a delay of 60 degrees(33 mS) may occur before the rectifier can respond. In addition to this the transducers require a period of 90 mS to register a change in DC voltage level (to 90% of steady state value) giving a total delay of 123 mS, or 17 mS less than the loop delay. The loop count multiplied by the loop delay is thus smaller than the load control routine entry intervals, ie., 7 x 140 mS = 980 mS compared with the 1 second entry intervals.

A power averaging count section in the routine allows the operator to make the choice of whether the value of wind power used in the control is taken anew on each entry to the load control routine or is averaged over the most recent two, three or four load control routine entries. This, to some degree, will allow for some control over system damping and response time.

Prevention of a positive feedback condition has also been made by testing each iteration for a decrease in power error, and has become necessary because of the unusual nature of the combined operation of the self

excited induction generator and controlled rectifier. If a positive feedback condition is detected the direction of control is changed by stepping the delay angle in the opposite direction.

Control software has been written in PL/M language because of its ease of use and suitability to control functions. It does however require that checks be made in all mathematical steps to ensure that overflow and underflow conditions do not arise. This is due to the use of unsigned integer arithmetic in the routines.

7.3: Operation with Mains Input to Rectifier.

As a first step in the assessment of system control the rectifier was fed with mains power and a simulated wind speed signal input to the processor. The purpose of this test was to determine if the processor can set the load power to a value suited to the wind speed signal. The use of mains input simplifies test conditions with the more complex case of generator input being shown in Section 7.4. The test arrangement is shown in Figure 7.5.

For a set power coefficient of 0.25 and wind speed changes of 12 m/s to 6 m/s and 18 m/s to 6 m/s recordings of wind speed and DC voltage were made for power averaging counts of one and four. The expected values of voltage can be calculated using Equations (7.1), (7.2) and (7.3), ie.,

$$V_d = \sqrt{C_p . U_1^3 . A . \rho . R_L / 2} \qquad (7.7)$$

or

$$V_d = \sqrt{171.1\ C_p . U_1^3} \qquad (7.8)$$

where

$A = \pi . R^2 = 28.27$ m

$\rho = 1.21$ kg/m^3

$R_L = 10\ \Omega$

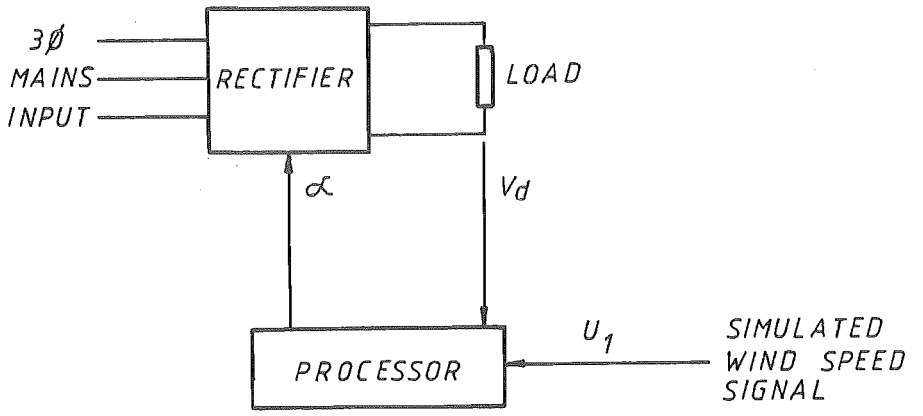

Figure 7.5: Controller Tests With Mains Input.

Plates 7.1(a) and 7.1(b) show the test recordings for the 12 m/s to 6 m/s change in wind speed and Plates 7.1(c) and 7.1(d) for the 18 m/s to 6m/s change. Measured steady state values are shown in Table 7.1, with calculated values found from by Equation (7.8). Measured and calculated values agree to within approximately 4% showing that the system is operating as expected under these conditions. For Plate 7.1(a) the DC voltage has responded in one entry or run of the load control routine, however for the change of 18 m/s to 6m/s of Plate 7.1(c) the routine required two runs, ie., approximately 2 seconds to respond. For Plates 7.1(b) and 7.1(d) where the power averaging count has been increased to 4, four runs or a total of four seconds have been required to obtain the correct DC voltage. In each of these four runs less than the maximum loop count has been used to achieve the required DC voltage for that run.

Wind Speed Input (m/s)	Calculated DC Voltage	Measured DC voltage
18	499	480
12	272	270
6	96	100

Table 7.1: Test Results, Mains Input.

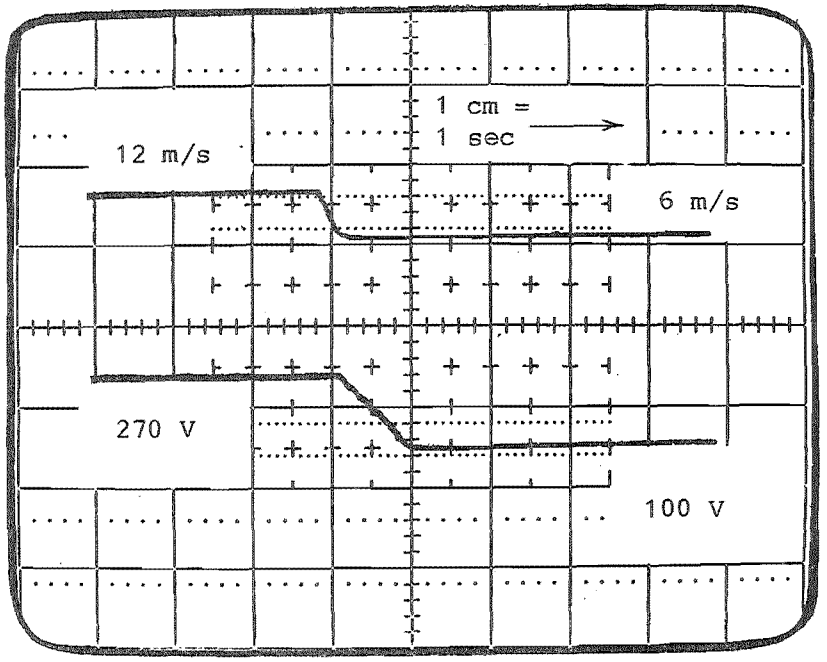

(a) 12 m/s - 6 m/s Wind Speed Change

Power Averaging Count = 1

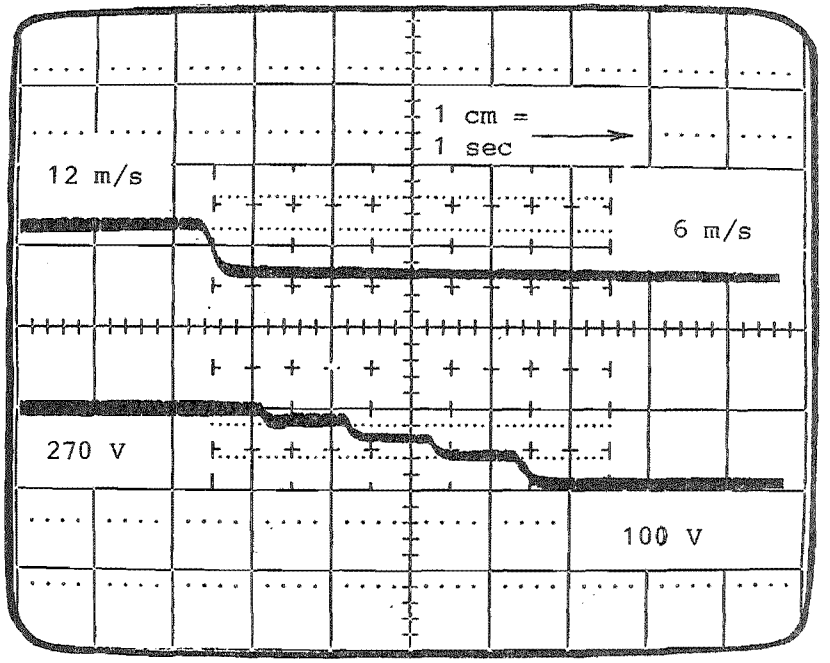

(b) 12 m/s - 6 m/s Wind Speed Change

Power Averaging Count = 4

Plate 7.1: Mains Fed Responses of Controller.

U_1 = Wind Speed (Upper Trace)

V_d = DC Voltage (Lower Trace)

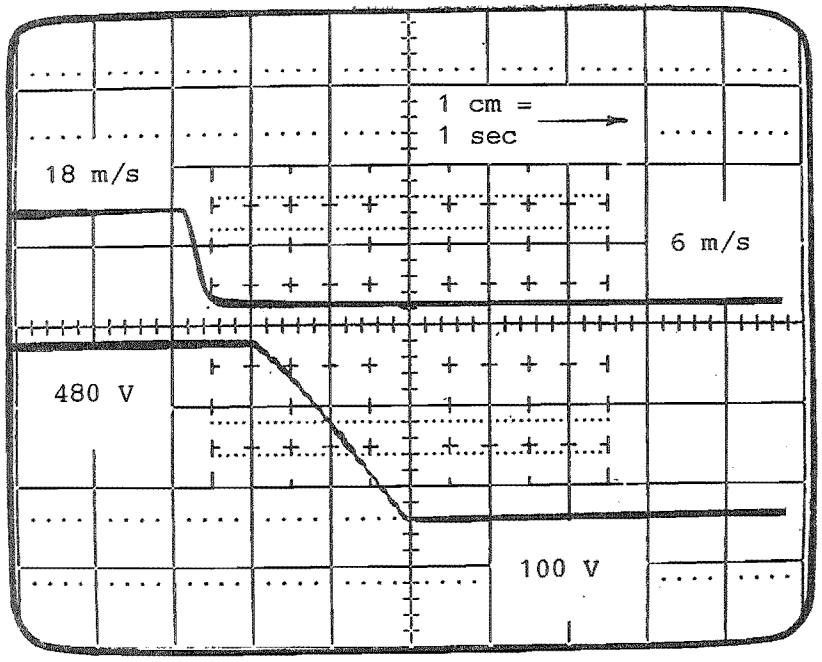

(c) 18 m/s - 6 m/s Wind Speed Change

Power Averaging Count = 1

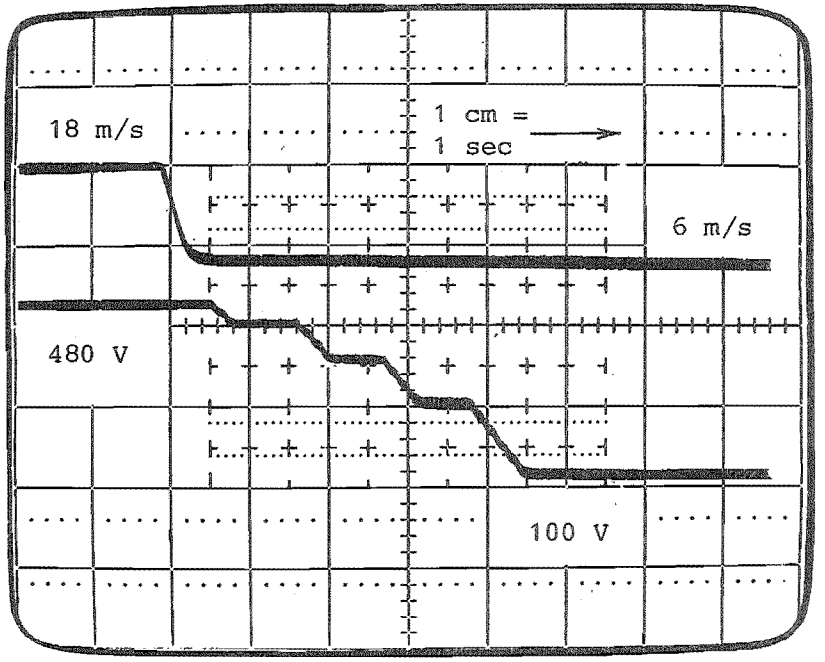

(d) 18 m/s - 6 m/s Wind Speed Change

Power Averaging Count = 4

Plate 7.1: Mains Fed Responses of Controller.

U_i = Wind Speed (Upper Trace)

V_d = DC Voltage (Lower Trace)

The effect of increasing the averaging count has thus been to alter the dynamic characteristics of the load control system in that the response times have been increased by the amounts shown above.

7.4: Operation With Generator Input to Rectifier.

As an extension of the mains fed controller tests the self excited induction generator was used as the source of power for the rectifier. The generator was driven by a Schrage motor which provided control over generator shaft speed.

7.4.1: Generator/Rectifier Interaction.

The role of capacitors as a source of lagging reactive current for excitation of the induction generator has been described in detail in Chapter 3. For an unloaded generator the lagging current required for generator excitation is approximately equal to the capacitative current as illustrated by Figures 3.9 and 3.13, ie.,

$$I_m = I_c \qquad (7.9)$$

For purely resistive loads the supply of this excitation current to the generator is largely unaffected, however if a complex lagging load is placed on the machine excitation current is effectively "stolen" from the generator resulting in a decrease in generated voltage (assuming constant speed). Referring to Figure 3.15, the magnetising current is now approximately described by:-

$$I_m = I_c - I_q \qquad (7.10)$$

In practical cases however the speed of the generator shaft will not remain constant as excitation changes. This is because a decrease in generated voltage, as a result of lower excitation current, generally results

in a decrease in real load power and a similar decrease in generator losses. This will usually give an increase in shaft speed since the prime mover is less heavily loaded.

The controllable rectifier affects the self excited induction generator in two ways:-

(i) As rectifier delay angle is decreased the generator becomes more heavily loaded since the rectifier is drawing increased real current, as shown by Equation (4.11).

(ii) A similar decrease in delay angle also changes the amount of lagging reactive current drawn by the rectifier resulting in a change in machine excitation as described in the above. Refer to Equation (4.12).

Equation (7.10) can now be modified for the rectifier/generator combination to:-

$$I_m = I_c - (\sqrt{6}/\pi).I_d.\sin(\alpha) \qquad (7.11)$$

or

$$I_m = 2\pi.f_1.V.C - (\sqrt{6}/\pi).(V_d/R_L).\sin(\alpha) \qquad (7.12)$$

Equating (7.12) with (4.6) gives:-

$$I_m = V.\ 2\pi.f_1.C - (18/\pi^2).\cos(\alpha).\sin(\alpha) \qquad (7.13)$$

The purpose of developing Equation (7.13) is to demonstrate the complex nature of the interaction between the self excited induction generator and the controllable rectifier. Equation (7.13) can be further complicated by including the expression relating generated voltage and magnetising current (Equation 3.2) and also an expression for frequency such as Equation (3.5). The result is a transcendental equation which is difficult to manipulate and because generator losses have been ignored it would provide results of dubious accuracy. Additionally, for a rectifier without an inductor on the

DC output the use of Equation (4.6) and Equations (4.11) and (4.12) is not valid, and the foregoing would need to be accordingly modified. However although these equations are only approximate they do demonstrate the underlying principles involved in the interaction of the generator and rectifier.

Equations (4.16) and (4.17) can be used for estimation of DC output voltages for known input AC voltages and delay angle. For the generator/ rectifier combination, the estimated and actual values of normalised DC voltage are shown in Figure 7.6 for a 400 Ω DC load. The points marked (a), (b), (c), (d) correspond to the photographed waveforms of Plate 5.2, which display large amounts of harmonic distortion on the input waves, primarily due to generator saturation. The fact that the harmonic content decreases as delay angle is decreased is due to a decrease in generated voltage as a result of less excitation current being available to the generator.

The discrepency between calculated and measured values for large delay angles is probably due to harmonics, based on two factors:-

(i) The difference between measured and calculated rectifier output voltages is less than 10% for mains input, i.e., negligible voltage harmonics present. Refer Figure 4.10. The difference between the mains fed case and this situation is that the voltage waveforms contain considerable harmonics in the generator fed case.

(ii) As delay angle is reduced the difference becomes less since the generated voltage is also decreasing and the harmonic generation is less due to a drop in saturation.

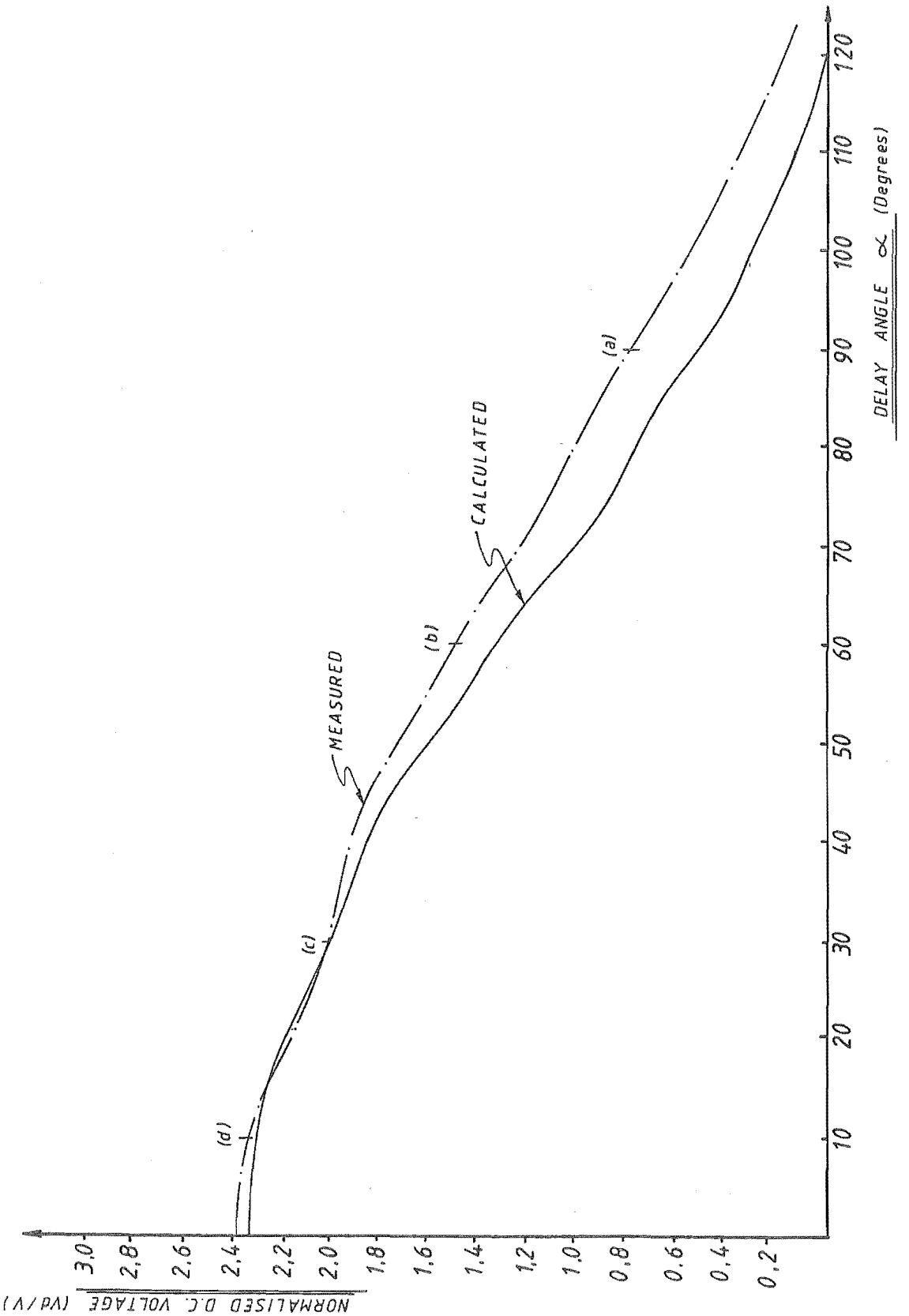

Figure 7.6: Rectifier Output Voltage For Generator Input, 400 Ω Load.

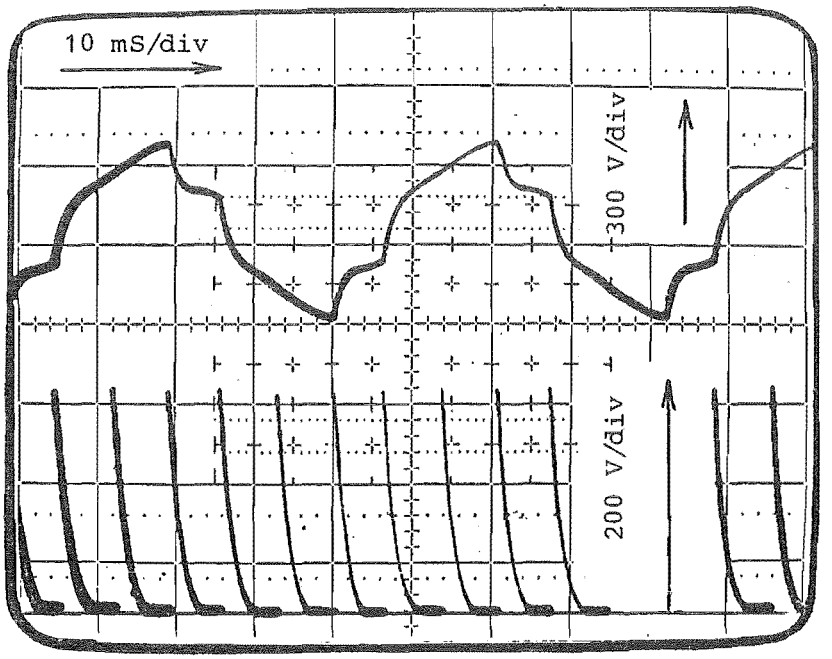

(a) α = 90 degrees.

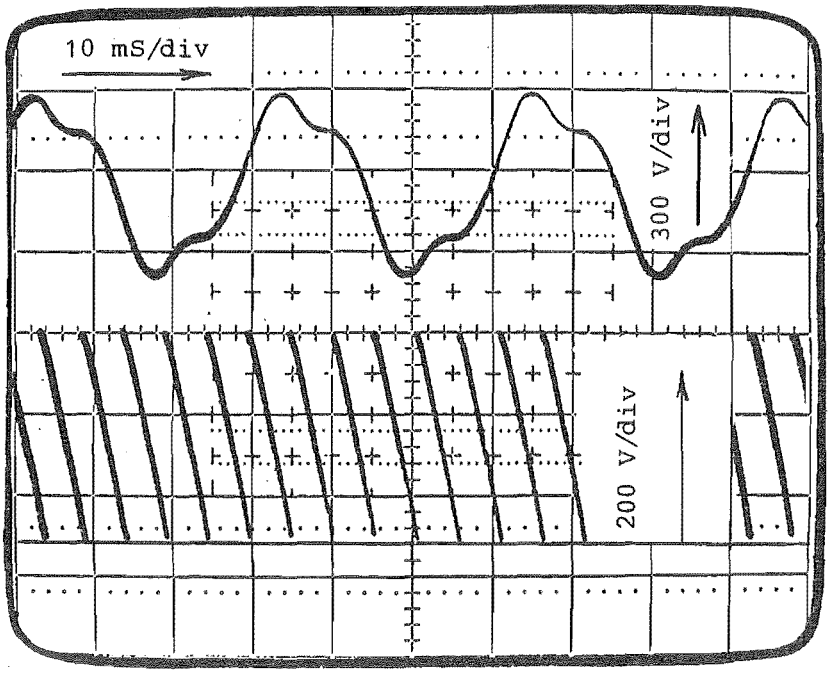

(b) α = 60 degrees.

Plate 7.2: Generator and Rectifier Output Waveforms, 400 Ω Load.

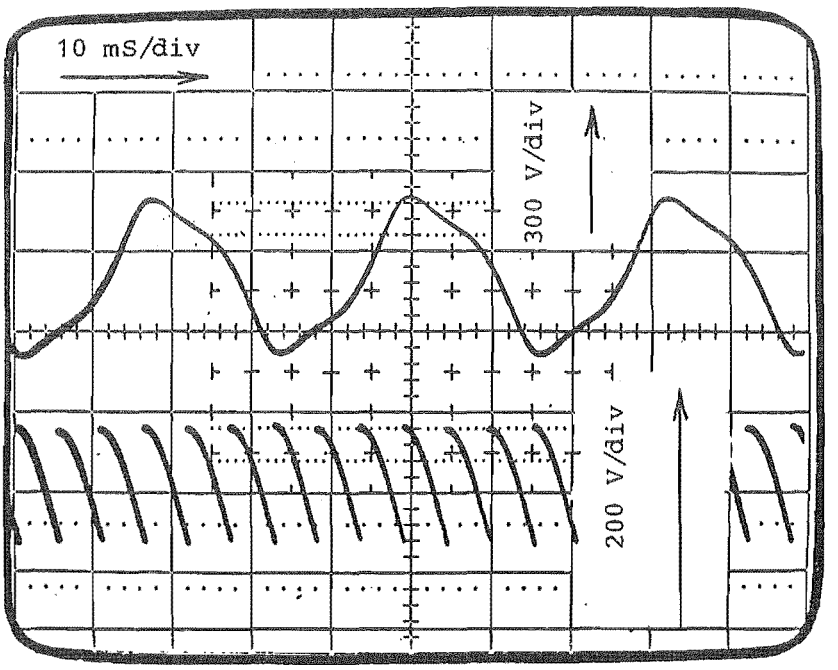

(c) α = 30 degrees.

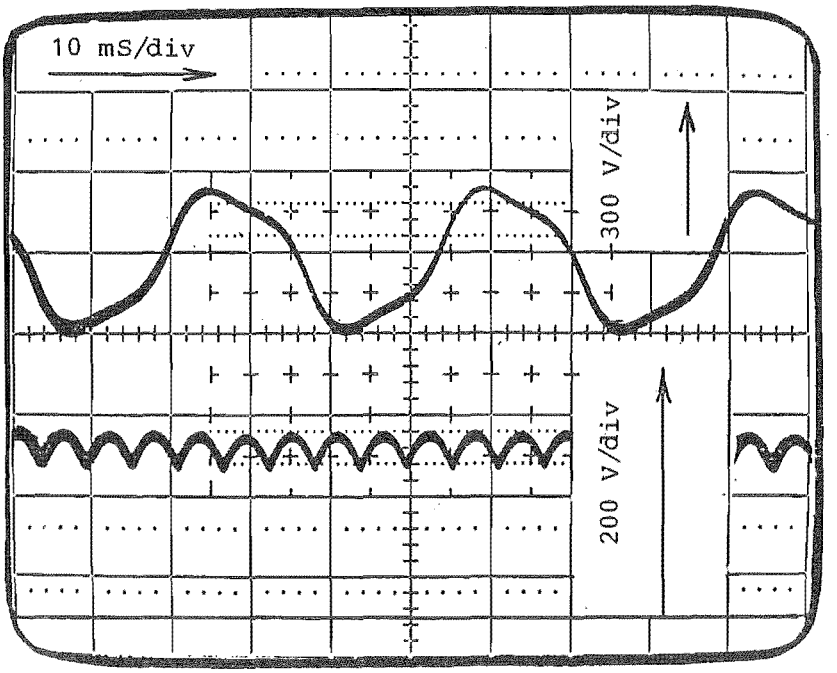

(d) α = 10 degrees.

Plate 7.2: Generator and Rectifier Output Waveforms, 400 Ω Load.

7.4.2: Controller Operation.

As in the case of mains input, tests were carried out for changes in wind speed signal. Changes in wind speed used were 15m/s to 6m/s and 12m/s to 6m/s. The test circuit is shown in Figure 7.7. Power coefficient was again set to 0.25.

For power averaging counts of one and four, Plate 7.3 shows the recorded responses. As for the mains fed case the responses are slowed by the increase in power averaging count. The results were similar to those for the mains fed tests in that the traces for power averaging counts of 4 yield response times corresponding to four load control routine runs or about 4 seconds. Also, for power averaging counts of one the response of Plate 7.3(c) required two runs and for the 12 m/s to 6 m/s response only one run was required. Measured and calculated values of DC voltage are shown by Table 7.2 and are within 7% of calculated values.

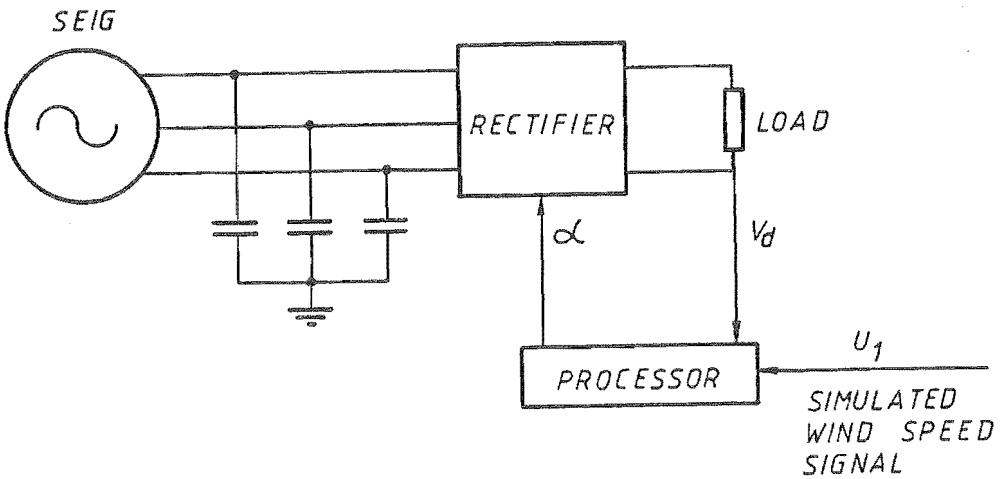

Figure 7.7: Controller Tests With Generator Input.

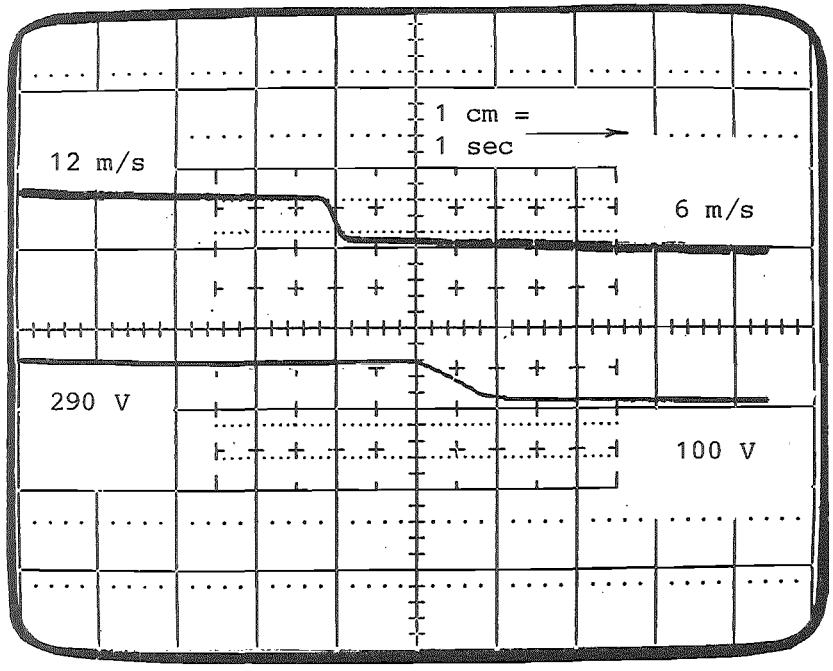

(a) 12 m/s - 6 m/s Wind Speed Change

Power Averaging Count = 1

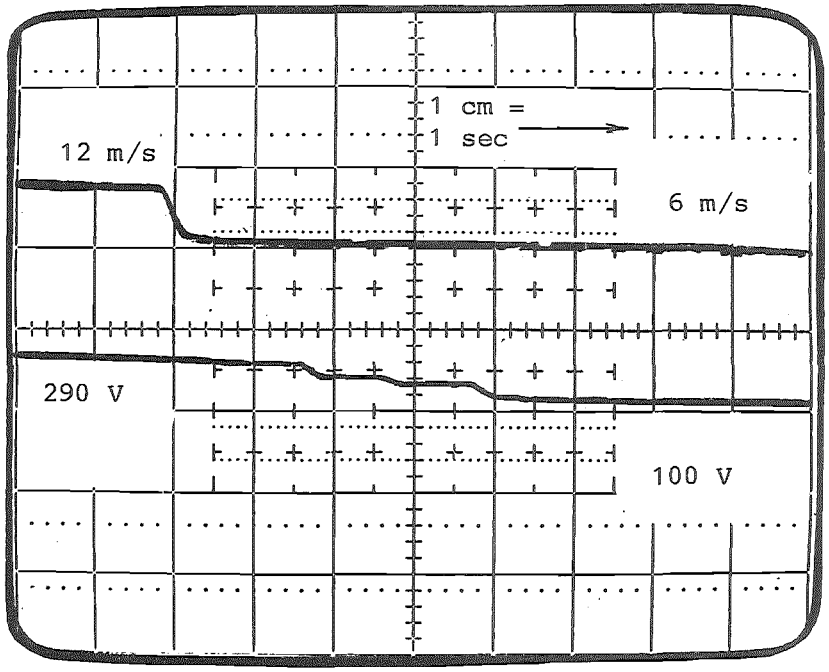

(b) 12 m/s - 6 m/s Wind Speed Change

Power Averaging Count = 4

U_1 = Wind Speed (Upper Trace)

V_d = DC Voltage (Lower Trace)

Plate 7.3: Generator Fed Responses of Controller.

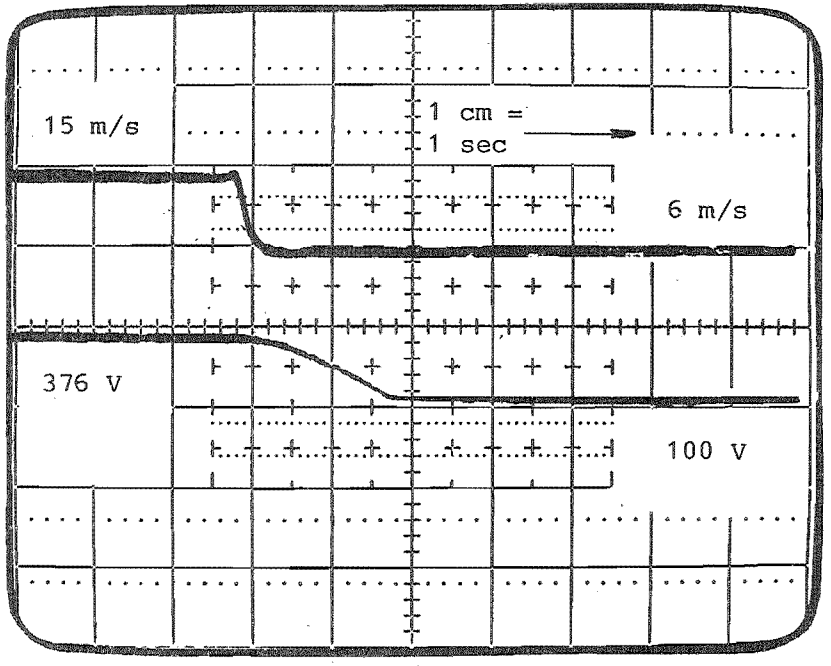

(c) 15 m/s - 6 m/s Wind Speed Change

Power Averaging Count = 1

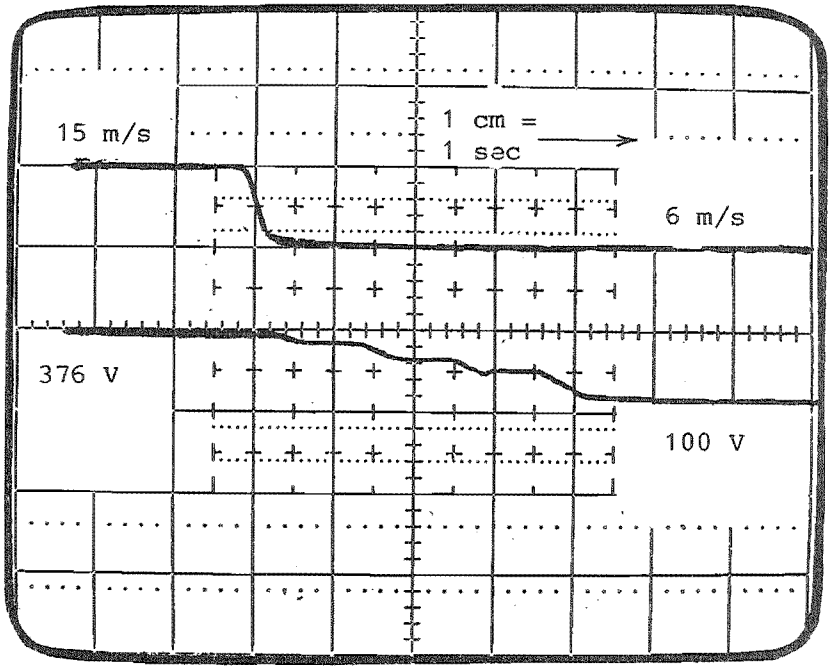

(d) 15 m/s - 6 m/s Wind Speed Change

Power Averaging Count = 4

Plate 7.3: Generator Fed Responses of Controller.

U_1 = Wind Speed (Upper Trace)

V_d = DC Voltage (Lower Trace)

Wind Speed Input (m/s)	Calculated DC Volts	Measured DC Volts
15	380	376
12	272	290
6	96	100

Table 7.2: Test Results, Generator Input.

7.5: Harmonics:- Loaded Generator - Rectifier Combination.

When the rectifier is operating under conditions of heavy load, large amounts of harmonic voltages are created by the rectifier, the generator simply acting as a load under these circumstances. The situation is similar to that explained in Chapter 3 where the appearance of these harmonic voltages becomes less evident as harmonic number increases since the excitation capacitors short circuit the high order harmonics.

For a high order harmonic current I_ν generated at the rectifier terminals, the voltage of the harmonic seen over the capacitors is:-

$$V_\nu = I_\nu/(\nu.\omega_1.C) \qquad (7.14)$$

where ν is the harmonic number.

The portion of harmonic current which passes into the generator is small for high order harmonics since the leakage reactances of the machine are large. As harmonic number decreases, more current will be shared between the capacitors and the generator, and Equation (7.14) will no longer hold true. For the third harmonic, the situation becomes even less clear since the generator will also be generating substantial voltage at this order of harmonic due to saturation.

A Wandel and Goltermann Power Line Harmonic Analyser was used to measure harmonic voltages and currents at the input terminals of the rectifier the

```
14JUL84 15:29 M1.A4

ν:01 54.86% 208.5 V
        I:    3.77 A
        P:  380.9 W
        Ψ:      61°

ν:02   0.85%  3.25 V
        I:   0.096 A
        P: -98.69mW
        Ψ:     109°

ν:03   1.29%  4.89 V
        I:   0.213 A
        P: -6.217mW
        Ψ:      99°

ν:04   0.35%  1.35 V
        I:   0.113 A
        P: -0.567mW
        Ψ:      90°

ν:05   7.27% 27.63 V
        I:    3.41 A
        P: -3.286 W
        Ψ:      92°

ν:06   0.43%  1.64 V
        I:   0.241 A
        P: -11.09mW
        Ψ:      92°

ν:07   3.88% 14.73 V
        I:    2.67 A
        P: -685.2mW
        Ψ:      91°

ν:08   0.28%  1.05 V
        I:   0.226 A
        P: -32.57mW
        Ψ:      98°

ν:09   0.42%  1.61 V
        I:   0.372 A
        P:  -8.07mW
        Ψ:      91°

ν:10   0.22%  0.85 V
        I:   0.230 A
        P: -17.91mW
        Ψ:      95°

ν:11   1.91%  7.25 V
        I:   2.134 A
        P: -345.3mW
        Ψ:      91°

ν:12   0.21%  0.79 V
        I:   0.305 A
        P:  -8.34mW
        Ψ:      92°

ν:13   1.05%  4.00 V
        I:   1.424 A
        P: -55.72mW
        Ψ:      91°

ν:14   0.16%  0.59 V
        I:   0.236 A
        P:  -8.36mW
        Ψ:      94°

ν:15   0.22%  0.85 V
        I:   0.383 A
        P:  12.58mW
        Ψ:      88°

ν:16   0.14%  0.53 V
        I:   0.264 A
        P:  21.25mW
        Ψ:      81°

ν:17   0.78%  2.95 V
        I:   1.430 A
        P: -160.3mW
        Ψ:      92°

ν:18   0.16%  0.59 V
        I:   0.314 A
        P:  43.45mW
        Ψ:      76°

ν:19   0.43%  1.64 V
        I:   0.929 A
        P: -78.18mW
        Ψ:      93°

ν:20   0.09%  0.36 V
        I:   0.239 A
        P:  4.605mW
        Ψ:      87°

ν:21   0.10%  0.69 V
        I:   0.394 A
        P:  24.53mW
        Ψ:      85°

ν:22   0.09%  0.36 V
        I:   0.275 A
        P: -13.44mW
        Ψ:      98°

ν:23   0.43%  1.64 V
        I:   1.072 A
        P: -39.87mW
        Ψ:      91°
```

Figure 7.8: Harmonic Analyser Results for Loaded Generator.

results of which are given in Figure 7.8 for line-neutral voltages. For the high order harmonics, Equation (7.14) is accurate to within about 5% (C = 90 μF, f_1 = 50 Hz)and as the harmonic order decreases it becomes obvious that the generator is taking a larger share of the harmonic current.

For the fundamental component, power flow can only be from the generator to the rectifier and this is the measured situation referred to in Figure (3.17). The total current flowing in the line is:-

$$I = \sqrt{I_1^2 + I_2^2 + I_3^2 + \ldots\ldots\ldots + I_n^2} = \sqrt{\Sigma\ I_\nu^2} \qquad (7.15)$$

For the results of Figure 7.8 this gives a total current of about 7 amperes which is substantially higher than would be expected, indicating that caution should prevail in using the SEIG/ rectifier combination since currents are likely to be greater than initially considered.

7.6: Wind Powered WTG Tests.

The tests conducted in the two previous sections indicate that the load control system should operate satisfactorily under wind powered conditions. It would not however be possible to operate the system at maximum power coefficient since appreciable winds would overload the generator. It was therefore decided that these tests would be carried out at a low selected value of power coefficient and if operation proved to be successful, it should also be successful at higher power coefficients (including C_{pm}). This would necessitate the installation of a larger capacity generator of the order of 20 kW.

System operation was tested under two circumstances:-

(i) Manual operation.

(ii) Automatic operation with a power averaging count of 1 and a set power coefficient of 0.1.

7.6.1: Manual Operation.

A manual test was carried out simply to provide some feel for the difficulty of obtaining a fixed power coefficient. Recordings of wind speed, DC voltage, shaft speed and delay angle were made and are shown in Plate 7.4. It can be seen that for increases in wind speed the operator has successively increased turbine load, however it was not at all possible to obtain a constant value of power coefficient or tip speed ratio by this means.

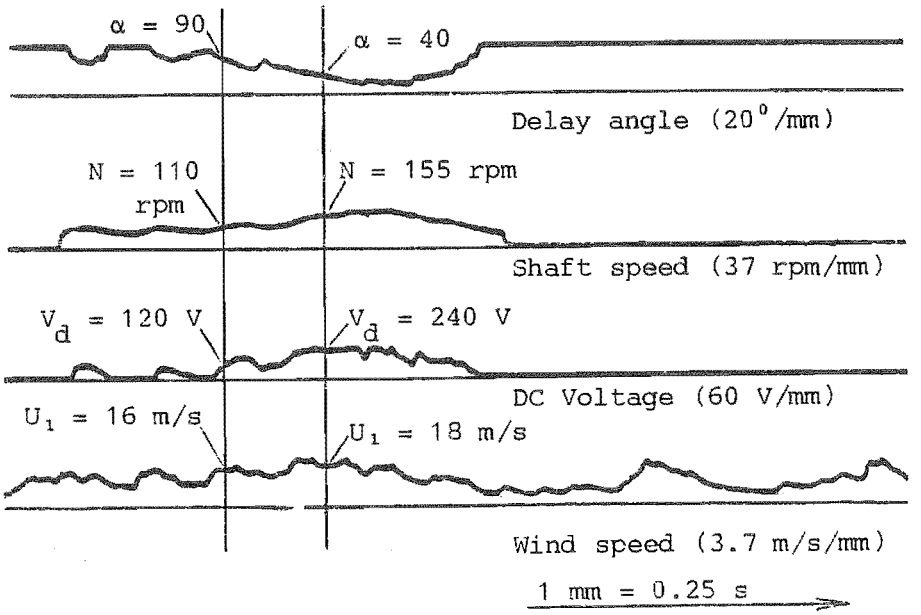

Plate 7.4: Manual Load Control Response.

7.6.2: Automatic Operation.

Plate 7.5 shows similar recordings for closed loop control of power coefficient. As wind speed changes the processor modifies delay angle so that the appropriate load is placed on the turbine. The vertical marks on Plate 7.5 show the points at which the load control routine is entered and a new wind speed reading is made. The marks are thus one second apart.

After entry to the load control routine , ie., at a mark, the processor will settle on a DC voltage at the end of a one second period, ie., at the next mark. The DC voltage at each mark will thus correspond to the wind speed reading at the previous mark. During the intervening period the processor is stepping the delay angle in order that correct voltage is found despite fluctuations is AC voltage due to excitation changes caused by the changing values in delay angle and also due to shaft speed changes.

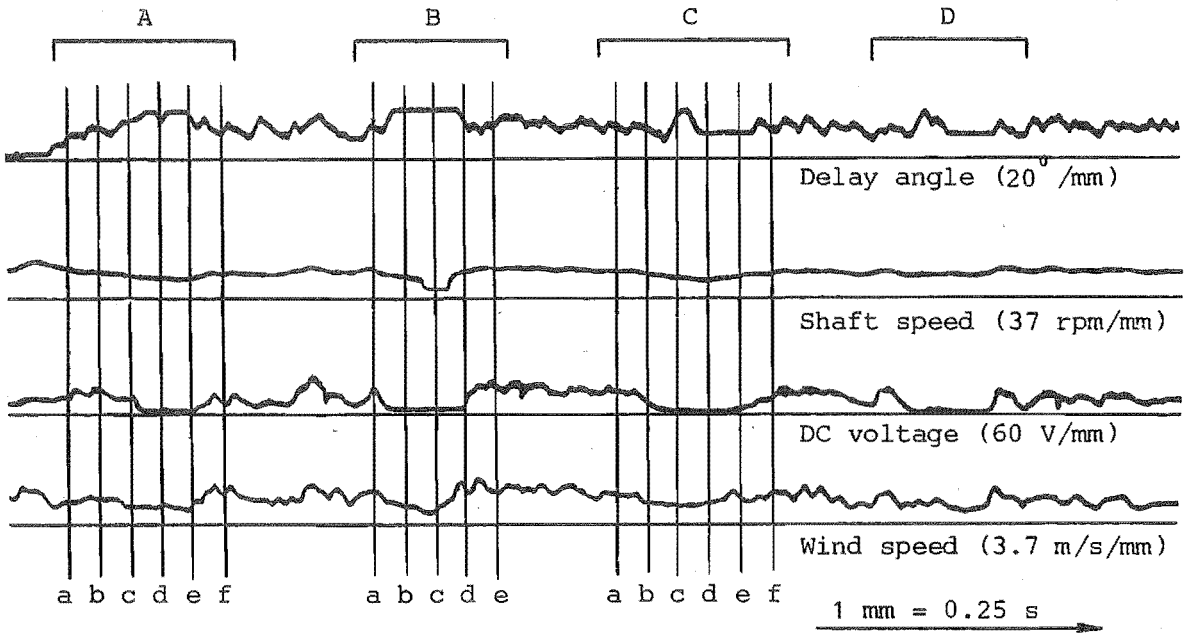

Plate 7.5: Automatic Load Control Response.

This is illustrated by the group of marks "A" in Plate 7.5. At mark (a) the measured wind speed is 10.5 m/s giving a wind power P_W of 19 800 W. The processor modifies the delay angle over the next one second period to give a DC output voltage of 150 V at (b). For a power coefficient of 0.1 the required power at (b) is 19 800 x 0.1 = 1 980 W, with a dead zone power P_D of 385 W. The actual power therefore should lie in the region of 1 595 W to 2 365 W. For the 150 V output the actual power P_A is 2 250 W, and is within the required dead zone area. Similarly for a new wind speed reading

taken at (b) of 11 m/s the required power P_R at mark (c) will be 22 770 x 0.1 ± 385 W, where the 385 W is the dead zone. This makes the required power lie in the region of 1 895 W to 2 665 W. The measured DC output voltage at (c) is 140 V giving an actual power of 2 000W, which is again within the dead zone area. Tip speed ratio has been maintained around 3.6 for the two cases. For the case of the measured 10.5 m/s wind speed at (a) the shaft speed at (b) is 130 rpm giving X = 3.8 and for the case of the 11 m/s wind speed at (b) the shaft speed at (c) is 120 rpm giving X = 3.5. These values will remain relatively constant where wind speed is not fluctuating quickly, because the changing conditions are not so extreme as to cause great variations in turbine speed in the intervening period.

For mark (c), a sudden decrease in DC voltage occurs and is caused by the drop in wind speed shortly before mark (c), and results in the drop in shaft speed with a corresponding fall in AC voltage. The wind speed is thus read at (c) and the processor attempts to modify delay angle to obtain the correct load, ie., it increases delay angle to reduce load to the extreme where it reaches 120 degrees. At this point the AC voltage has not totally collapsed to below the minimum allowable of 60 V and on the next mark (d) an attempt is made to increase load. This only lasts for a short period until the voltage begins to fall further due to the rectifier reducing generator excitation, whence it runs the delay angle back up to 120 degrees and prevents total de-excitation. At (e) the processor again attempts to reduce delay angle so that load will increase, but in this case the wind speed also picks up resulting in a return to normal operating conditions. For the wind speed reading taken at (e) of 9 m/s, the required power at (f) is 12 470 x 0.1 ± 385 W where the dead zone power is 385W. The actual power should therefore lie in the region of 960 W to 1 630 W. Measured DC voltage at (f) is 105 V giving an actual load power of 1 100 W, which falls within the dead zone. The shaft speed at (f) is 110 rpm corresponding to a tip speed ratio of X = 3.8 as measured before at (b).

Group "B" of marks exhibits the abnormality of delay angle being at 120 degrees for an extended period. For the high wind speed reading taken at mark (a) the processor reduces delay angle in order to increase load, but the

process runs into difficulty when the wind speed suddenly drops resulting in a loss of AC voltage since shaft speed decreases. The processor sees the situation as one of incorrect sign of delay angle steps and subsequently increases delay angle up to 120 degrees. The generator de-excites and the delay angle remains at 120 degrees since the load control routine is not being accessed because of the de-excited state of the generator. For mark (d) the wind speed again picks up and the turbine speed increases sufficiently for the generator to re-excite and allow normal control to take place over the period between (d) and (e). For the wind speed of 16 m/s at (d), the required power at (e) is 70 080 x 0.1 ± 1 535 W or in the range of 5 475 W to 8 545 W. 1 535 W is the dead zone power. The measured DC voltage at (e) is 240 V giving an actual load power of 5 760 W and is within the dead zone region. The tip speed ratio for the measured wind speed of 155 rpm is X = 3.1 and is seen to be less than the previously calculated values. This is primarily caused by the greatly fluctuating wind in the intervening period between marks (d) and (e) resulting in unanticipated variations in shaft speed. This would indicate that a faster control is required in order to account for quickly varying wind patterns. The apparent drop in shaft speed in the period between (b) and (d) results from the shaft speed being so low that the shaft speed transducer has dropped below its lower operating threshold.

For group "C" normal operation begins at mark (a) where a wind speed of 13.5 m/s is recorded giving a required load power of 42 100 x 0.1 ± 770 W where the 770 W is the dead zone power. The required DC voltage range to achieve this ranges from 185 V to 223 V. This voltage would have been achieved if it were not for the sudden drop in wind speed in the (a) to (b) period resulting in a drop in AC voltage and subsequent drop in DC voltage. As the AC voltage falls to below the minimum allowable value the processor forces the delay angle up to 120 degrees and as a result the AC voltage marginally exceeds the minimum allowable value. The load control loop is again entered at (c) and the delay angle decreased to increase load, with a subsequent drop in AC volts to below the minimum allowable value. The correct DC voltage is apparently achieved at (d), albeit below the minimum allowable value of AC voltage of 60 V. When the next entry occurs at mark

(d) the AC voltage is less than 60 V and the controller holds the delay angle at whatever value it was at before the new reading. At mark (e) the AC voltage, through an increase in wind speed, begins to rise to the extent where the control loop is again active and operation again returns to normal. The wind speed reading at (e) is 11 m/s giving an allowable range of actual powers of 1 895 W to 2 665 W. Measured DC voltage at (f) is 145 V giving an actual load power of 2 100 W which is within the dead zone area. Notice also that the wind speed between (e) and (f) is reasonably constant. The tip speed ratio of X = 3.3 results from a shaft speed of 115 rpm at (f).

A similar situation occurs in the area "D" as in the case of "C" above, where the wind speed unexpectedly falls shortly after a new wind speed reading has been taken. This case however is different in that the wind speed increases in short bursts whilst in a generally quiet period, resulting in the appearance of DC voltage spikes due to short periods of increased shaft speed.

7.7: Summary.

The load control system has been tested in a step by step manner and shown to operate satisfactorily under laboratory conditions. Self excited induction generator/controlled rectifier combined operation has been shown with test results. Wind powered operation has been tested and shown that operation is satisfactory under slowly varying wind conditions. For conditions where the wind is fluctuating rapidly the system is unable to maintain tip speed ratio at a relatively constant value and faster control of delay angle is required. The system would be improved if the generator was of a larger size so that higher loads could be placed on the turbine and thus operate at higher outputs near optimum power coefficient. Adjustment of the blade pitch angle may also be necessary for the turbine to operate at higher tip speed ratios.

CHAPTER 8.

PROSPECTS FOR THE FUTURE.

8.1: Introduction.

With the immediate objectives of the project achieved it is proposed to extend research in the form of application of the wind turbine generator to practical uses. Several such proposals are listed below along with several ideas for basic research on wind turbine generators.

8.2: Proposals for WTG Applications.

.Glasshouse Heating.

An application of the wind turbine generator to horticultural glasshouse heating is shown in Figure 8.1, and is based on the high heat loss that these buildings experience in cold windy conditions. During these periods the WTG is capable of supplying direct heating elements inside the glasshouse. Warm windy spells may occur however, when the glasshouse does not require heating and the energy from the WTG is stored in water storage tanks. This heat is then available for heating when the windmill is of little use, i.e., during cold still periods. The present control system is capable of controlling these functions. Refer to Appendix 3.

.Parallel Operation of WTG With Other Generators.

Also of considerable interest would be the operation of the WTG in parallel with other generators. This could take three forms:-

(1) Direct connection of the SEIG to a grid, bypassing the rectifier as in Figure 8.2. For a fixed frequency grid and a variable speed wind turbine the relationships between generator load, wind speed,

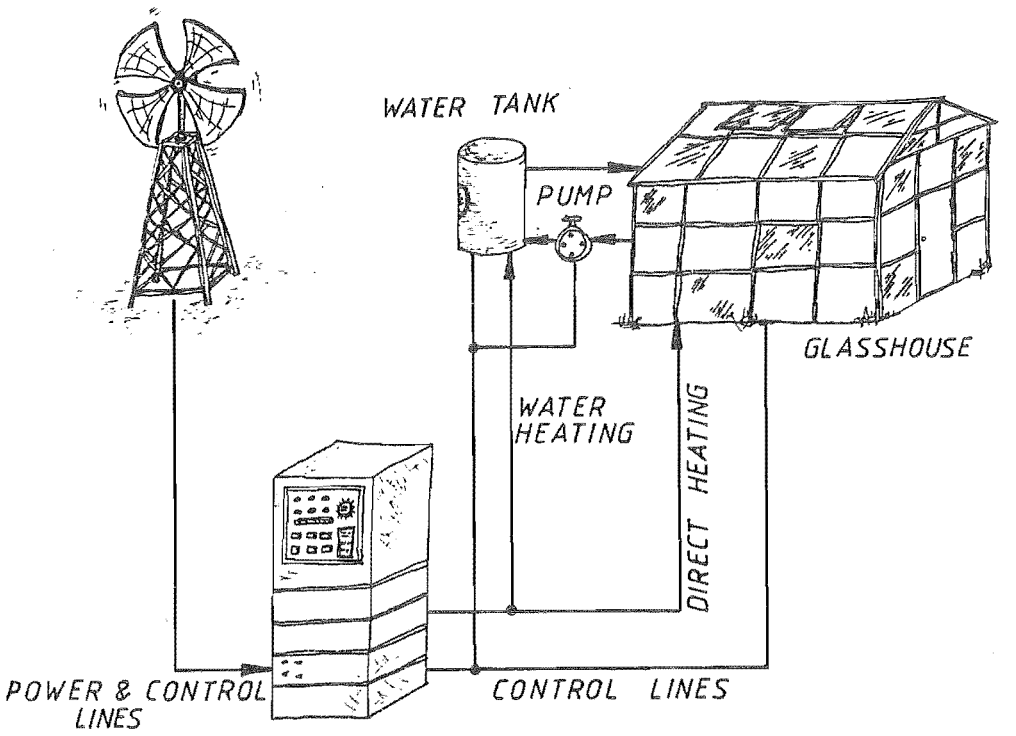

Figure 8.1: Glasshouse Heating by WTG.

turbine power coefficient and generator slip would be of considerable interest. In the case of all generators on the grid being of the asynchronous type as suggested by de Mello (de Mello 1981, 1982) then for n identical generators the total real power is zero , i.e., load and generated powers are equal (neglecting losses).

$$(V^2.s_1/R'_2) + (V^2.s_2/R'_2) + \ldots\ldots + (V^2.s_n/R'_2)$$

$$= V^2/R_L \qquad (8.1)$$

Where R_L is a load resistance. This leads to:

$$(s_1 + s_2 + \ldots\ldots + s_n) = R'_2/R_L = K_1 \qquad (8.2)$$

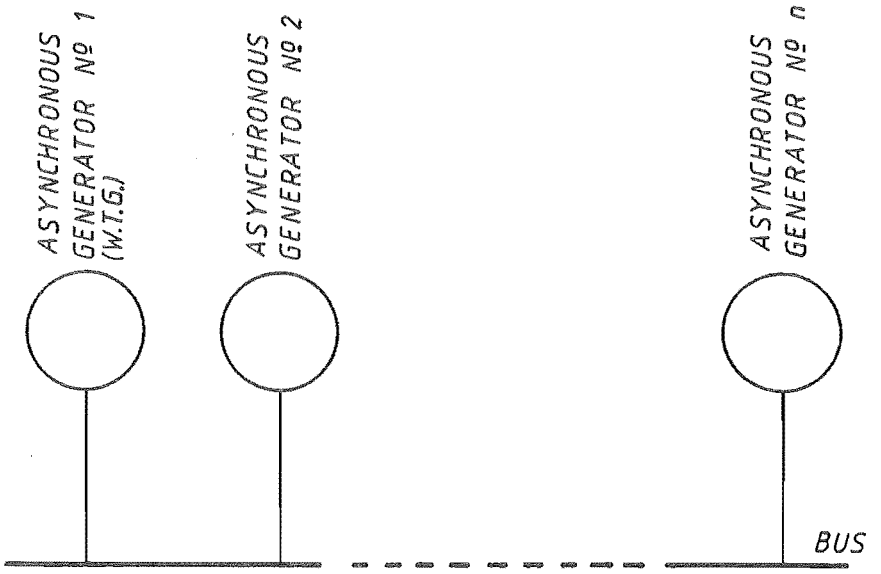

Figure 8.2: Parallel Operation of SEIG's.

Where K_1 is a constant value. Assuming generator 1 is a WTG operating at slip s_1 then it's generated power is:-

$$P_1 = P_W.C_p = 1/2.\rho.A.C_p.U_1^3 \qquad (8.3)$$

or

$$V^2.s_1/R_2' = 1/2.\rho.A.C_p.U_1^3 \qquad (8.4)$$

Assuming a large bus where the voltage is constant, then the steady state condition is:-

$$s_1 = K_2.C_p.U_1^3 \qquad (8.5)$$

where

$$K_2 = 1/2.\rho.A.R_2'/V^2 \qquad (8.6)$$

The resulting interaction between Equations (8.2) and (8.5) is significant and justifies further study. The equations could be extended by assuming non-identical generators, non-infinite bus and mixed generator types on the bus as well as transient effects.

(2) Connection of the WTG to a grid using an ADA system as shown by Figure 8.3. To accomplish this with the current WTG, inversion of the DC output would be required. This could be fixed frequency and voltage for connection to the existing New Zealand grid or variable frequency and voltage for connection to an fully asynchronous generator supplied experimental grid.

(3) Both (1) and (2) above could be modified for uses with different generator types.

.Wind/Hydro Electric Scheme.

New Zealand, as well as being a country particularly suited to generation of electricity from the winds, is well endowed with hydro-electric potential. Although this resource is currently well employed, some savings may be possible if wind power is used in conjuction, as shown by Figure 8.4. During peak load periods the hydro supplies the grid load, and if the wind is available, the WTG's output could constructively be put to use to pump water back up to the storage lake, thus preserving water supply. Studies into the feasability of such a scheme could also be made.

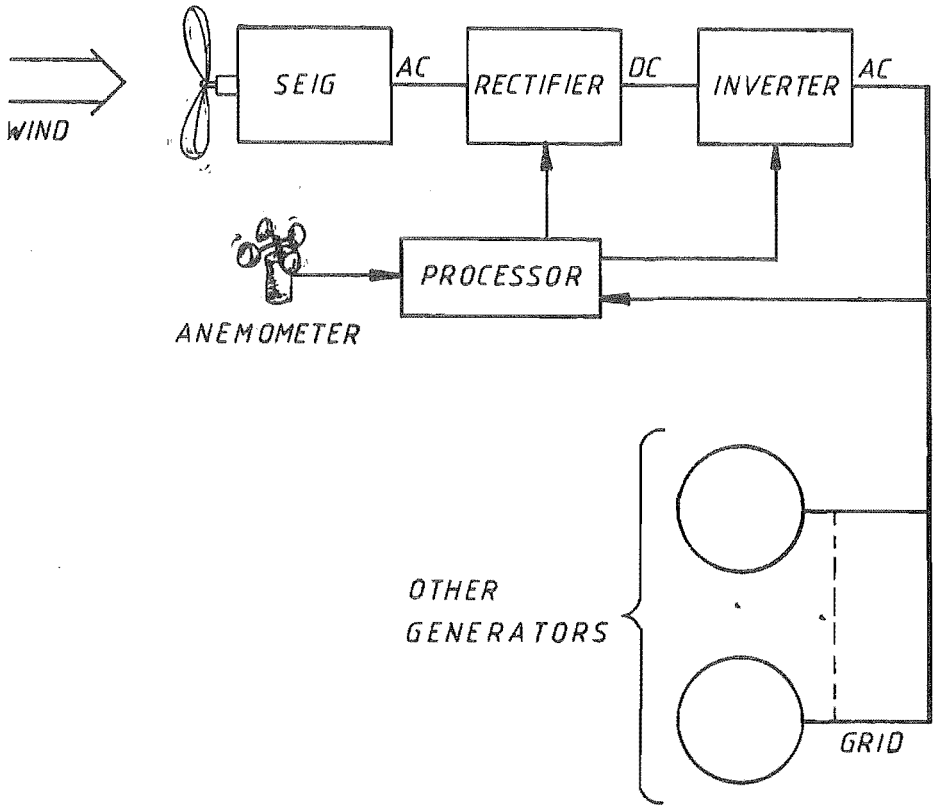

Figure 8.3: AC-DC-AC (ADA) Scheme.

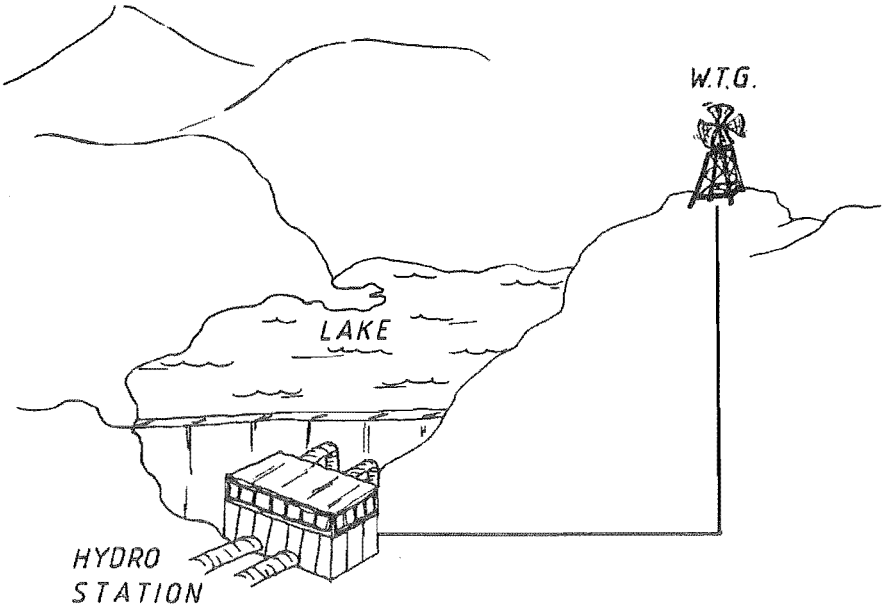

Figure 8.4: Wind/Hydro Electric Scheme.

8.3: Basic Research Proposals.

Studies on the wind turbine and its associated generator and control equipment which would be of interest are:-

.Turbine Blade Design.

The wind turbine generator constructed uses untwisted blades as described in Chapter 5. The use of untwisted blades was based on three factors:-

(1) Untwisted blades are easier to construct.

(2) A computer program PROP which computed performance showed only an 8% inprovement when optimally twisted blades are used over untwisted blades.

(3) Estimates from results produced by R.H. Miller (Miller 1983) suggest improvements of less than 5% are possible.

For the purposes of the current experiments it was considered that the advantages of improved performance of the turbine with twisted blades was outweighed by the simpler design and construction of flat blades. It is possible however that experiments could be carried out using differing blade designs, including those optimally twisted. This would necessitate construction of new blades, spars and spindles.

.Tip Vanes.

Tip vanes should also be considered following work by Van Holten (Van Holten 1978). The turbine is of a suitable scale such that work of this nature would not be of great difficulty.

.Mechanical Resonances.

The effects of resonances induced in wind turbines due to factors such as tower shadow can have serious consequences on the operation of the machines and should merit serious consideration for study on this wind turbine, since it is in this type of HAWT that tower shadow has its greatest effect.

.Generator and Rectifier Efficiencies.

The experiments described in this thesis are mainly concerned with obtaining controlled power transfer efficiency through the wind turbine, and uses a self excited induction generator and controlled rectifier for electricity generation and WTG control. The effects of generator and rectifier efficiencies have been neglected and it would seem appropriate to study these in the near future.

CHAPTER 9.

CONCLUSIONS.

A wind generation research facility has been designed, constructed and commissioned on the campus of the University of Canterbury. The facility is currently operating under microprocessor control using a self excited induction generator and controllable rectifier for the generation of electricity. Output at this stage is simply dumped in the form of heat.

It was possible to control wind turbine power coefficient by control of generator load. This was done by feeding the generator output through a controlled rectifier into a fixed resistive load. Control was achieved by varying the rectifier delay angle. Determination of required delay angle is made by detection of wind speed using the microprocessor based control system.

Self excited induction generator steady state operation has been discussed in terms of phasor diagrams and it was shown that diagrams drawn for currently used equivalent circuits inadequately describe the operation of the machine. An alternative equivalent circuit has been suggested. Further study of the steady state operation of the self excited induction generator to determine the exact nature of the relationships between the equivalent circuit and phasor diagram is recommended.

Design and operation of a controllable rectifier has been described, where linear control has been obtained over a wide range of frequencies and for distorted input waveforms. Interaction of the rectifier with the self excited induction generator has been described and shown to be of a complex, although workable nature.

Improvements in the load control system would increase its ability to demonstrate the practicability of this form of wind turbine control. Increasing the speed of the microprocessor software would be advantageous in that dynamic performance of load control system could be improved. Studies of this nature would be of great value. Increasing speed of the system would most simply be done by redesign of software, particularly in the operating system. Further improvements could also be made through study of the optimum pitch angle of the blades. Operating capacity would also be increased by installation of a larger generator, possibly in the region of 20 kW.

BIBLIOGRAPHY

Adamson C., Hingorani N.G. 1960 "High-Voltage Direct-Current Power Transmission", Garraway, 284p.

Almeida A.J., et al 1983 "Source Reliability in a Combined Wind-Solar-Hydro System", IEEE Trans. on Power Apparatus and Systems, Vol. PAS-102, No. 6, pp1515-1520.

Anderson M. 1979 "Horizontal Axis Wind Turbines in Yaw", Proc. First BWEA Wind Energy Workshop.

Anderson M.B. 1980 "A Vortex Wake Analysis for a Horizontal- Axis Wind Turbine and a Comparison with a Modified Blade Element Theory", Proc. BHRA Third International Symposium on Wind Energy Systems, pp357-374.

Anderson P.M., Bose A. 1983 "Stability Simulation of Wind Turbine Systems", IEEE Trans. on Power Apparatus and Systems, Vol. PAS-102, No. 12, pp3791-3795.

Arbouw J. 1982 "Electricity Generated by Flying Windmill", Engineers Australia, March 19, pp17-18.

Arrillaga J., Watson D.B. 1978 "Static Power Conversion from Self Excited Induction Generators", Proc. IEE, Vol. 125, No. 8, pp743-746.

Baird J.P. 1983 "Design Characteristics of the Mono Wind Turbine", Jou. Wind Engineering and Industrial Aerodynamics, Vol. 15, No. 1, pp31 -315.

Baker J.R. 1983 "Features to Aid or Enable Self Starting of Fixed Pitch Low Solidity Vertical Axis Wind Turbines", Jou. of Wind Engineering and Industrial Aerodynamics, Vol. 15, No. 3, pp369-380.

Barkle J.E., Ferguson R.W. 1954 "Induction Generator Theory and Application", Trans. AIEE, Vol. 73, Part III-A, pp12-18.

Bassett E.D., Potter F.M. 1935 "Capacitive Excitation for Induction Generators", Trans. AIEE, Vol. 54, pp540-545.

Bhumralkar C.M., et al 1980 "A Practical and Economic Method for Estimating Wind Characteristics at Potential Wind Energy Conversion Sites", Solar Energy, Vol. 25, No. 1, pp55-65.

Biederman N.P. 1975 "Wind Powered Hydrogen/Electric Systems for Farm and Rural Use", Proc. Second Workshop on Wind Energy Conversion Systems, Washington D.C., pp400-403.

Bolton H.R., Nicodemou V.C. 1979 "Operation of Self Excited Generators for Windmill Applications", Proc. IEE, Vol. 126, No. 9, pp815-820.

Bowen A.J. 1983 "The Prediction of Mean Wind Speeds Above Simple 2-D Hill Shapes", Jou. Wind Engineering and Industrial Aerodynamics, Vol. 15, No. 1, pp259-270.

Bradley E.F. 1983 "The Influence of Thermal Stability and Angle of Incidence on the Acceleration of Wind up a Slope", Jou. Wind Engineering and Industrial Aerodynamics, Vol. 15, No. 1, pp209-214.

Brennen M.B., Abbondanti A. 1977 "Static Exciters for Induction Generators", IEEE Trans. on Industry Applications, Vol. IA-13, No. 5, pp1020-1028.

Buehring I.K., Freris L.L. 1981 "Control Policies for Wind Energy Conversion Systems", Proc. IEE, Vol. 128, Pt. C, No. 5, pp253-261.

Buehring I.K., Freris L.L. 1980 "Some Aspects of Small Aerogenerator Design and Testing", Proc. BHRA Third International Symposium on Wind Energy Systems, Copenhagen, pp297-305.

Chan S.M., et al 1983 "Operations Requirements of Utilities with Wind Power Generation", IEEE Trans. on Power Apparatus and Systems, Vol. PAS-102, No. 9, pp2850-2860.

Chilcott R.E. 1976 "A Review of Renewable Energy in New Zealand with Emphasis on Wind Power Utilization", Dept. Agricultural Engineering, Lincoln College, Canterbury, New Zealand, 10p.

Daly S.A., et al 1983 "Modelling and Control of a Wind Driven Induction Generator for Water Storage Heating", Proc. IEE, Vol. 130, Pt. A, No. 9, pp596-603.

Davis R.M. 1979 "Power Diode and Thyristor Circuits", Peregrinus, 272p.

de Mello F.P., Hannett L.N. 1981 "Large Scale Induction Generators for Power Systems", IEEE Trans. on Power Apparatus and Systems, Vol. PAS-100, No. 5, pp2610-2618.

de Mello F.P., et al 1982 "Application of Induction Generators in Power Systems", IEEE Trans. on Power Apparatus and Systems, Vol. PAS-101, No.9, pp3385-3393.

Doherty R.E., Williamson E.T. 1921 "Short Circuit Current of Induction Motors and Generators", Trans. AIEE, Vol.40, pp509-551.

Doxey B.C. 1963 "Theory and Application of the Capacitor-Excited Induction Generator", The Engineer, November 29, pp893-896.

Dubyshev V.D., et al 1977 "Principles of Closed Loop Control Systems for Asynchronous Thyristorized Generators", Izv Vyssh Uchebn Zaved Elektromekh, No 10, pp1104-1109.

Edris A. 1980 "Dynamic Characteristics of a Wind Driven Induction Generator Equiped with Thyristor Controlled Inductances on the Stator Side", Proc. BHRA 3rd. International Symposium on Wind Energy Systems, pp279-296.

Elder J.M., et al 1983 "The Process of Self Excitation in Induction Generators", Proc. IEE, Vol. 130, Pt. B, No. 2, pp103-108.

Fung K.T., et al 1981 "Wind Energy - a Utility Perspective", IEEE Trans. on Power Apparatus and Systems, Vol. PAS-100, No. 3, pp1176-1182.

Golding E.W. 1955 "The Generation of Electricity by Wind Power", E and F.N. Spon Limited, 318p.

Gray A., Wallace G.A. "Principles and Practice of Electrical Engineering", McGraw-Hill, 8th. Edition, pp358-391.

Gustavsson B., Tornkvist G. 1978 "Test Results from the Swedish 60kW Experimental Wind Power Unit", Proc. BHRA 2nd. International Symposium on Wind Energy Systems, ppD1/1-D1/8.

Hau E. 1982 "Growian - Design, Manufacturing, Latest State of the Project", Proc. BHRA 4th. International Symposium on Wind Energy Systems, pp317-335.

Herapath R.G., Shi F.K.C. 1981 "Dynamics and Control of an Experimental 5m Diameter Variable Pitch Wind Powered Generator", IEE Conf. Publ. 192, International Conference on Future Energy Concepts, pp259-263.

Hinrichsen E.N., Nolan P.J. 1982 "Dynamics and Stability of Wind Turbine Generators", IEEE trans. on Power Apparatus and Systems, Vol. PAS-101, No. 8, pp2640-2648.

Hobart H.M., Knowlton E. 1912 "The Squirrel Cage Induction Generator", Proc. AIEE, Vol. XXXI, Pt. 2, pp1721-1747.

Holloway L. 1978 "Glass Reinforced Plastics in Construction", Surry University Press, pp7-51.

Igra O., Schulgasser K. 1978 "Design and Construction of a Pilot Plant for a Shrouded Wind Turbine", Proc. BHRA 2nd. International Symposium on Wind Energy Systems, ppF1/1-F1/12.

Jayadevaiah T.S., Smith R.T. 1975 "Generation Schemes for Wind Power Plants", IEEE Trans. on Aerospace and Electronic Systems, Vol. AES-11, No. 4, pp543-549.

Jayadev T.S. 1975 "Novel Electric Generation Schemes for Wind Power Plants", Proc. 2nd. Workshop on Wind Energy Conversion Systems, Washington D.C., pp298-306.

Jayadev T.S. 1976 "Windmills Stage a Comeback", IEEE Spectrum, November, pp44-49.

Jensen N.O. 1983 "Escarpment Induced Flow Pertubations, a Comparison of Measurements and Theory", Jou. of Wind Engineering and Industrial Aerodynamics, Vol. 15, No. 1, pp243-251.

Jensen S.A., Bjerregaard E.T.D. 1980 "Tests Performed on the 2MW Tvind WECS", Proc. BHRA 3rd. International Symposium on Wind Energy Systems, pp391-400.

Jian T.W., et al 1983 "Characteristic Induction Motor Slip Values for Variable Voltage Part Load Performance Optimization", IEEE Trans. on Power Apparatus and Systems, Vol. PAS-102, No. 1.

Johnson C.C., Smith R.T. 1976 "Dynamics of Wind Generators on Utility Networks", IEEE Trans. on Aerospace and Electronic Systems, Vol. AES-12, No. 4, pp483-493.

Jones C.V. 1967 "The Unified Theory of Electrical Machines", Butterworths, 542p.

Juul N.H. 1978 "Optimum Design Point Geometry and Performance of Propeller Type Wind Turbines", Wind Engineering, Vol. 2, No. 2, pp86-102.

Kalaitzakis K., Vachtsevanos G. 1982 "Power Optimization of Wind Electric Conversion Systems Integrated into the Electricity Grid", Wind Engineering, Vol. 6, No. 1, pp24-36.

Kant M., et al 1979 "Wind Energy Conversion System with Electromagnetic Stabilizer", Proc. IEE, Vol. 126, No. 11, pp1201-1203.

Kirchoff R.H., Kaminsky F.C. 1983 "Wind Shear Measurements and Synoptic Weather Categories for Siting Large Wind Turbines", Jou. of Wind Engineering and Industrial Aerodynamics, Vol. 15, No. 1, pp287-297.

Kitsis S.I. 1980 "Analytical Estimation of Magnetic Characteristic Curve of Asynchronous Self Excited Generator", Izv Vyssh Uchebn Zaved Elektromekh, No. 6, pp597-605.

Kitsis S.I. 1977 "Equivalent Circuit of a Loaded Asynchronous Generator in the Transient process of Self Excitation", Izv Vyssh Uchebn Zaved Elektromekh, No. 5, pp9-14.

Langsdorf A.S. 1955 "Theory of Alternating Current Machinery", 2nd. Edition, McGraw-Hill, pp164-362.

Larrabee E.E., French S.E. 1983 "Minimum Induced Loss Windmills and Propellers", Jou. of Wind Engineering and Industrial Aerodynamics, Vol. 15, No. 1, pp317-327.

Lindley D.F., Simpson P.B. 1980 "Assessment of Offshore Siting of Wind Turbine Generators", Proc. BHRA 3rd. International Symposium on Wind Energy Systems, pp17-42.

Lipman N.H., Halliday J. 1983 "Small Windpower Industry Needs a Government Boost", Electrical Review, Vol. 213, No. 4, pp23-24.

Lubin G. 1969 "Handbook of Fibreglass and Advanced Fibreglass Plastics Composites", Van Nostrand Reinhold Co., pp151-181.

Lundsager P., et al 1978 "Measurement of Performance and Structural Response of the Danish 200kW Gedser Windmill", Proc. BHRA 2nd. International Symposium on Wind Energy Systems, ppD2/9-D2/26.

Maeda J., Adachi K. 1983 "On the Spatial Structures of Longitudinal Wind Velocities Near the Ground in Strong Winds", Jou. of Wind Engineering and Industrial Aerodynamics, Vol. 15, No. 1, pp197-207.

Manigrasso R., et al 1971 "Regolazione Della Tensione Di Un Generatore Asincrono", L'Elettrotecnica, Vol. LVIII, No. 5, pp285-293.

Manning P.T. 1983 "The Environmental Impact of the Use of Large Wind Turbines", Wind Engineering, Vol. 7, No. 1, pp1-11.

Melkebeek J.A.A., Novotny D.W. 1983 "Steady State Modelling of Regeneration and Self Excitation in Induction Machines", IEEE Trans. on Power Apparatus and Systems, Vol. PAS-102, No. 8, pp2725-2733.

Meyer H., et al 1980"Requirements for a Cost Effective Wind-Powered Energy System for a Typical Rural Home or Farmhouse", Jou. of Engineering Education in South East Asia, Vol. 10, No. 1, pp70-75.

Milborrow D.J., et al 1982 "The UK Offshore Wind Power Resource", Proc. BHRA 4th. International Symposium on Wind Energy Systems, pp245-260.

Miller R.H. 1983 "The Aerodynamics and Dynamic Analysis of Horizontal Axis Wind Turbines", Jou. of Wind Engineering and Industrial Aerodynamics, Vol. 15, No. 12, pp329-340.

Miller R.H. 1982 "Simplified Free Wake Analysis for Rotors", The Aeronautical Research Institute of Sweden, FFA TN 1982-07, 73p.

Milner I.P., Watson D.B. 1982 "An Autonomous Wind Energy Converter Using a Self Excited Induction Generator for Heating Purposes", Wind Engineering, Vol. 6, No. 1, pp19-23.

Milner I.P., Watson D.B. 1983 "A Wind Power Generation Project", Unpblished paper, University of Canterbury.

Mitsuta Y., et al 1983 "Wind Characteristics over Complex Terrain", Jou. of Wind Engineering and Industrial Aerodynamics, Vol. 15, No. 1, pp185-196.

Mohan N., Riaz M. 1978 "Wind Driven, Capacitor-Excited Induction Generator for Residential Heating", Proc. 1978 Winter Power Meeting, IEEE Power Engineering Society, Paper A 78 050-7, 6p.

Moore D.J. 1979 "Depletion of Available Wind Power by a Large Network of Wind Generators", IEE Conference Publication No. 171, Future Energy Concepts, pp302-308.

Murakami S., Komine H. 1983 "Prediction Method for Surface Wind Velocity Distribution by Means of Regression Analysis of Topographic Effects on Local Wind Speed", Jou. of Wind Engineering and Industrial Aerodynamics, Vol. 15, No. 1, pp217-230.

Negushil A.V., Listvin V.S. 1977 "Autonomous Asynchronous Generator as a Nonlinear Oscillating System", Izv Vyssh Uchebn Zaved Elektromekh, No. 5, pp500-505.

Newman B.G. 1983 "Actuator-Disc Theory for Vertical-Axis Wind Turbines", Jou. of Wind Engineering and Industrial Aerodynamics, Vol. 15, No. 1, pp347-355.

Oberg E., Jones F.D. 1966 "Machinery's Handbook", Industrial Press Inc., 2103p.

Ouazene L., McPherson G. 1983 "Analysis of the Isolated Induction Generator", IEEE Trans. on Power Apparatus and Systems, Vol. PAS-102, No. 8, pp2793-2798.

Panofsky H.A., Zhao-Ming 1983 "Characteristics of Wind Profiles over Complex Terrain", Jou. of Wind Engineering and Industrial Aerodynamics, Vol. 15, No. 1, pp177-183.

Pass A.E., Vishnevskii L.V. 1980 "Dynamics of Asynchronous Self Excited Generator Close to Steady Regime", Izv Vyssh Uchebn Zaved Elektromekh, No. 6, pp591-596.

Poloujadoff M. 1982 "General Rotating MMF Theory of Squirrel Cage Induction Machines with Uniform Air Gap and Several Non- sinusoidally Distributed Windings", IEEE Trans. on Power Apparatus and Systems, Vol. PAS-101, No. 3, pp583-591.

Powell W.R. 1981 "An Analytical Expression for the Average Output Power of a Wind Machine", Solar Energy, Vol. 26, No. 1, pp77-80.

Power H.M. 1979 "Windmills on the Mind: A Study in Dynamics and Control", Electronics and Power, April, pp262-268.

Puthoff R.L. 1975 "Status of 100kW Experimental Wind Turbine Generator Project", Proc. 2nd. Workshop on Wind Energy Conversion Systems, Washington D.C., pp21-36.

Putnam P.C. 1948 "Power from the Wind", Van Nostrand, 224p.

Raina G., Malik O.P. 1983 "Wind Energy Conversion Using a Self Excited Induction Generator", IEEE Trans. on Power Apparatus and Systems, Vol. PAS-102, No. 12, pp3933-3935.

Ramakumar R. 1975 "Development and Adaptation of Field Modulated Generator Systems for Wind Energy Applications", Proc. 2nd. Workshop on Wind Energy Conversion Systems, Washington D.C., pp279-289.

Ramakumar R. 1983 "Renewable Energy Sources and Developing Countries", IEEE Trans. on Power Apparatus and Systems, Vol. PAS- 102, No. 2, pp502-510.

Reitan D.K. 1975 "A Progress Report on Employing a Non- synchronous AC/DC/AC Link in a Wind Power Application", Proc. 2nd. Workshop on Wind Energy Conversion Systems, Washington D.C., pp290-297.

Riegels F.W. 1961 "Aerofoil Sections", Butterworths, 281p.

Russell J.D. 1975 "The Induction Generator in Today's Industry", Petroleum and Chemical Conference Papers, 22nd. Milwaukee, pp80-84.

Say M.G. "The Performance and Design of Alternating Current Machines", 3rd. Edition, Pitman, pp344-347.

Schellens F.J.C. 1980 "The 25m Experimental Horizontal Axis Wind Turbine (25m HAT)", Proc. BHRA 3rd. International Symposium on Wind Energy Systems, pp375-390.

Seymour J. (Editor) 1968 "Semiconductor Devices in Power Engineering", Pitmans, 170p.

Simburger E.J., Cretcher C.K. 1983 "Load Following Impacts of a Large Wind Farm on an Interconnected Electric Utility System", IEEE Trans. on Power Apparatus and Systems, Vol. PAS-102, No. 3, pp687-692.

Sivasegaram S. 1980 "Transient Behaviour of Wind Energy Systems", Wind Engineering, Vol. 4, No. 2, pp53-63.

Somerville W.M. 1983 "55kW Aero-Generator Formally Commissioned on Fair Isle", NEI Review, Vol. 4, No. 4, pp15-19.

Spooner T., Barnes A.J. 1910 "The Induction Generator: A Discussion of its Operation in Parallel with Synchronous Apparatus", Electrical World, Vol. LV, No. 8, pp464-465.

Stanley H.C. 1938 "An Analysis of the Induction Machine", Trans. AIEE, Vol. 57, pp751-755.

Steinmetz C.P. 1897 "The Alternating Current Induction Motor", Trans. AIEE, Vol. 14, pp185-223.

Stickney G.H. 1983 "Performance Limitations of Wind Power Units" , Paper Preprints Vol. 3, Sixth International Conference on Wind Engineering, Session 22.

Stiller P.H., et al 1983 "Measured Effect of Wind Generation on the Fuel Consumption of an Isolated Diesel Power System", IEEE Trans. on Power Apparatus and Systems, Vol. PAS-102, No. 6, pp1788-1792.

Stodhart A.H. 1975 "Wind Power in Britain: Past Work and Present Position", Proc. 2nd. Workshop on Wind Energy Conversion Systems, Washington D.C., pp133-139.

Suzuki T., et al 1982 "Characteristics of a Small Wind-Power System with DC Generator", Proc. IEE, Vol. 129, Pt. B, No. 4, pp217-220.

Svensson J.E., Ulen E. 1982 "The Control System of WTS-3 Instrumentation and Testing", Proc. BHRA 4th. International Symposium on Wind Energy Systems, pp195-215.

Taylor D. 1982 "Wind Energy in the USA - Part 1", The Energy Journal, Vol. 55, No. 1, pp2-13.

Tesla N. 1888 "A New System of Alternate-Current Motors and Transformers", Trans. AIEE, Vol. 5, pp305-324.

Teunissen H.W. 1983 "Wind-Tunnel and Full-Scale Comparisons of Mean Wind Flow Over an Isolated Low Hill", Jou. of Wind Engineering and Industrial Aerodynamics, Vol. 15, No. 1, pp271-286.

United Nations 1981 "Renewable Sources of Energy, Vol. III Wind Energy", Economic and Social Commission for Asia and the Pacific, pp1-8.

van Holten T. 1978 "Tipvane Research at the Delft University of Technology", Proc. BHRA 2nd. Symposium on Wind Energy Systems, ppF2/13-F2/24.

Von Misis R. 1959 "Theory of Flight", Dover, 629p.

Wagner C.F. 1939 "Self Excitation of Induction Motors", Trans. AIEE, Vol. 58, pp47-51.

Warne D.F. 1983 "Wind Power Equipment", E. and F.N. Spon, 222p.

Warne D.F. 1977 "Generation of Electricity from the Wind", Proc. IEE, Vol. 124, No. 11R, pp963-985.

Waters W.L. 1901 "The Non-Synchronous Generator in Central Station and Other Work", Proc. AIEE, Vol. XXVII, Pt. 1, pp157-180.

Watson D.B., et al 1979 "Controllable DC Power Supply from Wind Driven Self Excited Induction Machines", Proc. IEE, Vol. 126, No. 12, pp1245-1249.

Weick F.E. 1930 "Aircraft Propeller Design", 1st. Edition, McGraw-Hill, pp5-81.

Westberg S. 1983 "A Strategy for Optimization of Wind Energy Systems", Wind Engineering, Vol. 7, No. 2, pp104-114.

Wilson R.E., Lissaman P.B.S. 1974 "Applied Aerodynamics of Wind Power Machines", Oregon State University, pp17-60.

Wood J.R., Chasteau V.A.L. 1981 "Wind Energy Utilization in New Zealand", NZERDC Report No. 67, p3.

Yadavalli S.R., Jayadev T.S. 1976 "A New Generation Scheme for Large Wind Energy Conversion Systems", Proc. of Intersociety Energy Conversion Engineering Conference, 11th., State Line, Nevada, pp1761-1765.

Young R.B. 1975 "A Concept for Converting Wind Energy to Methane", Proc. 2nd. Workshop on Wind Energy Conversion Systems, Washington D.C., pp461-464.

APPENDIX 1.

RESULTS OF BLADEB CALCULATIONS.

RESULTS OF BLADE CALCULATIONS
XXXXXXXXXXXXXXXXXXXXXXXXXXXX

BLADE DETAILS:-

ROOT RADIUS = 0.30

TIP RADIUS = 3.00

ROOT CHORD = 0.40

TIP CHORD = 0.20

TEST RADIUS = 0.17

NUMBER OF BLADES = 3.00

$C_p = 3.4\%$

PITCH ANGLE = 75.00

WIND VELOCITY M/S	START TORQUE NM	MAX SPEED RPM	AXIAL LOAD N	FORCE PLANE T N	FORCE NORMAL T N	MOM PLANE T NM	MOM NORMAL T NM
1.00	0.33	17.00	1.22	0.10	0.45	0.10	-0.45
2.00	1.32	34.00	4.89	0.40	1.79	0.39	-1.81
3.00	2.98	51.00	11.01	0.90	4.04	0.87	-4.08
4.00	5.29	68.00	19.57	1.60	7.18	1.55	-7.25
5.00	8.27	85.00	30.57	2.50	11.22	2.42	-11.33
6.00	11.91	102.00	44.02	3.59	16.15	3.49	-16.32
7.00	16.21	119.00	59.92	4.89	21.99	4.74	-22.21
8.00	21.17	136.00	78.26	6.39	28.72	6.20	-29.00
9.00	26.79	153.00	99.05	8.08	36.34	7.84	-36.71
10.00	33.08	170.00	122.28	9.98	44.87	9.68	-45.32
11.00	40.02	187.00	147.96	12.08	54.29	11.72	-54.84
12.00	47.63	204.00	176.09	14.37	64.61	13.94	-65.26
13.00	55.90	221.00	206.66	16.87	75.83	16.36	-76.59
14.00	64.83	238.00	239.67	19.56	87.94	18.98	-88.83
15.00	74.43	256.00	263.32	22.36	96.85	21.88	-111.14
16.00	84.68	273.00	301.20	25.46	110.75	24.91	-125.22
17.00	95.60	290.00	339.93	28.74	125.00	28.12	-141.29
18.00	107.17	307.00	381.31	32.25	140.22	31.52	-158.26
19.00	119.41	324.00	424.77	35.94	156.20	35.12	-176.26
20.00	132.31	341.00	473.76	39.80	174.14	38.81	-192.71
21.00	145.88	358.00	522.24	43.89	191.96	42.78	-212.39
22.00	160.10	375.00	574.90	48.16	211.28	46.98	-232.11
23.00	174.98	392.00	631.67	52.63	232.07	51.31	-251.08
24.00	190.53	409.00	689.12	57.36	253.16	55.91	-272.81
25.00	206.74	426.00	747.66	62.25	274.67	60.66	-295.95
26.00	223.61	443.00	808.57	67.33	297.05	65.60	-320.03
27.00	241.14	460.00	871.88	72.62	320.31	70.74	-345.05
28.00	259.33	477.00	937.57	78.11	344.45	76.08	-371.01
29.00	278.19	495.00	982.77	83.55	361.50	81.78	-416.08
30.00	297.71	512.00	1053.29	89.44	387.41	87.54	-444.58

RESULTS OF BLADE CALCULATIONS
XXXXXXXXXXXXXXXXXXXXXXXXXXXXXX

BLADE DETAILS:-

ROOT RADIUS = 0.30

TIP RADIUS = 3.00

ROOT CHORD = 0.40

TIP CHORD = 0.20

TEST RADIUS = 0.30

NUMBER OF BLADES = 3.00

$C_p = 3.47_0$

PITCH ANGLE = 75.00

WIND VELOCITY M/S	START TORQUE NM	MAX SPEED RPM	AXIAL LOAD N	FORCE PLANE T N	FORCE NORMAL T N	MOM PLANE T NM	MOM NORMAL T NM
1.00	0.33	17.00	1.22	0.10	0.45	0.08	-0.51
2.00	1.32	34.00	4.89	0.40	1.79	0.34	-2.05
3.00	2.98	51.00	11.01	0.90	4.04	0.75	-4.60
4.00	5.29	68.00	19.57	1.60	7.18	1.34	-8.18
5.00	8.27	85.00	30.57	2.50	11.22	2.10	-12.79
6.00	11.91	102.00	44.02	3.59	16.15	3.02	-18.41
7.00	16.21	119.00	59.92	4.89	21.99	4.11	-25.06
8.00	21.17	136.00	78.26	6.39	28.72	5.37	-32.74
9.00	26.79	153.00	99.05	8.08	36.34	6.79	-41.43
10.00	33.08	170.00	122.28	9.98	44.87	8.39	-51.15
11.00	40.02	187.00	147.96	12.08	54.29	10.15	-61.89
12.00	47.63	204.00	176.09	14.37	64.61	12.08	-73.66
13.00	55.90	221.00	206.66	16.87	75.83	14.17	-86.45
14.00	64.83	238.00	239.67	19.56	87.94	16.44	-100.26
15.00	74.43	256.00	263.32	22.36	96.85	18.98	-123.73
16.00	84.68	273.00	301.20	25.46	110.75	21.60	-139.62
17.00	95.60	290.00	339.93	28.74	125.00	24.38	-157.54
18.00	107.17	307.00	381.31	32.25	140.22	27.33	-176.49
19.00	119.41	324.00	424.77	35.94	156.20	30.45	-196.56
20.00	132.31	341.00	473.76	39.80	174.14	33.63	-215.35
21.00	145.88	358.00	522.24	43.89	191.96	37.07	-237.35
22.00	160.10	375.00	574.90	48.16	211.26	40.72	-259.58
23.00	174.98	392.00	631.67	52.63	232.07	44.47	-281.25
24.00	190.53	409.00	689.12	57.36	253.16	48.45	-305.73
25.00	206.74	426.00	747.66	62.25	274.67	52.57	-331.66
26.00	223.61	443.00	808.57	67.33	297.05	56.85	-358.65
27.00	241.14	460.00	871.88	72.62	320.31	61.30	-386.69
28.00	259.33	477.00	937.57	78.11	344.45	65.92	-415.79
29.00	278.19	495.00	982.77	83.55	361.50	70.92	-463.08
30.00	297.71	512.00	1053.29	89.44	387.41	75.91	-494.94

RESULTS OF BLADE CALCULATIONS
XXXXXXXXXXXXXXXXXXXXXXXXXXXX

BLADE DETAILS:-

ROOT RADIUS = 0.30

TIP RADIUS = 3.00

ROOT CHORD = 0.40

TIP CHORD = 0.20

TEST RADIUS = 0.90

NUMBER OF BLADES = 3.00

PITCH ANGLE = 75.00

WIND VELOCITY M/S	START TORQUE NM	MAX SPEED RPM	AXIAL LOAD N	FORCE PLANE T N	FORCE NORMAL T N	MOM PLANE T NM	MOM NORMAL T NM
1.00	0.33	17.00	1.22	0.07	0.15	0.02	-0.72
2.00	1.32	34.00	4.89	0.28	0.60	0.09	-2.86
3.00	2.98	51.00	11.01	0.63	1.35	0.21	-6.44
4.00	5.29	68.00	19.57	1.11	2.39	0.37	-11.45
5.00	8.27	85.00	30.57	1.74	3.74	0.58	-17.89
6.00	11.91	102.00	44.02	2.51	5.39	0.84	-25.76
7.00	16.21	119.00	59.92	3.41	7.33	1.14	-35.07
8.00	21.17	136.00	78.26	4.46	9.57	1.49	-45.80
9.00	26.79	153.00	99.05	5.64	12.12	1.89	-57.97
10.00	33.08	170.00	122.28	6.96	14.96	2.33	-71.57
11.00	40.02	187.00	147.96	8.42	18.10	2.82	-86.60
12.00	47.63	204.00	176.09	10.02	21.54	3.36	-103.06
13.00	55.90	221.00	206.66	11.76	25.28	3.94	-120.95
14.00	64.83	238.00	239.67	13.64	29.32	4.57	-140.27
15.00	74.43	256.00	263.32	15.58	29.35	5.42	-167.16
16.00	84.68	273.00	301.20	17.74	33.97	6.16	-189.37
17.00	95.60	290.00	339.93	20.03	38.35	6.95	-213.69
18.00	107.17	307.00	381.31	22.46	42.98	7.78	-239.47
19.00	119.41	324.00	424.77	25.02	47.89	8.66	-266.73
20.00	132.31	341.00	473.76	27.69	53.98	9.51	-293.73
21.00	145.88	358.00	522.24	30.53	59.51	10.47	-323.75
22.00	160.10	375.00	574.90	33.53	65.91	11.51	-354.75
23.00	174.98	392.00	631.67	36.64	73.21	12.54	-385.97
24.00	190.53	409.00	689.12	39.94	80.21	13.66	-420.03
25.00	206.74	426.00	747.66	43.34	87.02	14.81	-455.67
26.00	223.61	443.00	808.57	46.88	94.12	16.01	-492.77
27.00	241.14	460.00	871.88	50.56	101.49	17.26	-531.32
28.00	259.33	477.00	937.57	54.36	109.14	18.55	-571.31
29.00	278.19	495.00	982.77	56.20	109.15	20.25	-625.09
30.00	297.71	512.00	1053.29	62.34	117.41	21.67	-668.66

RESULTS OF BLADE CALCULATIONS
XXXXXXXXXXXXXXXXXXXXXXXXXXXX

BLADE DETAILS:-

ROOT RADIUS = 0.30

TIP RADIUS = 3.00

ROOT CHORD = 0.40

TIP CHORD = 0.20

TEST RADIUS = 2.70

NUMBER OF BLADES = 3.00

PITCH ANGLE = 75.00

WIND VELOCITY M/S	START TORQUE NM	MAX SPEED RPM	AXIAL LOAD N	FORCE PLANE T N	FORCE NORMAL T N	MOM PLANE T NM	MOM NORMAL T NM
1.00	0.33	17.00	1.22	0.01	-0.31	0.00	-0.05
2.00	1.32	34.00	4.89	0.04	-1.26	0.01	-0.20
3.00	2.98	51.00	11.01	0.08	-2.83	0.01	-0.45
4.00	5.29	68.00	19.57	0.15	-5.02	0.03	-0.79
5.00	8.27	85.00	30.57	0.23	-7.85	0.04	-1.24
6.00	11.91	102.00	44.02	0.33	-11.30	0.06	-1.78
7.00	16.21	119.00	59.92	0.44	-15.39	0.08	-2.43
8.00	21.17	136.00	78.26	0.58	-20.10	0.10	-3.17
9.00	26.79	153.00	99.05	0.74	-25.44	0.13	-4.01
10.00	33.08	170.00	122.28	0.91	-31.40	0.16	-4.95
11.00	40.02	187.00	147.96	1.10	-38.00	0.20	-5.99
12.00	47.63	204.00	176.09	1.31	-45.22	0.23	-7.13
13.00	55.90	221.00	206.66	1.53	-53.07	0.27	-8.37
14.00	64.83	238.00	239.67	1.78	-61.55	0.32	-9.71
15.00	74.43	256.00	263.32	2.14	-71.71	0.38	-11.26
16.00	84.68	273.00	301.20	2.43	-81.55	0.43	-12.81
17.00	95.60	290.00	339.93	2.73	-92.03	0.48	-14.45
18.00	107.17	307.00	381.31	3.06	-103.13	0.54	-16.19
19.00	119.41	324.00	424.77	3.40	-114.87	0.60	-18.04
20.00	132.31	341.00	473.76	3.72	-126.32	0.66	-19.93
21.00	145.88	358.00	522.24	4.10	-139.23	0.73	-21.97
22.00	160.10	375.00	574.90	4.50	-152.76	0.80	-24.10
23.00	174.98	392.00	631.67	4.91	-166.92	0.87	-26.34
24.00	190.53	409.00	689.12	5.34	-181.72	0.95	-28.67
25.00	206.74	426.00	747.66	5.79	-197.15	1.03	-31.10
26.00	223.61	443.00	808.57	6.26	-213.20	1.12	-33.64
27.00	241.14	460.00	871.88	6.74	-229.87	1.20	-36.27
28.00	259.33	477.00	937.57	7.25	-247.18	1.29	-39.00
29.00	278.19	495.00	982.77	7.99	-268.11	1.41	-42.10
30.00	297.71	512.00	1053.29	8.54	-286.84	1.51	-45.04

APPENDIX 2.

DETAILS OF TURBINE LOAD CALCULATIONS.

Locked Rotor Blade Loads.

Test Point	Z nn (mm^3)	A (mm^2)	Aerodynamic Loads
Point A	20 530	2 335	D = 575 N
			M = 855 Nm
Point B	12 360	1 358	D = 575 N
			M = 685 Nm
Point C	5 680 (Spar)	390 (Spar)	D = 415 N
	41 695 (GRP)	3 193 (GRP)	M = 350 Nm
Point D	19 420	2 020	D = 45 N
			M = 3 Nm

General Parameters for Blades:

Ultimate tensile strength of spindle	= 1 100 MPa
Ultimate tensile strength of spar	= 400 MPa
Ultimate tensile strength of GRP	= 250 MPa
Modulus of elasticity for spar	= 210 x 10^3 MPa
Modulus of elasticity for GRP	= 24 x 10^3 MPa

Main Shaft Loads.

Axial load	F	= 400 N
Out of balance force	F	= 660 N
Blade and hub weight	F	= 820 N
Precession couple	M	= 670 Nm
Torsional load	T	= 1 500 Nm
Coupling weight	F	= 90 N
Out of balance couple at foward end		= 86 Nm

Test Point	Z_{nn} (mm^3)	Z_{pp} (mm^3)	A (mm^2)	r (mm)	M (kg)	Aerodynamic Loads	Centrifugal Loads	Total Loads
Point A	20 530	20 530	2 335	0.99	17.1	F_{NT} = 395 N F_{PT} = 85 N M_{NT} = -425 Nm M_{PT} = 85 Nm	F_{AN} = -505 N F_{AP} = 135 N M_{AN} = -410 Nm M_{AP} = 110 Nm F_B = 7 445 N	F_N = -110 N F_P = 220 N M_N = -835 Nm M_P = 195 Nm
Point B	12 360	12 360	1 385	1.08	14.3	F_{NT} = 390 N F_{PT} = 90 N M_{NT} = -495 Nm M_{PT} = 75 Nm	F_{AN} = -480 N F_{AP} = 130 N M_{AN} = -375 Nm M_{AP} = 100 Nm F_B = 7 130 N	F_N = -90 N F_P = 480 N M_N = -870 Nm M_P = 175 Nm
Point C	5 680 Spar 41 695 GRP	15 820 Spar 434 540 GRP	390 Spar 3 193 GRP	1.43	6.8	F_{NT} = 120 N F_{PT} = 60 N M_{NT} = -670 Nm M_{PT} = 20 Nm	F_{AN} = -290 N F_{AP} = 80 N M_{AN} = -155 Nm M_{AP} = 45 Nm F_B = 4 280 N	F_N = -170 N F_P = 140 N M_N = -825 Nm M_P = 65 Nm
Point D	19 420	84 972	2 020	2.7	0.2	F_{NT} = -275 N F_{PT} = 8 N M_{NT} = -45 Nm M_{PT} = 2 Nm	F_{AN} = -15 N F_{AP} = 4 N M_{AN} = 0 Nm M_{AP} = 0 Nm F_B = 240 N	F_N = -290 N F_P = 12 N M_N = -45 Nm M_P = 2 Nm

Free Rotor Blade Loads.

Main Shaft Sections.

	Section Modulus Z (mm^3)	Polar Section Modulus Z (mm^3)	Area A (mm^2)	d (mm)
Stern End	21 205	42 410	2 825	60
Foward End	8 945	17 890	1 590	45

Main Shaft Splines.

Effective radius	R	= 27.9 mm
Ultimate tensile strength for main shaft		= 1 100 MPa
Torque rating of splines		= 206 235 Nm
Actual torque		= 110 Nm

Hub.

Section modulus at base of block shoulder		= 271 x 10^3 mm
Area		= 6 800 mm^2
Moment	M	= 850 Nm
Shear force	F	= 7 445 N
Ultimate tensile strength of plate		= 400 MPa

Bearing Loads.

	Main Shaft Stern Load (kN)	Yaw Shaft Upper Load (kN)
Dynamic load	2.2	20.96
Static load	3.9	13.26
Dynamic load rating	200	446
Static load rating	163	401

Support Column Loads.

Reaction to main shaft torque	T	= 1 500 Nm
Pod weight	F	= 6 470 N
Yaw torsional load	T	= 1 150 Nm
Drag force on pod	F	= 25 N
Precession couple	M	= 670 Nm
Drag force on blades	F	= 400 N
Out of balance force	F	= 660 N

Support Column Sections.

	Section Modulus Z (mm^3)	Polar Section Modulus Z (mm^3)	Area A (mm^2)	D (mm)	d (mm)
Yaw shaft, upper	67 895	135 785	3 970	95	63
Yaw shaft, lower	553 600	248 240	6 734	112	63
Column, lower			7 864	273	254

Yaw Shaft Gears and Spline.

Spline:

Effective radius	R	= 42.98 mm
Ultimate tensile strength, yaw shaft		= 400 MPa
Torque rating of spline		= 66 900 Nm
Actual torque		= 1 150 Nm

Yaw Gears:

	PCD (mm)	No. Teeth	Torque Rating (Nm)	Actual Torque (Nm)
Gear	420	134	12 600	1 150
Pinion	58	18	1 740	155

APPENDIX 3.

AUTHOR PUBLICATIONS.

An Autonomous Wind Energy Converter Using a Self Excited Induction Generator for Heating Purposes.

I.P. Milner, D.B. Watson.
Department of Electrical Engineering, University of Canterbury, Christchurch, New Zealand.

Abstract

A description is given of the design philosophy and construction for an autonomous wind energy conversion system using a self excited induction generator to provide heat for a plant propagation house. Emphasis is given to the method of optimisation of generator output to obtain maximum possible energy extraction from the wind.

Introduction

Wind energy conversion systems range from large scale systems interconnected to the electricity grid, to smaller autonomous systems for remote power supplies or for rural and domestic heating. This paper describes a small scale system under construction, and reviews some of the design philosophy.

The purpose of the project is to investigate power supply to a horticultural glass house. Rising fuel costs coupled with uncertainty of oil supplies have already influenced glass-house economies such that changes in heating methods, e.g. moves toward all electric heating, are now taking place. During this period of change there has been a renewed global interest in wind powered generation. The application of wind power to glass house heating therefore merits consideration particularly when it is realised that large heat losses occur in very windy weather [1]. Direct heating of resistive elements from a wind powered generator could meet the heating load, and during normal periods the wind powered generator would supply a heating element inside a large water tank, storing thermal energy for cold periods which occur when the wind speed is insignificant.

The proposed wind energy conversion system is autonomous in that it does not feed electrical power into an existing electrical grid, but whenever the wind speed is high enough it supplies electrical energy for use in an existing heating system. It is therefore not necessary to generate a constant voltage or constant frequency supply, and indeed direct current can be used in such heating applications. Furthermore, in order to obtain the maximum power available from the wind whenever it blows, a variable speed windmill is required. Finally the system must be relatively simple, cheap and rugged. These conditions are met by a variable speed windmill with fixed blade pitch driving a self excited induction generator, the electrical power being fed into the heating elements through a controlled rectifier unit.

The wind generator scheme described here is suitable for experimentation on this type of application. Since this study basically revolves around the subject of optimisation and its implementation on the experimental windmill, it is considered to be essentially electrical in nature.

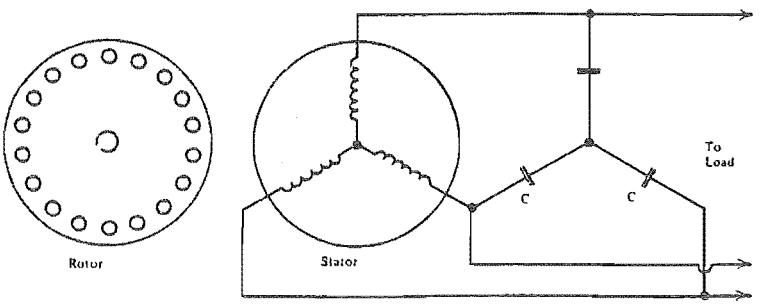

Figure 1 The Self Excited Induction Generator

Self Excited Induction Generator (SEIG)

In wind energy conversion systems the induction generator is seen to offer some advantages over synchronous or d.c. generators due mainly to its comparatively simple and rugged construction. Self excitation is achieved by connecting capacitors across the output terminals as illustrated in Fig. 1. An additional requirement for self excitation is, however, the existence of residual magnetism in the machine, for without this the subsequent buildup of voltage cannot occur.

There is a minimum value of capacitance and generator speed below which excitation will not occur, and for values which cause excitation the voltage buildup is limited by the intersection point of the generator magnetisation curve and the capacitor load line as shown in Fig. 2. For a wind generator using a SEIG the windmill must reach a speed above which excitation can occur before the generator is considered to be operational. This is the electrical cut-in speed. Above this speed the voltage and frequency are determined by complex relationships between speed, magnetization characteristics, and load impedance.

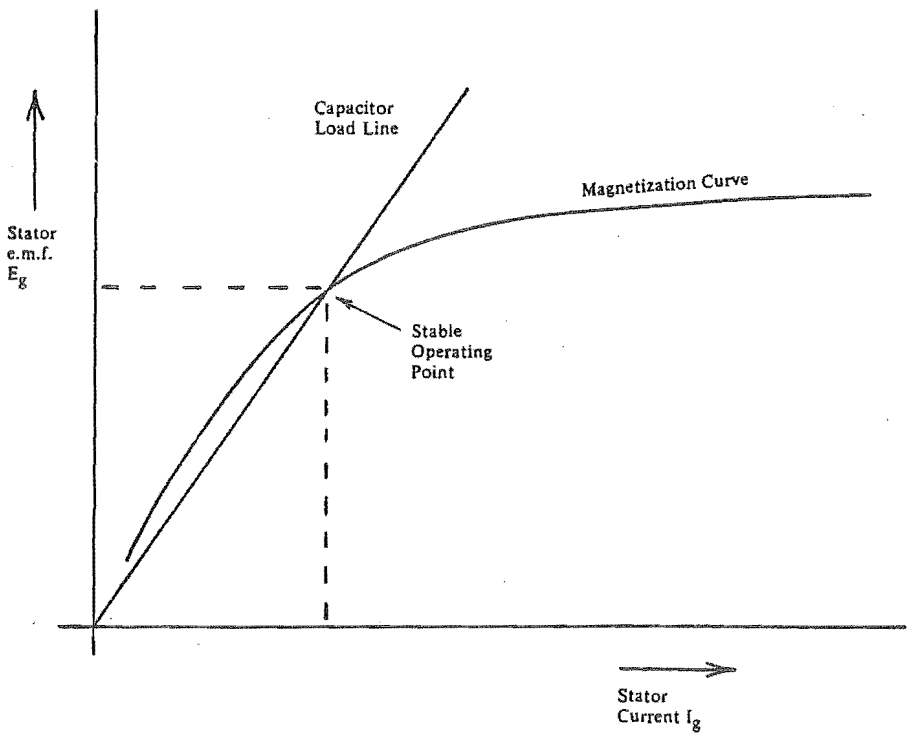

Figure 2 SEIG Excitation Characteristic

SEIG-Controlled Rectifier Combination

Recent publications [2,3] have described a method by which the SEIG output can be controlled using a controlled thyristor rectifier unit. The method relies on variation of rectifier delay angle to modify the active and reactive power flow from the generator, thus providing a form of variable excitation. Steady state investigations have shown that the generator output can be controlled over a very wide speed range. This makes it possible, between electrical cut-in speed and generator maximum rating, to optimise the power output from the system.

When the SEIG is driven by a fixed blade pitch windmill, the windmill speed is determined by the wind velocity and the generator output. Optimization of the performance of the system is obtained by control of rectifier delay angle, i.e. optimum tip-speed ratio is maintained by loading the generator to obtain a mill speed suitably matched to the incident wind speed. Under these conditions the power extracted from the wind is maximised, the power output from the generator increasing with the cube of the wind speed (Fig. 3).

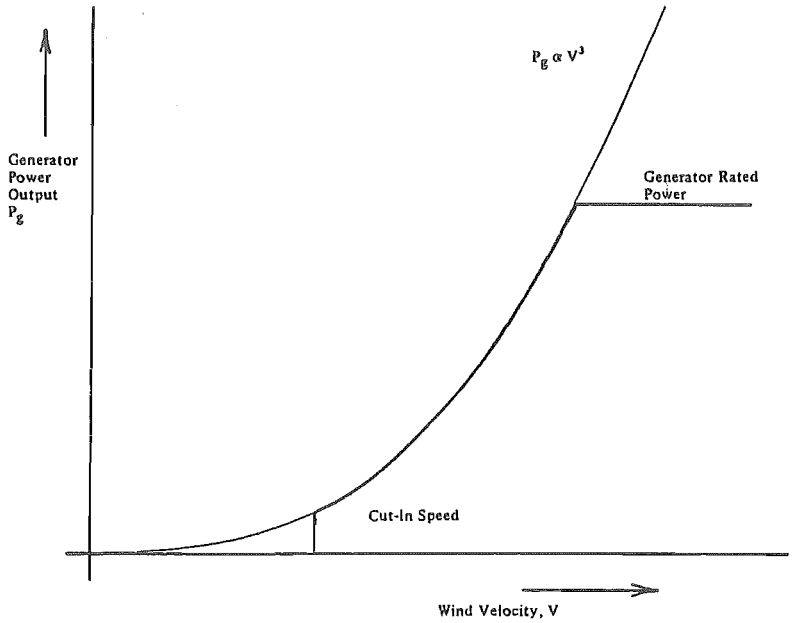

Figure 3 Wind Generation Power Characteristic

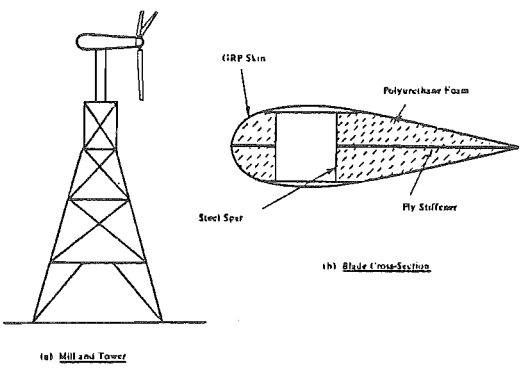

(a) Mill and Tower

(b) Blade Cross-Section

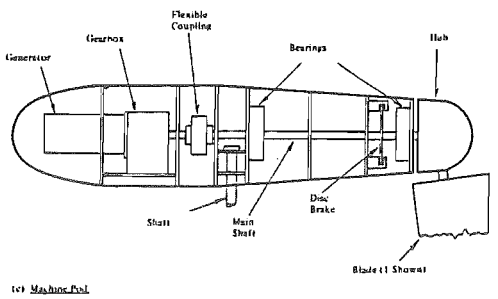

(c) Machine Pod

Figure 4

Fixed Blade Pitch Windmill

The experimental windmill is a trailing horizontal axis machine of 6 metre diameter with three fixed pitch blades and is mounted on an 18 metre steel tower (Fig. 4). The blades are a composite structure of folded sheet steel spar, polyurethane foam former, and glass reinforced plastic skin moulded to a NACA 0012 section. Blade pitch can be set manually when the mill is stationary to facilitate experimentation with differing pitch angles. Power transmission to the 8 pole 3-phase 10 KW induction generator is through a 1:10 helical gearbox with flexible coupling. Since the windmill is of the trailing type it is self aligning. However, the turntable does have a servo drive to obtain feathering by turning the whole mill sideways on to the wind, ensuring this position is maintained until disc brakes are applied.

Electrical cut in speed will occur for wind speeds in the order of 4 to 5 km per hour, while maximum generator output is expected to be realised for a wind speed of 40 km per hour. Response time of the mill to step changes in wind speed depend largely upon the requirement of adhesion to the optimum speed ratio, and for a step increase from zero wind speed to that required for maximum output it is estimated that response time will be in the order of 20 seconds.

The hothouse to be used during testing is approximately 12m by 4m and 2.2m high with glass ceiling and three glass walls to facilitate trapping of the sun's heat. When additional heating from the windmill is required it is accomplished either directly by resistive elements, or by circulation of preheated water if wind speed is too low to supply enough direct heating.

Overall control of the mill will be by the microprocessor based system of Fig. 5 designed around a general purpose 8 bit microprocessor controller data logger board. This allows flexible multipurpose control of a range of functions including plant optimisation, protection, data logging, telemetering and manual control.

By sensing incident wind velocity the rectifier delay angle is adjusted in order to obtain a maximum power coefficient for the mill. Limitations are set by electrical cut in speed and generator rating. As the response time of the microprocessor rectifier system is very small, less than a cycle of the generated voltage, response to changes in wind speed is limited only by the dynamics of the mill.

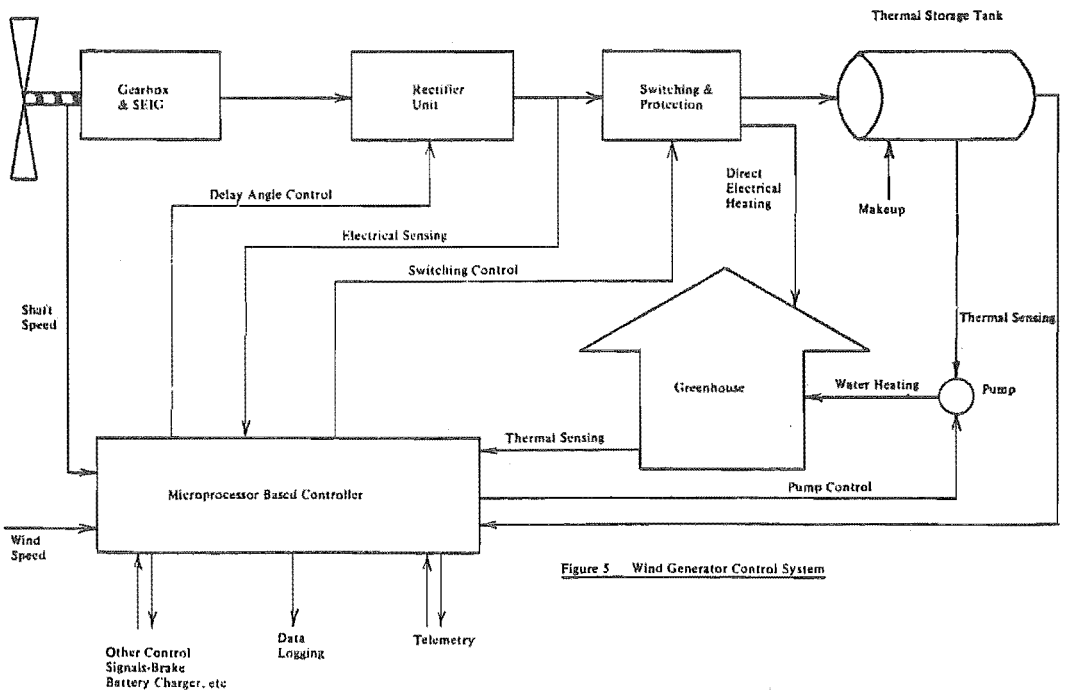

Figure 5 Wind Generator Control System

Discussion and Conclusions

A windmill with fixed blade pitch driving a self excited induction generator represents a cheap and rugged mechanical system. Controlled rectification provides a cheap, reliable method of power control. With microprocessor control the system can provide maximum heating power at all wind speeds, by variable speed operation.

The system described will be used to supply auxilliary heating for a small propagating house equipped with electric heating elements. A large water storage tank will provide alternative thermal storage.

The use of controlled rectifiers eliminates the need for mechanical blade pitch control, and for electromechanical actuators to operate at cut in and cut out speeds. Inclusion of a three phase inverter would make the plant suitable for interconnection to an electricity grid.

The SEIG has favourable characteristics under fault conditions, including de-excitation shortly after the application of a short-circuit fault on the generator terminals. Studies of the dynamic performance of the autonomous system are now required under such conditions as faults and rapid changes in wind conditions. On the completion of the basic wind generator it is intended to undertake such experiments.

References

[1] Brandenburg, W. *Canterbury Growers Review. May 1978.*

[2] Arrillaga, J., Watson, D.B. *"Static Power Conversion from Self Excited Induction Generators". Proc. I.E.E., Vol.125, No.8, 1978.*

[3] Watson, D.B., Arrillaga, J., Densem, T. *"Controllable D.C. Power Supply from Wind Driven Self Excited Induction Machines". Proc. I.E.E., Vol.126, No.12, 1979.*

APPENDIX 4.

SYSTEM CONTROL & LOAD CONTROL

PL/M CODE LISTINGS.

```
PL/M-80 COMPILER     SYSTEM CONTROL ROUTINE


ISIS-II PL/M-80 V3.1 COMPILATION OF MODULE PANELMODULE
OBJECT MODULE PLACED IN :F1:MILPAN.OBJ
COMPILER INVOKED BY:  PLM80 :F1:MILPAN.P80



             $INCLUDE(:F1:MILMN2.P80)
         =   $SYMBOLS XREF DEBUG PAGEWIDTH(132) PAGELENGTH(60) NOINTVECTOR IXREF
             $TITLE('    SYSTEM CONTROL ROUTINE')
   1         PANEL$MODULE:
             DO;
   2   1     DECLARE (PROALM,EXTALM) BYTE PUBLIC;
   3   1     DECLARE (INHIB,OZ,NANA,PETA) BYTE PUBLIC;
```

PL/M-80 COMPILER SYSTEM CONTROL ROUTINE

```
                $EJECT
  4   1     MILRUN: PROCEDURE EXTERNAL;
  5   2     END MILRUN;
  6   1     PHASE:  PROCEDURE (PNUM) EXTERNAL;
  7   2         DECLARE PNUM BYTE;
  8   2     END PHASE;
  9   1     GETAIC: PROCEDURE (CHAN) BYTE EXTERNAL;
 10   2         DECLARE CHAN BYTE;
 11   2     END GETAIC;
 12   1     SETAOC: PROCEDURE (CHAN,VALUE) EXTERNAL;
 13   2         DECLARE (CHAN,VALUE) BYTE;
 14   2     END SETAOC;
 15   1     GETDIC: PROCEDURE (CHAN) BYTE EXTERNAL;
 16   2         DECLARE CHAN BYTE;
 17   2     END GETDIC;
 18   1     SETDOC: PROCEDURE (CHAN,VALUE) EXTERNAL;
 19   2         DECLARE (CHAN,VALUE) BYTE;
 20   2     END SETDOC;
 21   1     RUNTSK: PROCEDURE (TASK$NUMBER) EXTERNAL;
 22   2         DECLARE TASK$NUMBER ADDRESS;
 23   2     END RUNTSK;
```

```
                $EJECT
 24   1         ALMCHK:                          /*THIS IS THE ALARM CHECKING SECTION*/
                    PROCEDURE;
 25   2          DECLARE JESS BYTE;              /*JESS IS MY WEE DAUGHTERS NAME*/
 26   2          CALL PHASE(8);
 27   2          EXTALM=GETDIC(7);               /*READ EXTERNAL ALARMS*/
 28   2          IF (PROALM<>0)THEN              /*ORDER SHUTDOWN IF A PROCESSOR ALARM EXISTS*/
 29   2              DO;
 30   3                  IF(JESS<>0)THEN         /*BUT ONLY DO IT IF THE ALARM PERSISTS*/
 31   3                      DO;
 32   4                      CALL SETDOC(1,0);   /*RESET P0*/
 33   4                      CALL SETDOC(2,0FFH);/*SET P1*/
 34   4                      CALL SETDOC(5,0FFH);/*SET ALARM INDICATION*/
 35   4                      INHIB=0FFH;         /*INHIBIT LOAD CONTROL*/
 36   4                      JESS=0;             /*RESET PERSISTANCE CHECK*/
 37   4                      PROALM=0;           /*RESET THE PROCESSOR ALARM*/
 38   4                      END;
                         ELSE
 39   3                      DO;
 40   4                      JESS=0FFH;          /*SET PERSISTANCE CHECK*/
 41   4                      PROALM=0;           /*RESET PROCESSOR ALARM AH TO BE SURE*/
 42   4                      END;
 43   3              END;
 44   2          ELSE JESS=0;                    /*RESET THE PERSISTANCE CHECKER AGAIN*/
 45   2          IF (EXTALM<>0)THEN              /*ORDER SHUTDOWN FOR AN EXTERNAL ALARM*/
 46   2              DO;
 47   3              CALL SETDOC(1,0);
 48   3              CALL SETDOC(2,0FFH);
 49   3              INHIB=0FFH;
 50   3              END;
 51   2          ELSE INHIB=0;
 52   2        END ALMCHK;
```

```
                $EJECT
 53   1         MILPAN: PROCEDURE PUBLIC;              /*THIS IS THE SYSTEM AND PANEL CONTROL SECTION*/
 54   2             DECLARE (PZERON,PZEROQ,DARN) BYTE; /*IT IS RUN EVERY HALF SECOND*/
 55   2             DECLARE (PONEN,PONEQ) BYTE;
 56   2             DECLARE (MBSN,MBSQ,CLRN) BYTE;
 57   2             DECLARE LIFE BYTE;
 58   2             CALL PHASE(2);
 59   2             PZERON=GETDIC(1);
 60   2             PONEN=GETDIC(2);
 61   2             DARN=GETDIC(3);
 62   2             CLRN=GETDIC(6);
 63   2             IF((PZERON<>PZEROQ) OR (PONEN<>PONEQ)) THEN /*HAVE ANY OF THE MILL*/
 64   2                 DO;                                     /*CONTROL BUTTONS BEEN PUSHED*/
 65   3                 IF((PZERON<>0) AND (PONEN<>0)) THEN
 66   3                     DO;
 67   4                     PZERON=0;
 68   4                     PONEN=0FFH;
 69   4                     END;
 70   3                 CALL SETDOC(1,PZERON);
 71   3                 CALL SETDOC(2,PONEN);
 72   3                 NANA=0FFH;
 73   3                 END;
 74   2             IF(DARN<>0) THEN                    /*HAS THE DELAY ANGLE CONTROL BUTTON BEEN PUSHED*/
 75   2                 DO;
 76   3                 CALL SETAOC(1,GETAIC(8));
 77   3                 NANA=0FFH;
 78   3                 PETA=0FFH;                      /*PETA IS MY OTHER DAUGHTERS NAME*/
 79   3                 END;
 80   2                 IF(MBSN<>MBSQ) THEN             /*HAS THE BREAKER CONTROL BUTTON BEEN PUSHED*/
 81   2                 DO;
 82   3                 IF(MBSN<>0)THEN
 83   3                     DO;
 84   4                     CALL SETAOC(1,0FFH);
 85   4                     END;
 86   3                 CALL SETDOC(4,MBSN);
 87   3                 NANA=0FFH;
 88   3                 IF(GETDIC(5)<>MBSQ) THEN
 89   3                     DO;
 90   4                     PROALM=0FFH;
 91   4                     END;
 92   3                 END;
 93   2             CALL SETDOC(6,NANA);
 94   2             OZ=OZ+1;                            /*OZ (THATS ME) IS USED TO SEE IF THE PROCESSOR IS ALIVE*/
 95   2             IF(OZ>1) THEN DO;
 97   3                 IF(LIFE=0) THEN LIFE=0FFH;      /*LIFE IS OUTPUT AS THE LIFE PULSE*/
 99   3                 ELSE LIFE=0;
100   3                 CALL SETDOC(3,LIFE);
101   3                 IF(PETA=0) THEN DO;             /*THIS BIT OF CODE CALLS THE LOAD CONTROL*/
103   4                     CALL PHASE(3);              /*CONTROL ROUTINE EVERY SECOND SCAN, IE.,*/
104   4                     CALL RUNTSK(2);             /*ONCE EVERY SECOND. RUNTSK(2) IS THE TASK*/
105   4                 END;                            /*TABLE ENTRY FOR MILRUN*/
106   3                 OZ=0;
107   3             END;
108   2             IF(CLRN<>0) THEN                    /*IF WE'RE FINISHED WITH THE PANEL CONTROL THEN*/
109   2                 DO;                             /*LETS RETURN TO AUTOMATIC CONTROL*/
110   3                 CALL PHASE(5);
111   3                 NANA=0;                         /*RESET ALL THE NASTIES THAT NEED TO BE RESET*/
```

```
112   3             PETA=0;
113   3             PZERON=0;
114   3             PONEN=0;
115   3             END;
116   2          PZEROO=PZERON;
117   2          PONEO=PONEN;
118   2          MBSO=MBSN;
119   2          CALL ALMCHK;
120   2       END MILPAN;
121   1       END PANEL$MODULE;
```

```
PL/M-80 COMPILER     LOAD CONTROL ROUTINE


ISIS-II PL/M-80 V3.1 COMPILATION OF MODULE MILLMODULE
OBJECT MODULE PLACED IN :F1:MILRUN.OBJ
COMPILER INVOKED BY:  PLM80 :F1:MILRUN.P80


                $INCLUDE(:F1:MILMN2.P80)
          =     $SYMBOLS XREF DEBUG PAGEWIDTH(132) PAGELENGTH(60) NOINTVECTOR IXREF
                $TITLE('    LOAD CONTROL ROUTINE')
   1            MILL$MODULE:
                DO;
   2    1       DECLARE (PROALM,EXTALM) BYTE EXTERNAL;
   3    1       DECLARE (INHIB,OZ,NANA) BYTE EXTERNAL;
   4    1       DECLARE PERR ADDRESS PUBLIC;
   5    1       DECLARE (FLAG1,FLAG2,FLAG3) BYTE PUBLIC;
   6    1       DECLARE ALPHAX BYTE PUBLIC;
   7    1       DECLARE (P1,P2,P3,P4) ADDRESS PUBLIC;
   8    1       PHASE:  PROCEDURE (PNUM) EXTERNAL;
   9    2           DECLARE PNUM BYTE;
  10    2       END PHASE;
  11    1       GETAIC: PROCEDURE (CHAN) BYTE EXTERNAL;
  12    2           DECLARE CHAN BYTE;
  13    2       END GETAIC;
  14    1       SETAOC: PROCEDURE (CHAN,VALUE) EXTERNAL;
  15    2           DECLARE (CHAN,VALUE) BYTE;
  16    2       END SETAOC;
  17    1       GETDIC: PROCEDURE (CHAN) BYTE EXTERNAL;
  18    2           DECLARE CHAN BYTE;
  19    2       END GETDIC;
  20    1       SETDOC: PROCEDURE (CHAN,VALUE) EXTERNAL;
  21    2           DECLARE (CHAN,VALUE) BYTE;
  22    2       END SETDOC;
  23    1       DELAY:
                    PROCEDURE (COUNT) EXTERNAL;
  24    2           DECLARE COUNT ADDRESS;
  25    2       END DELAY;
```

```
                $EJECT
 26   1         MILRUN: PROCEDURE PUBLIC;                /*HERE WE ARE - THE LOAD CONTROL SECTION*/
 27   2                 DECLARE (PMIN,PACT,PREQ,PDED) ADDRESS;
 28   2                 DECLARE (VD,VDR,PERRO) ADDRESS;
 29   2                 DECLARE (STEP,EN) BYTE;
 30   2                 DECLARE (U,CPM,A1,A2,WAY) BYTE;
 31   2                 DECLARE SET LITERALLY '0FFH';
 32   2                 DECLARE RIGHT LITERALLY '0FFH';
 33   2                 DECLARE INCREASE LITERALLY '0FFH';
 34   2                 DECLARE RESET LITERALLY '0';
 35   2                 DECLARE WRONG LITERALLY '0';
 36   2                 DECLARE DECREASE LITERALLY '0';
 37   2                 DECLARE LLIM LITERALLY '25';
                /*THIS LOOK UP TABLE TAKES THE VALUE OF WIND SPEED
                AND USES IT AS AN INDEX TO FIND THE POTENTIAL
                POWER AVAILABLE IN THE WIND, DIVIDED BY THE
                APPROPRIATE SCALE FACTOR WHICH MAXIMIZES ACCURACY*/
 38   2                 DECLARE WINDPWR$TABLE ($) ADDRESS DATA (0,0,0,0,
                         0,0,0,0,0,1,1,1,2,2,2,3,4,4,5,6,7,8,9,11,12,14,
                         15,17,19,21,24,26,29,31,34,37,41,44,48,52,56,60,
                         65,69,74,79,85,90,96,102,109,115,122,130,137,145,
                         153,161,170,179,188,198,208,218,228,239,250,262,
                         274,286,299,312,325,339,353,367,382,397,413,429,
                         446,463,480,498,516,535,554,573,593,614,635,656,
                         678,700,723,746,770,795,819,845,871,897,924,951,
                         979,1008,1037,1067,1097,1128,1159,1191,1223,1256,
                         1290,1324,1359,1394,1431,1467,1504,1542,1581,1620,
                         1660,1700,1742,1783,1826,1869,1913,1957,2002,2048,
                         2095,2142,2190,2239,2288,2338,2389,2441,2493,2546,
                         2600,2654,2710,2766,2822,2880,2938,2998,3058,3118,
                         3180,3242,3305,3369,3434,3500,3566,3633,3702,3771,
                         3840,3911,3983,4055,4128,4202,4278,4353,4430,4508,
                         4587,4666,4747,4828,4910,4993,5078,5163,5249,5336,
                         5424,5513,5603,5693,5785,5878,5972,6067,6162,6259,
                         6357,6456,6556,6656,6758,6861,6965,7070,7176,7283,
                         7392,7501,7611,7722,7835,7948,8063,8179,8296,8414,
                         8533,8653,8774,8897,9020,9145,9271,9398,9526,9655,
                         9786,9917,10050,10184,10319,10456,10593,10732,
                         10872,11013,11156,11299,11444,11590,11737,11886,
                         12036,12187,12339,12493,12648,12804,12961,13120,
                         13280,13441,13604,13768,13933,14100,14267,14437);
```

```
          $EJECT
          /* THIS IS THE START OF CODE FOR LOAD CONTROL SECTION*/
 39   2       CALL PHASE(4);
 40   2       IF(GETAIC(3)>250) THEN DO;        /*RUN IT ONLY IF AC VOLTS ARE OK*/
 42   3       IF(INHIB=RESET) THEN DO;          /*RUN IT ONLY IF INHIBIT IS RESET*/
 44   4       CALL PHASE(5);
 45   4       P4=P3;                            /*REORDER POWER READINGS*/
 46   4       P3=P2;
 47   4       P2=P1;
 48   4       U=GETAIC(1);                      /*HOW MUCH WIND WE GOT PARDNER*/
 49   4       IF(U>230) THEN PROALM=SET;        /*TO MUCH - SET THE ALARM*/
 51   4       P1=WINDPWR$TABLE(U);              /*DETERMINE SCALED WIND POWER VALUE*/
 52   4       A1=GETDIC(8);                     /*NOW LETS WORK OUT WHAT POWER AVERAGING COUNT*/
 53   4       A2=GETDIC(9);                     /*IS REQUIRED BY THE OPERATOR*/
 54   4       IF((NOT A2) AND (NOT A1)) THEN    /*WHAT IS THE AVERAGE VALUE OF*/
 55   4           PWIN=SHL(P1,2);               /*SCALED POWER THEN*/
 56   4       IF((NOT A2) AND A1) THEN
 57   4           DO;
 58   5           P1=SHL(P1,1);
 59   5           PWIN=P1+P2;
 60   5           END;
 61   4       IF(A2 AND (NOT A1)) THEN
 62   4           DO;
 63   5           P1=P1+(SHR(P1,1));
 64   5           PWIN=P1+P2+P3;
 65   5           END;
 66   4       IF(A1 AND A2) THEN
 67   4           PWIN=P1+P2+P3+P4;
 68   4       CPM=(GETAIC(9))/5;                /*FIND THE REQUIRED POWER COEFFICIENT*/
 69   4       IF(PWIN<=1285)THEN                /*NOW FIND THE SCALED REQUIRED LOAD POWER*/
 70   4           PREQ=(PWIN*CPM)/100;
               ELSE
 71   4           PREQ=(PWIN/100)*CPM;
 72   4       IF(U<32) THEN PDED=10;            /*SET THE VALUE OF SLIDING DEAD ZONE*/
               ELSE
 74   4           DO;
 75   5           IF(U<48) THEN PDED=12;
                   ELSE
 77   5               DO;
 78   6               IF(U<68) THEN PDED=24;
                       ELSE
 80   6                   DO;
 81   7                   IF(U<95) THEN PDED=48;
                           ELSE
 83   7                       DO;
 84   8                       IF(U<135) THEN PDED=96;
                               ELSE
 86   8                           DO;
 87   9                           IF(U<191) THEN PDED=192;
 89   9                           ELSE PDED=340;
 90   9                           END;
 91   8                       END;
 92   7                   END;
 93   6               END;
 94   5           END;
 95   4       EN=0;                             /*FOR A NEW RUN RESET LOOP COUNT*/
 96   4       DO WHILE(EN<8);                   /*ONLY DO IT IF LOOP COUNT IS OK*/
```

```
 97  5              IF(PREQ>PDED) THEN          /*NOT MUCH POINT IF REQUIRED POWER IS*/
 98  5                 DO;                     /*LESS THAN DEAD ZONE POWER*/
 99  6                 VDR=GETAIC(6);          /*FIND DC VOLTS AND CALCULATE ACTUAL POWER*/
100  6                 VD=SHL(VDR,1);
101  6                 PACT=((SHR(VD,3))*VD)/10;
102  6                 PERRD=PERR;             /*FLAGS FOR SOME OBSCURE USE (ALPHA DIRECTION*/
103  6                 FLAG2=FLAG1;            /*CONTROL)*/
104  6                 IF (PACT)(PREQ+PDED)) THEN      /*BIT TO INCREASE ALPHA*/
105  6                    DO;
106  7                    PERR=PACT-(PREQ+PDED);
107  7                    FLAG1=SET;
108  7                    END;
                       ELSE
109  6                    DO;
110  7                    IF (PACT<(PREQ-PDED)) THEN  /*BIT TO DECREASE ALPHA*/
111  7                       DO;
112  8                       PERR=(PREQ-PDED)-PACT;
113  8                       FLAG1=RESET;
114  8                       END;
115  7                    ELSE PERR=0;
116  7                    END;
117  6                 IF (PERR<>0) THEN       /*HERE WE GO - IS FEEDBACK NEGATIVE*/
118  6                    DO;
119  7                    IF ((PERR<=PERRD) AND (FLAG1=FLAG2)) THEN
120  7                       WAY=RIGHT;
121  7                    ELSE WAY=WRONG;
122  7                    IF (WAY<>RIGHT) THEN FLAG3=(NOT FLAG3);
124  7                    IF (PERR>50) THEN STEP=10;  /*BIG STEP FOR A BIG ERROR*/
126  7                    ELSE STEP=2;          /*LITTLE STEP FOR A LITTLE ERROR*/
127  7                    IF (FLAG1<>FLAG2) THEN STEP=2;  /*OR A DIRECTION CHANGE*/
129  7                    IF (FLAG3=DECREASE) THEN
130  7                       DO;
131  8                       CALL PHASE(6);
132  8                       IF(ALPHAX>STEP)THEN     /*LETS ACTUALLY OUTPUT A*/
133  8                          DO;          /*VALUE OF ALPHA*/
134  9                          ALPHAX=ALPHAX-STEP;
135  9                          IF (ALPHAX<LLIM)THEN ALPHAX=LLIM;   /*UNLESS ITS*/
137  9                          END;                                /*RUBBISH*/
138  8                       ELSE ALPHAX=LLIM;
139  8                       CALL SETAOC(1,ALPHAX);
140  8                       END;
141  7                    ELSE IF (FLAG3=INCREASE) THEN
142  7                       DO;
143  8                       CALL PHASE(7);
144  8                       IF((0FFH-ALPHAX)>STEP) THEN
145  8                          DO;
146  9                          ALPHAX=ALPHAX+STEP;
147  9                          END;
148  8                       ELSE ALPHAX=0FFH;
149  8                       CALL SETAOC(1,ALPHAX);
150  8                       END;
                          END;
152  6                 CALL DELAY(14);         /*OUR MAGICAL LOOP DELAY. THE 14 GIVES*/
153  6                 END;                    /*A 14 X 10 MS DELAY TIME*/
                    ELSE
154  5                 DO;                     /*BETTER SET ALPHA TO BLOCK IF WE CAN'T FIND ANYTHING*/
155  6                 ALPHAX=0FFH;            /*BETTER TO DO WITH IT*/
```

PL/M-80 COMPILER LOAD CONTROL ROUTINE

```
156  6                  CALL SETADC(1,ALPHAX);
157  6                  END;
158  5               EN=EN+1;                    /*INCREMENT THE LOOP COUNT*/
159  5               END;
160  4            IF(PACT)1250D) THEN PROALM=SET;   /*OH DEAR, POWER IS A BIT BIG - ALARM*/
162  4            IF(GETAIC(2)>1920) THEN PROALM=SET;     /* TURBINE REVS TOO BIG - ALARM*/
164  4            END;
165  3            END;
          /*THIS IS THE END OF THE LOAD CONTROL SECTION*/
166  2     END MILRUN;
167  1     END MILL$MODULE;
```

APPENDIX 5.

WIND TURBINE GENERATOR SPECIFICATIONS.

Rotor:

Number of Blades	3
Diameter	6 m
Maximum Speed	200 rpm
Coning Angle	4 degrees
Tilt Angle	0 degrees
Type	Downwind, bidirectional
Hub Type	Fixed

Blades:

Type	Tapered, untwisted
Material	Steel spar, GRP skin
Profile	RAF 39
Taper	50% of root chord

Drive Train:

Gearbox Ratio	1:10 Step up
Gearbox Type	Two stage, helically cut, oil bath
Coupling	Crown pin type, low speed shaft
Brake	2 Caliper disc, hydraulic

Generator:

Type	Asynchronous, 8 pole, squirrel cage
Rating	3 kW at 50 Hz, 415 V
Maximum Output	6 kW
Excitation	Self excited from static capacitors

Control System:

Type	Microprocessor based
Turbine control	By power feedback, rectifier delay angle control

Rectifier:

Type	3 Phase, 6 pulse controllable bridge
Frequency Range	5 Hz to 300 Hz
Rating	24 A_{dc} at 1000 V_{dc}

Yaw Drive:

Running	Self steering, hydraulically damped
Shutdown	Hydraulically driven
Maximum Yaw Rate	6 rpm

Tower:

Main Tower	15 m Steel lattice
Upper Column	Steel tube, seamless, 4m

APPENDIX 6.

WIND RECORDING SYSTEM.

WIND RECORDING SYSTEM.

A system has been constructed as a mobile wind speed and direction recorder. It is capable of recording wind speed up to 45 m/s and wind direction with a resolution of approximately 1.4 degrees ($360/2^8$ degrees). The system consists of:-

(1) A data logger (MIDAL = MIni DAta Logger) for processing and recording wind data. This is based on an INTEL 8085 processor with an architecture similar to that of Figure 6. 8. Software for reading and recording of wind data is interrupt driven, the interrupts arising from wind speed/frequency dependent pulses from the anemometer. Speed peaks are recorded from the delay between pulses and average 5 minute wind speed is also recorded. Wind direction is recorded as an 8 bit Grey Code averaged over a 5 minute period. All data, including time of day, is stored in RAM giving a maximum RAM recording time of about 30 minutes.

When RAM is full the processor dumps data, in Kansas City Format, on to a cassette recorder. The cassette is controlled by the processor and can store data for up to 5 days without changing of cassettes.

The processor also controlls the data logger console. Controls on the console allow for operator requested dumping of data from RAM to cassette immediately prior to a change of tape cassette. This is required to prevent the possibility of an automatic dump while changing cassettes. Other controls allow for the resetting of the time of day, processor resetting and analog display of wind speed.

Both the logger and cassette are 12 V_{DC} /230 V_{AC} operated. For 12 V_{DC} operation in remote areas a battery supply is needed. Logger operation requires 1 Amp at 12 V_{DC}.

(2) Anemometer and wind vane mounted on a stand. The anemometer is a

three cup type using an optical interruptor device located over a 16 slot drum. For one revolution of the cups, 16 pulses are thus output to the logger interrupt input. The wind vane uses an 8 segment optical interruptor array (paper tape reader array). The drum is slotted in Grey Code to facilitate processor checks of coded readings. The advantage of using optical interruptor devices is that they provide a system where shaft friction arises only from the bearings.

(3) Processing of data recorded on the cassettes. This is accomplished using an INTEL microprocessor development system with a cassette tape reading facility. Data is then transmitted to the Electrical and Electronics Engineering Department's VAX 11 /750 computer. Software on the VAX processes the data and caters for data presentation in yearly, weekly, monthly and seasonal formats. Ongoing averages and RMS values can also be shown.